ENHANCING THE DESIGN OF COMPLEX HYDRAULIC STRUCTURES APPLYING 3D HYDRODYNAMIC MODELLING

by

Getnet Kebede Demeke

PhD Dissertation submitted to Graduate School of Addis Ababa University, Addis Ababa Institute of Technology, School of Civil and Environmental Engineering in partial fulfilment of the requirements for the

Degree of

Doctor of Philosophy, PhD In

CIVIL ENGINEERING (HYDRAULIC ENGINEERING)

Addis Ababa University

Addis Ababa, Ethiopia

October 2019

The thesis committee of

Addis Ababa University (AAU), in Addis Ababa Institute of Technology (AAiT)

Certifies that this is the approved version of the following thesis

ENHANCING THE DESIGN OF COMPLEX HYDRAULIC STRUCTURES APPLYING 3D HYDRODYNAMIC MODELLING

By:

Getnet Kebede Demeke — Date

APPROVED BY

BOARD OF EXAMINNERS:

Supervisor: - Dereje Hailu (Assoc. Prof.) — Date

Co Supervisor: - Yilma Sileshi (Assoc. Prof.) — Date

Examiner 1: - — Date

Examiner 2: - — Date

Examiner 2: - — Date

Chairperson: - — Date

ABSTRACT

Hydraulic structures are often complex and in many cases their designs require attention so that the flow behaviour around hydraulic structures and their influence on the environment can be predicted accurately. Currently, more efficient computational fluid dynamics (CFD) codes can solve the Navier–Stokes equations in three-dimensions and free surface computation in a significantly improved manner. CFD has evolved into a powerful tool in simulating fluid flows. In addition, CFD with its advantages of lower cost and greater flexibility can reasonably predict the mean characteristics of flows such as velocity distributions, pressure distributions, and water surface profiles of complex problems in hydraulic engineering. Meanwhile, performance assessment of FLOW-3D hydrodynamic model using physical model result has been done and it was found that the 3D numerical model results showed a good agreement with the results of the physical model as well as the designed results.

In Ethiopia, Tendaho Dam Spillway was constructed recently, and one flood passed over the spillway. Using 3D hydrodynamic model Tendaho Spillway hydraulic performance was assessed and it is found stilling basin is inadequate. Because of this inadequacy the flood in 2011 created huge loses. It is recommended that the spillway bed level must be lowered by at least 15 m. Furthermore, the spillway size for its capacity to prevent overtopping of the dam has been checked with full Probable Maximum Flood (PMF) for a condition that if one of the gate malfunctions and the spillway crest length is reduced by one third. According to the result of 3D hydrodynamic model it is confirmed that the dam is safe from overtopping with the worst condition.

The unconventional stilling basin of the Ribb dam spillway in Ethiopia was checked with 3D hydrodynamic model and found that the designed and constructed wall height will be overtopped. Hence, the wall height requires to be raised by an additional 7 m, otherwise the spillway as well as the dam are not safe for operation. The capacity of the U-shaped side channel spillway also checked with full PMF and is found that it is safe for the operation however it is uneconomical design.

Hence, design of complex hydraulic structures using the state-of- art of 3D hydrodynamic modelling enhances the safety of the structures. Therefore, any complex hydraulic structure such as spillway, at least verification of its design must be done with 3D hydrodynamic numerical model before construction.

Keywords: velocity distributions; water surface profiles; computational fluid dynamics (CFD); 3D numerical models; spillway and superelevation.

ACKNOWLEDGEMENTS

I would like to express my special appreciation and thanks to my advisors Dr. Dereje Hailu Asfaw and Dr. Yilma Seleshi Shiferaw, you have been a tremendous mentor for me. I would like to thank you for encouraging my research and for allowing me to grow as a research scientist. Your advice on both research as well as on my career have been priceless. am also thankful to the School of Civil and Environmental Engineering of AAiT, Addis Ababa University for smoothly facilitating my PhD work throughout my study period. Words cannot express how grateful I am to my beloved wife Aster Tsegaye Abateneh who spent sleepless nights with and was always my support in the moments when there was no one to answer my queries. Thanks to my daughters Betel Getnet and Wudase Getnet and son Misgana Getnet for all of the sacrifices that you've made on my behalf.

I would like to thank Dawit Neri who supported me a lot and Engr. Mesfin Legesse, Engr. Kenneth Ifeanyi Nnadi and Dr. Andnet Shimelis who helped me for reviewing the work.

Finally, I am using this opportunity to express my gratitude to everyone who supported me throughout the course of this PhD thesis. I am thankful for their aspiring guidance, invaluable constructive criticism and friendly advice during the research work. I am sincerely grateful to them for sharing their truthful and illuminating views on a number of issues related to the project.

DECLARATION

By submitting this dissertation, I declare that the entirety of the work contained herein is my own, original work, that I am the sole author. The work contains no material that has been accepted for the award of any other degree or master in any university and, to the best of my knowledge and belief, contains no material previously published or written by another person, except where due reference has been made in the text.

The reproduction and publication thereof by Addis Ababa University will not infringe to my knowledge any third party right and so that I have not previously in its entirety or in part submitted it for obtaining any qualification

Getnet Kebede Demeke _____ _____

Name of the Author……. ……Signature……. …..…… Date……

DEDICATION

This work is dedicated to

The Almighty God, my Wife and Children

For dedicating their life for me and my wellbeing with endless love and support

TABLE OF CONTENT

LIST OF FIGURES

LIST OF PLATE

LIST OF TABLES

LIST OF ABBREVIATION

AEP	Annual Exceedance Probability
CCHE	Centre for Computational Hydro-science and Engineering
CFD	Computational Fluid Dynamics
ch	Chainage
CV	Control Volume
DHI	Danish Hydraulic Institute
DSD	Drainage Services Department
ECD	Enlarged Cotter Dam
EL	Elevation
FAO	Food and Agriculture Organization
FAVOR	Fractional Area Volume Obstacle Representation
FD	Finite Difference
FDM	Finite Difference Method
FEM	Finite Element Method
FRL	Full Reservoir Level
FV	Finite Volume
FVM	Finite Volume Method
HRI	Hydraulic Research Institute
IS	Indian Standard
MHL	Manly Hydraulics Laboratory

MMC	Million Meter Cubic
MWL	Maximum Water Level
NL	Normal Level
P.D.E	Partial Differential Equation
PMF	Probable Maximum Flood
RNG	Renormalization Group
SW	Shallow Water
STL	Stereolithographical
USACE	U.S.Army Corps of Engineers
USBR	U.S. Bureau of Reclamation
UWRL	Utah Water Research Laboratory
VOF	Volume Of Fluid
WS	Water Surface

CHAPTER ONE

1 INTRODUCTION

1.1 BACKGROUND

To predict the flow behaviour around hydraulic structures, it is usually carried out by means of hydraulic models of two types: numerical and physical model [1]. Hydraulic structures are very often complex and in many cases their designs require much attention so that the flow behaviour around hydraulic structures and their influence on the environment can be predicted accurately. Flows in curved and complex channels and in structures usually exhibit complex three-dimensional features by the presence of superelevation [2], [3], turbulence and vortex. Simulating such complex flow phenomena must rely on 3-D models rather than 1-D or 2-D models.

A spillway is a hydraulic structure that passes normal (operational) and/or flood flows in a manner that protects the structural integrity of the dam and/or dikes. Spillways are hydraulically sized to safely pass floods equal to or less than the inflow design flood [4], [5], [6] [7], [8]. It is of paramount importance for the spillway facilities to be designed with adequate capacity to dispose of the entire surplus water at the time of the arrival of the worst design flood.

From the researcher's experience, embankment spillway cost is a substantial part of the cost of the dam. Its cost can be as high as 40% of the total cost of dam, and a lot of these structures will be constructed in the future, hence, cost savings in spillway through proper design is important.

Traditionally, scaled physical hydraulic models have been constructed in laboratories to study the hydraulic behaviours. However, these models can be expensive, time consuming and there are many difficulties associated with scaling effects. Most models built are only kept for a limited time [9].

In early years, physical model studies would have been the only practical medium available to gain insight into the three- dimensional and time-dependent nature of fluid flow. However, physical modelling is typically undertaken during the final stages of design, and can be costly to execute [9], [10], [6]. With the advancements in computing power made since the 1980's, CFD analysis has emerged as a powerful alternative design tool, and can be used to provide insight into hydraulic design at all levels of study [10].

Advances in software and hardware technology mean more nonlinear, complex three-dimensional analyses are being performed. Now the use of numerical methods such as Computational Fluid Dynamics (CFD) analyses is attractive in term of lower cost and substantially reduces preparation time [11] and results can be obtained throughout the flow domain rather than at selected monitoring locations. Early difficulties involving mesh or grid to track the free water surface and to obtain a converged solution were

reported. CFD has evolved into a powerful tool and is used not only in simulating industrial and naturally occurring fluid flows, but also in the deeper understanding of the subject of Fluid Mechanics itself. For example, CFD models based on the Direct Numerical Simulation (DNS) are being used in understanding the very difficult problem of turbulence [12].

Turbulent flow in which the fluid undergoes irregular fluctuations, or mixing, in contrast to laminar flow, in which the fluid moves in smooth paths or layers. In turbulent flow the speed of the fluid at a point is continuously undergoing changes in both magnitude and direction [13], [14]. In a laminar flow, transport of momentum mostly occurs through viscosity (diffusion), while in a turbulent flow, transport can occur through the random motion embodied by the fluctuating terms [15], [16], [17].

CFD analysis involves the solution of the governing equations for fluid flow, the Navier Stokes equations, at thousands of discrete points on a computational grid, giving the analyst a full three-dimensional representation of the fluid flow domain. These numerical simulation capability gives engineers the power to quickly and inexpensively explore different design options and often demonstrates how a water resource project can be constructed and or operated more efficiently. It can be used early in the design phase to provide initial insight into critical design issues, and can also be used to compliment or reduce the need for any planned physical model studies [10], [18].

Currently, it is now feasible to undertake complex three-dimensional analyses with the use of high-performance computers and more efficient computational fluid dynamics

(CFD) codes. In addition, CFD with their advantages of lower cost and greater flexibility can reasonably predict the mean characteristics of flows such as velocity distributions, pressure distributions, and water surface profiles of complex problems in hydraulic engineering [12], [19], [20], [21].

FLOW-3D is a numerical technique and software package to solve the equations of motion for fluids to obtain transient, three-dimensional solutions to multi-scale, multi-physics flow problems. An array of physical and numerical options allows users to apply FLOW-3D to a wide variety of fluid flow and heat transfer phenomena [22], [23].

FLOW-3D uses a simple grid of rectangular elements, so it has the advantages of ease of generation, regularity for improved numerical accuracy; and it requires minimal memory storage. Geometry is then defined within the grid by computing the fractional face areas and fractional volumes of each element that are blocked by obstacles [10], [24].

FLOW-3D includes great many physical models, including shallow water, viscosity, cavitation, turbulence, sediment scour, homogenous and adiabatic bubbles, surface tension, porous media, particles and more. Among the industries in which FLOW-3D is put to use are: metal casting, ink jet design, process engineering, consumer products, civil hydraulics, environmental engineering, aerospace, coating, maritime, oil & gas [10].

Confidence gained through the use of the three-dimensional numerical model allowed engineers to eliminate the need for a costly comprehensive physical model at the final design level. The successful application of CFD analysis in the studies is a major step towards increasing the industry's confidence in the use of CFD techniques to assist in all types of hydraulic design whether for waterpower, flood control, irrigation, navigation or water supply [4], [25].

Nowadays, with the use of high-performance computers and more efficient computational fluid dynamics (CFD) software, it is feasible to investigate the hydraulic performance of full-scale spillways. It should be noted that this technology has been well established in the aerospace, automotive and maritime industries worldwide [9].

1.2 STATEMENT OF THE PROBLEM

Very often the equations for fluid flow are so complicated that they can be solved only by help of computers. Moreover, the equations usually contain empirical parts mainly associated with turbulence. From the physical point of view, the turbulence is not yet fully understood.

In recent years, mathematical models are used extensively to aid in the design of hydraulic structures. However, most of the complicated hydraulic structures cannot be modelled and analysed comprehensively by mathematical models alone using common 1 or 2-dimensional hydraulic software's such as HEC RAS. Even if these structures can be modelled by the software, the accuracies of the results may not

satisfy the requirements for local detailed design, particularly for large scale projects, due to: -

(i) The numerical assumptions and approximations necessary to construct the model;

(ii) Ignored or approximated hydraulic phenomena because the model has been set up to reproduce primarily flow routing only; and one dimensional.

(iii) Uncertainties in the user defined flow parameters.

In 1D or 2D no accuracy in: -

- areas of rapid acceleration or deceleration, where the assumption of a hydrostatic pressure distribution is no longer valid,
- areas of large turbulence and/or energy loss, and large change in cross-section
- supercritical flow, for which both discharge and water level are controlled by the upstream boundary.
- viscosity calculations particularly vulnerable to ‘water column’ effects when the vertical length scale approaches or exceeds the horizontal scale.

Flow in the complex structures requires 3D model to analyse the flow properties. Currently with development of high performing computer, it is possible to solve second order and none linear equations that describes the 3D nature of flow. FLOW-3D is a commercially available numerical model which has vast application. Results of numerical study must be carefully validated against physical experiments to establish their practical usefulness.

The bend at the end of the spillway channel for Zarema May Day Dam Spillway represents the key element of the spillway design. The bend permits to connect the spillway channel with the stepped chute, guiding the flow through a curve of nearly 65 degrees. Difficulty in the design arises because of the complexity of the flow around a curved path, which is not readily subject to analytical solutions. The challenging issue in the design of the channel bend is to reduce the superelevation, cross-waves disturbance pattern and provide a rather uniform transversal distribution of the flow at the entrance of the stepped chute.

The problem of using stepped spillway is the unknown of complex flow on each step. Even the flow through stepped spillway can dissipate a lot of energy and can decrease the cavitation problem, there is still no clarity of its processes.

Spillway is among the most important structures of a dam project that ensure the safety of the project. In addition, it has significant amount of cost for the project. Most of the recently designed and constructed spillways or complex hydraulic structures are not verified with either physical model or 3D hydrodynamic numerical models. Such gap made serious problem like Tendaho Dam Spillway. Meanwhile, in Ethiopia there are many dam projects which are planned to be constructed in the future. However, there is no standard for the design methodology to be followed for verification of complex hydraulic structures before construction.

1.3 OBJECTIVE OF THE STUDY

The main objective is to enhance the design of hydraulically safe structure for complex section using the state- of- art- of 3D hydrodynamic modelling. This helps to design hydraulically safe structure for complex section as a case study of Tendaho Dam Spillway and Ribb Dam Spillway found in Ethiopia which has been done in Chapter 5 and Chapter 6.

Accordingly, the purpose of this research is to test if FLOW-3D hydraulic model perform safe spillway/ hydraulic structures flow conditions by comparing its performance with physical model constructed Zarema May Day Dam Spillway physical model result which has been done in Chapter 4. In addition to propose methodology for design hydraulically safe structure for complex section.

1.4 SIGNIFICANCE OF THE STUDY

The problem of using complex structure like bends, stepped spillway, etc. is unknown of complex flow on each structure. Even the flow through stepped spillway can dissipate a lot of energy and can decrease the cavitation problem, there is still no clarity of its processes. The physical model cannot describe these processes clearly and completely. Therefore, if the numerical model can describe flow pattern and flow characteristics correctly, it would be the advantage for the design of complex structures. Furthermore, it can be conducted with full scale model, which will minimize problems arises due to scale reduction.

Flows in curved and complex channels and in structures usually exhibit complex three-dimensional features by the presence of superelevation, turbulence and vortex. Realistically simulating these complex flow phenomena must rely on 3-D models rather than 1-D or 2-D models [2].

3D numerical modelling is therefore useful for identifying unusual hydraulic performance and obtaining design data and information for complicated structures like vortex-intake structure, pumping stations, cascades, portal structures and large-size channels with abrupt bends etc., where three-dimensional (3D) flows dominate.

1.5 SCOPES AND LIMITATIONS

The numerical model is done for open channel flow with ungated ogee spillway. This study is limited with one case study. Although it is limited with one case study, this project is a representative for other water resource structures and, the output of the present study can imply how to improve the design of any hydraulic structures. Optimal shape of hydraulic structure causes increasing the performance of hydraulic structures and numerical simulation helps designers to propose the required size for hydraulics structures. Hence, 3D hydrodynamic modelling helps the designers to improve the hydraulic performance of existing or new hydraulic structures.

1.6 ORGANIZATION OF THE THESIS

The followings are the structure of this thesis.

Dissertation

Chapter 1 presents introduction including background, problems, objectives, significance and limitations.

Chapter 2 presents the review of 3D numerical model conducted using FLOW-3D hydrodynamic model in an open channel hydraulic structure.

Chapter 3 presents the description of 1D and 3D numerical model and describes about model setup of FLOW-3D based on Zarema May Day Dam Spillway.

Chapter 4 presents performance assessment of numerical 3D hydraulic model using physical model. For a case study of Zarema May Day Dam Spillway, the numerical model was done with full scale model at the design flow rate of 680 m^3/s. The results have been verified against physical scale model result and standard design results.

Chapter 5 presents 3D hydrodynamic modelling enhances the design of Tendaho Dam Spillway, Ethiopia. The numerical model was done with full scale model at the design flow rate of 1,700 m^3/s. In addition, for full PMF 2,194 m^3/s to check the safety of the dam from being overtopped if for some reason, one of the control gates is faulty.

Chapter 6 presents to check the design of Ribb Dam side channel spillway using FLOW-3D numerical model. The performance of the U-shaped side channel has been checked using FLOW-3D hydrodynamic numerical model and found that it is uneconomical design. In addition, the stilling

basin wall height is required to be raised by 7 m otherwise the dam is not safe.

Chapter 7 presents conclusion and recommendation of the Thesis.

CHAPTER TWO

2 LITERATURE REVIEW

2.1 GENERAL

FLOW-3D is a powerful CFD commercial code, developed by Flowscience, Inc., capable of solving a wide range of fluid flow problems. FLOW-3D uses the finite volume method to solve the Navier-Stokes system of equations in three dimensions to simulate the flow of fluid. Two-fluid and one-fluid solvers are available, both of which use a proprietary volume-of-fluid (VOF) method to track the free surface. The VOF technique was developed mathematically by the founder of Flow Science and was described by Nichols and Hirt [26].

Deniz Velioglu et al. studied on a Numerical and Experimental Study on the Characteristics of Hydraulic Jumps on Rough Beds. Roughness elements are used to stabilize a hydraulic jump, to shorten the length of a stilling basin and to increase the energy dissipation on a channel bed. Baffle blocks and sills are the most common energy dissipation devices used on stilling basins. However, this study recommends strip rectangular bars as roughness elements. In this study, an attempt is made to investigate the effects of strip roughness elements on the characteristics of hydraulic jumps both experimentally and numerically. For numerical modelling, Flow 3D code, which is rather satisfactory for free surface flow equations, was used. Comparison of

the experimental data with Flow 3D results proved that the code indeed gives reliable results. The data obtained from experiments are used to determine the change in the conjugate depth ratio, jump length and energy dissipation occurring due to the introduction of strip roughness elements to the stilling basin. In short, this study is expected to contribute to the available knowledge concerning the effects of rectangular prismatic roughness elements on the main characteristics of the hydraulic jump and to support the findings of the previous investigations [27].

When a hydraulic jump takes place on a rough bed, the concept of bed shear stress comes into picture. It is possible to neglect the boundary channel resistance on smooth channels because it is rather small compared to the other forces. However, if the channel bed is rough, the effect of the boundary resistance should be included in the momentum equation. To include this effect, a coefficient, β, is introduced to the momentum equation to modify the classical hydraulic jump relation for rough beds. In the first phase of the analyses, reliability of Flow 3D code is assessed. The experiments are also carried out on a smooth bed. Therefore, a separate model without roughness elements is prepared for Flow 3D simulations. The cell size used in the model was 0.5 cm. In order to test the soundness of the experimental and numerical data, the conjugate depth of each y1 on smooth bed is compared with the ones obtained equation. The deviation of experimental and numerical results from the analytical solution is also computed. It is seen that % error for both experimental and numerical results are in acceptable limits. For lower mesh resolutions, it is possible to obtain better results with the numerical model [27].

Another channel bed with strip roughness elements is modelled in Flow 3D to assess the capability of the code when roughness elements are present on a stilling basin. The mesh resolution of this model is taken as 0.3 in order to reach more accurate results around the roughness elements. The deviation between experimental and numerical results on smooth and rough beds is tolerable; therefore, Flow 3D is accepted as a satisfactory code to model hydraulic jumps even in the presence of roughness elements. However, as per the researcher, while calculating coefficients related to hydraulic jump characteristics, experimental values are preferred in the rest of the study to reflect the real-life data as much as possible. Therefore, this study suggests that rectangular strip bars are used as an alternative method to stabilize the location of a hydraulic jump and shorten the length of a stilling basin. Experimental and numerical investigations both show that when strip rectangular bars are introduced to the channel bed, they have a positive effect on the characteristics of a hydraulic jump. The tail water depth reduction compared to classical jump was 18-20%. The length of the jump was reduced about by 20-25%. This type of roughness elements induces 2-3% more energy dissipation than that of a classical jump. Hence, strip bed roughness elements may be considered as an alternative for baffle blocks and sills. The reliability of a CFD model, Flow 3D, is also tested and it is seen that Flow 3D gives satisfactory results regarding free surface flows and turbulence models. However, the test was only conducted in one type of arrangement and uniform roughness height [27].

Jose Carlos and etl. studied for hydraulic jump in stilling basin using physical model of the Porto Colombia Power Plant basin and a computational fluid dynamics (CFD)

model. These studies had two goals. The first goal was to determine if the additional tools of CFD augment the physical basin investigation, such as plots of flow fields, will improve understanding of the transient nature and optimize the recommended modifications. To simulate the highly transient and turbulent flow conditions in the stilling basin, a free-surface CFD numerical model has been applied using Flow 3D. The characteristics of the turbulence, it was also checked. Validating the numerical performance was done from a physical model at scale of 1:100. The model represents 1000 $m^{3/}s$, 4000 m^3/s and 8000 m^3/s [28].

The main objective was to determine the characteristics of the turbulent flow in stilling basins using physical model and numerical model and then compare the two models results. In addition, the behaviour of the flow inside of a stilling basin is described, aiming the surface profile, estimating velocities and of the instantaneous and mean pressures at specified points of the flow, and the hydraulic efficiency, using the Flow 3D modelling techniques [28].

The behaviour of the turbulent flow inside the stilling basin was well represented by the numerical model. The model reproduced the recirculation due to the formation of the roller associated to the hydraulic jump. The model comparison for the average pressure has general agreement, however difference also exist. The limitation of the numerical model was that it was considered two-dimensional model on the other hand flow in the stilling basin was three-dimensional flow is dominant [28].

The ogee-crested spillway has been one of the most studied hydraulic structures. Its ability to pass flows efficiently and safely, when properly designed, with relatively good flow measuring capabilities, has enabled engineers to use it in a wide variety of situations. Although much is understood about the general ogee shape and its flow characteristics, it is also understood that a deviation from the standard design parameters such as a change in upstream flow conditions, slightly modified crest shape, or construction variances can change the flow properties. These small changes often require engineers to evaluate the crest and determine whether or not the change or deviation will be detrimental to the spillway's performance. Such is the case when an updated probable maximum flood calculation requires a spillway to pass a larger flow than it was designed to handle [29].

Therefore, a study by Bruce et al. was completed to compare flow parameters over a standard ogee-crested spillway using a physical model, numerical model, and existing literature. The physical model was constructed of Plexiglas and placed in a test flume. Pressure taps were installed along the entire length of the spillway. Discharge and pressure data were recorded for 10 different flow conditions. FLOW-3D program was used to model the physical model setup. Data interpolated from U.S. Bureau of Reclamation and U.S. Army Corps of Engineers design nomographs provided discharge and pressure data from the literature. None dimensional discharge curves are used to compare the results from the different methods. Pressures are compared at low, mid, and high flow conditions [29].

This study, in conjunction with the many previous studies, shows that, for uncontrolled flow over an ogee spillway, numerical tools are sufficiently advanced to calculate discharge and pressures on the spillway. New numerical techniques provide engineers with an additional tool in the design or analysis of spillways. This tool may be very useful when re-evaluating a dam for higher flows or improved hydrologic event flood calculations. It is apparent that, within the range tested, the numerical method has an improved accuracy over the design nomographs for flow rates and pressures [29].

Neda Sharif and Amin Rostami Ravori did the Experimental and Numerical Study of the Effect of Flow Separation on Dissipating Energy in compound Bucket. In this research by making three different buckets, separation effect has been analysed. First model was a bucket with lip angle of 40 degrees and the two others were compound bucket which have two equally division in bucket width with different lip angle in each part; one of them has 20, 40 degrees angle and another one has 40, 80 degrees. The major amount of energy dissipation occurs in the region where the jet plunges into the tail water. So, the hydraulic jump sequent depth is used to evaluate energy dissipation at downstream. Experimental results showed that the compound bucket with less lip angle is more efficient. Also, this paper discusses two and three-dimensional numerical modelling of bucket configurations using the CFD software FLOW-3D and compares the fluid depth curves and Energy loss to corresponding physical model experimental values. The numerical model results were generally in agreement with physical model data [30].

Yuehua Wang and et al studied on the safety of shipping, flood discharging and energy dissipation which is important issue in hydraulic engineering, especially in cases of low water head. Low head sluice is widely used in shipping improvement, flood control and ecological environment protection, which has the characteristics of low-head, large unit discharge and low energy dissipation [31].

In their study, the original stilling basin is only one stilling basin where the energy cannot be dissipated as per the requirement. The proposed second type of stilling basin contains two end sills where one end sill after the other with different levels. For both types of stilling basins, they conducted test with physical and numerical models. FLOW-3D numerical model was used to study the characteristics of the hydraulic jumps in the study [31].

Based on the original design, the flow pattern agrees very well with that measured from the physical model. At the end of the stilling basin, the velocity of water flow is large and water depth is none uniform along transect and the energy was not dissipated as per the required [31].

As per the proposed design, the submerged hydraulic jump in stilling basin agrees well with the measured. Hydraulic jump is occurred in the first stilling basin completely. Then the flow enters slope section of the second stilling basin through first stilling basin section, submerged hydraulic jump is also forced successfully. After stilling basin, the flow evenly spread. Water depth is uniform along transect and there is no obvious phenomenon of shock wave. The computed maximum vertical mean velocity

at the end of anti-scour trench is lower than that of the original design. It is said that the energy dissipation effect is improved. It is said that two stilling basins can effectively reduce the water flow velocity at the downstream river and make velocity distribution more uniform [31].

The calculated results, such as discharge capacity, flow pattern, velocity, and water surface profile are in good agreement with those obtained by experiments. It indicates that the turbulence models are valid. The energy loss ratio is calculated, and results showed that two stilling basins can increase the energy dissipation. Besides, the turbulent kinetic energy distribution is also simulated by using turbulence mode, and simulated results agree better with the practical situation of the water flow movement [31].

Ho, Boyes, Donohoo, and Cooper (2003) made comparisons of crest pressures and discharges over a standard ogee spillway from 2D and 3D simulations in FLOW-3D to USACE data and empirical discharge equations. Their study found that simulated 2D and 3D crest pressures followed the general trend of data published by USACE, however, in both cases the CFD results predicted slightly larger negative pressures. It was also found that the 2D simulation over-predicted the flow-rates by about 10 to 20 percent depending on the headwater elevation. The 3D CFD simulation results were much better, within 5 percent of the empirical calculations for the three headwater levels considered [32].

A study completed by Savage and Johnson used a FLOW-3D model to compute discharge and crest pressures over an uncontrolled USACE and USBR standard ogee-crested spillway. Results from the CFD modelling were subsequently compared to results from a physical model study as well as existing USACE and USBR data. It was found that the FLOW-3D discharges were in between the physical model study and the USACE and USBR data for heads ranging from about 0.1 to 0.7 times the design head higher than this, up to 1.2 times Hd, the FLOW-3D results slightly over predicted discharge when compared to all three other sources, however, remained within 1% of the physical model results in that range. A good agreement between the FLOW-3D results, the physical model study, and USACE data was also obtained for crest pressures with various headwater conditions including 0.51Hd, 0.82Hd, and 1.20Hd [33].

CFD modelling has been shown in the applications summarized herein to be an effective modelling tool for spillway design applications. This assessment was however limited to consideration of static conditions. Comparisons with scale modelling data show that excellent results can be produced, especially in areas where the velocity is relatively low, for example the spillway approach and crest region. For studies of these regions, CFD models using relatively coarse grids can produce accurate results very rapidly and allow for design alternatives and multiple upstream water levels or discharges to be evaluated and optimized rapidly [33].

It is critical to note that further work is required to improve CFD modelling techniques in relation to transient pressures, turbulence, and cavitation, effects of air, two-phase

flows, structure vibration and pressure pulsations in hydraulic jumps and on structure boundaries. Complementary use of CFD and scale models allows for a degree of cross checking between the two sets of model results, allows for innovation and refinement of designs, provides greater confidence in the final design and will inevitably lead to improvements in both CFD modelling methodologies and scale modelling practices [33].

Saeed-reza Sabbagh-yazdi and etl. analysed a comparison of the results of 2D and 3D numerical modelling of flow over spillway chutes with vertical curvatures. In their research, a model of FLOW-3D, and a depth average version of NASIR flow solver are applied to model the free surface flow over the two small scale test cases. First, flow from horizontal to a steep slope with a circular arc transition is modelled. Second, flow over a symmetric and an asymmetric bed profile is tested. The results of present numerical investigations show that the water surface elevation computed by both FLOW-3D (which uses True-VOF technique for computation of water free surface) and a 2D depth average version of NASIR flow solver (which is developed for variable steep slope bed) match well with the measured data [34].

The computed pressures by the utilized 3D flow solver are in good agreements with the experimental measurements. However, the computed pressures at the bottom surface of chutes with vertical curvatures slightly differ from the measured pressure in some parts of the super-critical flow parts. The computed pressures along the conduit differ from the hydrostatic assumption due to curved bed and effect of centrifugal acceleration. The differences are more pronounce at the zones with considerably large

vertical curvatures, particularly for high flow rates. Therefore, it can be stated that, in the regions with large bottom curvature the pressure distribution does not follow the hydrostatic pressure profile. For the convex bottom curvature, the hydrostatic assumption for pressure is more than the actual pressure, while in concave curvature the contrary condition is observed [34].

In typical spillways over small embankment dams, the skimming, non-aerated region of the flow is of importance for their hydraulic design. A good agreement between simulated and measured results have been achieved. In the broad crested weir, the relative differences between experimental and numerical water depths were less than 8.9% (average difference of 3.8%), and the relative differences between experimental and numerical velocities were less than 10.2% (average difference of 5.4%). In the stepped spillway, the relative differences between experimental and numerical water depths were less than 13.6% (average difference of 7.4%), and the relative differences between experimental and numerical velocities were less than 20.0% (average difference of 14.3%). The validation confirms that FLOW-3D is able to simulate, in general with good accuracy, the flow rate, water depths and velocity distribution of the skimming flow in the non-aerated region of the spillway [35].

2.2 COMPARISON WITH PHYSICAL MODELLING

2.2.1 Principle of Scaling

Physical scale modelling has been used in the design and investigation of hydraulic

structures for over 100 years. The design process has typically involved the development of a preliminary design on the basis of theoretical and empirical methods. A physical scale model of this arrangement would then be constructed in two- or three-dimensions and various scenarios run to confirm whether the hydraulic performance was acceptable and to extract data for input to the design. The methods are tried and tested and the outputs from the model testing in terms of data and observations are invaluable in the design process. However, the construction, operation, and testing of physical models is often a time-consuming and expensive exercise. Furthermore, the modification of the model to trial alternative arrangements or to optimize features can add weeks to a testing programme, [8], [36].

In free-surface flows, gravity effects are predominant. Similarity in physical models is performed usually with a Froude similitude ensuring the ratio between inertia and gravity to be the same for the model and the prototype [37]. Scale effects in hydraulic models are defined as distortions introduced by effects other than the dominant model law. They occur where one or more dimensionless parameter differs between the model and the prototype. In most cases scale effects are small but not always negligible [38]. In general, for a hydraulic model with a scale ratio of 40, verification needs to be done to ensure and realize possible scale effects and their influence on the study. Examples of scale effects include scaling from model to prototype of friction, turbulence, cavitation, air entrainment and air release, fluid structure interaction and local scouring [39].

The principle of the use of scale models consists of the possibility to reproduce the

real problem (the prototype) on a smaller scale in such a way that the phenomena in the scale model are similar to the prototype.

The similarity can be divided into various aspects:

i. Geometric similarity
ii. Kinematic similarity
iii. Dynamic similarity, etc.

In a physical model, the flow conditions are said to be similar to those in the prototype (p) if the model (m) displays similarity of form (geometric similarity), similarity of motion (kinematic similarity) and similarity of forces (dynamic similarity).

I. Geometric Similarity

Geometric similarity implies that the ratios of prototype characteristic lengths to model lengths are equal [7]:

$$\alpha_L = \frac{l_p}{l_m} = \frac{d_p}{d_m} = \frac{H_p}{H_m} - - - - - - - - - - - - - - (2-1)$$

Where l = length, d = depth, H = Hight

II. Kinematic Similarity

Kinematic similarity implies that the ratios of prototype characteristic velocities to model velocities are the same [7]:

$$\alpha_V = \frac{V_p}{V_m} = \frac{(V_1)p}{(V_1)m} = \frac{(V_2)p}{(V_2)m} - - - - - - - - - - - (2-2)$$

III. Dynamic Similarity

Dynamic similarity implies that the ratios of prototype forces to model forces are equal [7]:

$$\alpha_F = \frac{F_{1p}}{F_{1m}} = \frac{F_{2p}}{F_{2m}} - - - - - - - - - - - - - (2-3)$$

The relation between the model and the prototype is found by defining for each parameter a scale (or scale factor). For complete similarity between the proto type and the model, the ratio of each variable of the model and the corresponding one for the proto type must conform to the specific principles.

It is important to achieve dynamic similarity between model and the prototype. The two most important parameters for dynamic similarity are Froude number and Reynolds number.

$$F_r = \frac{V}{\sqrt{Dg}}$$

Where Fr= Froude number, V=velocity of flow, D=flow depth, g = gravitational acceleration

The Froude Law

This is applicable when the gravitational forces are predominant in the flow condition. Similitude (proto type /model similarity) can be obtained if the ratios of gravitational forces to the inertia forces in the proto type and model are equal. Other forces may be neglected. This law implies that there must be equality of Froude number between the prototype and the model in the case where gravitational forces predominate.

Froude number can be regarded as a ratio of the inertia force of a water particle to the gravitational force acting on it. Hence, for a high Froude number, inertia dominates and gravity has little influence on the motion of the particle. Conversely, for a low Froude number, gravitational force becomes the major factor controlling water motion.

The Reynolds Law

A similar interpretation applies to the Reynolds number, which represents the ratio of the inertia force of the water particle to the viscous force acting upon it. When viscous forces predominate, the similitude is based on the equality of the ratio of the inertia force and the viscous force between the proto type and the model.

It is impossible to make the pair of Froude number and Reynolds number identical in both model and proto type if the same fluid is used. For open channel flow, equality of Froude numbers in modelling is commonly used. Otherwise, water surface elevations in the model bear no relationship to the proto type. Therefore, a model with a free water surface is almost in variably Froude-scale model while at the same time allowance is made for influence due to the non-scaled Reynolds number because Reynolds number is used to classify flow type (laminar to turbulent etc.). In open channel flow, both proto type and model are usually in the turbulent state. There is a large similarity between the use of scale models and mathematical models. The same process of modelling, solving and interpretation is required for both types of models [10].

Scale models are used if the physical phenomena can be reproduced with sufficient similarity by reducing the length dimensions of the real problem area. Mathematical or numerical models can be used if the problem can be described mathematically with sufficient details. Now a days, computers are used to solve these problems. However, not for all hydraulic problems such a large selection of possibilities is present. The computational methods may not be powerful enough to solve all problems. The accuracy of numerically predicted results relies on the initial and boundary conditions that are sometimes difficult to determine, especially for new designs and setups [10].

Physical model tests also were carried out to reproduce construction of the cofferdam needed to build the spillway during a constant flow of 3,930 m^3/s (1:2 year mean daily

discharge), [4]. The physical model test results for diversion and final rollway conditions with the gates fully open were compared to FLOW-3D simulations carried out by McGill university. The result of the CFD and physical modelling for this aspect agreed very closely. With the diversion sluiceway fully open, the difference in results was 0.85 percent or less. With the final rollways fully open, the difference in results was 5.25 percent or less [4].

On major design projects, it is recommended that both modelling techniques be integrated during design to provide the optimum hydraulic engineering solution. During the early stages of design, CFD modelling is quite adequate for purposes of feasibility and pre-engineering design. Before advancing to final design, the element of risk should be evaluated to determine whether confirmatory physical modelling would add value engineering to the final design [4].

2.2.2 Weir Experiment

The weir experiment consisted of a 3.2 m long, 0.25 m wide flat channel with a streamlined weir located approximately 1m from the upstream end Figure 2- 1 the crest of the weir is ‘broad’ enough for the streamlines to become parallel to the weir crest, the pressure distribution will be approximately hydrostatic and the flow on the weir can be considered as gradually varied flow. If the upstream head is large compared to the crest length, the flow across the weir will be rapidly varied. Both conditions were examined on the physical model and compared with numerical model predictions. The objective of this comparison was to examine the capability of the

software in the gradually and rapidly varying flow conditions that occurred along the weir. The model results are presented in Figure 2- 2 and discussed below [40].

HEC RAS: The backwater equation is not valid for rapidly varied flow. Nevertheless, HEC RAS identifies that the weir acts as a hydraulic control and predicts that a transition from subcritical to supercritical flow occurs on the weir. For the low-flow case, HEC RAS achieves a good match of the flow across the weir, with only minor differences occurring in the rapidly varying flow at the upstream and downstream end. Significant differences are observed across the weir for the high-flow case, where the entire weir is rapidly varied flow. The profiles upstream and downstream of the weir are nevertheless predicted with good accuracy [40].

MIKE 11: Because of its numerical limitations, MIKE 11 cannot model the supercritical flow downstream of the weir. For the low-flow case, the downstream water level is over estimated by a factor of 8. This high tailwater impacts on the flow conditions on the weir, causing a significant error in the upstream water level. The incorrect tailwater has less impact for the high-flow case. There is still significant error in the predictions across the weir, but the upstream water level is almost correct [40].

MIKE 21: The numerical algorithms used by MIKE 21 allow it to achieve a good match of the flow across the weir. Some differences are observed at the ends of the weir crest, particularly for the low-flow case. This is believed to be partly numerical limitation and partly due to the difficulty of representing a smooth transition with a fixed space grid (i.e. a physical limitation) [40].

FLOW-3D: With the ability to model vertical velocity components, flow acceleration and none hydrostatic pressure, FLOW-3D achieves an excellent match of the physical model data [40], [34]

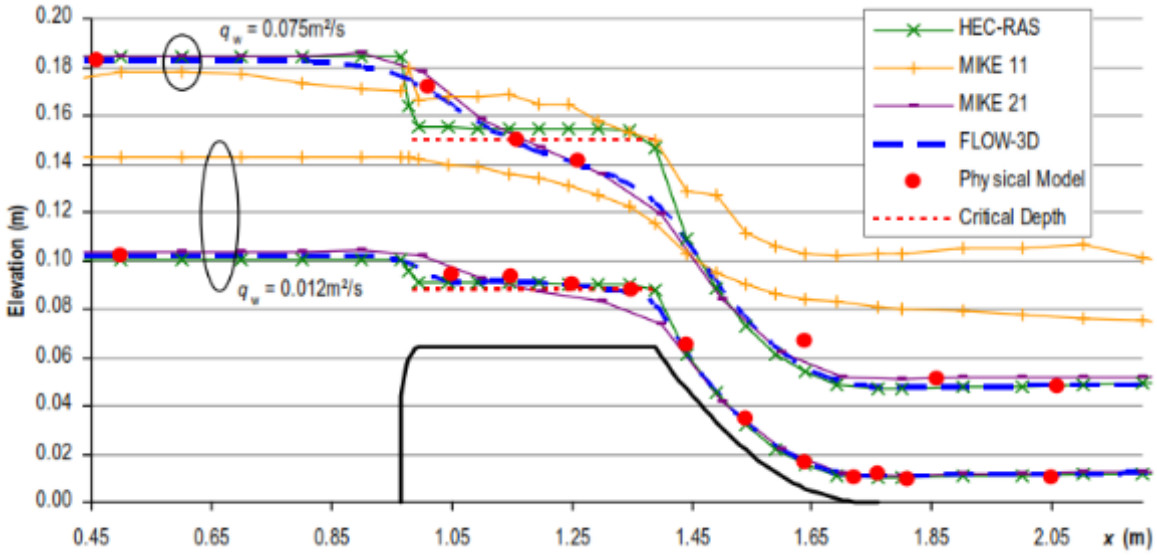

Figure 2- 1 Weir Water Level Predictions of the Physical and Numerical Models [40].

2.2.3 Open Channel Flow Experiment

The Open Channel Flow experiment apparatus was a 12 m long, 0.5m wide rectangular flume set with a slope of 1.6º. Upstream and downstream water levels were controlled by a rounded gate, while constant inflow was provided by an upstream reservoir supplied from a constant-head tank. Key objectives of the physical model were to demonstrate: (a) the basic principles of open channel flow and the backwater equation, (b) the control mechanisms (i.e. subcritical from downstream and supercritical from upstream), and (c) the transition from supercritical to subcritical flow

in the form of a hydraulic jump. Physical and numerical model results are shown in Figure 2- 2 and discussed below [40].

HEC RAS: The HEC RAS (steady-state) model prediction shows good agreement with the physical model measurements. The steady-state solution of the Backwater Equation in HEC RAS can model both subcritical and supercritical flow. HEC RAS also identifies the occurrence of a hydraulic jump transition and predicts its location with reasonable accuracy. The jump is modelled as an instantaneous transition between cross-sections, and there is no attempt to describe the length or strength of the jump [40].

MIKE 11: The solutions of the Saint Venant equation in both MIKE 11 and the unsteady solver of HEC RAS are incapable of modelling supercritical flow. Although able to match the subcritical flow measurements, significant disparity is observed in both the supercritical flow region and hydraulic jump. While at first glance the result may appear conservative (i.e. predicted water levels higher than measured), this cannot be guaranteed in all circumstances. Additionally, when water levels are over-predicted, velocities will be under-predicted, which could have potentially catastrophic consequences [40].

MIKE 21: Based on the Saint Venant equation, the solution within MIKE 21 demonstrates the ability to model both subcritical and supercritical flow with good accuracy (although a supercritical upstream boundary cannot be modelled, and defaults to critical depth). The hydraulic jump is also modelled with reasonable

accuracy. The model lacks the capability to model the complex flow patterns within the hydraulic jump, and predictions in this region should be treated with caution [40].

FLOW-3D: Considering the technological superiority of the FLOW-3D modelling package, it is just as well that the model prediction displays excellent agreement with the physical model. The software can also model additional flow properties such as turbulence intensity and air entrainment [40].

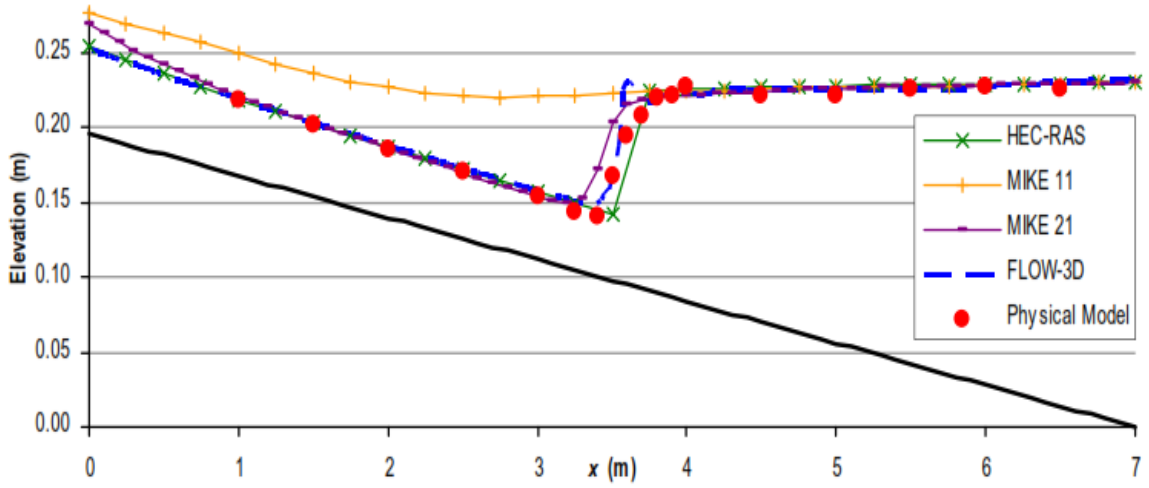

Figure 2- 2 Open channel flow water level predictions of the physical and numerical modes [40].

Verification of Model [10]

Manitoba Hydro and Acres International Ltd., both of Winnipeg, Manitoba, Canada, have undertaken an extensive 3-dimensional modelling program as a part of pre-commitment level studies for three proposed hydropower projects in Northern Manitoba. These three projects are the Gull Generating Station (680 MW) on the

Nelson River, near Gillam, Manitoba, and the Notigi (100 MW) and Wuskwatim (200 MW) Generating Stations, both on the Burntwood River, near Thompson, Manitoba. A sophisticated computer model, FLOW-3D, was carefully reviewed and tested prior to ensure its use as a design tool would be appropriate. Following this confirmation, the 3-dimensional model was used to evaluate a number of complex hydraulic design issues associated with these three plants [10].

In order to ensure the utmost quality in the hydraulic design of the structures, a state-of-the-art FLOW-3D numerical model was selected and used to test and refine design concepts. Normally, physical model studies would have been the only means available to provide additional insight into the complex flow conditions resulting from the interaction of hydraulic structures with flowing water, but such costly studies would not typically be undertaken until the final design phase of the project. By using advanced numerical modelling techniques, the design engineers were able to identify and address critical design issues early in the design phase and optimize the overall hydraulic design [10].

These projects included the successful modelling of [10]:

- Two- and three-dimensional dam break studies
- Hydroelectric Intake and Spillway design
- Channel Improvement studies on a large northern river
- Replication of past physical model studies to verify model performance
- Fish way design
- Trash boom design
- Dilution studies of a contaminated lake

- Confirmation of existing Spillway capacity
- Prediction of Intake head loss.

But perhaps what most impressed the design team over this period of time was the ability of the model to replicate the results of past physical model studies and observed field measurements, with very good success. Three such example applications are described below [10].

Simulation of Conawapa Diversion Port [10]

Physical model study tests were previously carried out to refine estimates of discharge through the 8-m high diversion ports of the proposed 1390 MW Conawapa Generating Station on the Nelson River. Flow conditions through the ports are highly three dimensional in nature. To establish confidence in the FLOW-3D model's ability to predict discharge capacity through a diversion port structure, the model was configured to replicate the Conawapa physical model study [10].

The physical dimensions of the diversion port simulated with the FLOW-3D model were based on the prototype dimensions used to configure the actual physical model. Fluid properties in the numerical model (viscosity, density, etc) were set to standard properties for water at a temperature of 20 degrees Celsius. Two test cases were then simulated representing operation of the fully open port at head pond elevations covering the anticipated operating range during diversion. A comparison of the FLOW-3D results, confirmed the FLOW-3D model's accuracy in matching the physical model test results [10].

Simulation of Conawapa Stage II Diversion [10]

A second simulation was undertaken which tested the model's ability to replicate complicated flow patterns. For this case a simulation developed for a diversion scheme proposed to be used during the construction of the Conawapa hydropower project. Flow was being diverted through the partially completed powerhouse and the completed spillway structure. The partially removed Stage I cofferdam created a significant barrier to flow, particularly as it approached the north bank powerhouse location. FLOW-3D model closely reproduced both the flow patterns and the magnitudes of flow velocity observed in the physical model [10].

Simulation of Kelsey Generating Station [10]

The quality of flow approaching a powerhouse and the resulting intake velocity distribution will have an impact on the turbine performance characteristics of a hydroelectric plant. Asymmetrical flow conditions resulting from an upstream flow obstruction, or a curved approach channel can reduce a plant's generating capacity significantly. This was the case at Manitoba Hydro's 223 MW Kelsey hydroelectric plant located in northern Manitoba [10].

Based on gathered observations, it was known that this hydraulic problem is highly three-dimensional in nature, and would not be adequately addressed using 1-D or even 2-D numerical models. To compound the complexity of the problem, flow conditions are affected not only by the approach channel geometry, but also by the accumulation of debris and trash at the two units. These conditions result in the

formation of a large eddy and vortex formation results in the loss of hydraulic efficiency [10].

The FLOW-3D model was setup to simulate the Kelsey Generating Station approach channel and intakes. FLOW-3D was able to simulate the eddy, and its approximate location under typical operating conditions. Head losses resulting from the asymmetric approach channel configuration were found by the model. Although slightly low, these simulated losses agreed well with observed losses [10].

Sample Design Applications [10]

After gaining confidence in the numerical model's capabilities, the model was used to assist in the pre-commitment level design studies for the proposed Wuskwatim Generating Station. The model was setup and used to provide guidance on a number of technical design issues, including but not limited to [10]:

- Spillway design, including confirmation of spillway discharge estimates
- Simulation of three-dimensional flow patterns in the project's forebay and tailrace area
- Refinement of cofferdam layouts
- Refinement of powerhouse intake design
- Channel design
- Refinement of river management strategies, including river closure.

A number of representative examples have been done. Few of them are as follow.

Intake Design Comparison [10]

The proposed Wuskwatim powerhouse is equipped with three units, and has a maximum plant capacity of 1100 m^3/s. As a part of the powerhouse design, the FLOW-3D model was used to evaluate the overall hydraulic performance of a number of powerhouse intake configurations [10].

The use of a three-dimensional numerical model allowed design engineers to quickly visualize resultant flow fields, and evaluate alternative designs early in the design process. Based on the simulation results, it was concluded that each of the tested alternatives produced a relatively streamlined flow field, minimizing the potential for formation of air entraining vortices. Each alternative was also tested to ensure that cross flow velocities within the intake were minimized, and that there was an equal distribution of flow between all three units. The primary difference between alternatives was in the vertical distribution of flow at the Intake entrance. Of the designs tested, the alternative exhibited the most even distribution of velocity, resulting in the lowest estimated trash rack losses at the entrance to the Intake [10].

3-D Spillway Model [10]

Three-dimensional numerical simulations were also undertaken to assist in the hydraulic design of the Wuskwatim spillway structure. The proposed spillway for this project is comprised of three gated sluiceways, each nine meters wide, separated by intermediate piers. The spillway is designed to handle the Probable Maximum Flood

(PMF) of 2650 m^3/s at a design head of 15.8 m. The approach channel to the spillway consists of a relatively deep channel excavated into rock. In order to maximize spillway efficiency, designers aligned the approach channel sidewalls to coincide closely with the spillway entrance wall that a feature was expected to reduce abutment contraction losses for the structure [10].

A three-dimensional numerical model was setup and utilized to confirm the anticipated hydraulic performance of the proposed arrangement. The results indicated lateral contraction effects, and therefore abutment losses, would be substantially decreased for the proposed design, and as a result an approximate 5% increase in spillway capacity at the design head was realized. This in turn allowed designers to raise the spillway invert, thereby reducing overall construction costs [10].

The model was also utilized to assess the need for downstream stoplogs and guides for the spillway structure. The spillway discharges into a relatively steep channel, and as a result it was anticipated that little would be required to protect against tailwater effects in the event that one of the bays were to be closed for maintenance, while other bays continued to operate. To test this assumption, a three-dimensional model was setup of the spillway in which a single bay was assumed to be closed, while the other two bays operated with the gates fully raised. The result of the simulation shows, the momentum of the water being discharged from the operating bays prevents water from entering the “dry” bay from downstream. Accordingly, downstream stoplog requirements for the structure were reduced, again lowering overall anticipated construction costs [10].

Finally, CFD analysis has been successfully utilized to provide considerable design support for advanced hydropower design. The use of this tool has allowed engineers at Manitoba Hydro and Acres Manitoba Ltd. to provide early input to critical design issues, and to refine hydraulic design to a level normally achieved only through the undertaking of physical model studies. The CFD model can also be used to provide insight into any planned physical models, allowing designers to streamline the testing program by reducing the number of options to be evaluated. In the case of the Wuskwatim project, the confidence gained through the use of the three-dimensional numerical model allowed engineers to eliminate the need for a costly comprehensive physical model at the final design level [4].

The successful application of CFD analysis in these studies is a major step towards increasing the industry's confidence in the use of CFD techniques to assist in all types of hydraulic design whether for waterpower, flood control, irrigation, navigation or water supply [4].

The spillway of the Cabinet Gorge Dam produces high concentrations of dissolved gas in the downstream river. Avista is therefore looking to reconstruct the original river bypass tunnels to reduce the use of the spillway when the hydraulic capacity of the powerhouse is exceeded. The bypass tunnel design is intended to reduce downstream dissolved gas concentration by avoiding use of the spillway and air entrainment in the tunnel discharge [41].

Avista chose to use physical and numerical modelling efforts to address the risks and issues associated with this highly complex project. 1:50 scale physical model was constructed to define the hydraulic performance of an initial tunnel design concept, support design development of the tunnels, and to confirm the hydraulic performance of the final concept. FLOW-3D, was used to evaluate design alternatives prior to testing final concepts in the physical model [41].

The location and magnitude of low pressures in the intake are of particular importance to avoid cavitation and to verify the actual discharge capacity of the tunnel. The CFD model was used to identify low pressure areas in the intake. Piezometric taps were installed in the physical model at the corresponding locations and connected to calibrated pressure transducers [41].

Various runs were undertaken with both the physical and numerical models. Although the models were used in complementary roles, their results were compared to determine how well they matched in terms of pressure distribution and magnitude. The models showed a good match in predicted pressure patterns, and their identification of the minimum pressure location within the intake. Both models show that lowest pressure will likely occur in the upper corners of the intake section, where flow accelerations and velocities are largest [41].

The models also showed a good match in predicting the magnitude of average pressures within the tunnel entrance. Match shown for all tunnel discharges is

reasonable, providing confidence in the numerical model's ability to replicate real world processes [41].

Overall, the match in average pressure predicted with the two models was very good, and it was of value to have input from both models in planning and executing these design studies [41].

Application of Numerical Modelling to Spillways in Australia

Revision to design flood estimates of a number of Australian dams have required their spillways to be upgraded to cope with increased discharge rates. In coping with the increased discharges, the existing spillways may face potential problems such as the generation of excessive negative pressure over the spillway crest, erosion of unprotected cut banks, overtopping of chute walls, and flow impact on crest bridges and gates. Furthermore, the discharge coefficient and rating curve usually need to be re-evaluated for greater operating heads. Their hydraulic performance was investigated by numerical modelling instead of using scaled physical model. For most projects, where possible, a rigorous validation exercise using published or physical test results was performed to ensure its correctness and reliability before embarking on further parametric study [9].

Traditionally, scaled physical hydraulic models have been constructed in laboratories to study these behaviours. However, these models can be expensive, time

consuming and there are many difficulties associated with scaling effects. Most models built are only kept for a limited time [9].

Nowadays, with the use of high-performance computers and more efficient computational fluid dynamics (CFD) software, it is feasible to investigate the hydraulic performance of full-scale spillways. It should be noted that this technology has been well established in the aerospace, automotive and maritime industries worldwide [9].

The application of this numerical modelling technique has benefited a number of dam upgrade projects in Australia. As this type of spillway analysis technique was used for the first time in this country, the need to carryout validation was essential. A rigorous staged validation process was conducted for the Warragarnba Dam drum gate upgrade project. In all the subsequent spillway upgrade projects, comparisons were made between computed and measured values, using the results of physical modelling carried out during the original design of the dam, where available, to raise the confidence level of the analysis technique [9].

Use of numerical modelling has led to the development of innovative devices to mitigate the impact of flows on gate structures and concept designs to reduce excessive negative pressure over a spillway crest. Significant cost savings were achieved for these upgrade projects [9].

The validation process was carried out in a multi-staged approach. The validation of the standard ogee spillway profile using the US Army Corp of Engineers Waterways

Experimental Station (USACE-WES, 1952) design guides was carried out both two- and three-dimensionally to determine the suitability of the code. The influence of the piers was correctly captured by the 3D analysis. Then the actual spillway geometry in question was analysed and the results compared with those obtained by physical testing. A reasonable agreement was achieved for practical purposes [9].

Typically, the discharge rate, pressure distribution and flow surface profile were used for comparison purposes. In some cases, velocity profiles were also available for comparison. In general, the flow rate computed by the numerical model can be up to 5% greater than physical model results for head levels equal to and greater than the design head of the spillway. Typically, the overestimation is around 3% [9].

It is inevitable that information technology will continue to improve in the future. Fast computers and CFD codes will become more accessible to engineers. The role of physical modelling will need to be reappraised. Although physical models will still provide valuable information, it is anticipated that numerical models may be routinely used during the initial phase of design or feasibility study. When the preferred solution is selected, the physical model may serve to confirm design expectation. This computer aided rapid prototyping approach is already a common practice in the automotive and aerospace industries [9].

The use of numerical modelling of eight spillway upgrade projects in Australia demonstrated that it is a viable technology. The benefits gained from these experiences have been highlighted. It must be emphasized that this technology must

be treated like any other numerical design tool or design calculation it is not a substitute for competent engineering experience and sound judgment. The various analysis capabilities allowing better understanding of the flow behaviour taken from eight spillway upgrade projects. With prudent engineering guidance, it is anticipated this emerging technology may become a standard design tool for analysing spillway flow in the future [9].

CHAPTER THREE

3 NUMERICAL MODEL USING HEC RAS 1D AND FLOW-3D

3.1 GENERAL

There are different types of Numerical models called ‘Computational Fluid Dynamic’ (CFD) programs, available for one, two and three-dimensional analysis with varying degree of sophistication and reliability. Some of them are: - HEC RAS 1D, HEC RAS 2D, ANSYS-CFX 3D, FLOW-3D, CCHE2D, PHOENICS, STAR-CD, FLUENT, TELEMAC, MIKE21, DELFT-3D, TABS and SSIIM.

3.2 HEC RAS

HEC RAS is a software developed by the US Army Corps of Engineers and stands for Hydrologic Engineering Centres River Analysis System. The present version of HEC RAS system contains four one-dimensional river analysis components for: (1) steady flow water surface profile computations; (2) unsteady flow simulation (one-dimensional and two- dimensional hydrodynamics); (3) movable boundary sediment transport computations; and (4) water quality analysis. A key element is that all four components use a common geometric data representation and common geometric and hydraulic computation routines. In addition to the four river analysis components, the system

contains several hydraulic design features that can be invoked once the basic water surface profiles are computed. The steady/unsteady flow components are capable of modelling sub critical, super critical, and mixed flow regime water surface profiles. The graphics include X- Y plots of the river system, schematic cross sections, profiles, rating curves, hydrographs, and many other hydraulic variables [42], [43].

The current version of HEC RAS supports steady and unsteady flow water surface profile calculations; combined 1D and 2D hydrodynamics; sediment transport/mobile bed computations; water temperature analysis; water quality and spatial mapping of many computed parameters (Depth, water surface elevation, velocity, etc.) [42].

HEC RAS 1D model is a numerical model which uses the Finite Difference Method for analysis [42]. HEC RAS 1D is used for comparison for this research since it is widely applicable for river hydraulics and its availability is free. In addition, its model set up are not complex, simulation time are very short and has different options. For further information refer Annex E.

3.2.1 HEC RAS Hydraulic Model Structure

In HEC RAS terminology, a project is a set of data files associated with a particular river system. Steady flow analysis, unsteady flow analysis, and sediment transport computations may be performed as part of the project. The data files for a project are categorize as follows: (1) plan data, (2) geometric data, (3) steady flow data, (4) unsteady flow data, (5) sediment data, and (6) hydraulic data [44].

3.3 FLOW-3D

FLOW-3D is a numerical technique to solve the equations of motion for fluids to obtain transient, three-dimensional solutions to multi-scale, multi-physics flow problems. An array of physical and numerical options allows users to apply FLOW-3D to a wide variety of fluid flow and heat transfer phenomena [22].

FLOW-3D has been broadly applicable for the past three decades and appears to be the most popular program for spillway. Several researches were conducted using FLOW-3D and it is commercially available model. Hence, for these main reasons, FLOW-3D has been chosen to be applied in this research.

FLOW-3D allows either one or two fluid flow, with or without a free surface, and a multitude of available physics options to suit the specific application. Various meshing and geometry options are available including multi-block grids and the ability to draw simple objects in the software or import different forms of more complex geometry or topographic files. A large selection of boundary conditions is also available to properly model each specific application. Another benefit of FLOW-3D is the ability to select from several different implicit and explicit numerical solver options. All these model set-up parameters can easily be specified by either encoding selections in the text editor or by making radio button selections in the graphical user interface. FLOW-3D is a pre-processor of major model setup and run performance. For post processer FLOWSIGHT application was the main part to analyse the required output [22].

FLOW-3D in Collaboration with FLOWSIGHT provides a powerful and simple method for understanding and sharing simulation results. Results can be compared by viewing both numerical and visual formats, analysing Isosurfaces from all six degrees simultaneously and linking and viewing separate cases together in the same viewport [22].

It has the following main components:

- Flow Type Options
- Flow Definition Options
- Thermal Modelling Options
- Turbulence Models
- Numerical Modelling Options
- Fluid Modelling Options
- Shallow Flow Models
- Advanced Physical Models
- Chemistry Models
- Porous Media Models
- Discrete Particle Models
- Two-Phase & Two-Component Models
- Coupling with Other Programs
- Data Processing Options
- User Conveniences
- Multi-Processor Computing
- FlowSight

3.4 BRIEF DESCRIPTION OF FLOW-3D

FLOW-3D is a powerful CFD commercial code, developed by Flowscience, Inc., capable of solving a wide range of fluid flow problems. FLOW-3D uses the finite volume method to solve the Navier-Stokes system of equations in three dimensions to simulate the flow of fluid. Two-fluid and one-fluid solvers are available, both of which use a proprietary volume-of-fluid (VOF) method to track the free surface. The VOF technique was developed mathematically by the founder of Flow Science and was described by Nichols and Hirt and more thoroughly detailed by Hirt and Nichols [45].

The model includes many optional models that add to or modify the basic Navier-Stokes equations. For further information refer Annex E. Additional models that are used frequently in hydraulics, include options for describing the effects of turbulence, surface tension, heat transfer, fluid solidification, sediment scour, Lagrangian particles, granular flows, moving solids, solid deformation, air entrainment, cavitation, and porous media [22].

The equation of motion for the fluid velocity components (u, v, w) in the three coordinate directions are the Navier-Stokes equations with some additional terms in numerical method of FLOW-3D expressed as follows.

The general mass continuity equation is:

$$V_F \frac{\partial p}{\partial t} + \frac{\partial}{\partial x}(\rho u A_x) + R\frac{\partial}{\partial y}(\rho v A_y) + \frac{\partial}{\partial z}(\rho w A_z) + \xi\frac{\rho u A_x}{x} = R_{DIF} + R_{SOR} ----(3-1)$$

[22].

Momentum Equations

$$\frac{\partial u}{\partial t}+\frac{1}{V_F}\left\{uA_x\frac{\partial u}{\partial x}+vA_yR\frac{\partial u}{\partial y}+wA_z\frac{\partial u}{\partial z}\right\}-\xi\frac{A_yv^2}{xV_F}=-\frac{1}{\rho}\frac{\partial p}{\partial x}+G_x+f_x-b_x-\frac{R_{SOR}}{\rho V_F}(u-u_w-\delta u_s)------(3-2)$$ [22].

$$\frac{\partial v}{\partial t}+\frac{1}{V_F}\left\{uA_x\frac{\partial v}{\partial x}+vA_yR\frac{\partial v}{\partial y}+wA_z\frac{\partial v}{\partial z}\right\}+\xi\frac{A_yuv}{xV_F}=-\frac{1}{\rho}\left(R\frac{\partial p}{\partial y}\right)+G_y+f_y-b_y-\frac{R_{SOR}}{\rho V_F}(v-v_w-\delta v_s)--------------------(3-3)$$ [22].

$$\frac{\partial w}{\partial t}+\frac{1}{V_F}\left\{uA_x\frac{\partial w}{\partial x}+vA_yR\frac{\partial w}{\partial y}+wA_z\frac{\partial w}{\partial z}\right\}=-\frac{1}{\rho}\frac{\partial p}{\partial z}+G_z+f_z-b_z-\frac{R_{SOR}}{\rho V_F}(w-w_w-\delta w_s)-----------(3-4)$$ [22].

In these equations:

(Gx,Gy ,Gz) are body accelerations,

(fx,fy ,fz) are viscous accelerations,

(bx,by ,bz) are flow losses in porous media or across porous baffle plates, and the final terms account for the injection of mass at a source represented by a geometry component.

The term Uw = (uw, vw, ww) is the velocity of the source component, which will generally be non-zero for a mass source at a General Moving Object (GMO).

The term Us = (us, vs, ws) is the velocity of the fluid at the surface of the source relative to the source itself.

VF = is the fractional volume open to flow

P = the fluid density

RDIF = is a turbulent diffusion term

RSOR = is a mass source

Ax = is the fractional area open to flow in the x- direction, Ay and Az are similar area fractions for flow in the y and z directions, respectively.

R = is the coefficient for the choice of coordinate system. When Cartesian coordinates are to be used, R is set to unity and ξ is set to zero.

There are two methods of simulation in FLOW-3D called Volume of Fluid (VOF) that is used to show the behaviour of fluid at the free surface and the Fractional Area Volume Obstacle Representation (FAVOR) method, a program used for surfaces modelling and rigid volumes such as geometric borders. The model is considered as incompressible flow and for a free surface, the boundary between water and air, the VOF by NICHOLS, C. W. HIRT [46] function is defined to meet the governing equation. If F(x,y,z,t) is equal to 1, the control volume will be full of fluid, and if F is equal to 0, no fluid will exist in a control volume. Furthermore, in the case of a free water surface, F is shown to have the value between 0 and 1.

The Pressure Solution Algorithm in numerical treatment of mass conservation mass equation leads to an algorithm for determining cell pressures and updating velocities. In FLOW-3D this can be done in an automated way.

The FLOW-3D distribution includes a variety of FORTRAN source subroutines that allow the user to customize FLOW-3D to meet their requirements. The FORTRAN subroutines provided allow the user to customize boundary conditions, include their

own material property correlations, specify custom fluid forces (i.e., electromagnetic forces), add physical models to FLOW-3D, and more [22].

Accordingly, the subsequent chapters are mainly following the research analysis as a general methodology shown in Figure 3- 1 for model verification and modification of hydraulic structures design.

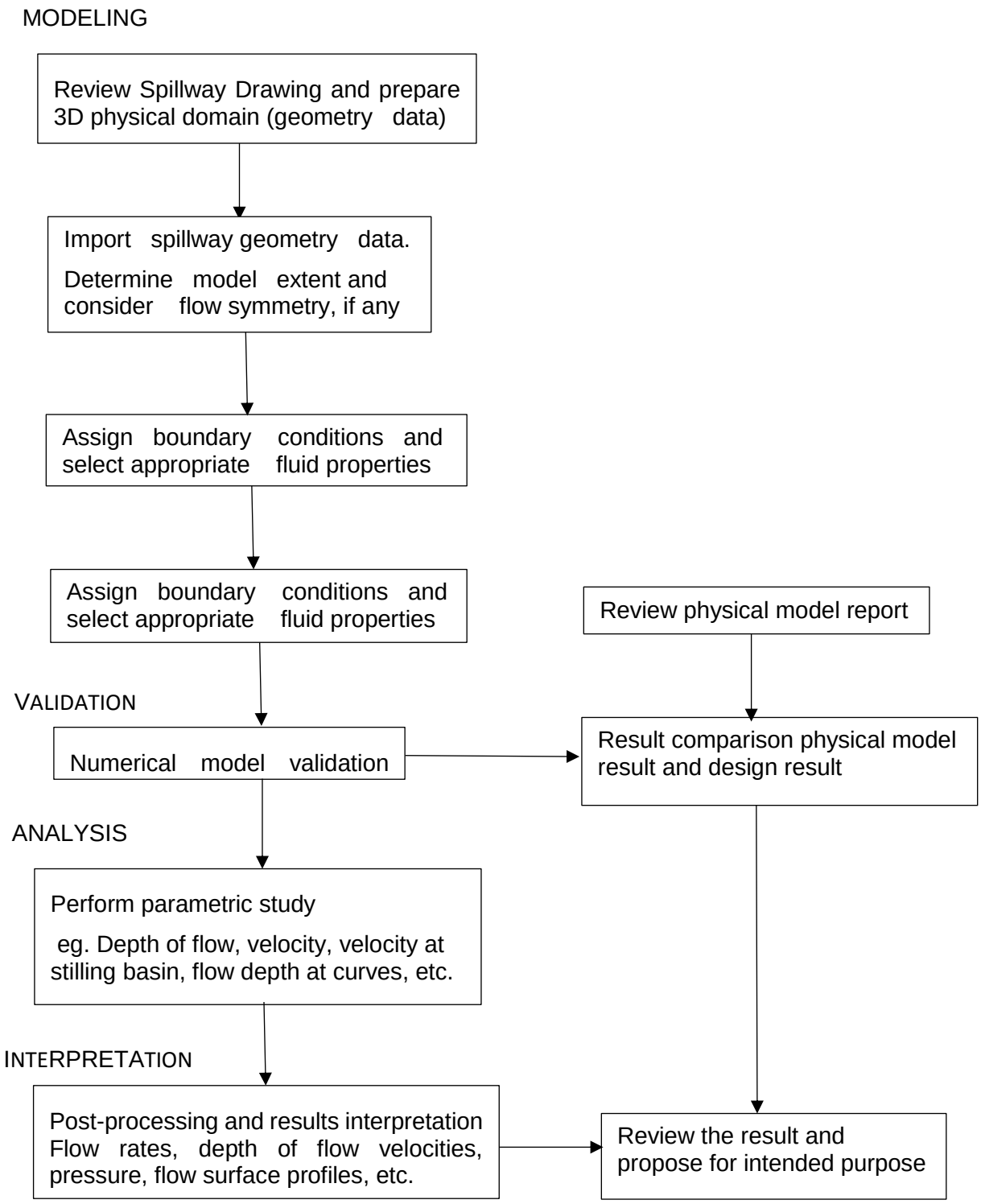

Figure 3- 1 Flowchart showing a general methodology

CHAPTER FOUR

4 PERFORMANCE ASSESSMENT OF NUMERICAL 3D HYDRAULIC MODEL USING PHYSICAL MODEL

4.1 BACKGROUND

Zarema May Day Dam is found in the Northern Tigray region of Ethiopia 37^0 47' 55''E and 13^0 44' 13''N. It is 152 m high, 900 m long, asphalt-core rock fill dam, collecting the water potential of the Zarema Basin, a tributary of the Tekeze. The reservoir has a capacity of 3.6 billion m^3 which will feed a 45,000-ha plantation for sugarcane production of Wolkaite Project, owned and operated by the Ethiopian Sugar Corporation. The dam is currently under construction, supposed to be completed by 2018 [47]. Figure 4- 1 shows the location of project.

Flood control is provided through 680 m^3/s capacity spillway located on the left dam abutment. The spillway consists of a 30 m wide ogee crest of shallow approach flow, an approximately 250 m long channel running along the contours and a 130 m head stepped chute, designed to dissipate the flow energy through a 390 m long nappe flow cascade, before releasing the water back to the river. A relatively sharp 65° bend connects the upstream channel to the stepped chute and represents the unique distinctive features of the design. The bend includes three vanes and related deflecting walls, a set of diagonal steps on the channel bottom and two rows of baffle blocks at

the terminal sill. The stepped chute is almost entirely rock surface after excavation and shaping of spillway channel, [47].

The spillway discharge is estimated in 290 m^3/s for the design flood with return period 1000-years and in 680 m^3/s for the PMF. Since the spillway has been checked with the PMF, the maximum flow has been taken for the model which is 680 m^3/s. Table 4-1 shows the flood routed flow [47].

Table 4- 1 Zarema May Day Flood Routing [47]

Return Period	Inflow		Outflow		Max. water Level
	Peak	Volume	Peak	Volume	
Years	m^3/s	Mm^3	m^3/s	Mm^3	m
25	2914	172	119	30	948.08
50	3372	199	147	37	948.33
100	3831	226	178	44	948.58
500	4904	289	255	63	949.15
1,000	5369	317	291	72	949.40
10,000	6921	408	420	102	950.20
PMF	9690	572	676	163	951.56

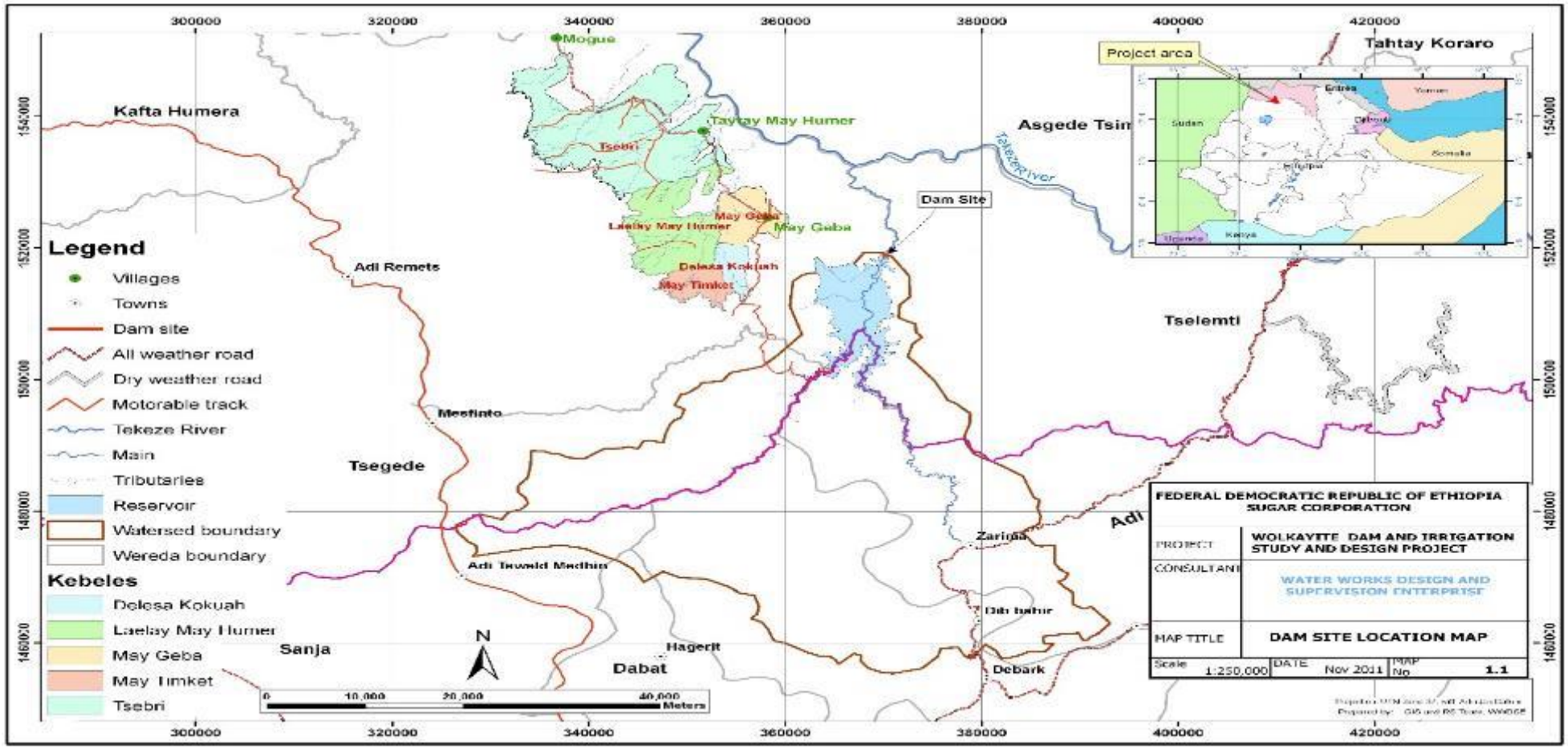

Figure 4- 1 Zarema May Day Dam Site Location Map [47]

4.2 OBJECTIVE

The spillway presents an unconventional and challenging scheme, involving different hydraulic solutions. The hydraulic performance was investigated with the aid of a 1:60 physical scale model developed at the PITLAB Laboratory of the University of Pisa, Italy. The model reproduces the entire spillway structure from the ogee crest to the chute toe, for an overall remarkable length of around 12 m [47].

Accordingly, the purpose of this research is to test if FLOW-3D hydraulic model perform safe spillway/ hydraulic structures flow conditions by comparing its performance with physical model constructed Zarema May Day Dam Spillway physical model result in Ethiopia.

4.3 HYDRAULIC FEATURES

4.3.1 Spillway

The spillway walls extended nearly 19 m into the approach channel in form of training walls (or wing walls). The wing walls are streamlined to reduce the flow contraction and suppress unfavourable eddies. The layout conforms to a constant curvature of 10 m radius [47]. Figure 4- 2 and Figure 4- 3 show elements of the spillway.

The crest of the spillway is at El. 946.4 m, and its height is 2 m. The ogee crest consists of an effective hydraulic crest length of 29 m has been selected. A 1m wide reinforced concrete bridge pier is integrated into the spillway crest giving it a total crest length of 30 m. The overall pier length is around 26 m.

4.3.2 Spillway Channel

From the spillway toe 20 m downstream, the rectangular channel depth decreased from 9 m to 6 m in 10 m distance. From the beginning of 6 m depth of rectangular spill channel, there is a transition of channel width from 30 m to 23 m with a convergence angle of around 4.5 degree. The overall length of the transition is 45 m and the bottom grade of rectangular channel is 0.5%. After the transition 150 m long with 23 m wide and 6 m depth of concrete channel extends with 0.5% slope and joins a 65-degree channel bend.

4.3.3 Channel Bend

Difficulty in the design arises because of the complexity of the flow around a curved path, that is not readily subject to any analytical solutions. The challenging issue in the design of the channel bend is to reduce the superelevation, cross waves disturbance pattern and provide a rather uniform transversal distribution of the flow at the entrance of the stepped chute. To achieve this objective, the following elements have been considered [47]:

1. The channel section has been divided into 3 curved vanes, 7 m wide each, separated by a nearly 1.5 m thick deflecting wall, which extends over the entire bend. This solution creates a series of narrow curved channels of lower discharge with the purpose of reducing the effect of the centrifugal force on the flow;
2. Near the end of the bend, two diagonal steps have been created in the channel bottom. Each step is around 1.8 m high and extend across the entire vane. The steps show an angle of 30 degree with respect of the channel axis and are intended to attract the flow toward the inner boundary;
3. Immediately downstream from the end of the bend, 2 rows of baffle block have been installed. The baffle blocks extend across the entire channel width, following a staggering pattern, for a total of 29 baffle blocks. Each baffle block is 1.5 m wide, 1.8 m long and 1.8 m high. The first row is located around 4 m downstream from the end of the deflecting walls, followed 2 m by the second row. The baffle blocks have been designed to both reduce the flow velocity at the entrance of the stepped chute and promote a uniform transversal distribution of the flow.

4.3.4 Stepped Chute

Downstream of the baffles, the rectangular cascade drop channel joins a trapezoidal channel. The trapezoidal channel is with cascade drops and unlined rock extends. A total of 33 cascades drops with drop height 4 m and length of cascade 4.9 m and at

the end it has variable, with larger length. The cascade drops have a 50 m bed width and 1:1 side slope of more than 10 m depth. The grade of the chute, which progressively decreases from the initial 45 degrees at the entrance to approximately 30 degrees in the vicinity of the toe. The total drop head is 130 m for 390 m long nearly 50 m wide will joins the natural river. The channel for the cascade is entirely unlined, founded on fresh rock. Figure 4- 3 shows the elements of the spillway design.

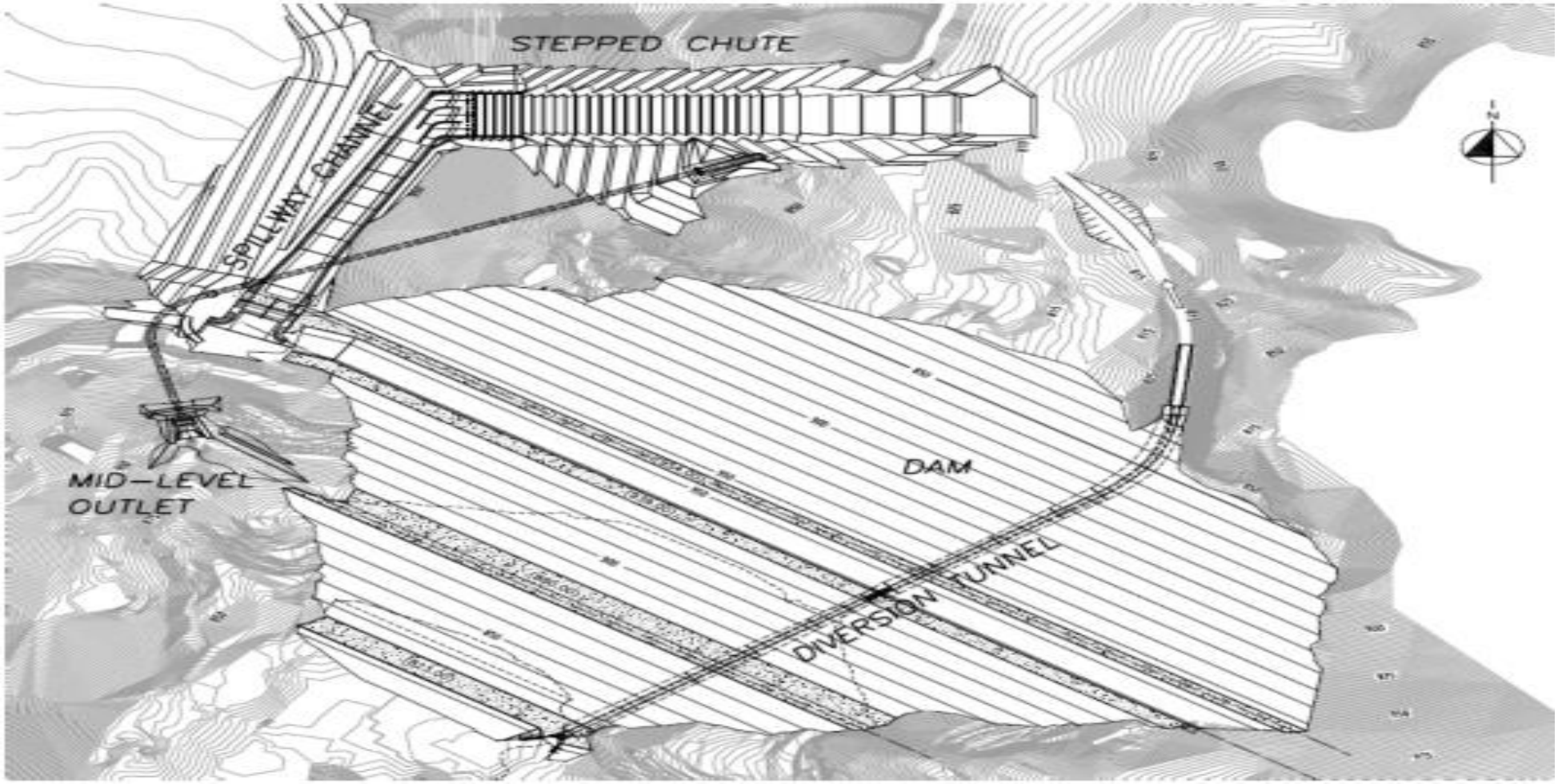

Figure 4- 2 General Project layout [47]

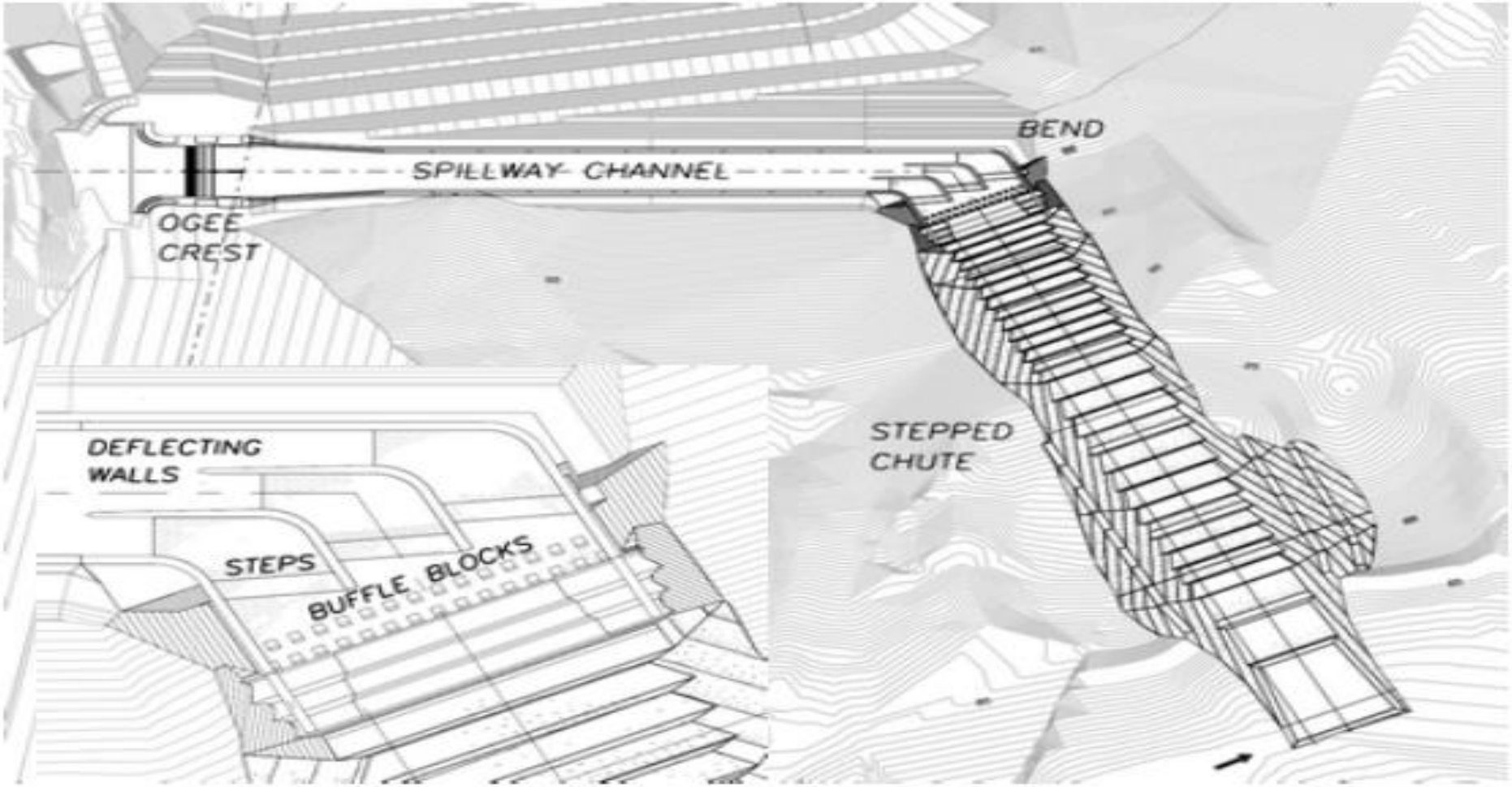

Figure 4- 3 Elements of the spillway design [47]

4.4 NUMERICAL MODEL SETUP

4.4.1 General

During physical modelling three model configurations have been tested and the final model were used for design of the spillway. In this research, the verification of the model was done based on the final model output.

FLOW-3D uses the finite volume method to solve the Navier-Stokes system of equations in three dimensions to simulate the flow of fluid. The general model set-up has time for simulation, specified with one fluid, incompressible flow, and a free surface or sharp interface being selected. Water at 20 degrees Celsius for all simulations were specified for fluid properties. Metric system of unit was selected. Furthermore, some other model parameters remained generally constant.

4.4.2 Physics

The gravity option was activated with gravitational acceleration in the vertical or z-direction being set to negative 9.81 m/s^2. The viscosity and turbulence option were also activated with Newtonian viscosity being applied to the flow along with the selection of an appropriate turbulence model. Once the FLOW-3D model was completely prepared, simulations can be performed with different turbulence models

activated. There are many different physics options available, activation of only two selections are required which are related to this research.

4.4.3 Geometry and Mesh

The spillway geometry design was generated using AutoCAD 3D model, based on the dimensions of the design and was exported into the code as an STL file. The domain was discretized using different blocks to minimize space outside the structure which is useful to reduce unnecessary mesh that will increase the simulation time. Therefore, the mesh blocks are prepared in accordance to the given geometry. Figure 4- 4 to Figure 4- 7 show the model set up.

Eight numerical hexagon meshes blocks were built with uniform cubic elements in order to properly capture the geometry of the structure and correctly simulate the water flow from the reservoir to the outlet. Accordingly, it was observed that the cells at the ogee, near the baffle and drops were not resolved well when grid size was given higher than 0.5 m. Hence, 0.5 m grid size showed good resolution. Hence all mesh block grids were 0.5 m for all grid sizes. The model for 1D was set up to get overall information at different location along the spillway by dividing the length of spillway at 5 m intervals starting from the river (Outlet) up to reservoir (Inlet) with full scale model. The total length of the spillway model is 702 m.

The operations of geometry building, and grid generation are independent of one another. After both the geometry and the grid are defined, the geometry is then

embedded in the computational grid by the pre-processor using a technique called FAVOR (Fractional Area Volume Obstacle Representation).

Discretization errors can be reduced by using more accurate interpolation or approximations or by applying the approximations to smaller regions, but this usually increases the time and cost of obtaining the solution. Compromise is usually needed [48].

A useful option in FLOW-3D that makes this process even more effective is the restart option. This allows the user to run a simulation and then make a variety of model changes, including mesh size and configuration, before restarting the simulation using information from the last time step of the previous simulation. Solving the fluid flow equations are based on discretization procedures such as FVM in which one needs to divide the domain to a numerous cell and create a mesh system. Cartesian coordinate system was used.

4.4.4 Boundary and Initial Conditions

The spillway was modelled in different blocks to properly capture the space occupied by the structure. The initial boundary condition for flow data from free surface flows is desired and so the top boundary was set as atmospheric pressure while the bottom boundary was specified as a wall. As for the extent of the mesh in the vertical or z-direction, the bottom boundary was set just below the model geometry in order to capture the channel bed, while the top boundary was set just above the highest water

elevation and above the wing walls. Since the goal of many of these simulations was to model flow rate over a spillway with headwater level for comparison to physical model data, the upstream boundary was set as a specified fluid height.

Since the flow domain is defined as a hexagonal in the Cartesian coordinates, there are six different boundaries on each mesh blocks. The boundaries on the mesh and their coordinate directions were set as follows.

The boundary condition for flow data in Block 1, the upstream boundary condition (Xmin) was defined as volume flow rate 680 m^3/s at inlet of spillway, the downstream boundary condition (Xmax) was defined as symmetry. The bottom boundary (Zmin) was defined as Wall (no-slip condition) and the top boundary (Zmax) was set as Specified Pressure (with Fluid Fraction = 0) which is specified with water elevation 1008 m. In Block 8 at the outlet, Ymin was given as an outlet. All the other blocks were either Symmetry or Wall condition.

The initial conditions that represent on the upstream sides of the spillways at the same level as the specified fluid heights was proposed fluid elevation. The free surface water elevation option was given as an initial condition at the Block-1. The Zmax-coordinate of the free water surface was fixed for the estimated initial condition which is 1008 m.

Another geometry option, that remained constant for all spillway modelling completed as part of this study, was the inclusion of surface roughness value applied on the surface of all spillway geometry. The roughness friction factor = 0.013 for a concrete

lined channel and 0.025 for cascade drops were utilized the model. This was done in FLOW-3D by specifying a surface roughness value, equal to the average height of surface imperfections to the desired components in the meshing and geometry tab since Manning roughness was converted to FLOW-3D's Surface Roughness.

At different locations along the spillway probes and baffles were proposed. A baffle is a plane that was defined as a flux surface and specified to be 100 percent porous so that it would have no effect on the flow. This baffle was normally located in a plane near the crest and was responsible for providing the discharge measurement over the spillway. In a similar way probes were used to measure as a staff gauge for measuring the depth of flow. Hence, history probes which shows stage discharge curve was located at various locations.

4.4.5 Numerical Simulations Options

Several types of options are available in the Numeric tab of the FLOW-3D model set-up. These options present modifications to the way the Reynolds-Averaged Navier Stokes (RANS) equations, which are the fundamental underlying equations in FLOW-3D, are solved. In most cases, the default selections were used; however, in case of momentum advection algorithm, the default momentum advection algorithm is a first-order upwind differencing method. This method is first order accurate in space and time. It is robust and sufficiently accurate in most situations, although, as in any first-order method, it introduces numerical diffusion into the solution. For this it has its own controlling system. When better accuracy is needed for the resolution of flow

velocities, e.g., in vortices, then a second-order monotonicity-preserving upwind differencing method can be used by selecting second order monotonicity preserving. This method is second order accurate in space and first order accurate in time. Another second-order method based on central differencing of the advection terms can be used by selecting second order. This method is second order accurate in both space and time. As such, it is the preferred method for minimizing numerical dissipation in swirling flows. This method is the least diffusive of the three, and performs well for circulating flows and free surface waves [22]. In this numerical simulation second order momentum advection was given since there is a sharp bend at the end of the chute channel.

Starting from smaller time steps that is from 0.5 seconds up to 75 seconds, were given to get the final numerical simulation result. A larger time step will lead to numerical instabilities and nonphysical results. Hence simulations were stable. Implicit pressure solver was used.

A numerical solution method is said to be stable if it does not magnify the errors that appear during numerical solution process. FLOW-3D uses the self-corrective procedure as well as an automatic setting of the convergence criteria that adjusts to whatever is happening during numerical solution process. Generalized Minimum Residual (GMRES) method was preferred due to its rapid convergence and parallel efficiency [22].

The runs were developed in a personal computer with a Pentium 4 Ghz processor and 16 GB of RAM; the evolution in time was used as a relaxation to the final steady state. Simulation time was given 75 second and accordingly 22 days were taken to finalize simulation. The required output memory size was 200 GB carried out with eight multi processes parallel. 2.0×10^9 number of cycles were run.

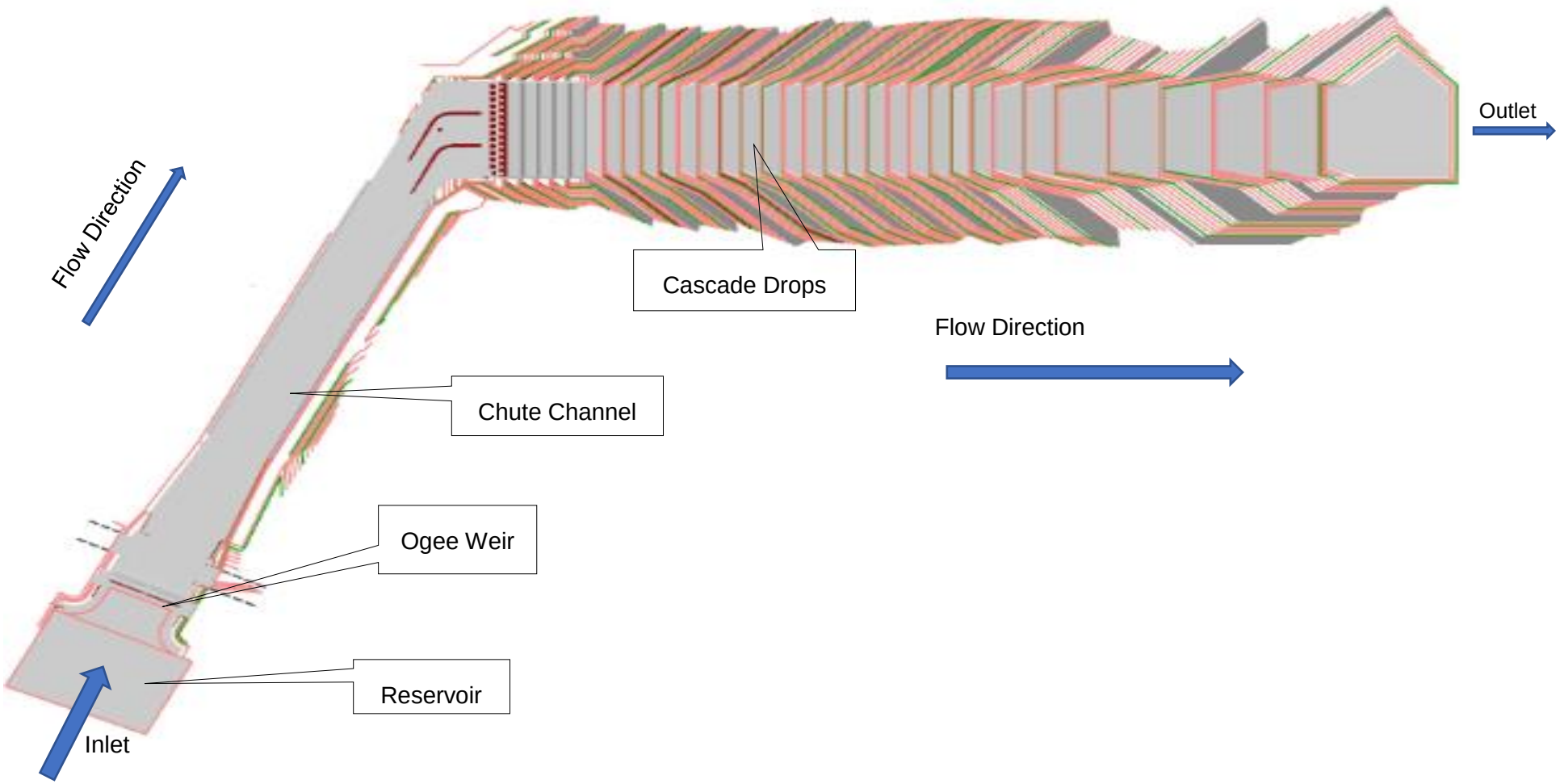

Figure 4- 4 Plan of the Spillway

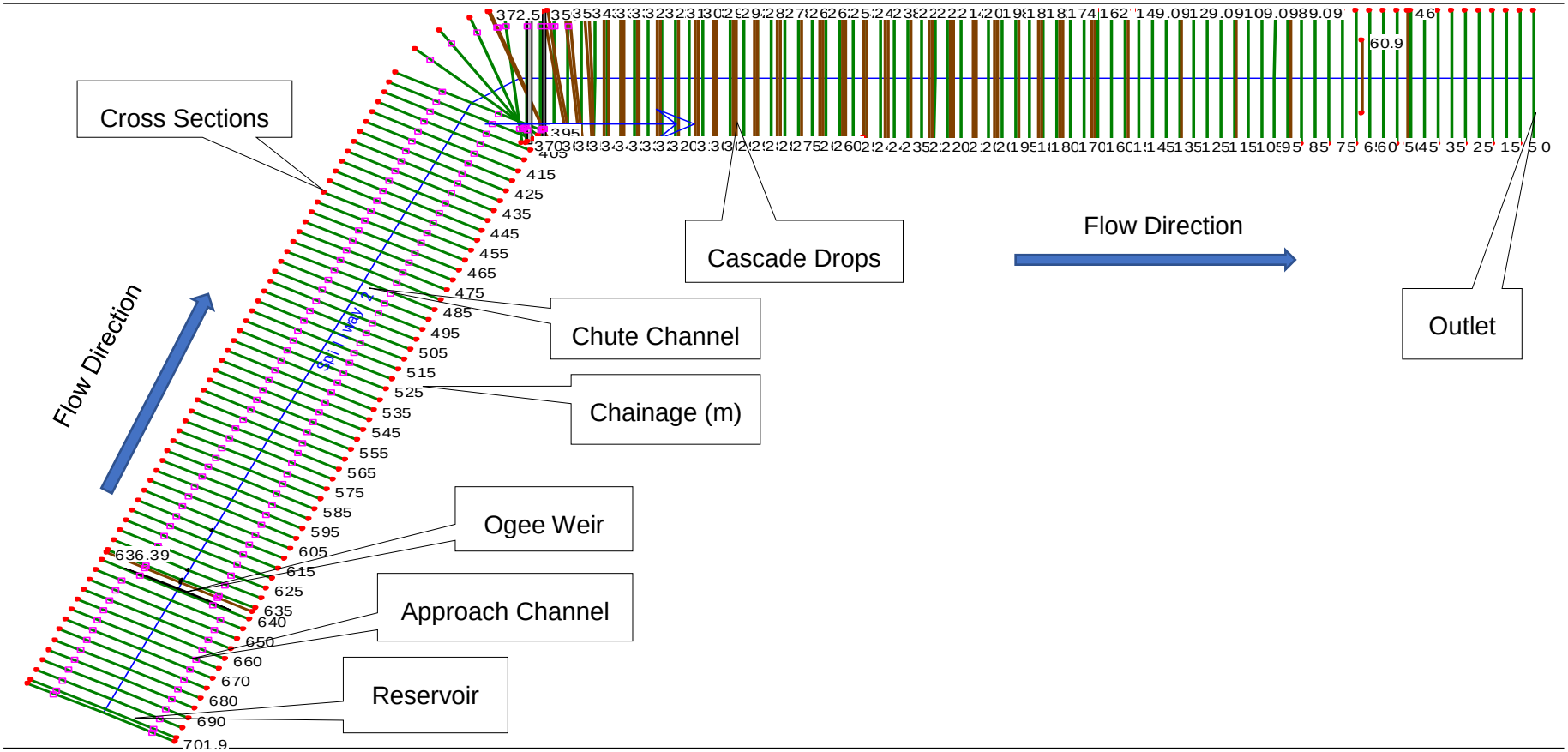

Figure 4- 5 Spillway Model Chainage distance (m)

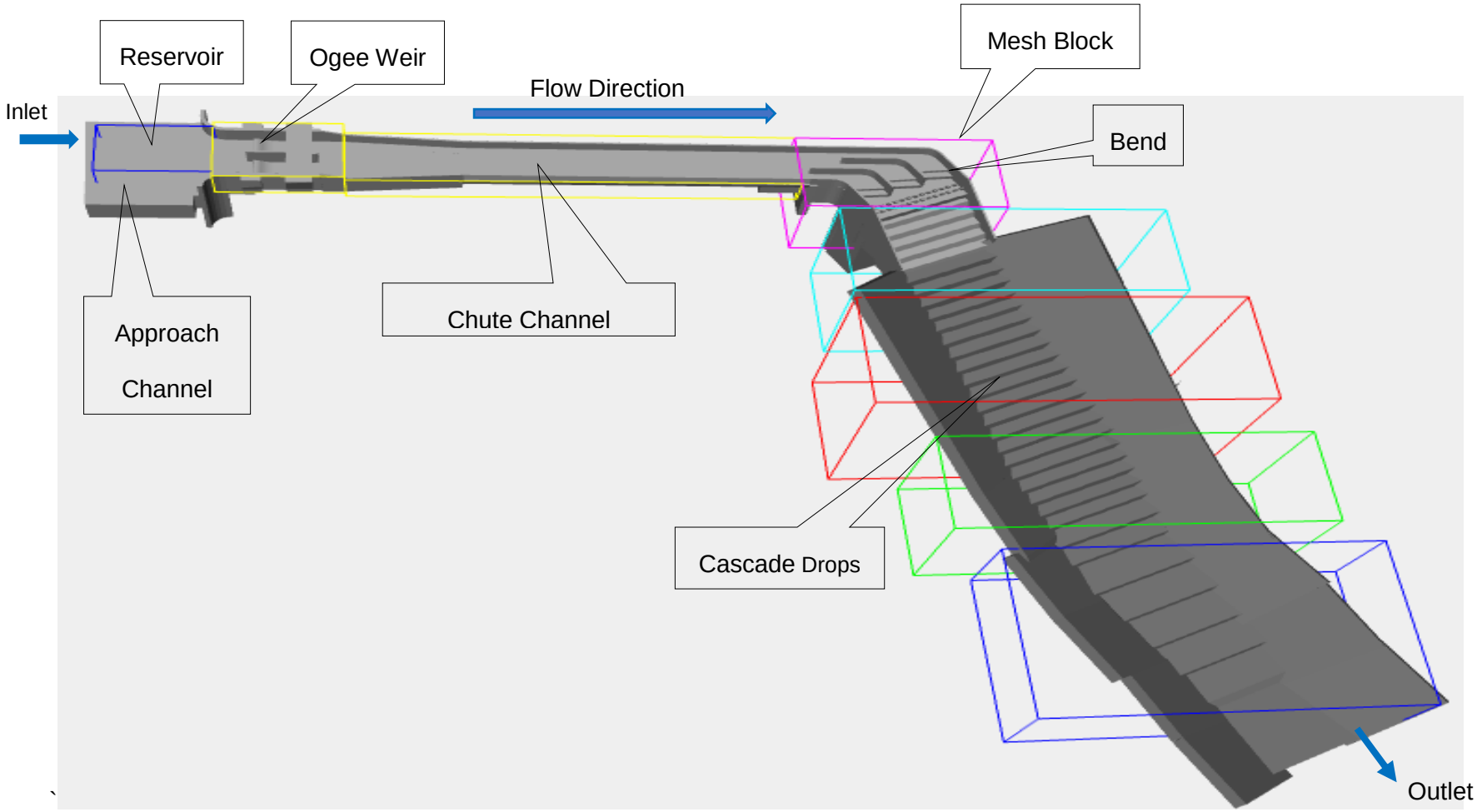

Figure 4- 6 3D Spillway mesh blocks prepared for the model

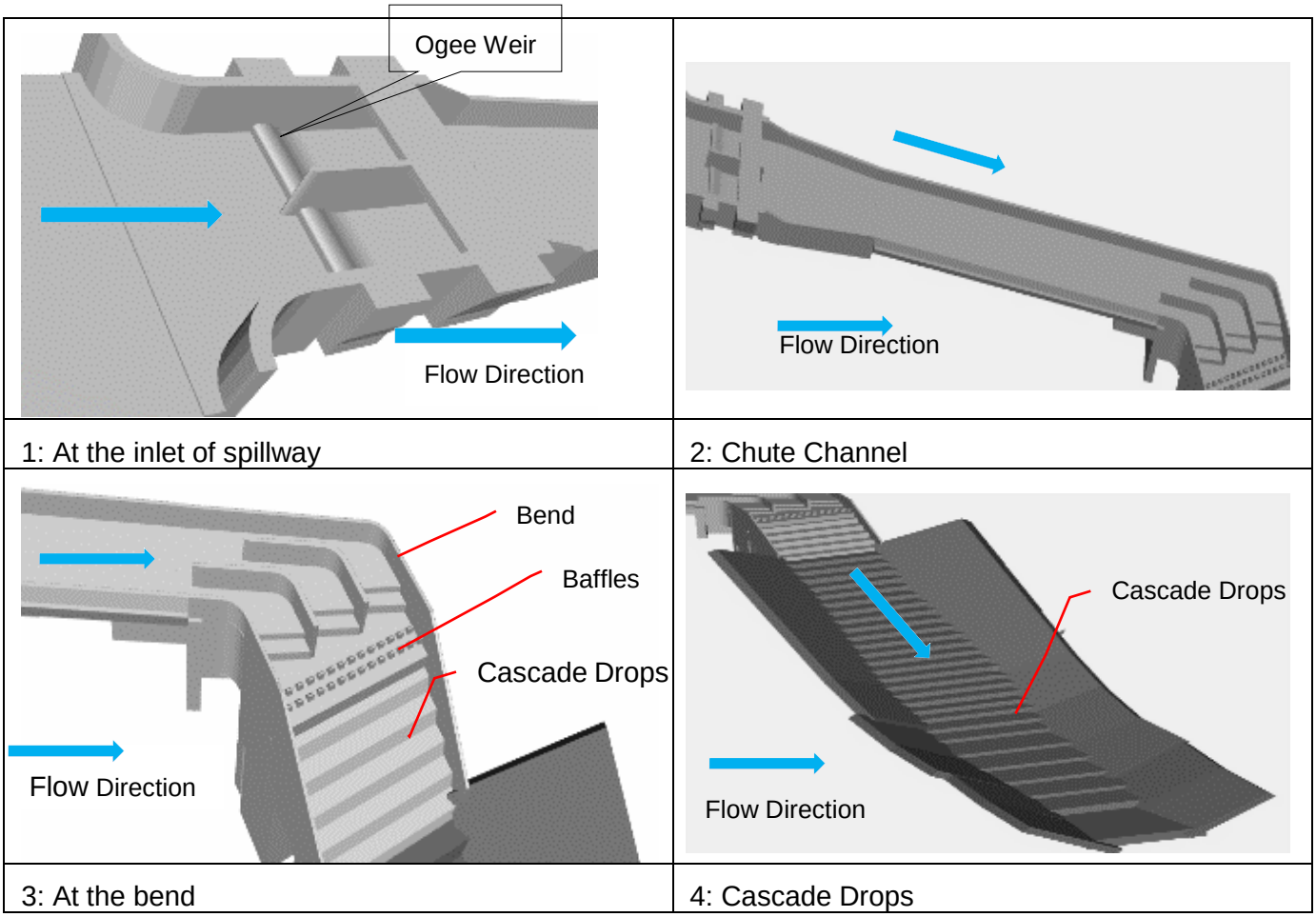

Figure 4- 7 3D Spillway mesh blocks at different sections

4.5 COMPARISON OF PHYSICAL AND NUMERICAL MODEL

4.5.1 Model Geometry

Comparison for validation of the 3D numerical model is the main objective based on the physical model results. Accordingly, during research, the design for the spillway sections were verified by numerical methods using FLOW-3D models based on physical model results. In addition, for the general information, HEC RAS 1D results

are also checked. For the section where there is no physical model data, it was checked with the pictures from the physical model and section provided as per the design. The design data is basically computed based on USBR.

The model consists of an upstream metallic tank, which simulates the dam reservoir and permits to reduce the flow disturbance in the approach channel. The ogee crest, the spillway channel, the connecting curve and the flow deflecting walls have been realized in Plexiglas to correctly simulate the roughness of the concrete lining. The transparency of the Plexiglas also facilitates examination of the flow in the channel and along the curve. The stepped chute and the riverbed have been realized with bricks and mortar to simulate the roughness of the unlined rock cut [47].

The longitudinal and transversal flow profiles have been carefully measured in the spillway channel, along the flow deflecting walls, in the stepped chute and at the chute toe with the aid of a 0.1 mm precise point gauge installed on a movable trolley. Plate 4- 1 shows the physical model setup. In addition, Figure 4- 2 shows the discharge with different return period.

Table 4- 2 Physical Model discharge with different flows [47].

Model Test			Design	
Test Number	Qm (l/s)	Qp*(m^3/s)	Return Period Tr (Years)	Qp (m^3/s)
2	4.14	115.4	25	122
1	4.93	137.5	50	152
3	6.54	182.4	100	183
4	9.4	262.1	500	264
5	10.68	297.8	1000	302
6	15.9	443.4	10000	437
7	25.1	699.9	PMF	709

Where: - Discharge (Qm) (l/s), Proto type (Qp*) (m^3/s), Routed out flow (Qp) (m^3/s) and Return Period Tr (Years)

Physical Model Setup

1: Ogee crest at the spillway entrance, view from downstream

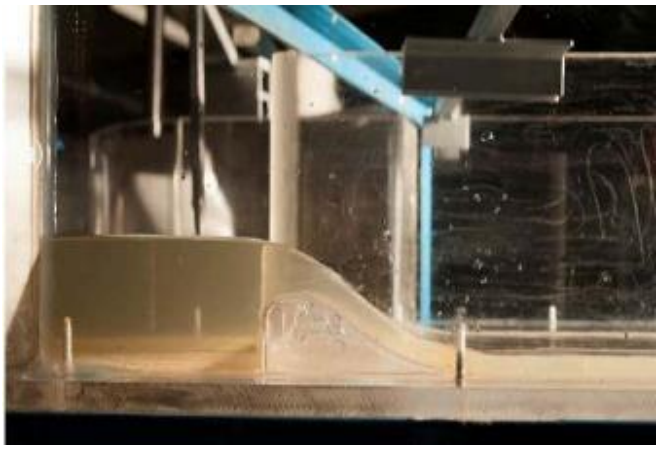

2: Ogee crest, detail of the flow profile

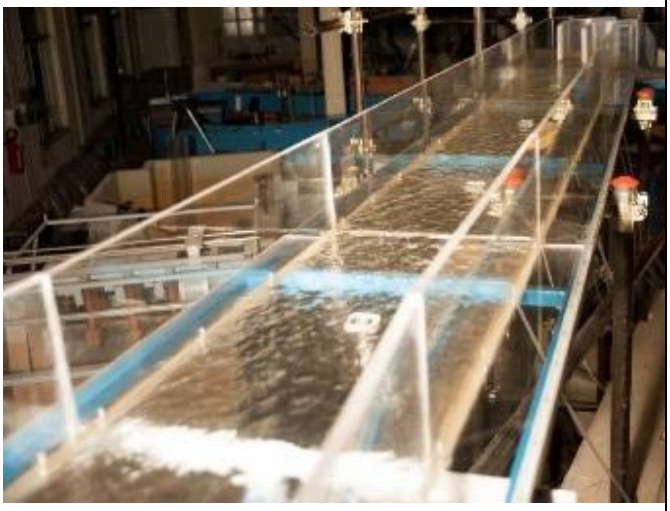

3: Spillway channel, in the foreground the channel transition

4: Channel bend and the first steps of the stepped chute

Physical Model Setup	
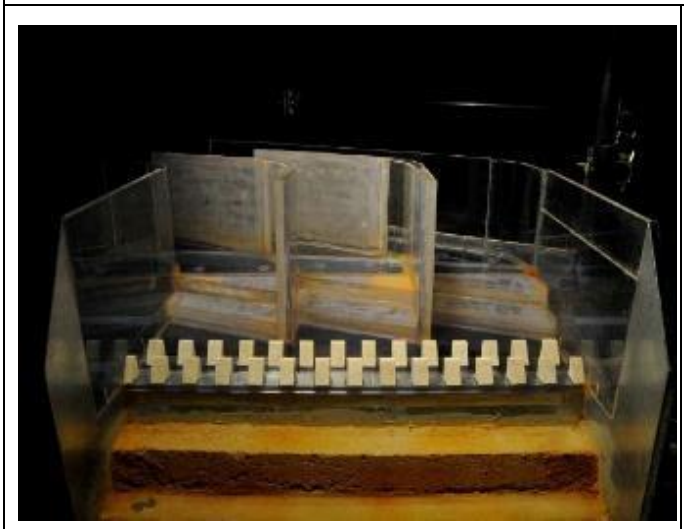	
5 : Configuration of the baffle blocks	6 : Stepped chute

Plate 4- 1 Physical model setup [47]

The general flow pattern for the 1D and 3D numerical model results are shown below. From Figure 4- 8 to Figure 4- 13 are the general information and main comparison for different sections of the spillway from the approach channel to the end of cascade drops.

The 1D model result shown in Figure 4- 8 and Figure 4-9 show the longitudinal profile of flow condition as per the design section. The first part of ch 0+450 to 0+550, the designed wall height is not sufficient which shows overtopping. Therefore, modification has been done during research and based on modification, the result of 1D refer Figure 4- 10 shows no overtopping. On the other hand, Figure 4- 11 to Figure 4- 12 are the 3D model output which show no overtopping without any modification. Detail

description has been given from section 4.5.2 to 4.5.12. Figure 4- 13 is the typical model output results used to get information about average depth, maximum depth, average velocity and local velocity at the end of simulation. This typical model is also applicable for the information given to the other model output. Across the channel, points were located at the top of the flow to get information. The average depth and velocity at a point shows the average velocity and depth during simulation time at that section. In addition, to get average information, data were taken at different locations of the 3D model output and arranged in table from left to right looking in downstream at respective cross sections.

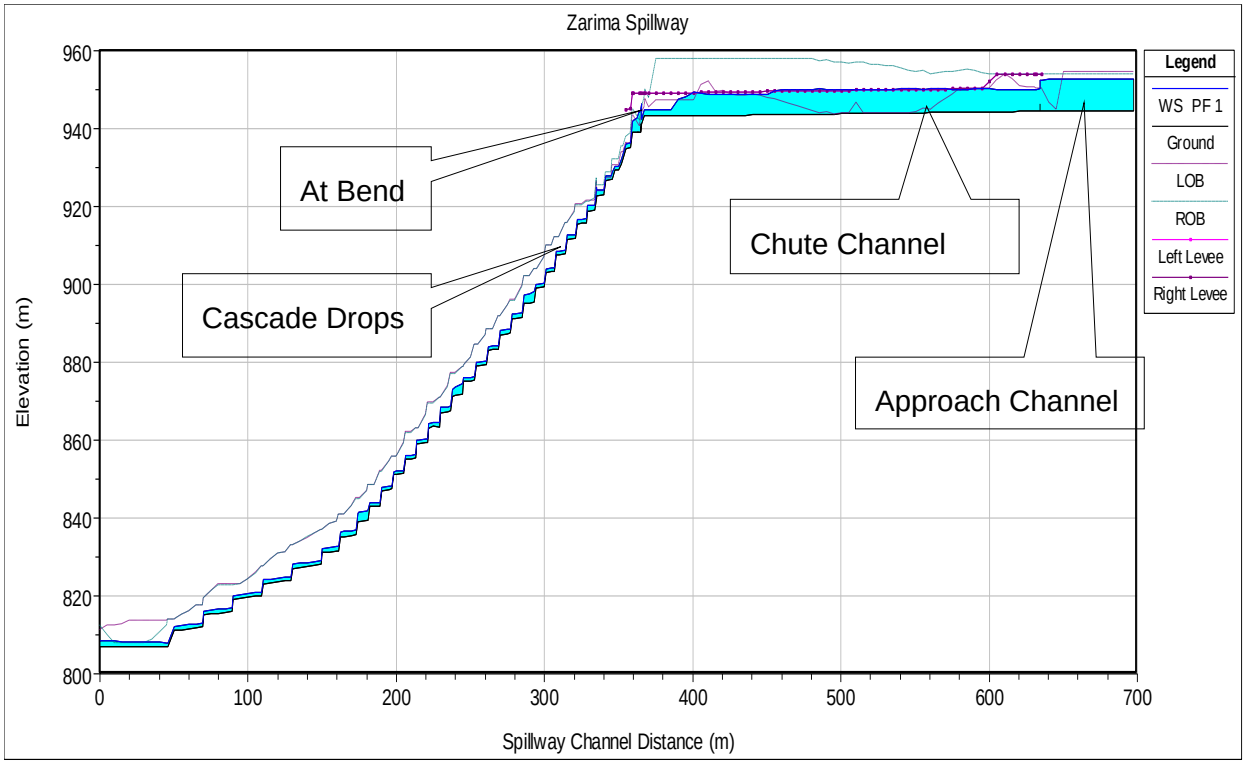

Figure 4- 8 1D model longitudinal profile result as per the design section

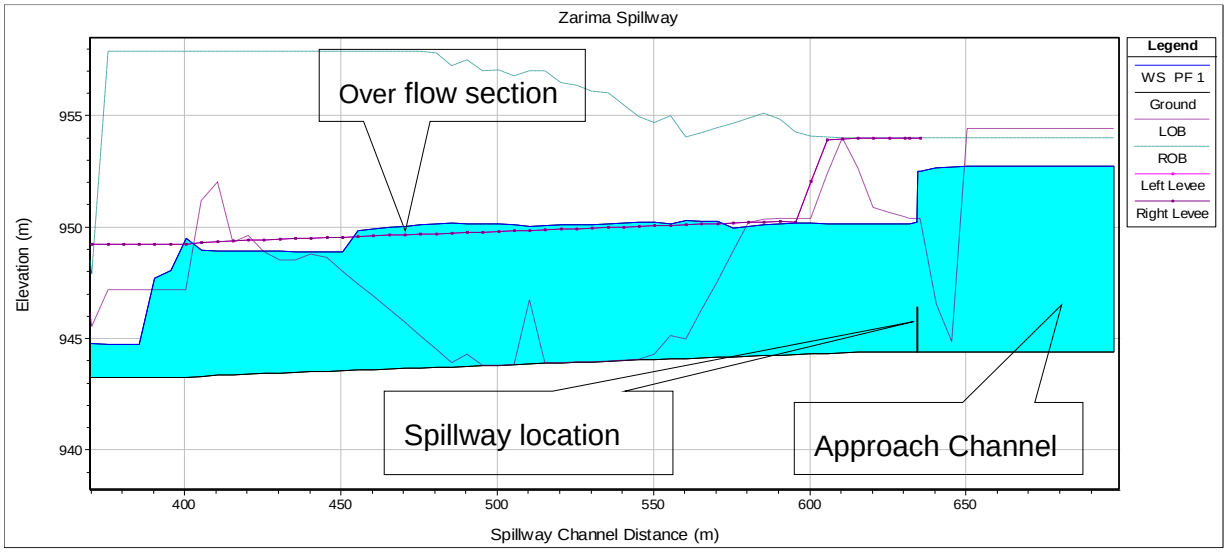

Figure 4-9 1D model longitudinal profile as per the design section which shows overtopping

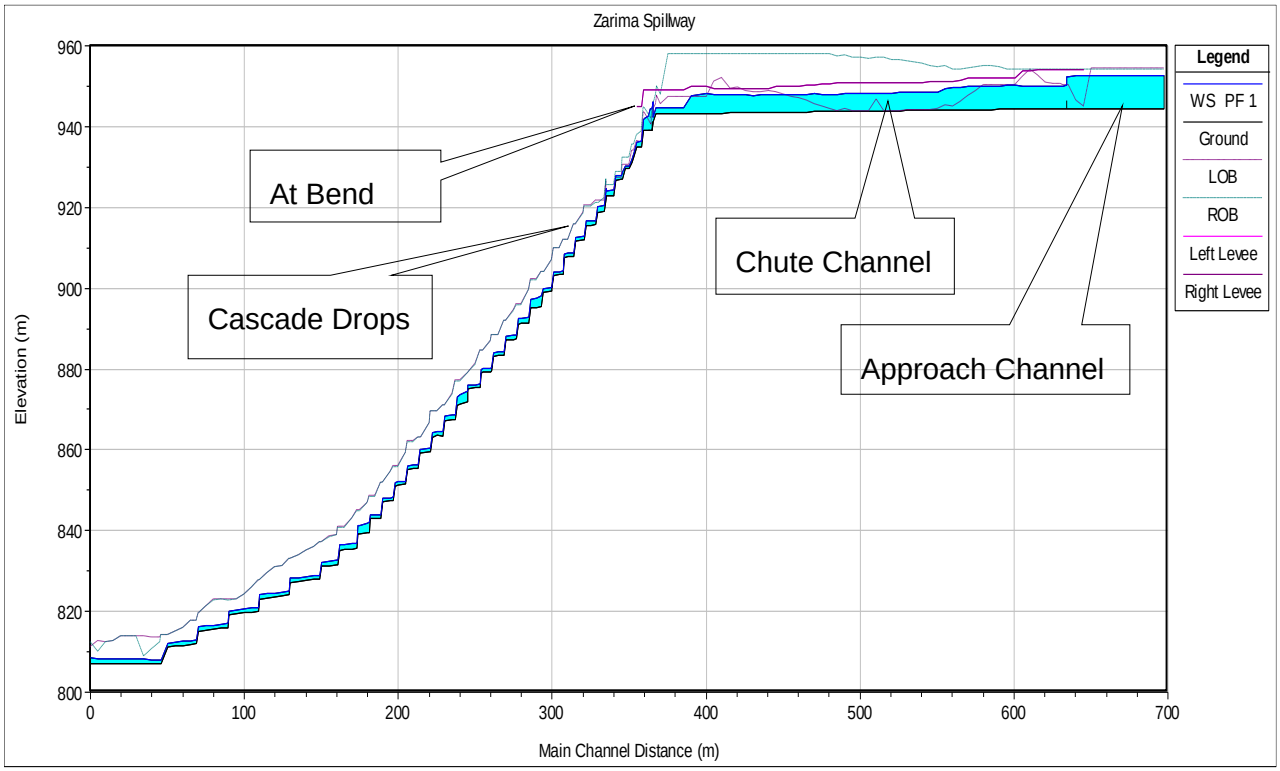

Figure 4- 10 1D model longitudinal profile for the Spillway after modification of the design section

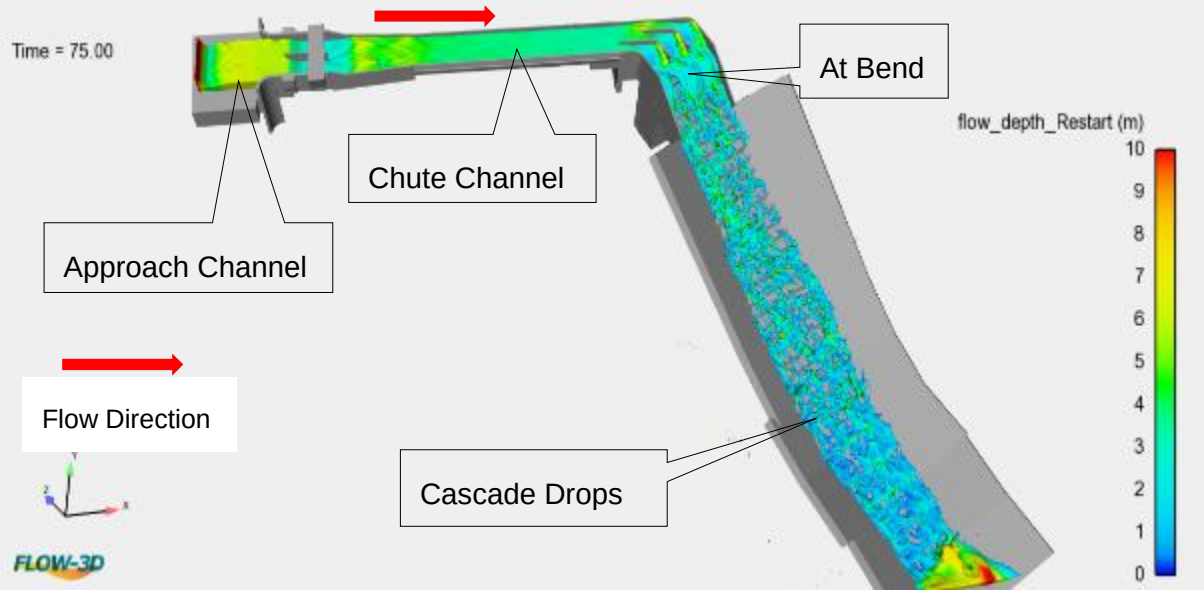

Figure 4- 11 3D model result for the whole part of Spillway in reference to flow depth

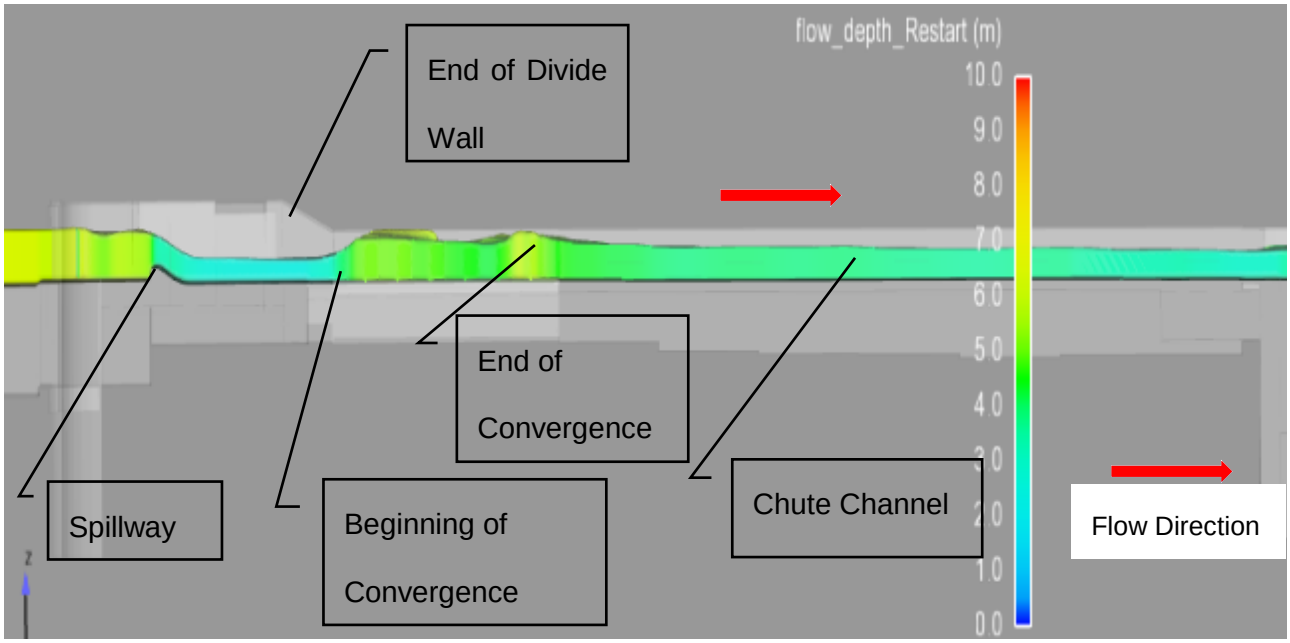

Figure 4- 12 Flow Profile of 3D from approach channel to bend

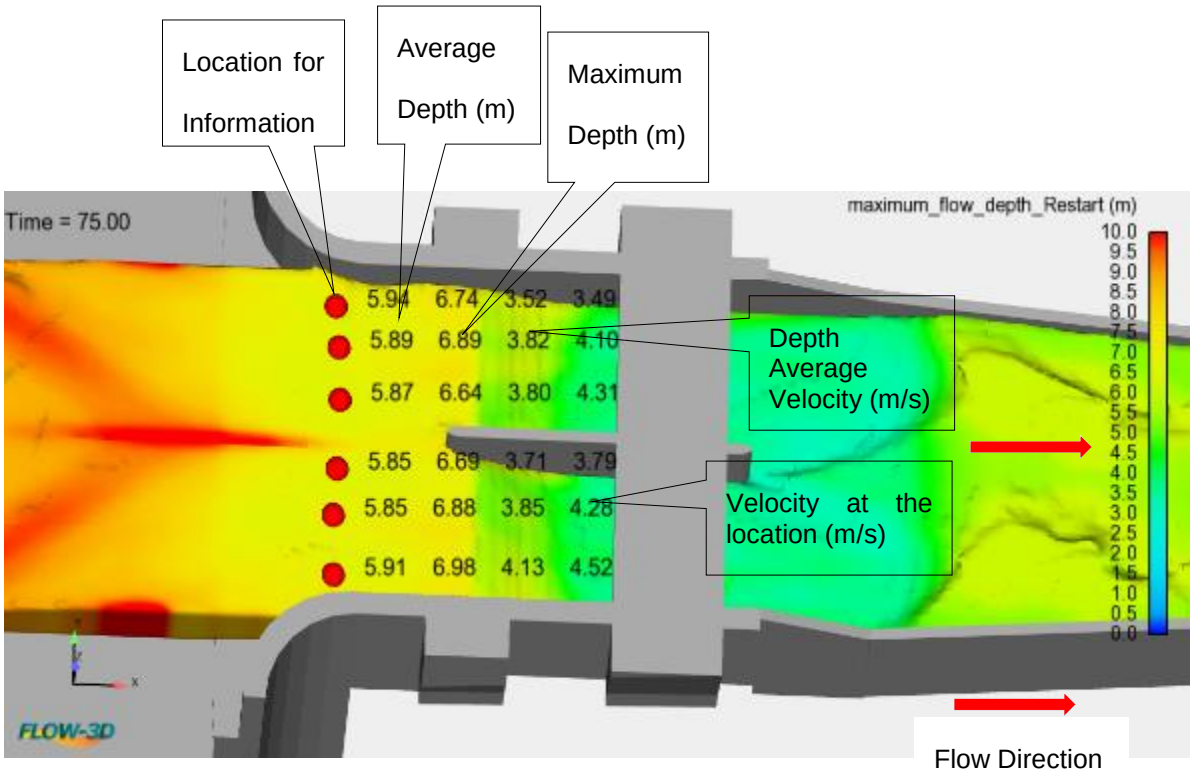

Figure 4- 13 3D typical model output results

4.5.2 Water Surface Profile Along Approach Channel

Approach channel was checked at ch 0+660 with 1D and 3D numerical models and cross checked with the design output and proposed wall height. There is no available data from the physical model. Figure 4- 14 section 1 and 2 show the comparison of flow depth and velocity. The flow depths from design 5.4 m, from 1D 8 m, from 3D average 5.89 m and from 3D maximum 6.8 m respectively. The velocities from design 3.4 m/s, from 1D 1.6 m/s and from 3D 3.81 m/s. There was 10% difference between design and 3D average depth of flow and 10.76% difference in velocity. From the

results, the proposed side wall height is sufficient enough to protect overtopping. For further information refer Table 4- 9, Table 4- 10 and Annex A.

Comparison Along Approach Channel at Chainage 0 + 660

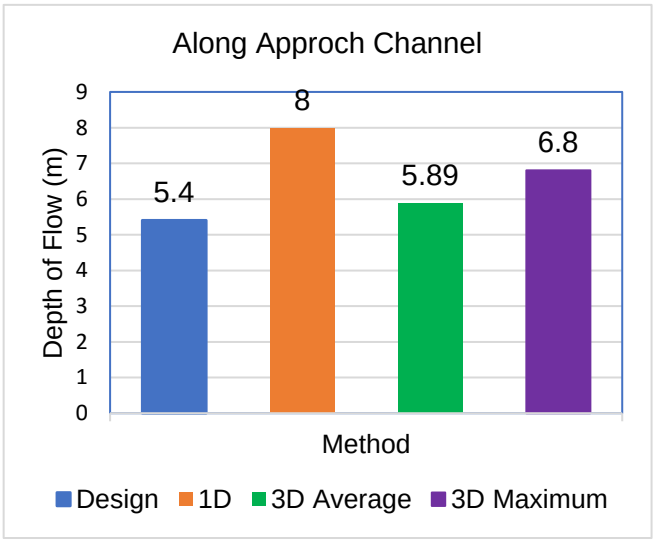

1: Depth comparison along Approach Channel

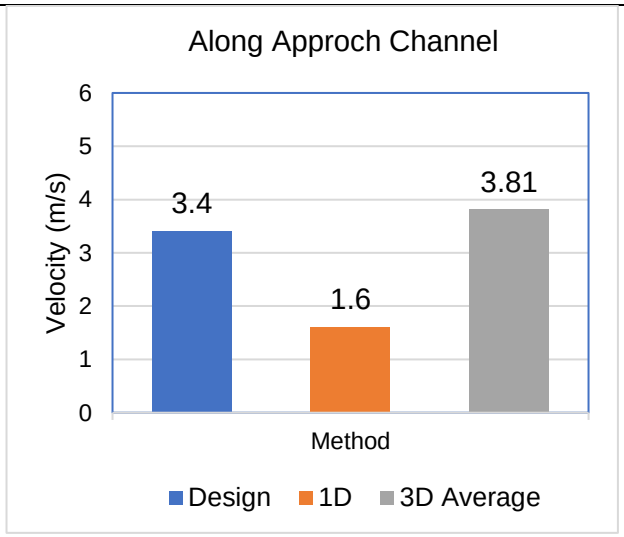

2 : Velocity comparison along Approach Channel

Figure 4- 14 Comparison and Model Results Along Approach Channel

4.5.3 Flow over the spillway crest

Since the spillway has been checked with the PMF, the maximum flow has been taken for the model which is 680 m^3/s. There is a physical model result and design result for the rating curve of the spillway crest at ch 0+639. During research, the rating curve was checked using USBR and the results are matching well. On the other hand, the research result and the physical model result at the end have closer agreement than the design. Hence, the physical model result and research results are matching with Trend Line R^2 = 0.981. Figure 4- 15 shows the comparison result of the above

approaches. Furthermore, the comparison has been checked using performance statistics. For detail information refer section 4.5.3.1 and Annex A.

4.5.3.1 Approach and performance Statistics

Assessment has been done for the performance accuracy of each simulation by comparison with observed flow. The comparison is made based on physical model result, 3D model result and design result through the following performance statistics: Coefficient of Determination (R^2), Relative bias (Rbias), and Nash-Sutcliffe Efficiency (NSE) [49], [50]:

$$R^2 = \left[\frac{\sum_{i=1}^{n}(\mathrm{SIM}_i - \overline{\mathrm{SIM}})\,(\mathrm{OBS}_\mathrm{i} - \overline{OBS})}{\sqrt{\sum_{i=1}^{n}(\mathrm{SIM}_i - \overline{\mathrm{SIM}})^2}\sqrt{\sum_{i=1}^{n}(\mathrm{OBS}_\mathrm{i} - \overline{\mathrm{OBS}})^2}}\right]^2 \quad (4-1)$$

$$\mathrm{Rbias} = \frac{\sum_{\mathrm{i}=1}^{\mathrm{n}}(\mathrm{SIM}_\mathrm{i} - \mathrm{OBS}_\mathrm{i})}{\sum_{\mathrm{i}=1}^{\mathrm{n}}\mathrm{OBS}_\mathrm{i}} * 100 \quad (4-2)$$

$$\mathrm{NSE} = 1 - \left[\frac{\sum_{\mathrm{i}=1}^{\mathrm{n}}(\mathrm{SIM}_\mathrm{i} - \mathrm{OBS}_\mathrm{i})^2}{\sum_{\mathrm{i}=1}^{\mathrm{n}}(\mathrm{OBS}_\mathrm{i} - \overline{\mathrm{OBS}})^2}\right] \quad (4-3)$$

Where SIM is the simulated flow, OBS is the observed flow or designed flow, n is the total number of pairs of simulated and observed data, and the bar indicates average value over n. NSE indicates how well the plot of the observed value versus the simulated value fits the 1:1 line, and ranges from −∞ to 1, with higher values indicating better agreement. R^2 measures the variance of observed values explained by the simulated values. Rbias measures the relative error in total flow volume [49], [50].

The best skill occurs with R^2=1, NSCE = 1, and Rbias = 0%. From the rating curve of Zarema May Day Dam spillway simulation result of performance are as follows: R^2= 0.956, NSCE = 0.927 and Rbias = 2.19%. Figure 4- 15 shows the comparison result for R^2 of the above three approaches. In addition, for detail computation refer Annex A.

Comparison of depth and velocity over the crest shown in Figure 4- 16 section 1 are as follow. The flow depths from design 4.99 m, from 1D 5.72 m, from physical model 4.88 m, from 3D average 4.21 m and from 3D maximum 6.05 m respectively. The velocities from design 3.4 m/s, from 1D 4.1 m/s and from 3D 6.18 m/s. Section 2 shows 3D model result and its average are shown in Table 4- 3. There was 13 % difference in depth of flow between physical model and 3D average and 23.36% difference in velocity. For further information refer Table 4- 8, Table 4- 9, Table 4- 10 and Annex A.

Figure 4- 16 section 3 shows the 1D profile over the crest was a sharp drop over the weir which was not actual. The flow profile of 1D did not show the reality. This shows that 1D has a limitation of showing flow profile along the vertical curvature. On the other hand, the 3D model captured the real flow. Figure 4- 16 section 4 shows the 3D model longitudinal flow profile over the spillway crest. There was no measured velocity data for the physical model.

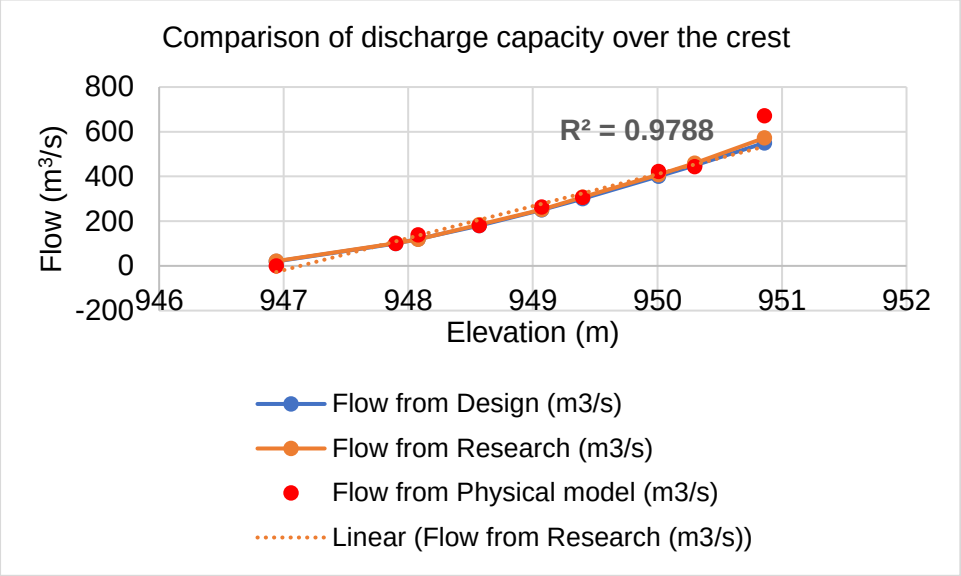

Figure 4- 15 Comparison of discharge capacity for Rating Curve of spillway

Water Surface Profile over the spillway crest ch 0+639

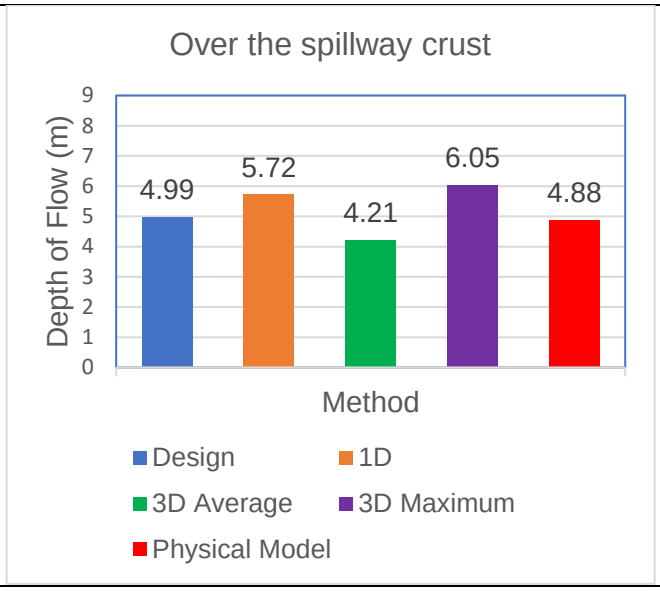

1 : Depth comparison

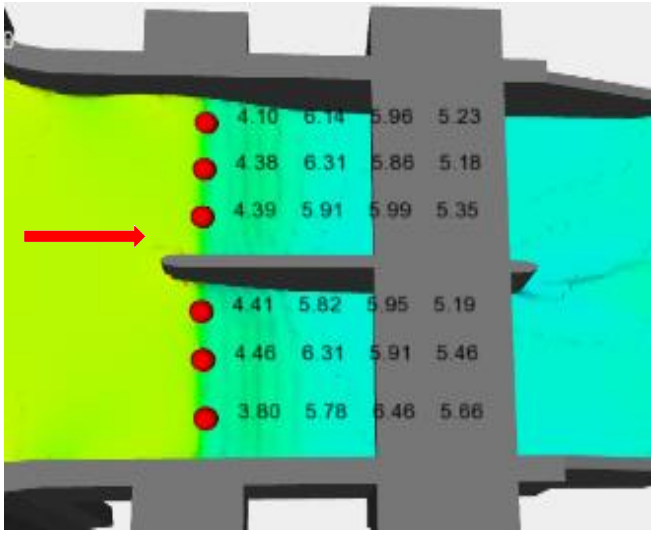

2 : 3D model result for depth and velocity

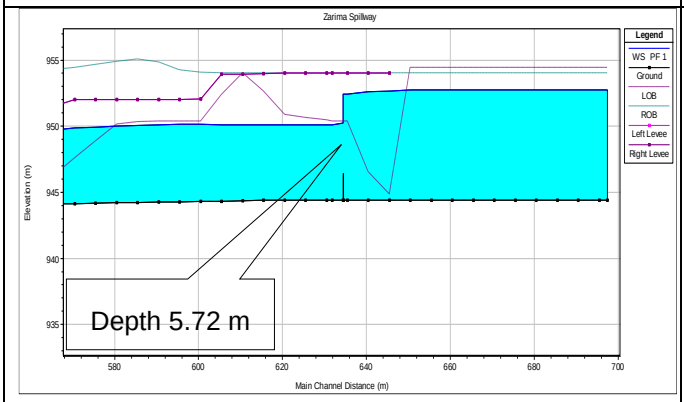

3 : 1D model result longitudinal profile over the spillway crest

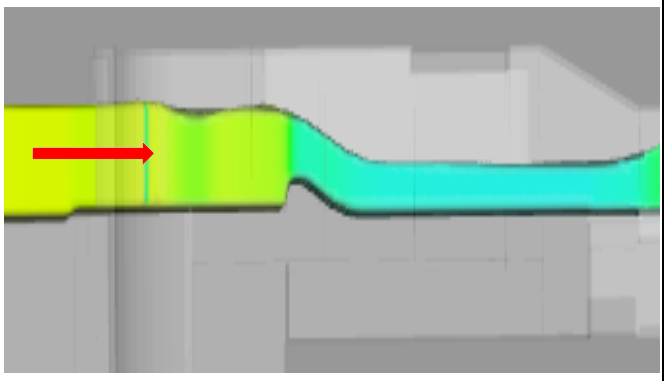

4 : 3D model result longitudinal profile over the spillway crest

Figure 4- 16 Over the spillway crest

Table 4- 3 shows the 3D model output from Figure 4- 16 section 2 was computed based on the results of the depth and velocity obtained across the spillway section.

Table 4- 3 Model Output Over the spillway Crest

	Average Depth	Maximum Flow Depth	Average Velocity
	m	m	m/s
	4.1	6.14	4.9
	4.38	6.31	5.01
	4.39	5.91	5.18
	4.1	5.82	5.47
	4.46	6.31	5.34
	3.8	5.78	6.18
Average	4.21	6.05	5.35

4.5.4 At the Toe of the spillway

There is no physical model data for flow depth at ch 0+620 of spillway toe. However, estimation was done during design. Figure 4- 17 section 1 shows the depth of flow: from design 2.5 m, from 1D 5.71 m, from 3D average 2.71 m and from 3D maximum depth 3.92 m. There is a difference of 8.4% between 3D and design. The flow profile of 1D did not capture the reality since the flow condition at the toe is supercritical and this is the limitation in 1D. On the other hand, 3D model captured the real flow profile. For further information refer Table 4- 9 and Annex A.

Water Surface Profile at the Spillway Toe ch 0+620

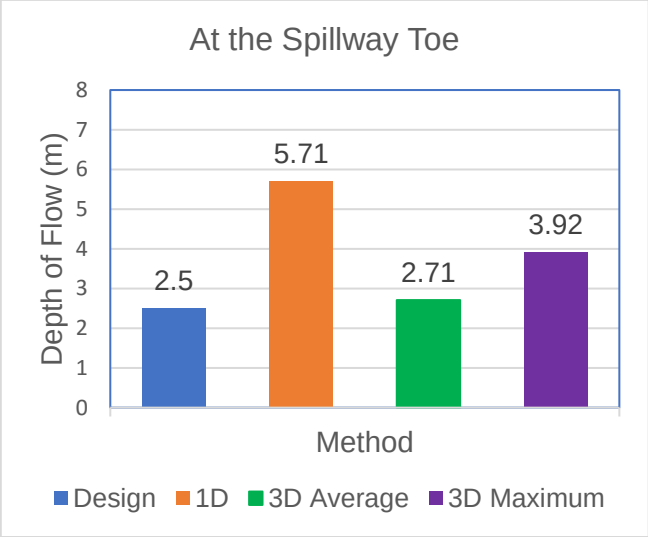

1 : Depth comparison

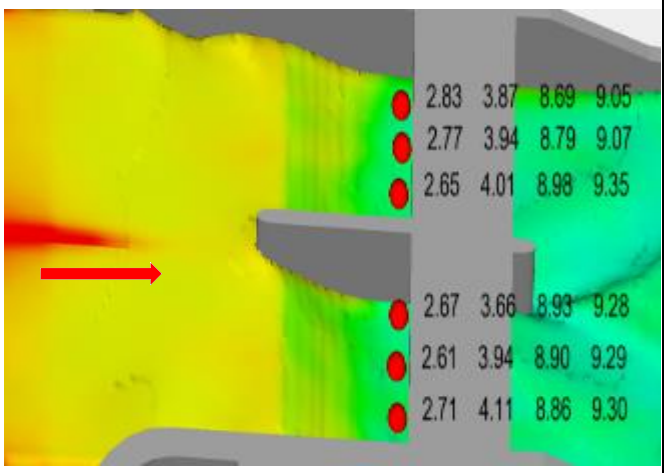

2 : 3D model result

Figure 4- 17 At the Spillway Toe

Table 4- 4 shows the 3D model output from Figure 4- 17 section 2 was computed based on the results of the depth and velocity obtained across the spillway section.

Table 4- 4 3D Model Output at the Spillway Toe

	Average Depth	Maximum Flow Depth	Average Velocity
	m	m	m/s
	2.83	3.87	8.69
	2.77	3.94	8.79
	2.65	4.01	8.98
	2.67	3.66	8.93
	2.61	3.94	8.9
	2.71	4.11	8.86
Average	2.71	3.92	8.86

4.5.5 At the End of Divide Wall

Figure 4- 18 section 1 shows depth of flow comparison at the end of divided wall and section 2 shows profile. Section 3 to 4 in both physical model and 3D numerical model shock wave was created which shows similarity between the two models. As per physical model result the pier on the ogee crest generates shock-waves that develop downstream in the channel and shows a typical oscillating transversal profile [47]. In 3D model an increase in depth of flow was observed due to hydraulic jump and reduced section of the chute. Similar observation has been seen in physical model. “the contraction of the flow due to the deflecting walls produces a back-water that extends upstream in the channel. For the higher discharges a transition from supercritical to subcritical flow with the formation of an oscillating (low-Froude number) hydraulic jump is observed. The hydraulic jump gradually moves upstream until reaching the toe of the ogee crest” [47].

On the other hand, no hydraulic jump and increase in depth was seen in 1D. The jump in 3D was contained in the proposed section of the chute after the toe of the spillway. The 1D model did not capture the flow pattern of the jump. 3D model properly captured the flow profile by showing the hydraulic jump. Table 4- 5 shows the 3D model output from Figure 4- 18 based on the results of the depth and velocity obtained across the spillway section. The percentage difference of flow depth between design and average 3D was 10.4%. No velocity was recorded from physical model. For further information refer Table 4- 9 and Annex A.

Water Surface Profile at the End of Divide Wall 0+590

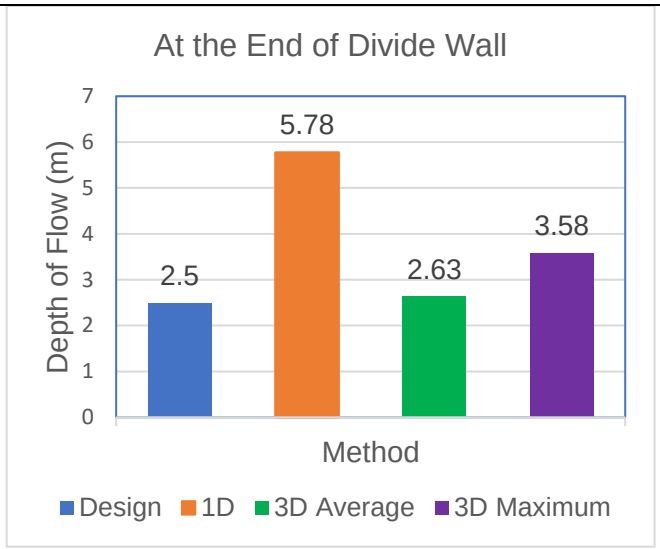

1 : Depth comparison

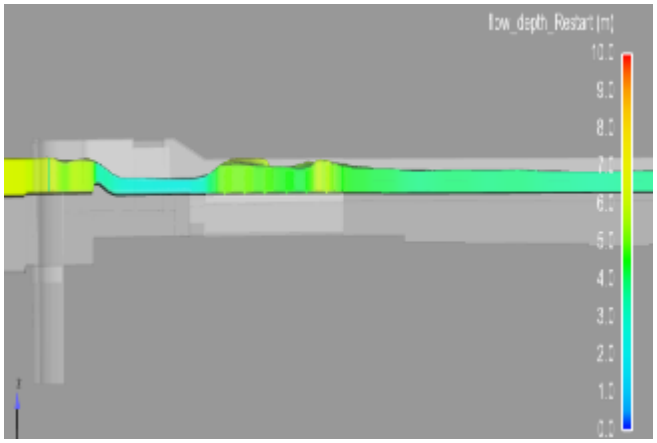

2 : 3D model flow profile

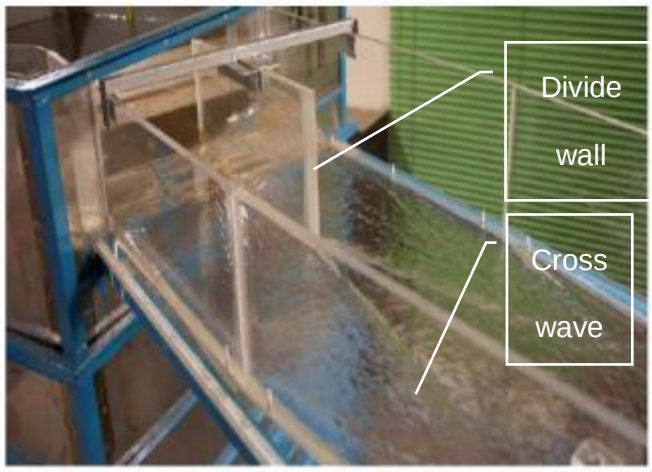

3 : Physical Scale model of Detail Shock – Waves [47]

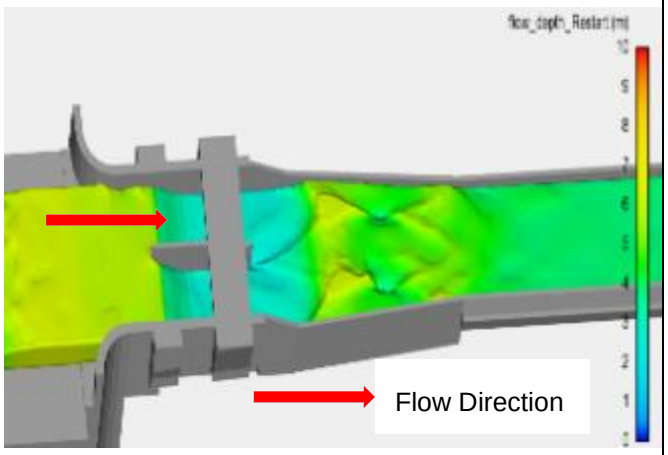

4 : 3D model of Detail Shock – Waves

Figure 4- 18 At the end of divide wall

Table 4- 5 Model Outputs at the End of Divide wall

	Average Depth	Maximum Flow Depth	Average Velocity
	m	m	m/s
	2.6	3.68	8.82
	2.69	3.81	8.79
	2.76	3.51	8.8
	2.41	3.31	8.97
	2.59	3.39	8.81
	2.73	3.75	8.72
Average	2.63	3.58	8.82

4.5.6 Beginning of Convergence

At the beginning of convergence, the hydraulic jump from the spillway ends at this section. There is no physical model result however there is design result. Figure 4- 19 section 1 shows the depth of flow: as per the design 2.39 m, 1D model 5.87 m, 3D model 5.64 m and 5.72 m for both average and maximum flow depths. The design depth cannot show the increased in depth due to convergence hence, it showed low depth of flow than 1D and 3D model.

As per the 3D model, flow was increased at the central part of the channel and 1D cannot show flow across the channel section. As a result, overtopping was observed in 1D but not in 3D. Figure 4- 19 section 2 shows the 3D model output. In FLOW-3D, the depth of flow was increased at the central part of the channel and decreased close to the walls. Basically, the cause of the difference in depth is that, the channel section is changed from the larger section to narrower section. Thus, middle portion of the channel was congested with the flow. Due to convergence at downstream, the water

depth was also raised and this flow condition was seen in both 1D and 3D model. However, 1D numerical model showed as if there is overtopping but not in 3D since the increased in depth was only at the center of the channel.

Since the 1D model for this section showed overflow, adjustment was done in the section of the channel during research. Before modification of the section and after the modified section in the profile was shown in Figure 4- 8 and Figure 4-9. In 3D model, the depth of flow in central portion of the channel increased but near to the walls not. Hence, no overflow was seen.

Overall, both 1D and 3D models agree for the depth of flow and 3.92% difference between 3D and 1D model and 27.39% difference in velocity. However, the 3D model has the ability to show the actual flow behaviour by showing its profile and the results can be obtained at different level and location across the spillway section. For further information refer Table 4- 9, Table 4- 10 and Annex A.

Water Surface Profile Before Convergence at ch 0+585

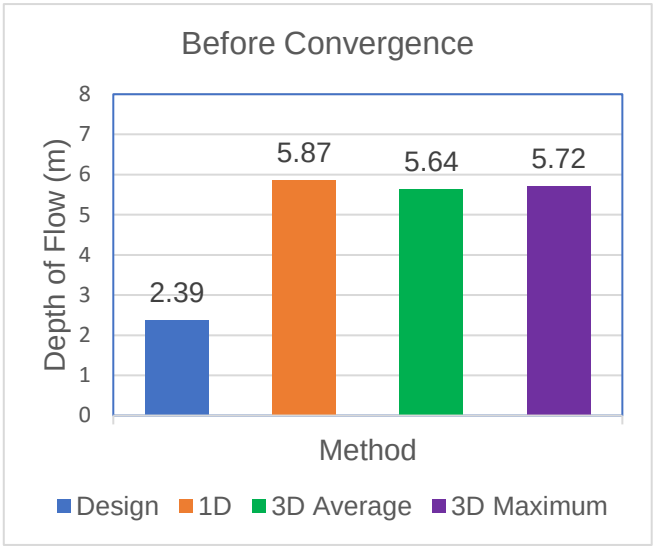

1 : Depth comparison

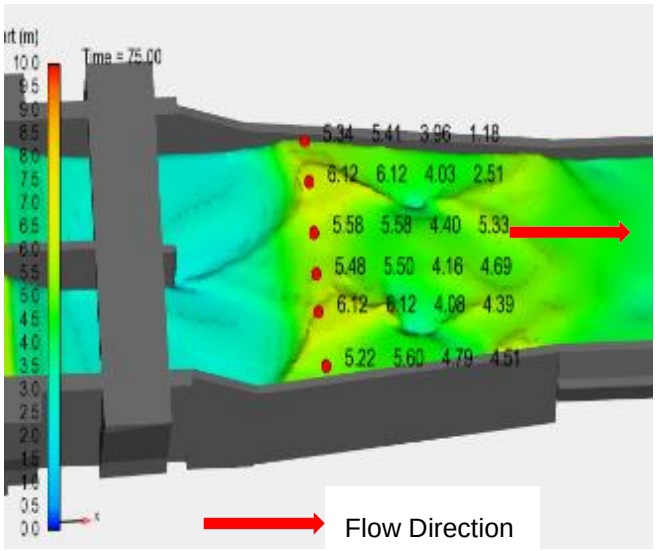

2 : 3D model result

Figure 4- 19 Before Convergence

Table 4- 6 shows the 3D model output from Figure 4- 19 section 2 was computed based on the results of the depth and velocity obtained across the spillway section.

Table 4- 6 Model Output Before Convergence

	Average Depth	Maximum Depth	Average Velocity	Velocity at Final Simulation
	m	m	m/s	m/s
	5.34	5.41	3.96	1.18
	6.12	6.12	4.03	2.51
	5.58	5.58	4.04	5.33
	5.48	5.5	4.16	4.69
	6.12	6.12	4.08	4.39
	5.22	5.6	4.79	4.51
Average	5.64	5.72	4.18	3.77

4.5.7 End of Convergence

Figure 4- 20 section 1 and section 2 show depth of flow comparison and 3D model result at the end of convergence. The following were the flow depths from the design 3.6 m, from 1D 4.5 m, from 3D average 5.06 m and from 3D maximum 5.6 m respectively. There was 12.44% difference between 3D and 1D model and 24.43% difference in velocity. Table 4- 7 shows the 3D model output from Figure 4- 20 section 2 was computed based on the results of the flow depth and velocity obtained across the spillway section. For further information refer Table 4- 9, Table 4- 10 and Annex A.

Water Surface Profile End of Convergence at ch 0+575

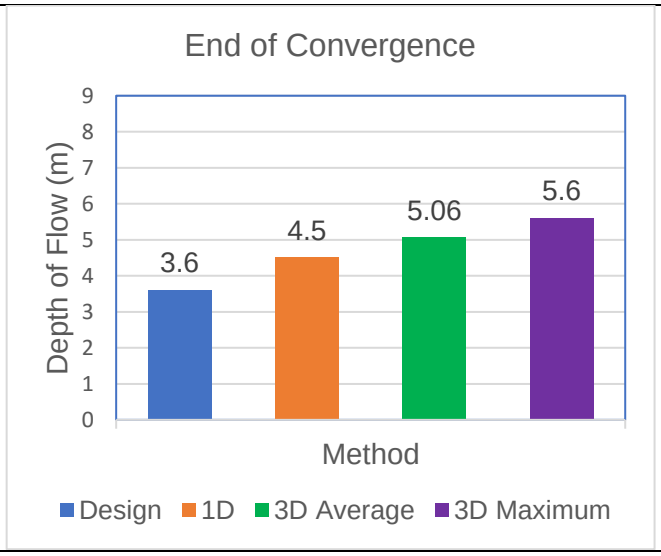

1 : Depth comparison

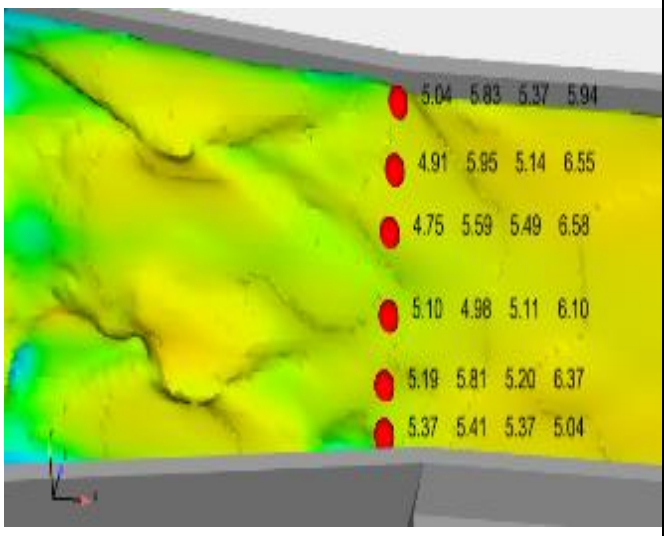

2 : 3D model result

Figure 4- 20 End of Convergence

Table 4- 7 3D Model Output at the End of Convergence

	Average Depth	Maximum Flow Depth	Average Velocity
	m	m	m/s
	5.04	5.83	5.37
	4.91	5.95	5.14
	4.75	5.59	5.49
	5.1	4.98	5.11
	5.19	5.81	5.2
	5.37	5.41	5.37
Average	5.06	5.6	5.28

4.5.8 Along the Chute Channel

There is no physical model result but there is design result. In this section compared to other sections of the spillway, it has uniform section and the flow depths were more or less uniform across the chute channel. Figure 4- 21 section 1 shows the depth of flow: as per the design 3.25 m, 1D model 4.38 m, 3D model average 3.6 m and, 3D model maximum 3.69 m. Section 2 also shows the velocity comparison. There was 2.15% percentage difference of flow depth between the design and 3D model output and 15.03% difference in velocity. For further information refer Table 4- 9, Table 4- 10 and Annex A.

Water Surface Profile Along the Chute Channel at ch 0+475

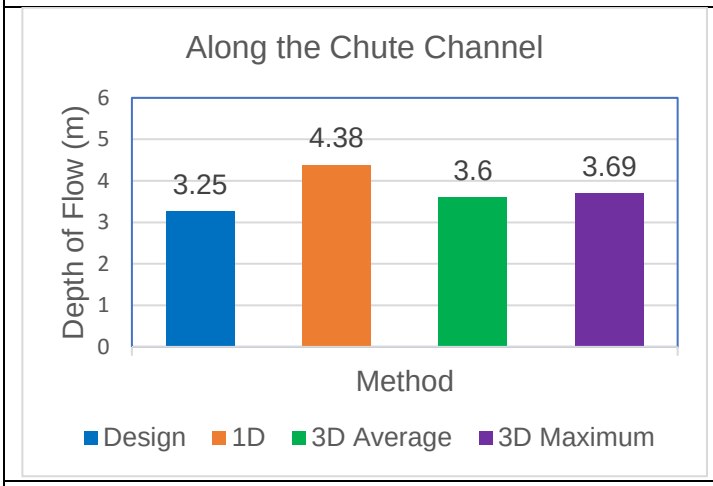

1: Depth comparison

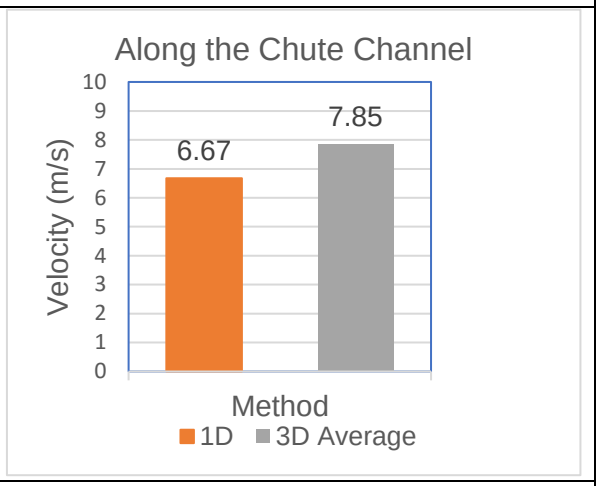

2: Velocity comparison

3 : 3D model result

Figure 4- 21 Along the Chute Channel

4.5.9 Before Bend

In this section there is a physical model result for depth of flow. Accordingly, Figure 4-22 section 1 to 4 shows the flow depths as follows: for physical model 6.24 m, 1D model 4.85 m, for 3D average 6.16 m and 6.2 m for maximum. The 3D model flow depth is by 1% differ from the physical model. As per the physical model, the maximum

water depth in the spillway chute channel occurs just upstream of the deflecting walls where the flow enters the bend. This agrees with the numerical model result. On the other hand, 1D model did not properly capture the depth of the flow since there is sudden change in hydraulic section. However, the difference in depth of flow for 1D model is not much exaggerated from the physical and 3D model. The percentage difference in velocity between 3D model and 1D was 11.34%. Figure 4- 22 shows detail information. For further information refer Table 4- 8, Table 4- 9, Table 4- 10 and Annex A.

Water Surface Profile Before Bend at ch 0+390

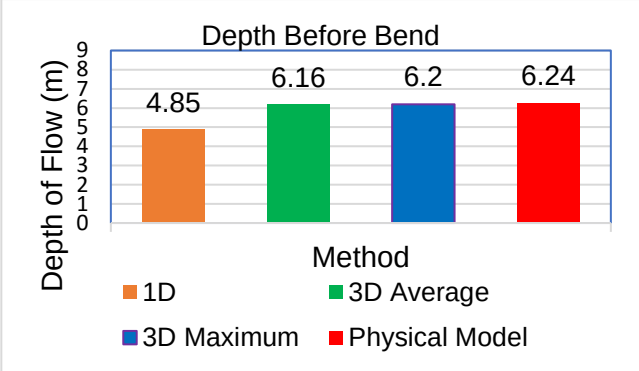

1 : Depth comparison

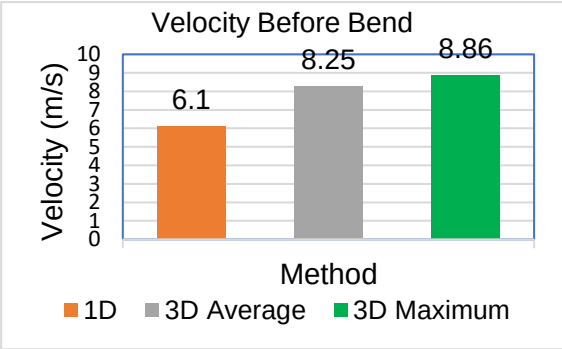

2 : Velocity comparison

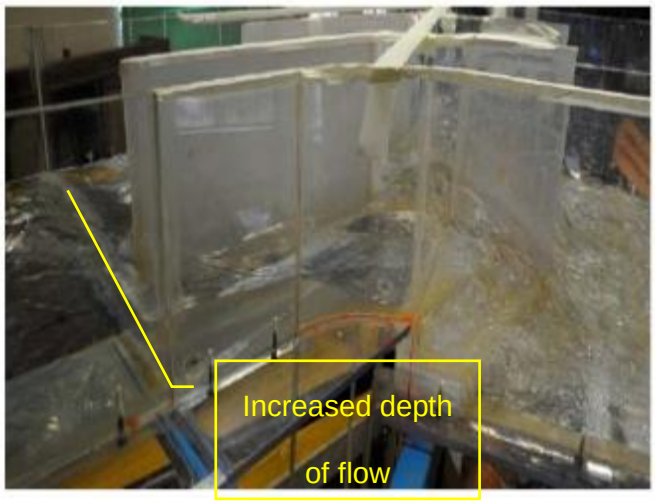

3 : Physical scale model, flow characteristics [47]

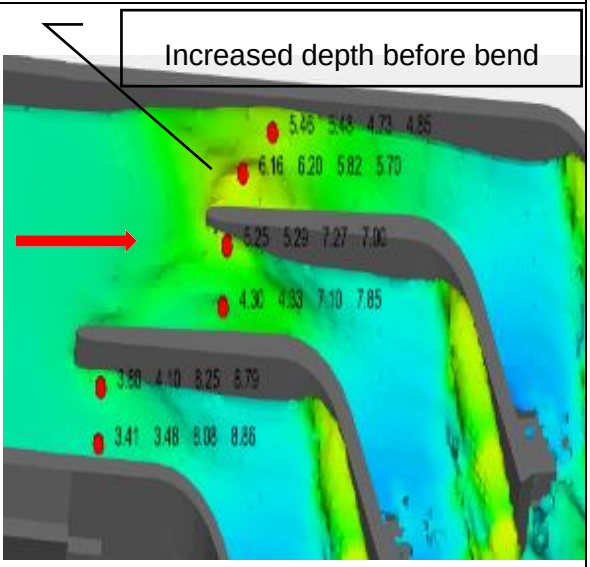

4 : 3D model result

Figure 4- 22 Before Bend

4.5.10 Along Channel Bend

Difficulty in the design arises because of the complexity of the flow around a curved path that is not readily subject to any analytical solutions. Hence it was not possible to predict the depth of flow at the bend. As per the design to reduce the superelevation,

guide walls are proposed. In the design report, the depth of flow along the bend is not mentioned. However, during research, the required superelevation was checked with USACE [51]. Accordingly, because of superelevation, the outer wall requires 8 m height. This shows that the provided 6 m wall height is not sufficient. For details refer Annex A.

Although there is no measured data from physical model, different information was given by stating the depth of flow is lower than 6.24 m. In addition, picture was also cross checked with the 3D numerical model. In the curved region there are two guide walls. The purpose of these walls is to reduce the superelevation of the flow.

Along the bend the provided channel depth is 6 m. As it is mentioned above the design report stated that the depth of flow at bend is lower than the depth of flow before the bend that is lower than 6.24 m. As per the numerical model the superelevation was significantly high enough for overtopping in both deflecting walls as well as the outer wall. On the other hand, this was not seen in the physical model. This difference in physical model could be due to the scale effect. 1D numerical model has a limitation to identify flow in a complex structure like superelevation flow in curved section. However, the 3D numerical model has the ability to show the flow pattern in a complex hydraulic structure.

Figure 4- 23 section 1 to 4 shows the flow depths as follows: from design 7.76 m, from 1D 1.52 m, from 3D average 6.06 m and from 3D maximum 6.97 m and from the physical model 6.18 m. This shows that there was 1.94% difference between the 3D

model and physical model and 21.97% difference in velocity between design and 3D model. The 3D model can show the flow conditions in detail in a complex structure. As per the result of the 3D model, the spillway at this location is not safe and it requires the outer part of the wall to be raised by 2 m. For further information refer Table 4- 8, Table 4- 9, Table 4- 10 and Annex A.

Figure 4- 23 section 5 and 6 shows drops are provided at an angle towards the center of the channel to reduce the flow separation and to distribute along the cross section of the channel before it passes the baffle blocks. From the 3D numerical model simulation result, there was still separation of flow but not seen in 1D. However, drops provided at angle towards the center of the channel blocks played a significant role to reduce flow separation and distribute along the cross section of the channel which agreed with the result of physical model.

Finally, the deflecting walls made good performance to reduce the superelevation flow. Similarly, inclined drops distribute the flow across the chute cross section before it passes through the baffle blocks.

Water Surface Profile Along the Bend at ch 0+375

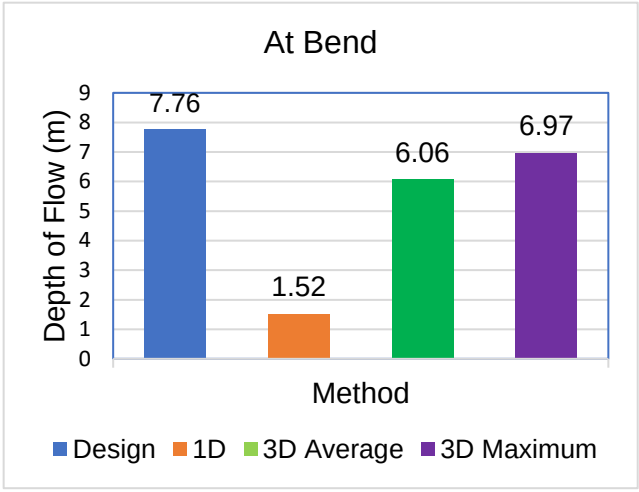

1: Depth comparison

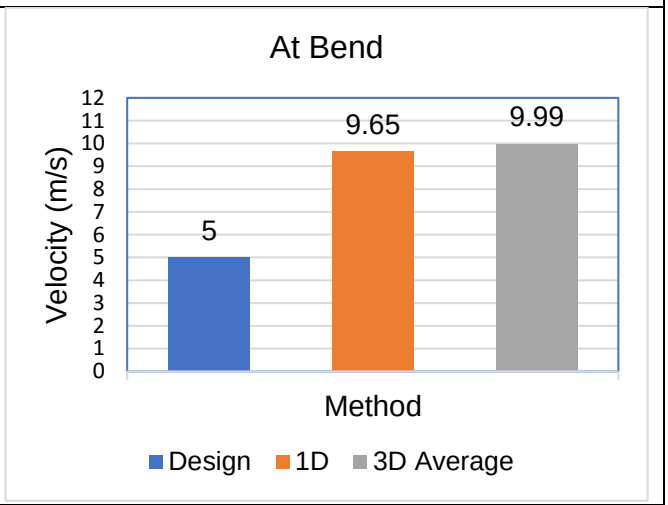

2: Velocity comparison

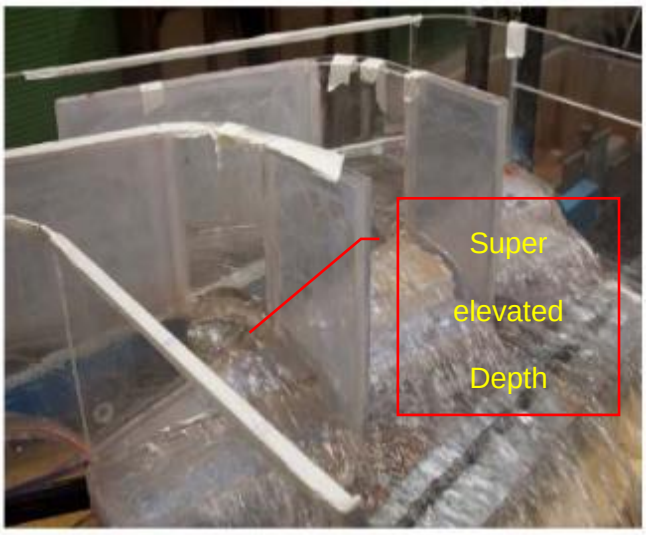

3: Physical Scale Model flow characteristics [47]

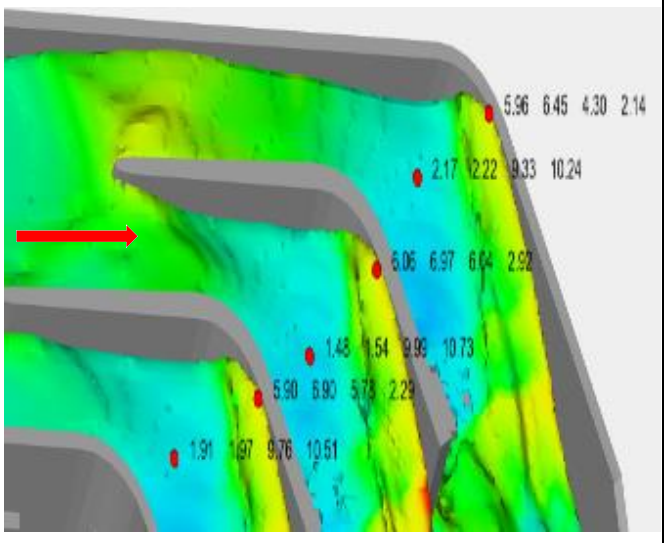

4: 3D model result

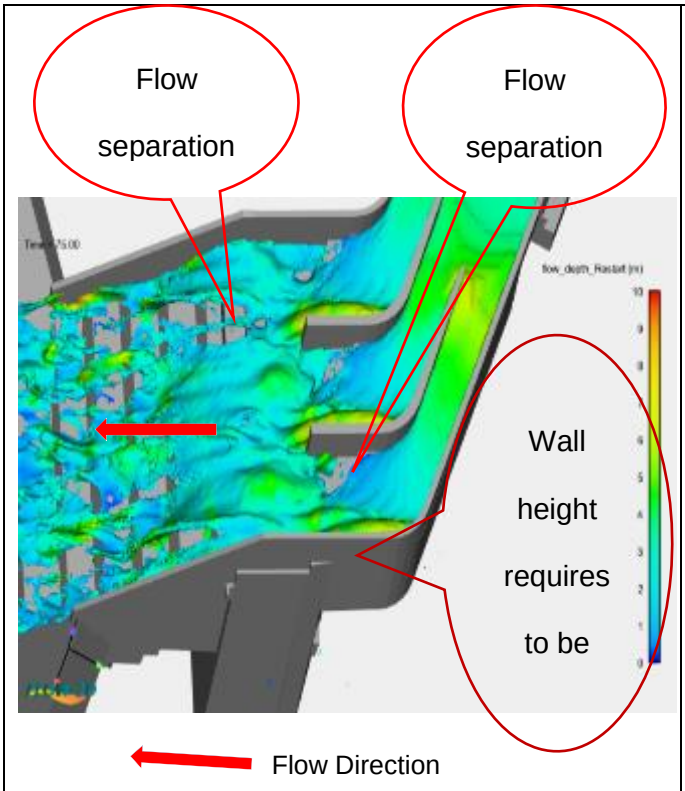

5 : 3D model result for flow separation

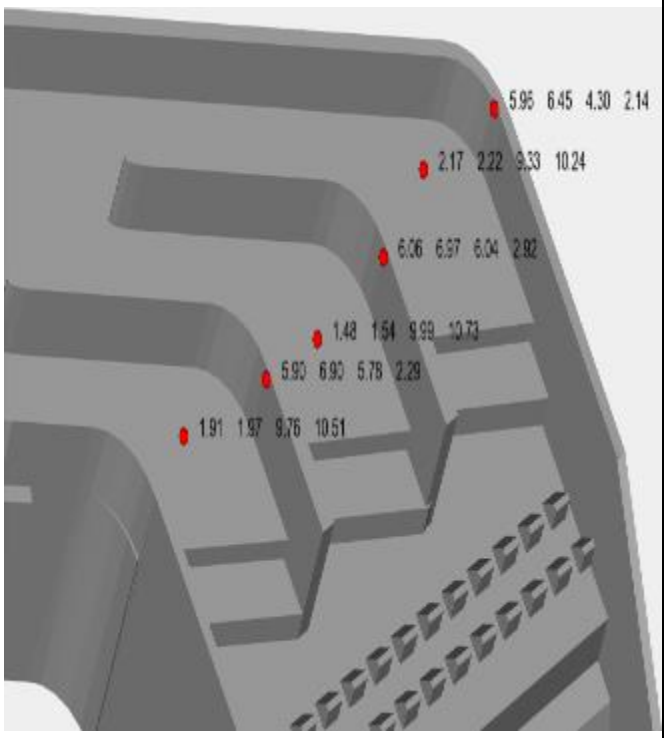

6 : 3D model result with channel detail

Figure 4- 23 Along Bend

4.5.11 At Baffles

The flow depths were for 1D model 5.14 m, for 3D average 4.35 m. Thus, 3D model showed the required depth of channel proposed by design was sufficient. Figure 4- 24 section 2 to 4 shows detail information.

The flow exiting the bend exhibits plunging jets at the baffles which is also shown in the physical model. Meanwhile the drops inclined towards the center serves a significant role to distribute the flow across the width of the channel and to reduce flow separations.

After the bend, there are two rows of baffle blocks and these baffles significantly dissipate the flow energy and made flow distribution in the section of the cascade drops. This flow condition was also seen in physical model however there is no measured data.

To confirm the performance of the baffles, in 3D model, data was taken before and after the baffles. Accordingly, from 1.6 m average depth of flow before baffles to 4.2 m depth of flow after baffles of hydraulic jump was observed. This shows that the baffles dissipated the energy of the flow and it was contained in the channel section. Meanwhile, baffles were also distributed the flow across the channel [52].

Water Surface Profile at Baffles ch 0+372

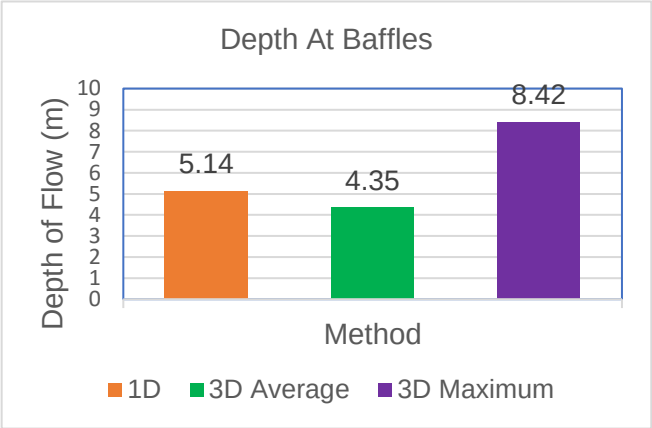

1 : Depth comparison

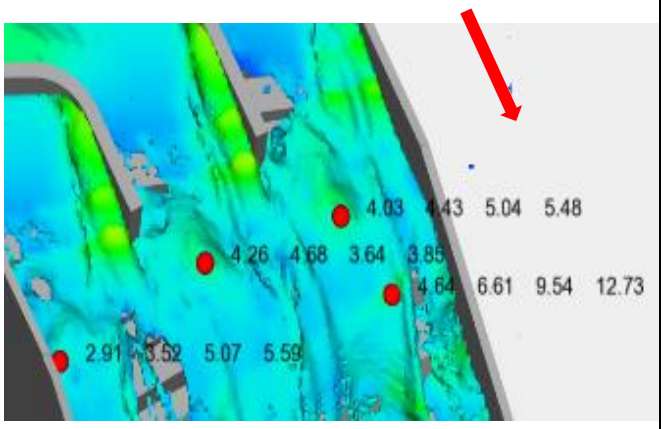

2 : 3D model result after the Baffles

3: Physical scale model flow characteristics [47]

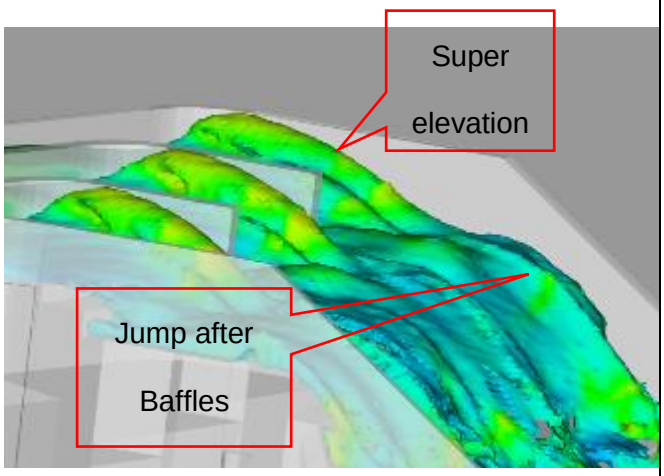

4: 3D model result for superelevation and jump

Figure 4- 24 At Baffles

4.5.12 Along Cascade

The grade of the chute, progressively decreases from initial 45 degrees at the entrance to approximately 30 degrees near the toe. Flow in the cascade steps started with

aerated flow due to flow separation created by the three chambers and two rows of baffle blocks on the entrance of the cascade. Such condition has direct impact on the transition flow from skimming to nape flow. Hence, there was no point of inception and no none aerated flow region. Thus, flow in the cascade drops was nape flow which agrees with the physical model result.

Figure 4- 25 section 5 to 7 shows the 3D numerical model simulation result, due to hydraulic jump, the first three portion of the drops has no role in dissipating the energy since they are under the trajectory flow. This jump agrees with physical model result. Starting from the first three drops, nape flow was seen however separation of flow continues splash due to water fall. Nape flow existed till the end of the cascade channel and at the last portion of the cascade, the slope of the cascade drops decreases, and the flow of water flows nearly covering the whole section of the channel bed.

Along the steeped drops, the numerical model and the physical model have comparable results. The water spreads randomly along the entire width of the channel and there were void spaces in the channel bed width along the cascade drops which was also seen in the physical model.

The cascade channel bed width was not fully covered by flowing water. Figure 4- 25 section 1 and 2 show the flow depth result for 1D was 1.07 m, 3D average and maximum were 1.9 m and 7.55 m. Similarly, the velocity for 1D was 13.56 m/s, 3D average was 17.14 m/s. The provided depth of channel was sufficient even for 3D maximum flow depth since as per the design, 10 m depth of channel is given.

Overtopping was not seen in the trapezoidal section. However, as per the result of the 3D model, the width of the cascade drops could have been reduced to reduce the cost for construction. The velocity close to the outlet was reduced so as not to cause scoring. For further information refer Table 4- 9.

The flow depth was contained in the section of cascade drops. The potential energy of the water was dissipated with successive drops with the process of turbulence which spread the water depth from the average 6 m to less than 1.5 m. When it reached at the end of the cascade, it joined the river water. During the research time, it was difficult to get the rating curve of the river. However, as per the 3D numerical result 8 m depth of water is required for proper termination of the flow or it requires to lower the outlet by 8 m to create pool for dissipation of the energy. With this, the energy was fully dissipated and the velocity is reduced, hence there will not be a scoring problem at the outlet. Figure 4- 25 shows detail flow in the cascade.

Water Surface Profile Along Cascade

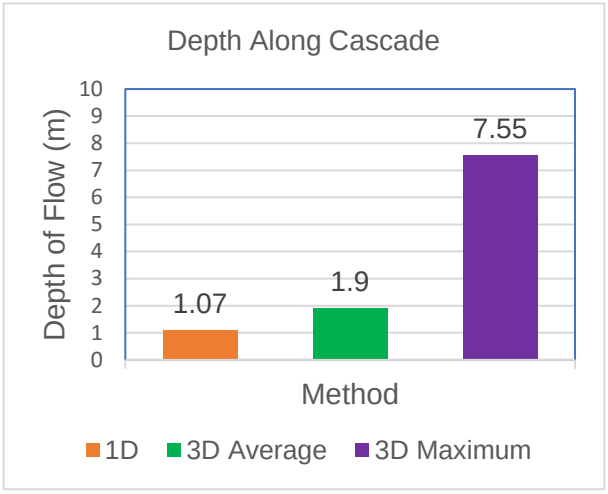

1 : Depth comparison

2 : Physical model along stepped chute [47]

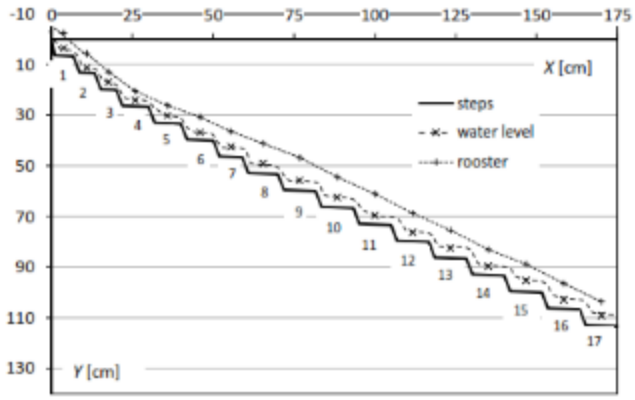

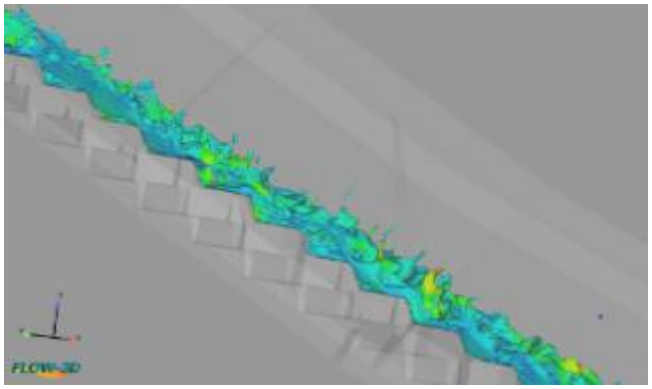

3: Nappe flow and rooster profile in the upper segment of the stepped chute [47].

4: 3D model result for nappe flow and rooster profile in the upper segment of the stepped chute.

Water Surface Profile Along Cascade

5 : Physical model for nappe flow and rooster profile in the upper segment of the stepped chute [47]

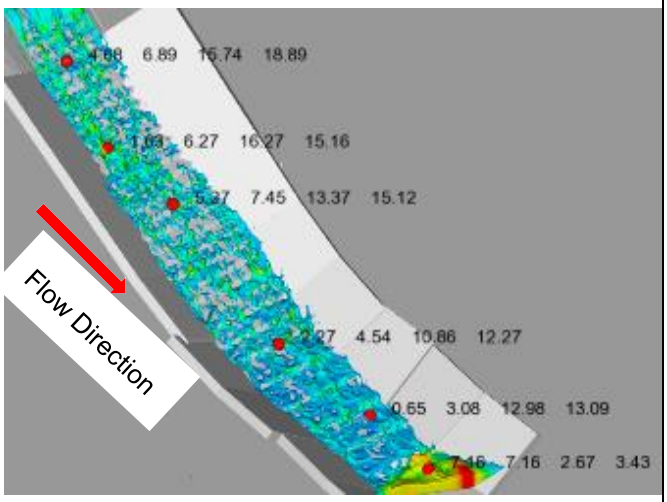

6 : 3D model result

Figure 4- 25 Along Cascade

The following Table 4- 8 to Table 4- 10 gives the summary results showing the performance indicators and percentage difference of physical mode, 3D and design or depth of flow and velocity comparisons. For additional information see Annex A.

Table 4- 8 Zarema May Day Dam performance indicators 3D with Physical Model for flow depth

Measurement Location	Depth of flow from 3D model (m)	Depth of flow from Physical Model (m)	Percentage difference (%)
At the Crest of Spillway	4.460	4.880	-8.610
Before Bend	6.160	6.240	-1.300
At Bend	6.060	6.180	-1.940
Sum	16.680	17.300	
Average	5.560	5.767	
	R^2 =	0.9998	
	NSCE =	0.833	
	Rbias =	-3.584%	

Table 4- 9 Zarema May Day Dam performance indicators 3D with Design for flow depth

Measurement Location	Depth of flow from 3D model (m)	Depth of flow from Design or 1D or physical model (m)	Percentage difference (%)
At Approach channel	5.94	5.4	10
At the Crest of Spillway	4.21	4.88	-13.73
At the Spillway Toe	2.71	2.5	8.4
At the End of Divide Wall	2.76	2.5	10.4
Before Convergence	5.64	5.87	-3.92
End of Convergence	5.06	4.5	12.44
Along the Chute Channel	3.32	3.25	2.15
Before Bend	6.16	6.24	-1.28
At Bend	6.06	7.76	-21.91
Along Cascade	7.55	8	-5.63
Sum	49.41	50.9	
Average	4.941	5.09	
	R^2 =	0.904	
	NSCE =	0.871	
	Rbias =	-2.77%	

Table 4- 10 Zarema May Day Dam performance indicators 3D with Design for flow velocity

Measurement Location	Velocity of flow from 3D model (m/s)	Velocity of flow from Design or 1D model (m/s)	Percentage difference (%)
At Approach channel	3.81	3.4	10.76
At the Crest of Spillway	5.35	4.1	23.36
Before Convergence	5.44	3.95	27.39
End of Convergence	5.28	6.57	-24.43
Along the Chute Channel	7.85	6.67	15.03
Before Bend	6.88	6.1	11.34
At Bend	7.53	9.65	-28.15
Sum	42.14	40.44	
Average	6.02	5.777	
	R^2 =	0.698	
	NSCE =	0.573	
	Rbias =	4.204%	

4.6 CONCLUSIONS AND RECOMMENDATIONS

4.6.1 Conclusions

Open channel flow in a complex hydraulic structure is difficult to predict the flow behaviour in 1D or 2D model. Such flow conditions in a constricted cross sections, bends and cascade flows need to be verified by at least 3D hydrodynamic numerical model. Understanding the flow condition in a complex hydraulic structure is of great importance for the designers and decision making. Physical modelling is a tool to validate the numerical modelling to understand the flow condition along the hydraulic structure. This dissertation is focused on study and validation of FLOW-3D finite volume numerical model for three dimensional flows on Zarema May Day Dam spillway based on the physical model result and design result. The concluding remarks for the dissertation are as follow:

This research confirmed that the FLOW-3D model based hydraulic analysis of spillway has a good agreement with the physical model result. In addition, based on the physical model output the provided section for the spillway agrees with the 3D numerical model result. The model shows the overall performance of the spillway system for complex hydraulic section in supercritical flow condition. The comparison of the results at the channel bend showed that the numerical solution can well predict the superelevation.

The performance indicator of flow depth comparison between 3D model result and physical model result are as follow: R^2= 0.9998, NSCE = 0.833 and Rbias =-3.584%. The performance indicator of flow depth comparison between 3D model result and design results are as follow: R^2= 0.902, NSCE = 0.860 and Rbias = -0.804%. For detail information, refer Annex A.

From above results FLOW-3D model has very good agreement with the physical model result and the design results. Thus, FLOW-3D can well predict the flow behaviour in a complex hydraulic section and also different information can be obtained from the model.

The drawback of the model is the simulation time. When there is a complex and void space it will take few days. The simulation time will be reduced when high capacity of computer involved.

Due to the development of science and technology, the emerging of the 3D numerical model is one of the base lines for the design of the complex hydraulic structures that can operate safely. Modelling flow in a complex geometry using the state- of- art of 3D numerical model will enhance recognizing the complex hydrodynamic flow conditions and its velocity distribution, depth variation, energy dissipation, etc. This will enable the engineers to provide the required section and sufficient energy dissipation. Therefore, for a complex flow structure the design or verification must be done with at least 3D numerical model.

4.6.2 Recommendations

It is a significant technological development to use 3D hydrodynamic numerical model for design of complex hydraulic structures. Flow condition at the curve or complex section cannot be seen by 1D numerical model. Therefore, any complex hydraulic structure design such as spillway of the dam requires to be verified with 3D hydrodynamic model or physical model. In addition, 3D hydrodynamic modelling helps for the designers to improve the hydraulic performance of existing or new hydraulic structures.

During research the result of the physical model for Zarema May Day Dam spillway was very scarce. Detail result must be seen at the divide wall, chute channel, along bend and cascade. The data have to be in detail along and across the channel sections. Therefore, it is recommended that at the above locations physical model measurement are required to be conducted.

CHAPTER FIVE

5 3D HYDRODYNAMIC MODELLING ENHANCES THE DESIGN OF TENDAHO DAM SPILLWAY, ETHIOPIA

This paper has been published on line and is currently available on Water 2019, 11(1), 82; https://doi.org/10.3390/w11010082, Published: 4 January 2019.

5.1 INTRODUCTION

Water is the world's most important natural resource; however, it is estimated that by 2030, the world is projected to face a 40% global water deficit. Research development and modern technology enhances and provide an improved and optimized hydraulic structures for water resource projects worldwide [53].

In Ethiopia, large scale water resources development is at its beginning stage. Currently large-scale projects such as Tendaho Dam, Kesem Dam, Gidabo Dam, Ribb Dam, Megech Dam, Welkait (Zarima May Day) Dam, Kuraz Barrage, Jema Dam, Gigel Abbay Dam, Gibe 1 Dam, Gibe 3 Dam, Renaissance Dam, Upper Guder Dam, etc are under design, under construction or recently constructed. Huge water resource development projects such as the aforementioned have a significant impact on the country's economy; hence, the successful implementation of water resource projects require special attention from envision to completion. Therefore, proper design and analysis of the hydraulics structures is essential [54].

Tendaho dam and appurtenant structures were designed and constructed in 2008 in Ethiopia. The spillway was designed based on Indian Standards [55], [56] and [57] which is similar to USBR. However, the design safety for its operation has not been confirmed either with physical model or 3D numerical model. The estimated design inflow discharge into reservoir is 3,042 m^3/s [58] and in 2011, there was an inflow discharge of 2,100 m^3/s and the water spilled accordingly. The designed flow depth over the spillway crest is 9.2 m and during this flood time, 5.5 m depth of water passed over the spillway crest. At the time of flooding, the gates were not installed. The flow of water leaving the stilling basin and entering the Downstream Channel had high velocity and wavy since the water in the stilling basin was not properly dissipated.

In addition, the flow had superelvation at the bend and due to this superelevation, the water overtopped the spillway channel in the outer side of the bend and entered to Main Canal at a location where the spillway channel cross over the Main Canal. Because of this problem there was significant losses occurred in the Main Canal.

3D hydrodynamic numerical modelling of the spillway was carried out for Tendaho Dam, Ethiopia, which is constructed with a routed half PMF (Probable Maximum Flood) design flow rate of 1,700 m^3/s. The routed hydrograph is characterized by the attenuation of flood peak of the inflow hydrograph. The design results were compared with FLOW-3D model results. As per the result, redesign of the hydraulic section at stilling basin was proposed and verified with the 3D numerical model.

Using 3D hydrodynamic model, Tendaho Spillway hydraulic performance was assessed and it is found stilling basin is inadequate. Because of this inadequacy the flood in 2011 created huge loses. It is recommended that the spillway bed level must be lowered by at least 15 m.

5.2 BACKGROUND

Tendaho dam is constructed across the river Awash, nearly 7 km upstream of its confluence with Logia tributary. The location of the dam is Latitude 11.30 (North), Longitude 41.00 (East). Figure 5- 1, Plate 5- 1 and Figure 5- 2 show the Location of Tendaho Dam. The dam site lies across a gap in rock ridge adjacent to and immediately east of the present Addis Ababa-Assab highway. The dam is as an earth dam with impervious clay core [59].

Tendaho dam is a part of Tendaho Dam & Irrigation Project, which aims at harnessing the inflows of River Awash at Tendaho for irrigating sugarcane plantation in an area of about 60,000 hectares. The project has sugar factory and it has target production of five hundred thousand tons of sugar per annum, as part of development of Lower Awash Valley [60].

Tendaho Dam spillway structure comprises an approach channel leading the water to the control structure, a control structure and an inclined chute terminating into a stilling basin. Energy dissipation is by means of the hydraulic jump forming in the

stilling basin [61]. A dentated sill is provided at the end of stilling basin to facilitate formation of the hydraulic jump for a large range of discharge passing over the control structure. After the dissipation of energy in the stilling basin, the flow will be conveyed back to the river through an outlet channel (Downstream Discharge Channel). After the stilling basin, the Downstream Discharge Channel has a bend with deflection of 68^0. Just downstream of the bend, the Downstream Discharge Channel crosses over the Main Canal at chainage ch 0+390 m.

The bend along the Downstream Discharge Channel represents the key element of the spillway design. Difficulty in the design arises because of the complexity of the flow around a curved path, which is not readily subject to analytical solutions [62].

The downstream channel was constructed with cemented stone pitching and concrete blocks for 110 m downstream of the stilling basin. it is unlined channel after it cross the Main Canal until it joins River Awash.

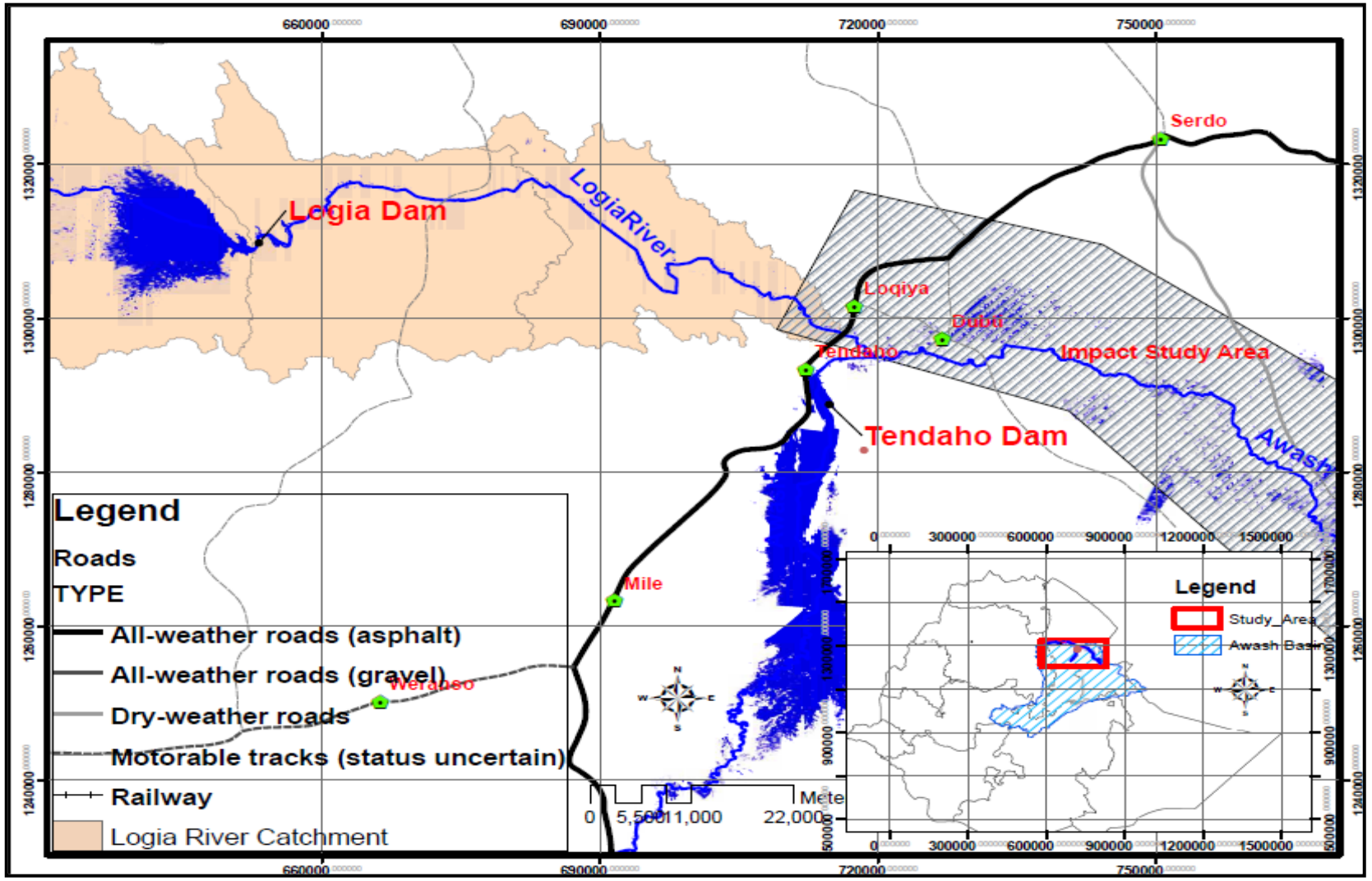

Figure 5- 1 Location of Tendaho Dam [63]

Plate 5- 1 Tendaho Spillway Image

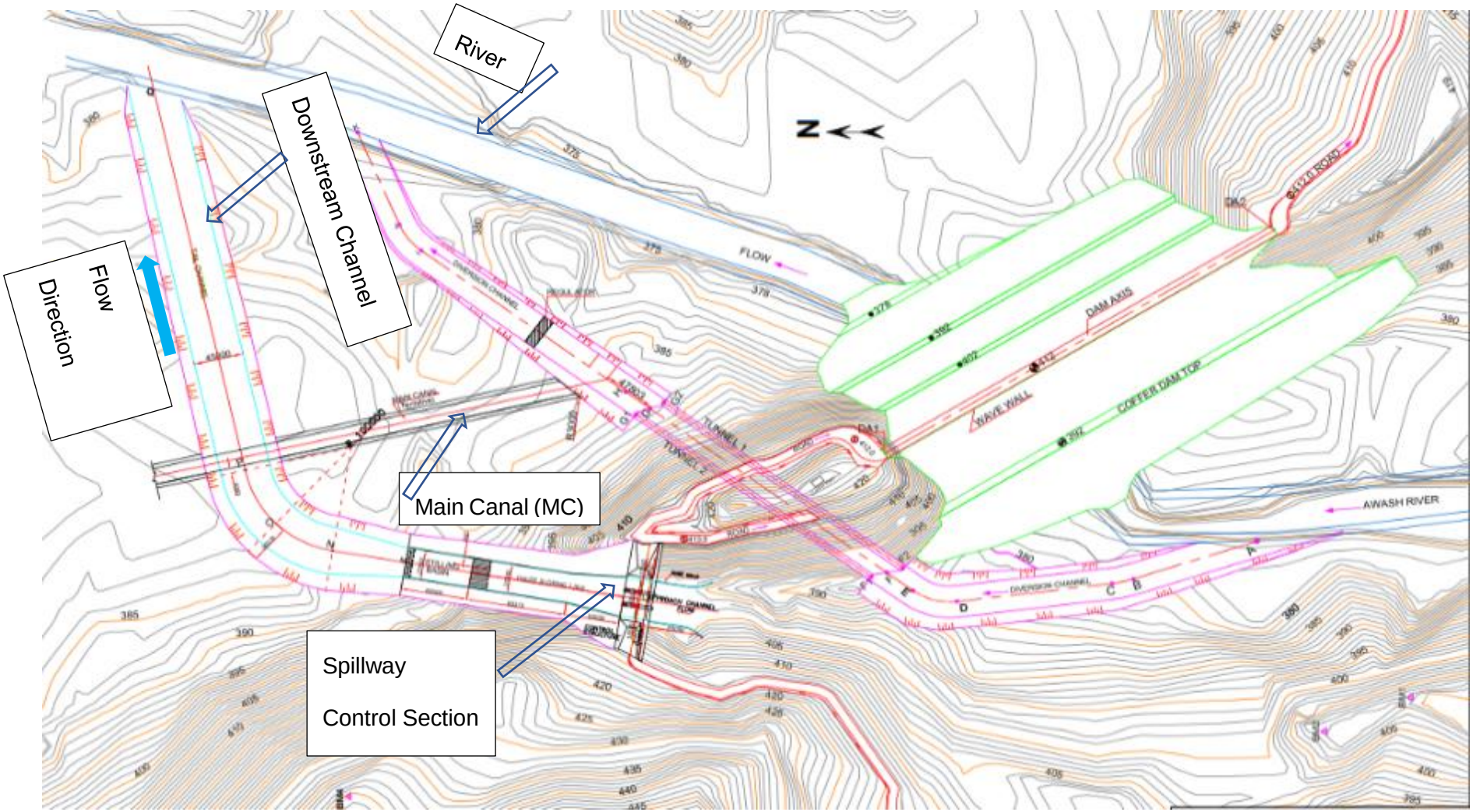

Figure 5- 2 Spillway and Dam Layout Plan [64].

5.3 STATEMENT OF THE PROBLEM

Currently in Ethiopia large-scale projects are under design, under construction or recently constructed. Spillway is among the most important structures of a dam project for effective disposal of the surplus water from the reservoir to the channel downstream to ensure the safety of the project. However, most of the recently designed and constructed spillways or complex hydraulic structures are not verified with either physical model or 3D hydrodynamic numerical models. Such gap made serious problem like Tendaho Dam Spillway.

During the flood time in Tendaho Dam Spillway, the concrete blocks and stone pitching were taken away by the flood. In addition, the flow had superelvation at the bend and due to this superelevation, the water overtopped the spillway channel and entered to the Main Canal at a location where the spillway channel cross over the Main Canal. Because of this problem there was significant losses occurred in the Main Canal. The researcher had an opportunity to see the problem while it was occurring, and this problem inspired him to conduct research to investigating the hydraulic problems and propose solutions. In addition, the maintenance work after the problem was carried out based on the original design which shows that still the spillway is in danger of being unsafe. The following Plate 5- 2 was taken at the spillway during flood.

Meanwhile, in Ethiopia there are many dam projects which are planned to be constructed in the future. However, there is no standard for the design methodology to be followed for verification of complex hydraulic structures before construction.

Most of the complicated hydraulic structures cannot be modelled and analysed comprehensively by mathematical models alone using common 1 or 2- dimensional hydraulic model such as HEC RAS. Since 1D or 2D has no accuracy in:

- Areas of rapid acceleration or deceleration, where the assumption of a hydrostatic pressure distribution is no longer valid,
- Areas of large turbulence and/or energy loss, and large change in cross-section
- Supercritical flow, for which both discharge and water level are controlled by the upstream boundary.
- Shallow water equations implying that vertical velocities are negligible, additional limitations such as viscous shear stresses.
- Viscosity calculations which is particularly vulnerable to ‘water column’ effects when the vertical length scale approaches or exceeds the horizontal scale.

Tendaho Spillway	
	
1: Reservoir	2: Approach Channel
	
3: Flow over the spillway and Stilling Basin	4: Flow along the chute
	
5: Flow after Stilling Basin	6: Flow after Stilling Basin

Plate 5- 2 Tendaho Spillway during Spillway operation

The following Plate 5- 3 was taken at the spillway during flood which shows damages along the Main Canal.

Loss Occurred After Flood

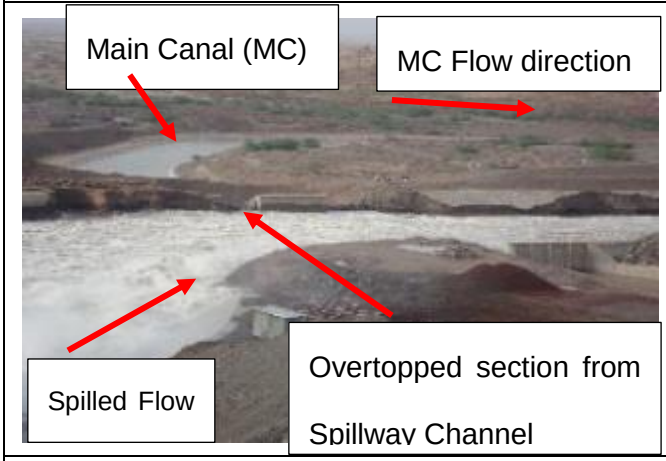

1: Overtopped at Spillway Channel in to MC

2: Canal Breach at Main Canal (MC)

3: Structure Failed in MC

4 : Canal Breach at Main Canal (MC)

5: Canal Breach at Main Canal (MC)

6: Irrigation Field During Flooding

Plate 5- 3 Tendaho Spillway during operation at Spill Channel

5.4 OBJECTIVE OF THE STUDY

The main objective is to enhance the design of hydraulically safe structure for complex section using the state- of- art of 3D hydrodynamic modelling. In addition, to propose methodology for design hydraulically safe structure for complex section.

5.5 HYDRAULIC FEATURES AND DESIGNED DATA

5.5.1 General Arrangement

The total length of the approach channel is 50.0 m. The control structure is in the form of an ogee weir. It has three bays of 10.5 m clear width each separated by two intermediate piers of 3.0 m thickness. The remaining gap on either side of the abutments are closed and sealed in a manner like non-spilling sections of a concrete dam. The stilling basin has length of 60.0 m and is provided with only chute blocks at the start of the basin and a dentated sill at the end of the basin. The total length of the spillway is 868 m and drop height is 38m. [64]. Details of design report is shown in Annex C.

5.6 METHODS

5.6.1 Validation of the FLOW-3D numerical model

Tedaho Dam spillway was designed and constructed without the physical model or 3D hydrodynamic model being verified due to its complexity of flow conditions. Therefore, the objective of this study is to verify the design and propose a solution which will

enhance the design of the spillway using 3D hydrodynamic model. Accordingly, FLOW-3D hydrodynamic model has been used for verification and modification of the Tendaho spillway design. According to the design and proposed section and dimensions, using the AUTO CAD 3D model, the physical domain was prepared and exported to the FLOW-3D model in stl format to produce computational domain. Figure 5- 3 and Figure 5- 4 show the plan of the spillway.

The FLOW-3D program subdivides the Cartesian computational domain into a grid of hexagonal cells. For each cell, the program calculates average and maximum values for the flow parameters (depth, velocity, pressure) at discrete times.

5.6.2 Boundary and Initial Conditions

Since the flow domain is defined as a hexagonal in the Cartesian coordinates, there are six different boundaries on each mesh block. The boundaries on the mesh and their coordinate directions were set as follows.

For optimal simulation, the spillway was modelled in seven mesh blocks. The boundary condition for flow data in Block 1, the upstream boundary condition (Xmin) was defined as volume flow rate 1,700 m^3/s at the inlet of the spillway, the downstream boundary condition (Xmax) was defined as symmetry. The spillway has three bays with radial gates. However, these test cases were simulated representing operation of the fully opened gates. The bottom boundary (Zmin) was defined as the Wall (no-slip condition) where the approach channel invert elevation 396 m and the spillway crest elevation are 400 m. The top boundary (Zmax) was set as Specified Pressure (with Fluid Fraction = 0) that was specified with water elevation 410 m which is flow depth

over the crest is 10 m. In Block 7 at the outlet, Ymin was given as an outflow. All the other blocks between Block 1 and 7 were either Symmetry or Wall condition. Symmetry means a zero-gradient condition which is continuative at the boundary. Wall means no-slip condition at the boundary as well as a zero-velocity condition normal to the boundary [22]. Figure 5- 5 and Figure 5- 6 show the boundary conditions

The initial conditions that represent on the upstream sides of the spillways at the same level as the specified fluid heights were proposed fluid elevation. The free surface water elevation option was given as an initial condition at the Block 1. The Zmax-coordinate of the free surface was fixed for the estimated initial condition which is 410 m.

5.6.3 Numerical Simulations Options

In most cases, the default selections were used; however, in case of momentum advection algorithm, the default momentum advection algorithm is a first-order upwind differencing method. This method is first order accurate in space and time. It is robust and sufficiently accurate in most situations, although, as in any first-order method, it introduces numerical diffusion into the solution. For this it has its own controlling system. When better accuracy is needed for the resolution of flow velocities, e.g., in vortices, then a second-order monotonicity-preserving upwind differencing method can be used by selecting second order monotonicity preserving. This method is second order accurate in space and first order accurate in time. Another second-order method based on central differencing of the advection terms can be used by selecting second order. This method is second order accurate in both space and time. As such, it is the preferred method for minimizing numerical dissipation in swirling flows. This

method is the least diffusive of the three, and performs well for circulating flows and free surface waves [22]. In this numerical simulation second order momentum advection was given since there is a sharp bend along the chute channel. Starting from smaller time steps that is from 0.5 seconds up to 100 seconds, were given to get the final numerical simulation result. Implicit pressure solver was used.

5.6.4 Discretization Approach

Various computational trials are conducted with different grid cells size in x, y and z directions and it was observed that the cells at the ogee, near the baffles and along the curve were not resolved well when the grid size was given above 0.5 m. Hence, 0.5 m width was given for all hexagonal grid widths.

5.6.5 Model Geometry

The numerical analysis was carried out based on the original design and modified design. In addition, the designed data obtained from the report which was not done with the numerical method, was also compared with the numerical results of design and modified numerical results. The model for 1D was set up to get overall information at different location along the spillway by dividing the length of spillway at 5 m intervals starting from the river (Outlet) up to the reservoir (Inlet). The total length of the spillway model is 868 m. Therefore, the mesh blocks are prepared in accordance to the given geometry. Figure 5- 7 to Figure 5- 9 show the model set up.

Another geometry option, that remained constant for all spillway modelling completed as part of this study, was the inclusion of surface roughness value applied on the

surface of all spillway geometry. The roughness friction factor = 0.016 for a concrete lined channel and 0.025 for the Downstream Channel were utilized in the model. This was done in FLOW-3D by specifying a surface roughness value, equal to the average height of surface imperfections to the desired components in the meshing and geometry tab since Manning roughness was converted to FLOW-3D's Surface Roughness. Also included in the geometry tab for all simulations was a baffle, which is a plane that was defined as a flux surface and specified to be 100% porous so that it would have no effect on the flow. This baffle was normally located in a plane at different sections along the spillway which was responsible for providing the discharge measurement. The numerical model comprises the approach channel, ogee crest, crest pier, chute channel, stilling basin, channel bend, downstream channel [59].

The 3D numerical model has different types of options for the output result that includes hydraulic data of average flow depth, maximum flow depth, average velocity, maximum velocity, specific hydraulic head and total head, pressure, etc.

The runs were developed in a personal computer with a Pentium 4 Ghz processor and 16 GB of RAM; the evolution in time was used as a relaxation to the final steady state. Simulation time was given as 100 second and accordingly 8 days were taken to finalize simulation. The required output memory size was 138 GB carried out with eight multi processes parallel.

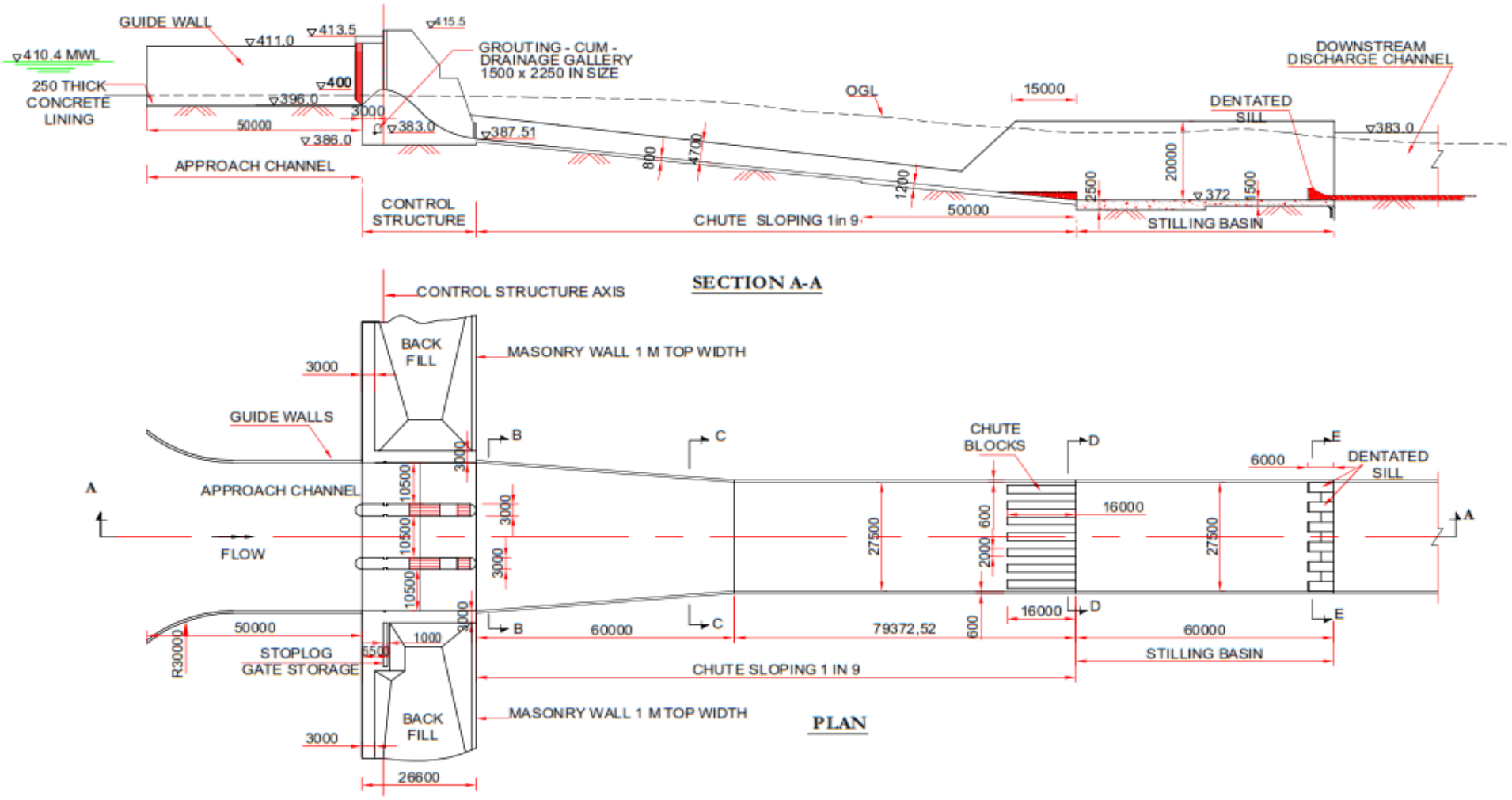

Figure 5- 3 Plan and Section of the Spillway as per the Design [64].

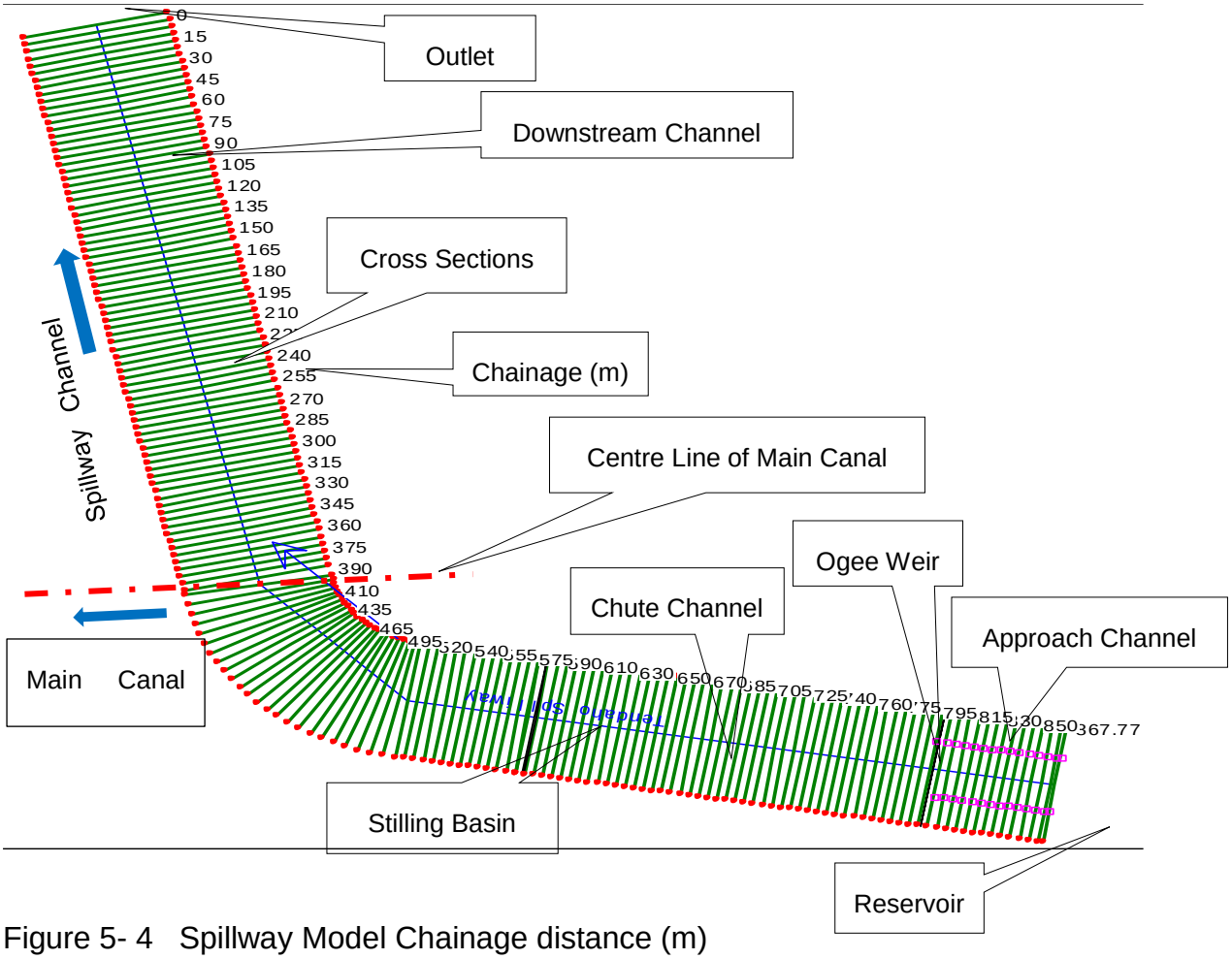

Figure 5- 4 Spillway Model Chainage distance (m)

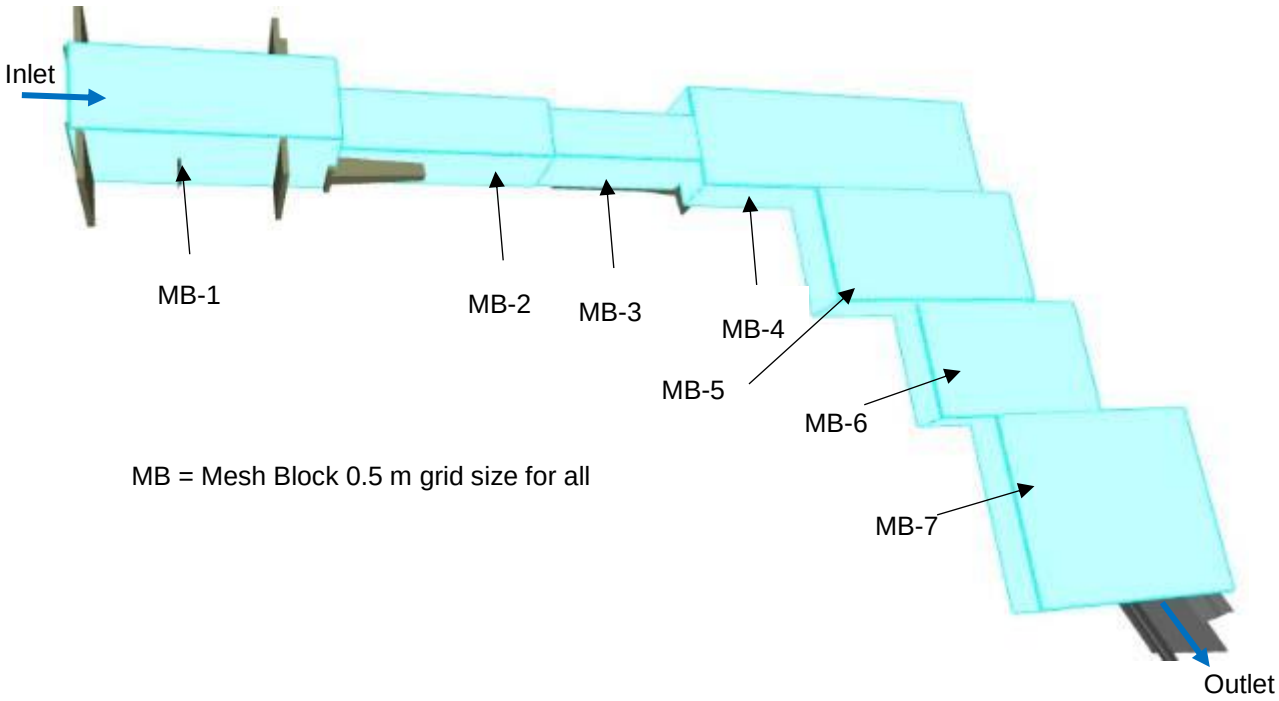

Figure 5- 5 Different mesh blocks for the spillway model 0.5 m grid length for all grid

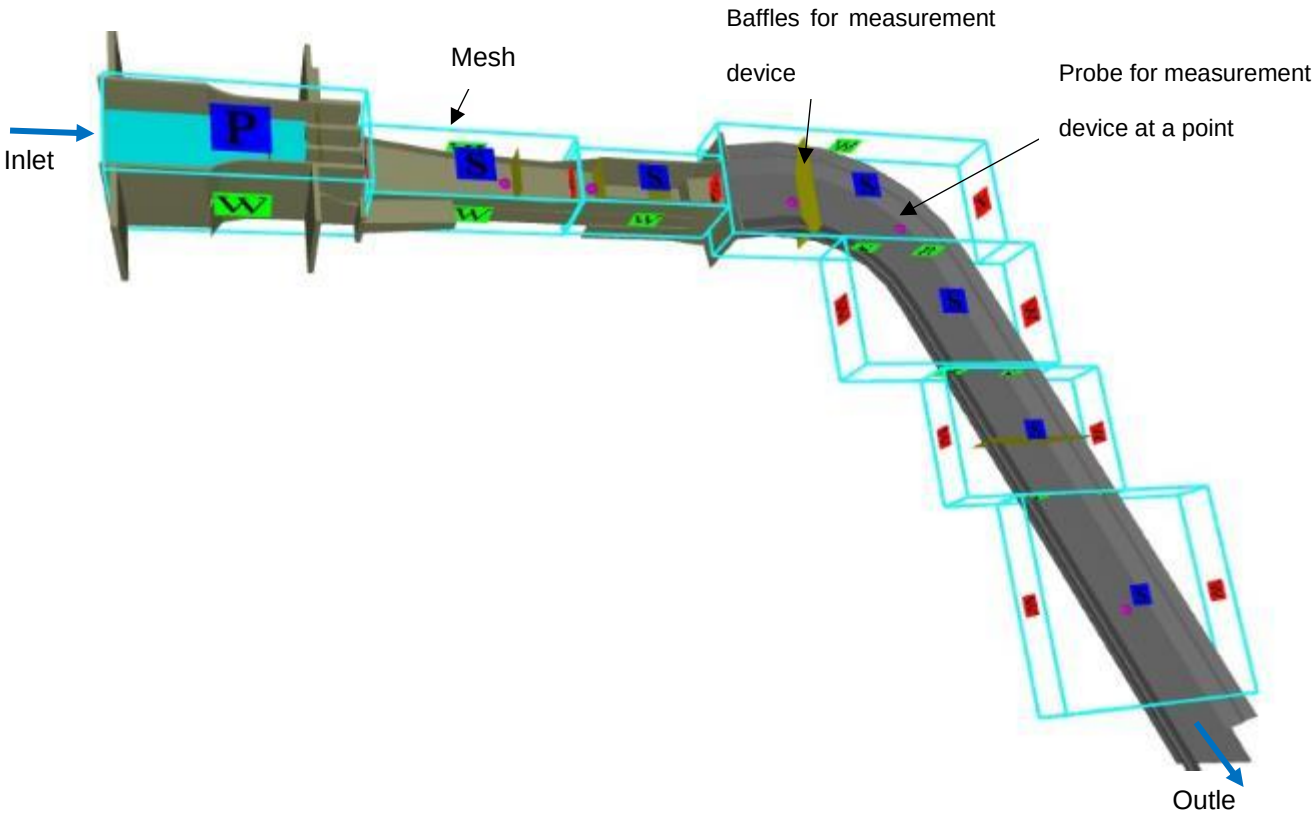

Figure 5- 6 Boundary conditions and location of hydraulic measuring devices

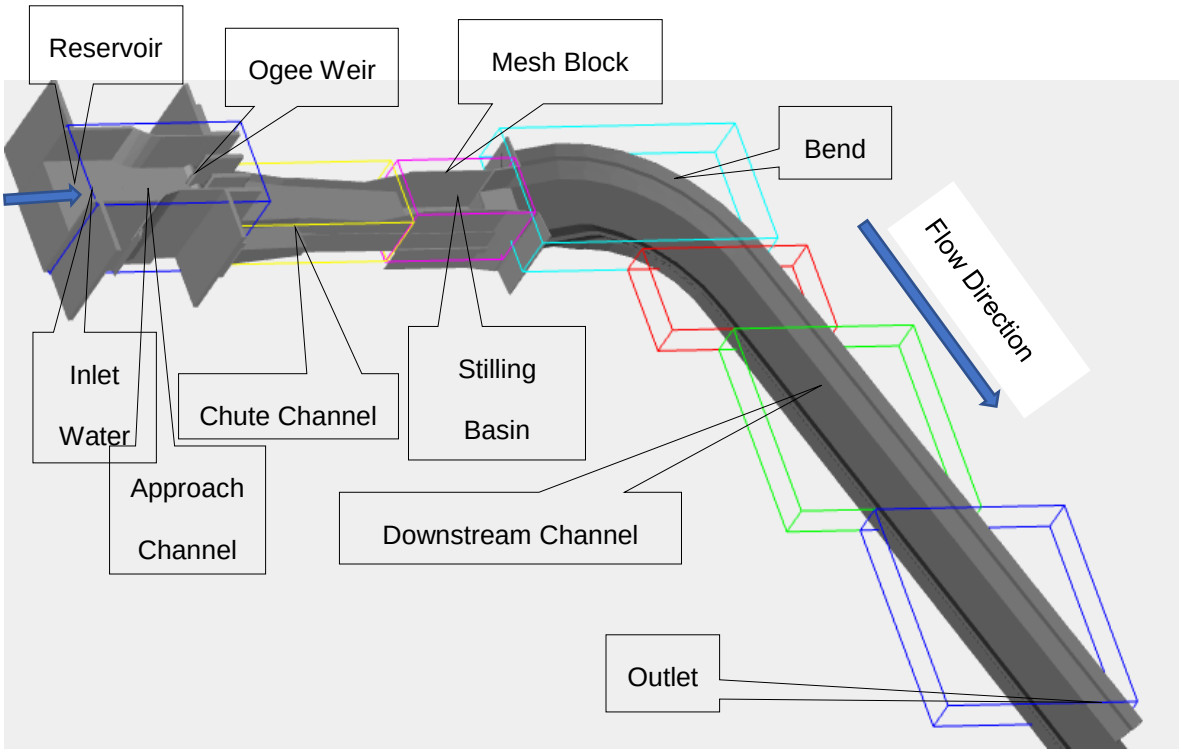

Figure 5- 7 Plan of the Spillway and mesh blocks prepared for the model. Per Modified

3D Mode at Different Sections	
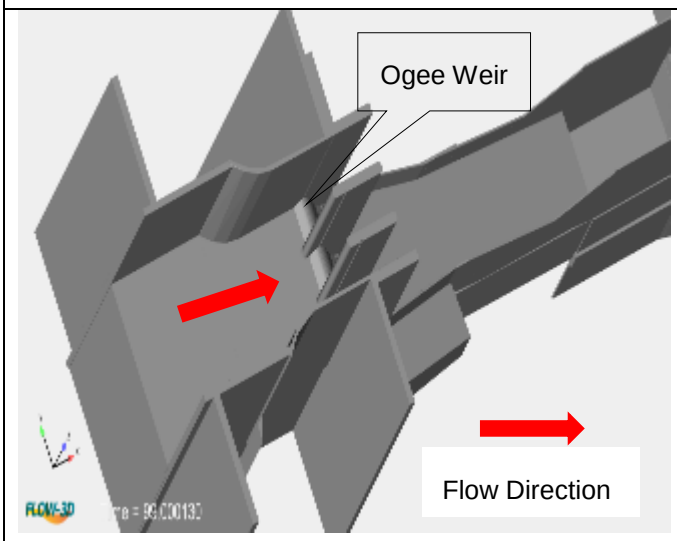	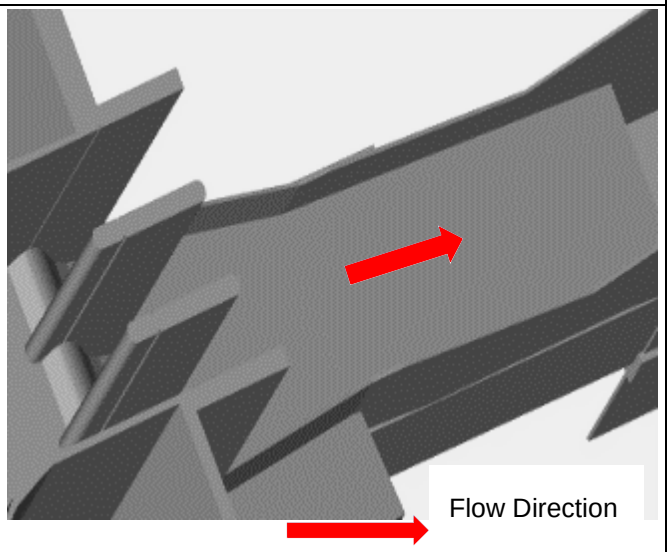
1 : At the inlet of spillway	2 : Chute Channel
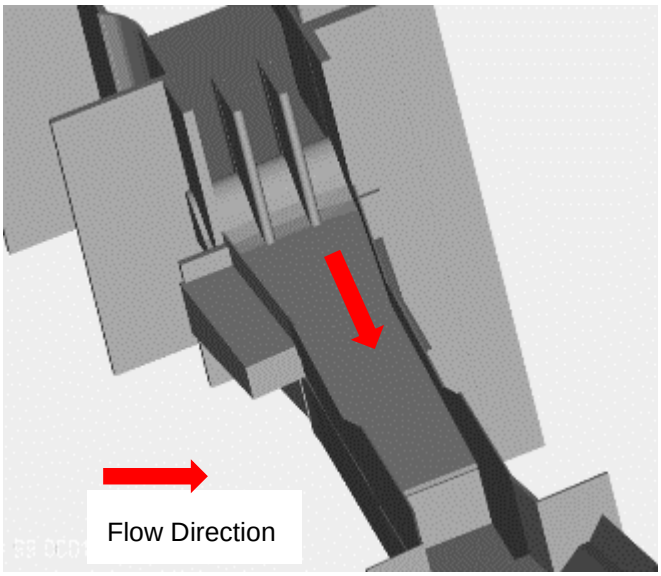	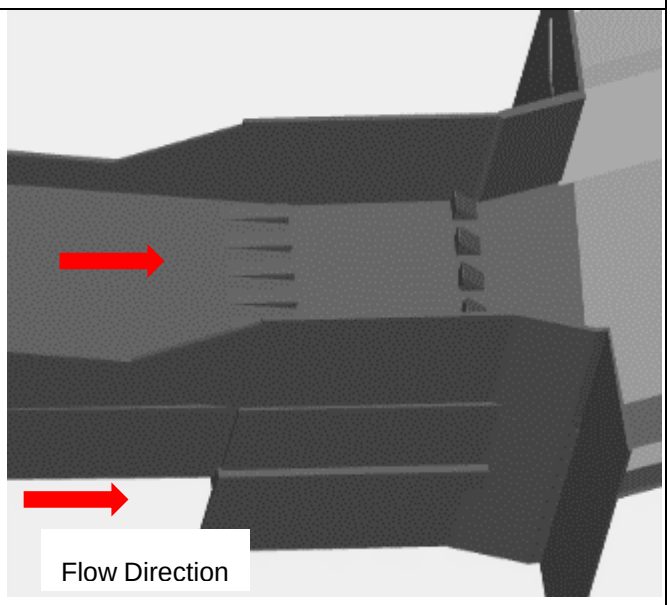
3 : Converging Section	4: Stilling Basin as Per Design

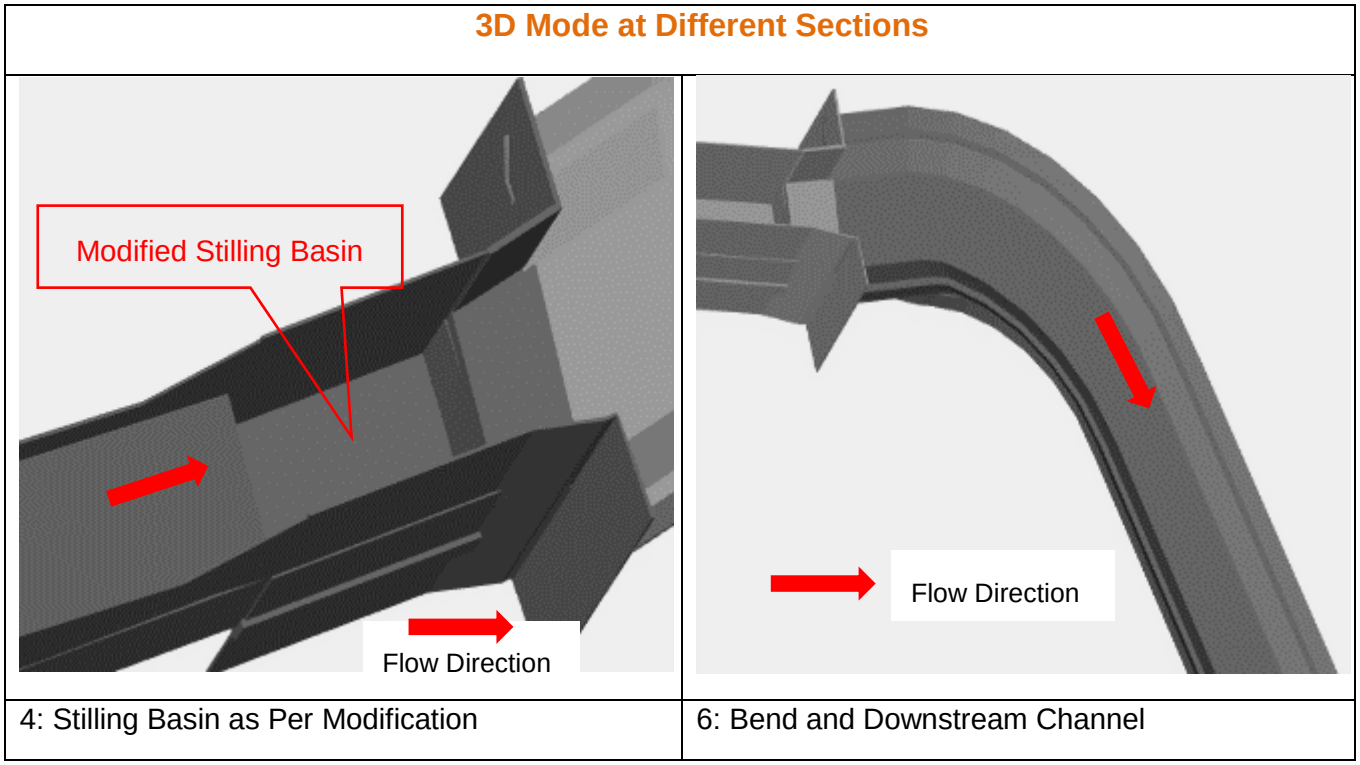

Figure 5- 8 3D Spillway mesh blocks at different sections of the Spillway.

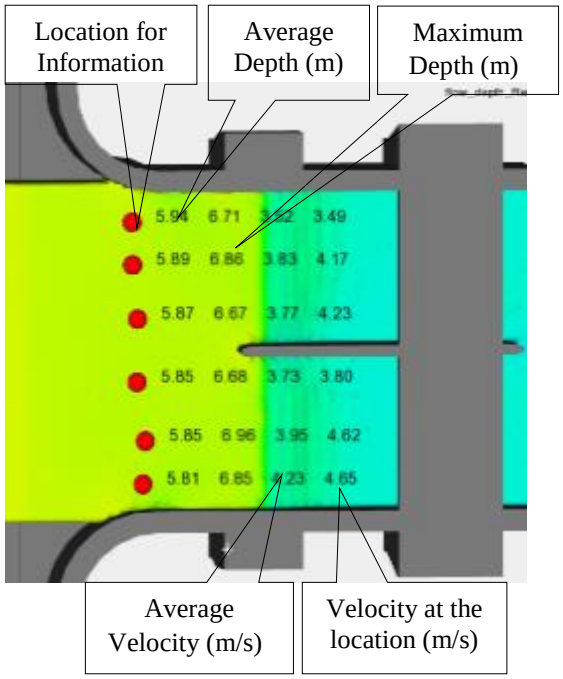

At seven locations hydraulics data were taken across the flow direction and the results are: -

Average Depth, Maximum Depth, Average Velocity and Maximum Velocity

Figure 5- 9 3D model Result Information.

5.7 RESULTS

5.7.1 Along Approach Channel

Along approach channel, the model data at CH 0+835 showed that the design flow depth was 12.4 m, the 3D model result for average flow depth was 11.43 m and for maximum depth 14.29 m. The velocity as per the design was 3.5 m/s and for the 3D model average was 3.52 m/s. There was 7.82% difference between design and 3D average depth of flow and 0.57% difference in velocity. Figure 5- 10 shows detail information. For further information refer Table 5- 2, Table 5- 3 and Annex C.

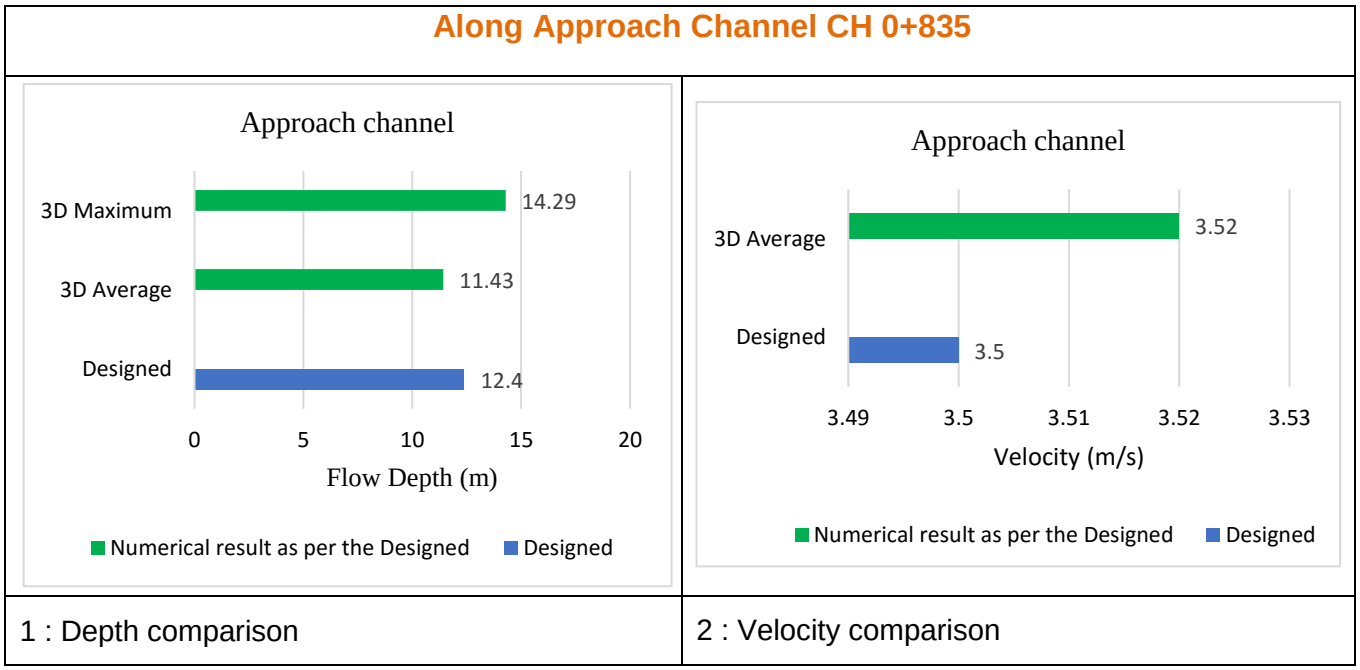

1 : Depth comparison

2 : Velocity comparison

Figure 5- 10 Along Approach Channel

5.7.2 Flow over the Spillway Crest

The design of Tendaho dam spillway is sized to pass the routed half Probable Maximum Flood (½ PMF) and dam overtopping is checked for full PMF. Furthermore,

dam overtopping is checked for full PMF if for some reason, one of the control gates is faulty. The routed peak discharge for half PMF is 1,700 m^3/s with 8.4 m depth of water above the spillway crest and the routed discharge for full PMF is 2,194 m^3/s with 9.2 m depth of water above the spillway clear crest length of spillway (3 bays of 10.0 m each) although actual length of each bay has 10.5 m length. The routed discharge for full PMF is 2,194 m^3/s for the worst condition that is if one of the three control gates malfunctions, restricting the overflow length to 21.0 m only (2 bays of 10.5 m each) with 10.4 m depth of water above the spillway crest [64], [60].

During research simulation has been done for two scenarios to check the performance of the spillway control section based on the design. The first simulation was for half PMF and the second simulation was for full PMF to check the safety of the dam from being overtopped if for some reason, one of the control gates is faulty. Accordingly, the followings are the results.

At chainage 0+800 m, the routed ½ PMF flow which is 1,700 m^3/s was considered as flow over the spillway crest. In addition, the initial boundary condition for the FLOW-3D model was given as the top boundary (Zmax) and was set as Specified Pressure that was specified with water elevation 410 m.

The flow depths from design 8.4 m, from 3D average 5.37 m and from 3D maximum were 10.2 m respectively. The velocities from design 6.86 m/s and from 3D model 9.47 m/s. There was 56.42% difference between design and 3D average depth of flow and 18.33% difference in velocity. Figure 5- 11 section 1 and 2 show detail information. In addition, refer Table 5- 2, Table 5- 3 and Annex C.

For the worst condition that is one of the three control gates malfunctions, restricting the overflow length to 21.0 m only. The depth of flow as per the design is 10.4 m without overtopping of the dam. The 3D model result for depth of flow over the crest was 7.75 m. The 3D model result for depth of flow from the design was lower than the design flow depth over the crest even though the spillway was operating only by two bays. This shows that the dam is safe from overtopping during malfunction of one gate. Figure 5- 11 section 3 and 4 show detail information.

Over the Crest 0+800

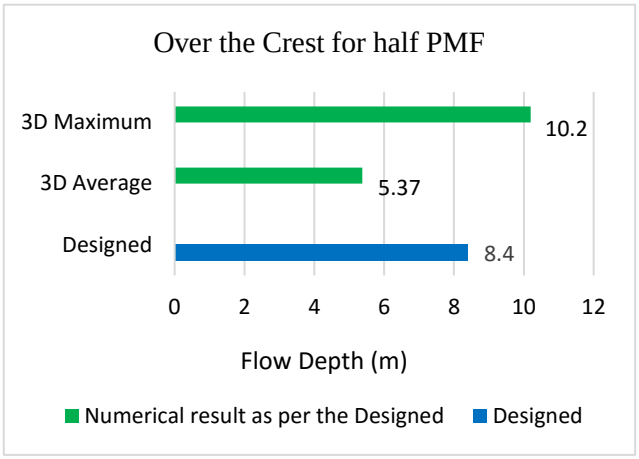

1 : Depth comparison for half PMF

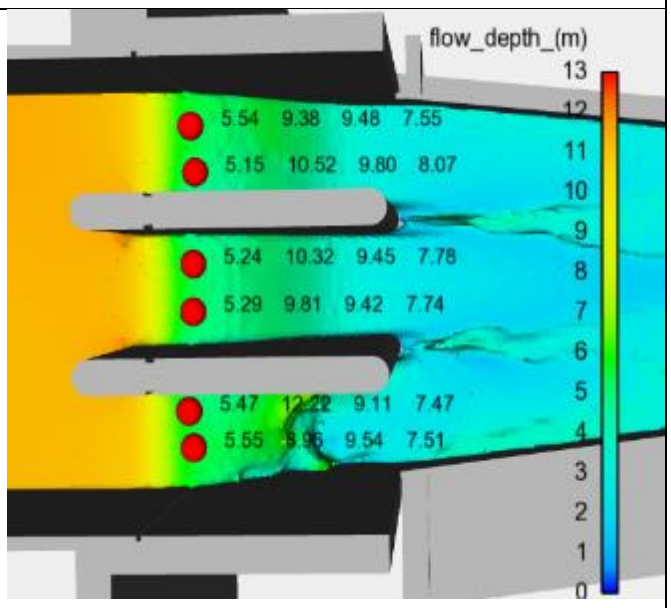

2 : 3D model output for half PMF

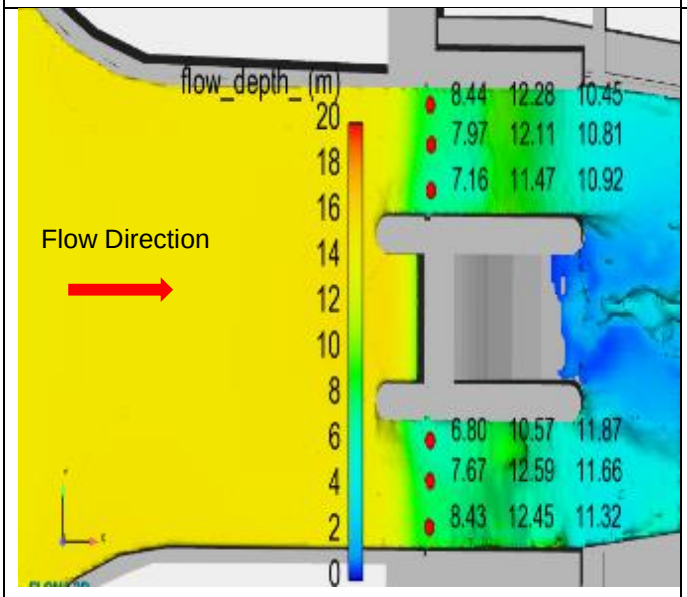

3 : 3D model output for full PMF with One gate malfunctions

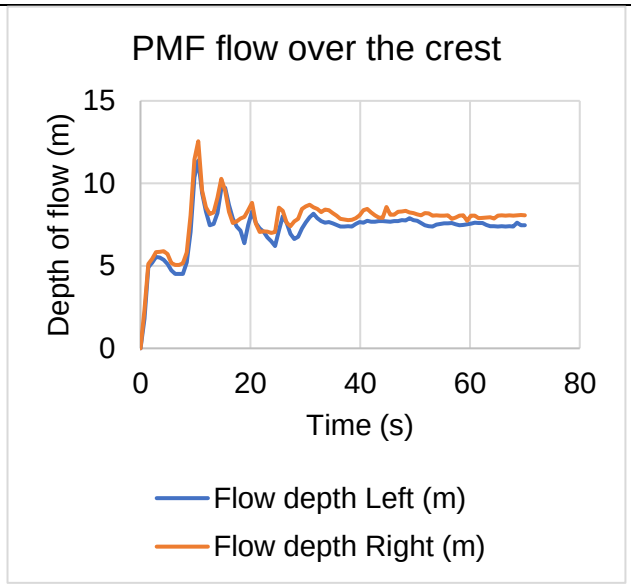

4 : 3D model output for PMF data from both sides with One gate malfunctions

Figure 5- 11 Model result Over Spillway Crest

5.7.3 At the Toe

At CH 0+ 755 Toe of the spillway, the design flow depth was 2.34 m with a velocity of 19.4 m/s. The 3D average flow depth was 3.88 m with average velocity of 14.78 m/s

and the maximum flow depth was 9.67 m. There was 39.69% difference between design and 3D average depth of flow and 45.76% difference in velocity. Refer Table 5- 2, Table 5- 3 and Annex C.

5.7.4 At the End of Convergence

At CH 0+ 730 End of Convergence of the spillway, the design flow depth was 2.91 m with a velocity of 21.25 m/s. The 3D average flow depth was 3.0 m with average velocity of 18.59 m/s and the maximum flow depth was 5.73 m. There was 3.0% difference between design and 3D average depth of flow and 16.44% difference in velocity. Refer Table 5- 2 and Table 5- 3.

5.7.5 Along Chute Channel

The results of flow Along Chute Channel at ch 0+ 685 are shown in Figure 5- 12. All the flow depth in this section were similar with the 3D model. The design depth and 3D average depth are almost the same. The flow depths from design 2.91 m, from 3D average 2.83 m and from 3D maximum were 5.54 m respectively. The velocities from design 21.25 m/s and from 3D model 19.31 m/s. There was 2.83% difference between design and 3D average depth of flow and 10.05% difference in velocity. Refer Figure 5- 12, Table 5- 2 and Table 5- 3.

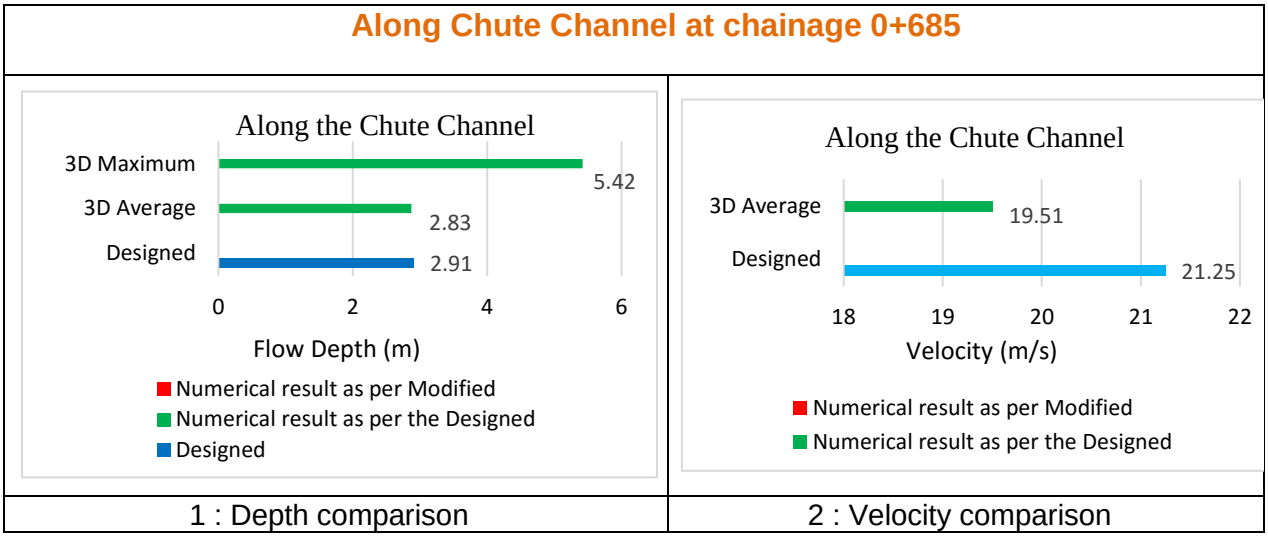

Figure 5- 12 Models result Along Chute Channel.

5.7.6 Upstream of Stilling Basin

The flow at Upstream of Stilling Basin at CH 0+ 650 results are as follow. The flow depths from design 2.72 m, from 3D average 2.58 m and from 3D maximum were 4.28 m respectively. The velocities from design 23.9 m/s and from 3D model 20.15 m/s. There was 5.15% difference between design and 3D average depth of flow and 10.05% difference in velocity. Refer Figure 5- 13, Table 5- 2 and Table 5- 3.

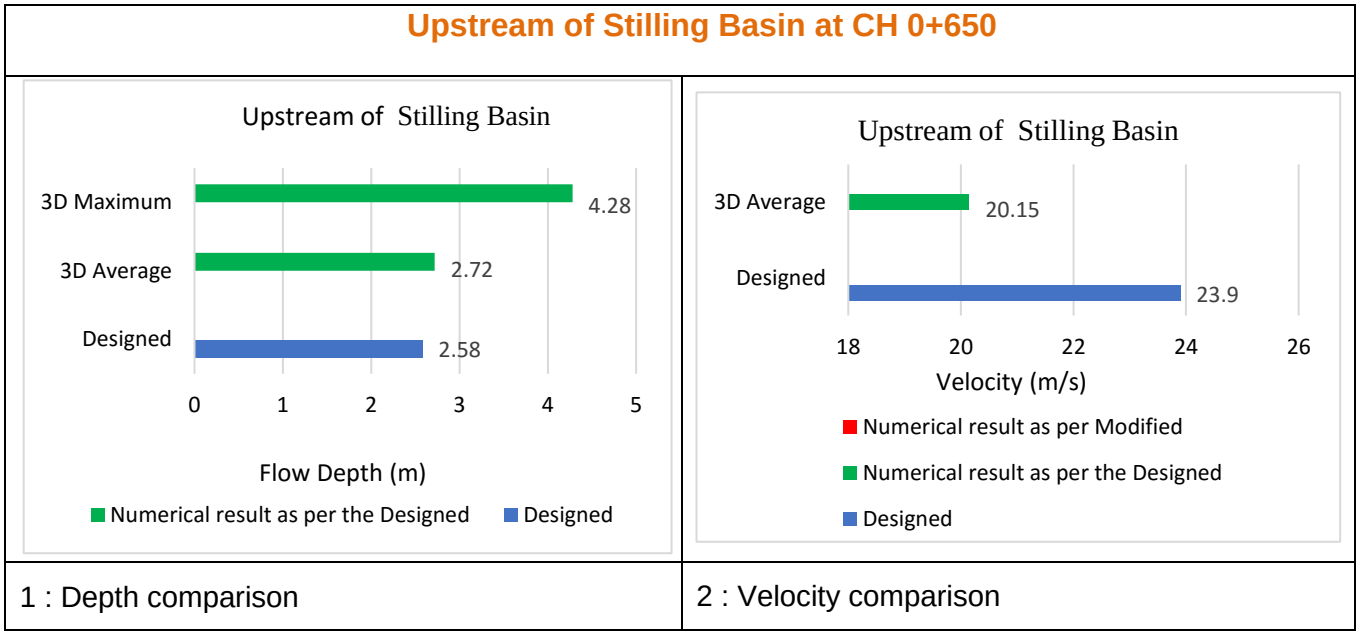

Figure 5- 13 Upstream of Stilling Basin

5.7.7 At Stilling Basin

As per the design report, the depth of flow in the stilling basin is 16 m, however in the 3D numerical model the result showed that no such depth of flow at stilling basin. Instead, based on the design section using FLOW-3D model it was checked and found that the depth of flow was 2.81 m. In addition, there is no data for the velocity; however, the velocity as per the designed section using 3D numerical model showed that, it is more than 19 m/s.

Therefore, to dissipate the energy and reduce the flow velocity, the researcher suggests the stilling basin type needs to be modified and verified with the 3D numerical model. Accordingly, the stilling basin was modified by lowering the stilling basin floor to a depth of 15 m. After modification, it was verified with the 3D numerical model. Accordingly, the velocity was reduced from 20.15 m/s to less than 5.81 m/s. Results after modification are shown in Figure 5- 14. In addition, the overall comparisons before modification and after modification are shown in Figure 5- 14 and Figure 5- 15.

Figure 5- 14 section 1 and 2 shows the flow results of Stilling Basin at ch 0+ 600 are as follow. As per the design, the depth of flow was 16.1 m. The numerical result as per the designed and modified 3D average 2.81 m and 19.85 m. For 3D maximum flow depth as per the designed and modified were 4.03 m and 26.88 m. Meanwhile, no designed velocity. The numerical result of velocity as per the design section and modified section of 3D average were 19.7 m/s and 5.81 m/s. The energy in terms of hydraulic head has decreased from 23 m to 20 m as per design and as per the modification decreased from 23 m to 13 m which is nearly by half.

At Stilling Basin at chainage 0+600

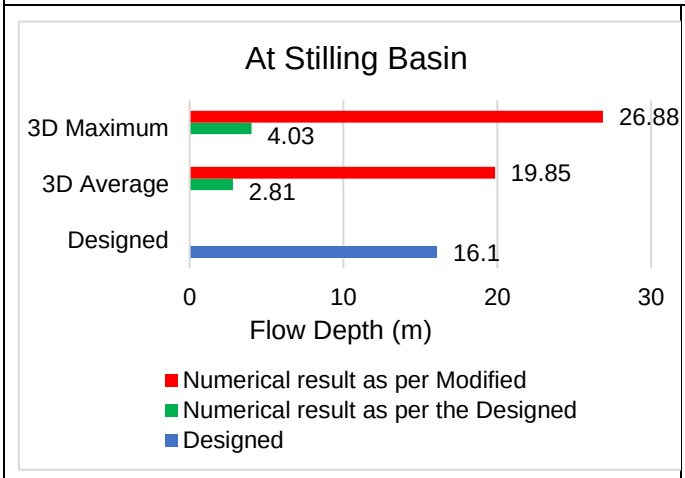

1 : Depth comparison at ch 0+600

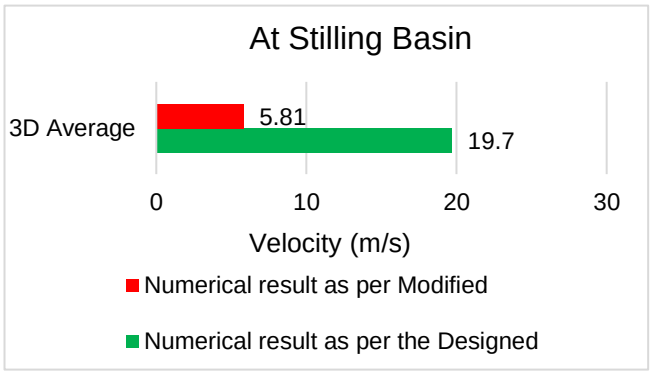

2 : Velocity comparison at ch 0+600

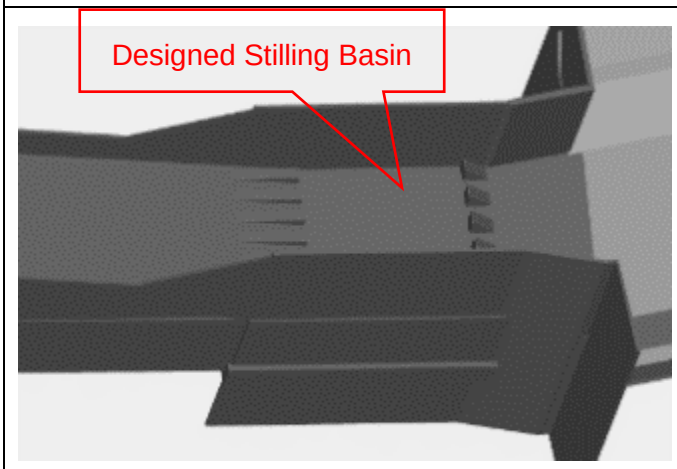

3: 3D Stilling Basin as per the design

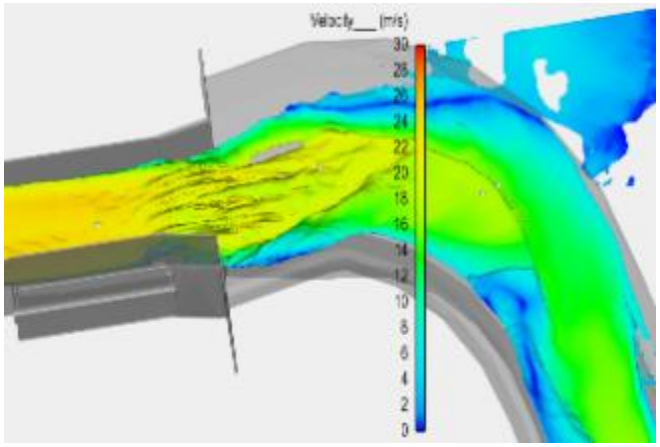

4: 3D model flow as per the design shows overtopping at the bend

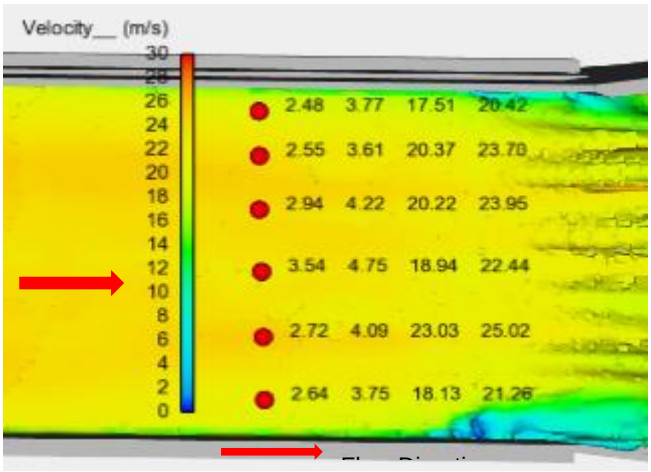

5 : 3D model flow result as per the design at Stilling Basin

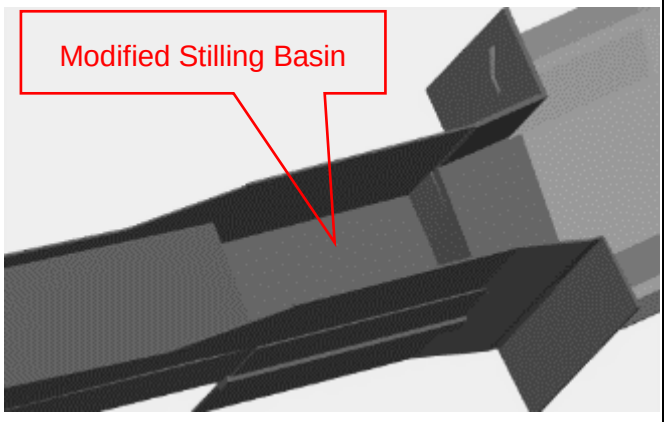

6: 3D model as per modification at Stilling Basin

At Stilling Basin at chainage 0+600	
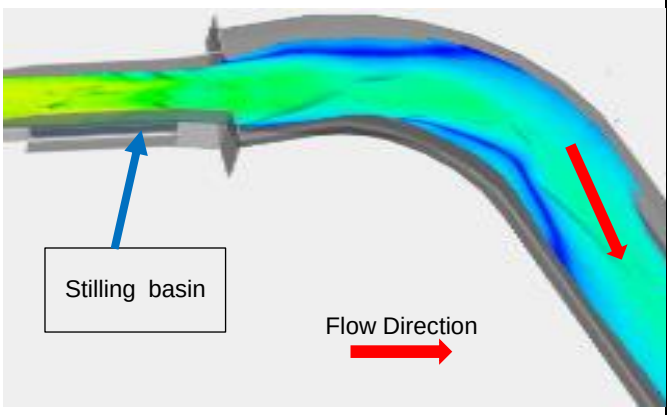	- The designed value in the design report has very large difference than the 3D average depth of flow before modification. - After modification the 3D average depth of flow has increase significantly. - No overtopping at the bend.
7 : 3D model result as per modification	

Figure 5- 14 At Stilling Basin

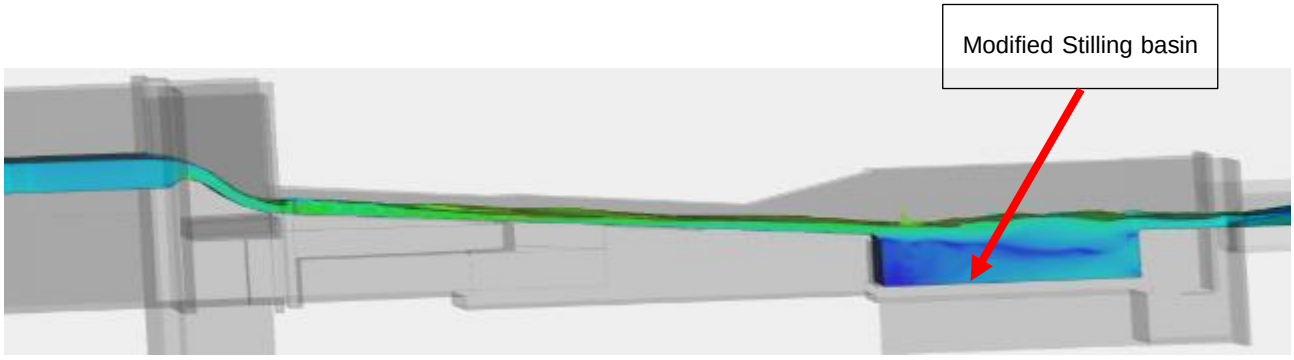

Figure 5- 15 Flow Profile of 3D upto Stilling basin as per the proposed design adjustments

5.7.8 Downstream of Stilling Basin or At the Beginning of Downstream Channel

The flow results Downstream of stilling basin at CH 0+ 550, were as follow. There is no designed data for the flow depth. The numerical result as per the designed section and modified section 3D average 3.15 m and 4.04 m. For 3D maximum flow depth were 5.13 m and 5.09 m for design and modified conditions. No designed velocity

data. Using the numerical model velocity as per the design 14.72 m/s and modified 7.13 m/s respectively.

The velocity as per the designed was higher than the velocity of proposed section. This shows that the existing structure is not enough to dissipate the energy. On the other hand, the proposed section of stilling basin can dissipate the energy and reduce the flow velocity. After modification, the velocity was reduced from more than 14 m/s to less than 7 m/s. Figure 5- 16 shows detail information of the results.

Downstream of Stilling Basin at CH 0+520

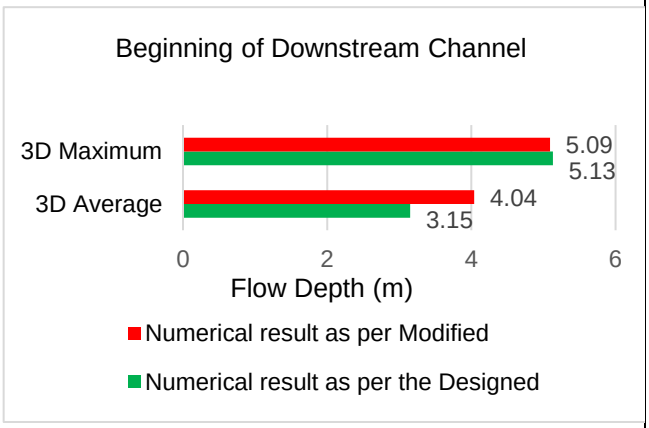

1 : Depth comparison

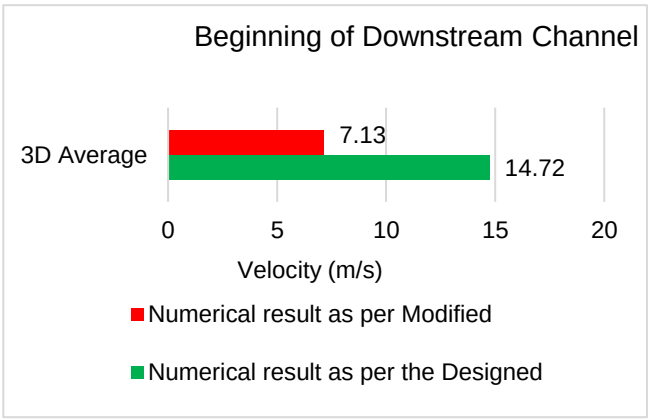

2 : Velocity comparison

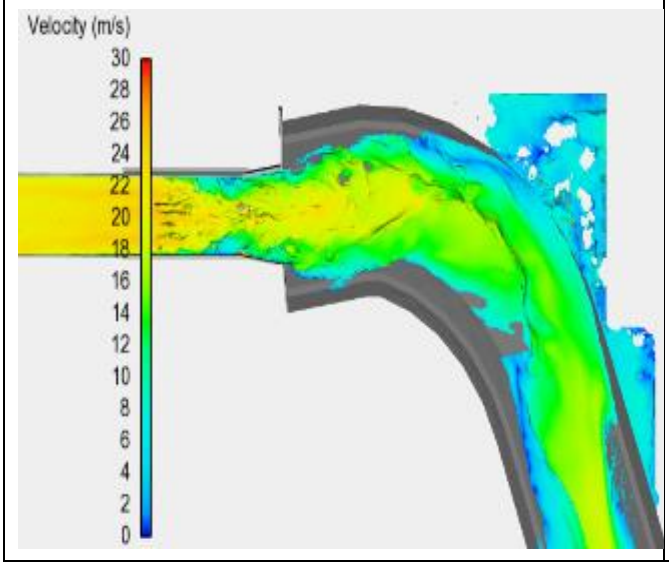

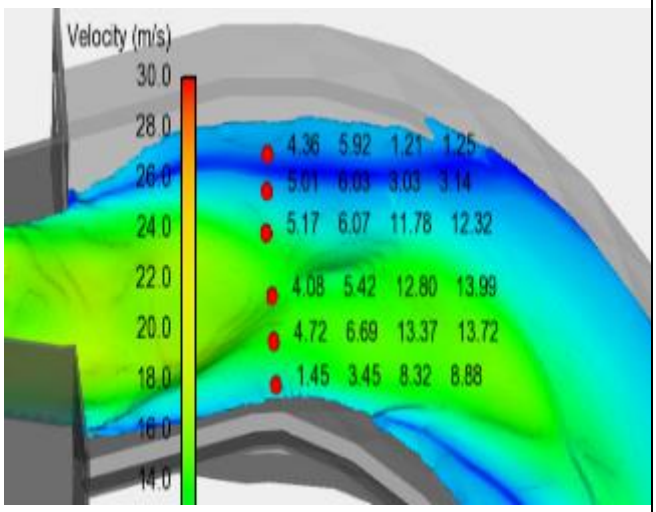

Downstream of Stilling Basin at CH 0+520	
3 : 3D model result as per the design	4 : 3D model result as per the modification
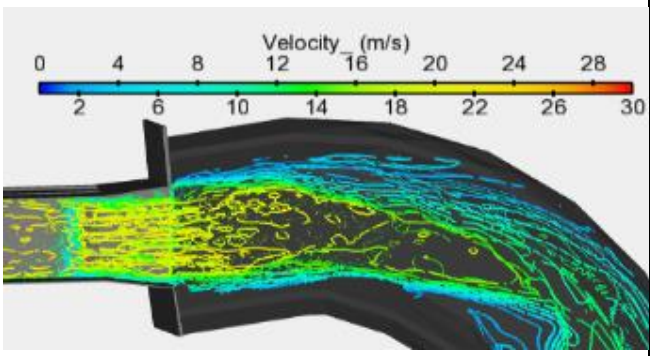	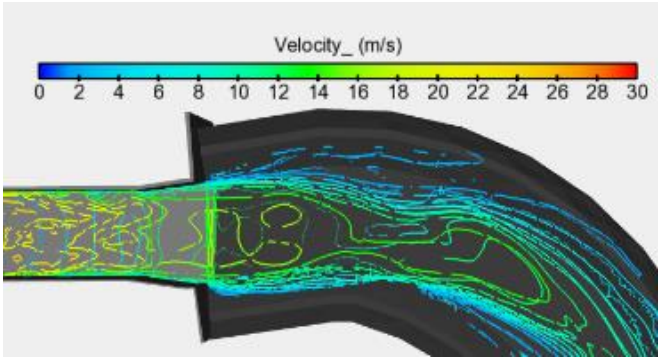
5: Contour for velocity at downstream of stilling basin as per the design	6: Contour for velocity at downstream of stilling basin as per modification
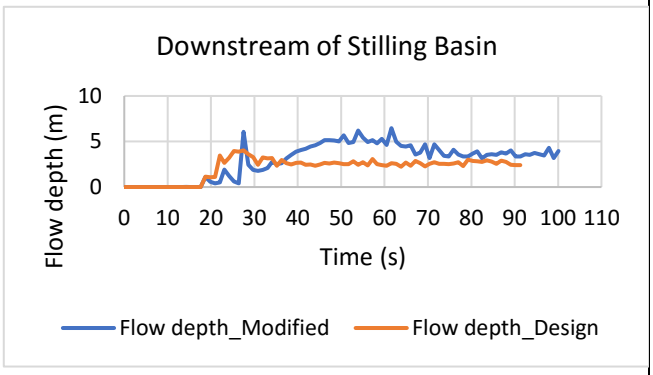	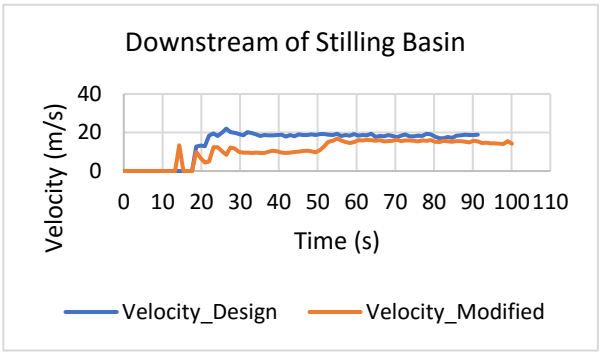
7 : Numerical model result for depth with two simulation results	8: Numerical model result for velocity with two simulation results
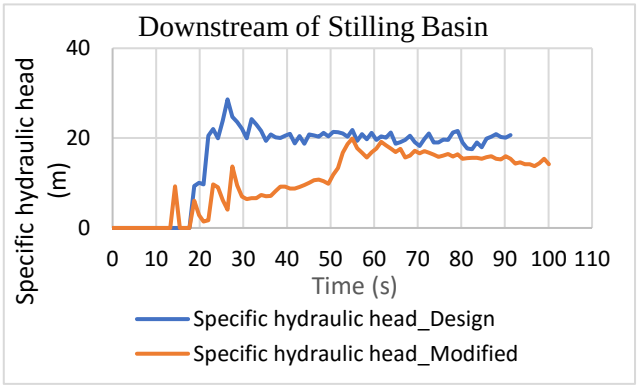	- Before modification flow coming from stilling basin has high turbulence or fluctuating in flow depth and wavy with has high velocity which is more than 20 m/s. Refer section 3 and 5. - After modification flow coming from stilling basin has less turbulence and wavy and the velocity which was less than 13 m/s. Refer section 4 and 6. - After modification flow depth has increased which shows that there is significance energy dissipation. Refer section 7. - Velocity after modification has significantly reduced which shows that there is significance energy dissipation. Refer section 8. - After modification the hydraulic head has decreased. Refer section 9.
9: Numerical model result	

Figure 5- 16 Beginning of Downstream Channel

5.7.9 Flow along Channel Bend

Flow along the bend at ch 0+ 370 has different features than expected [65], [66]. There is no design data for the depth and velocity. The numerical result as per the designed and modified 3D average were 3.14 m and 4.04 m. 3D maximum flow depth were 5.02 m and 5.09 m for design and modified conditions.

The incoming velocity towards the bend was more than 14.72 m/s before modification. There was superelevation and the flow overtopped the channel at the bend. According to the numerical result of velocity at bend as per the design was 9.27 m/s and as per modified section 7.13 m/s.

As per the design shown in Figure 5- 17 at section 3 and Figure 5- 19 due to superelevation, the water overtopped the channel. This is one of the advantages to use 3D hydrodynamic model that identify whether the section is safe for its operation or not. Such result can only be identified by 3D numerical model. Meanwhile, similar phenomena occurred during the flood time as shown in Plate 5- 3. Depth across the cross section varies and wavy flow. On the other hand, after modification, there were less wavy flow and relatively uniform depth across the channel. Figure 5- 17 and Figure 5- 20 shows detail information of the results.

At Bend chainage 0+ 370

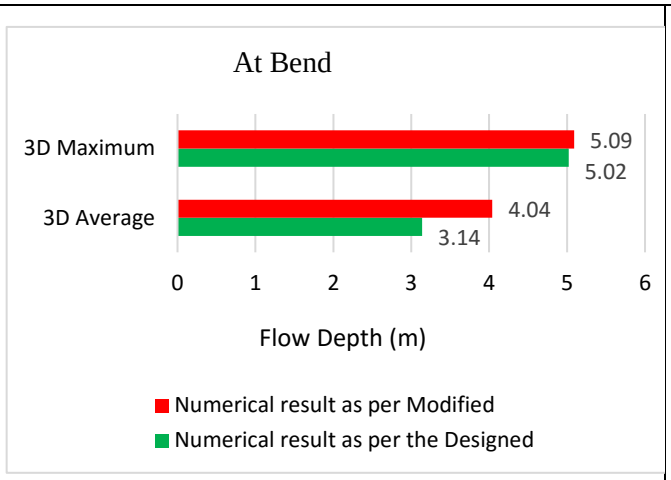

1 : Depth comparison

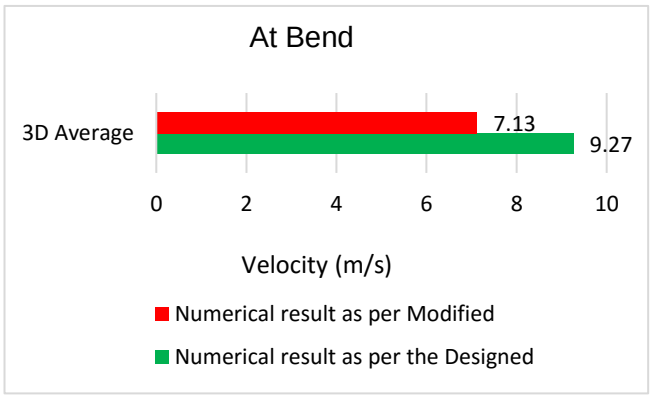

2 : Velocity comparison

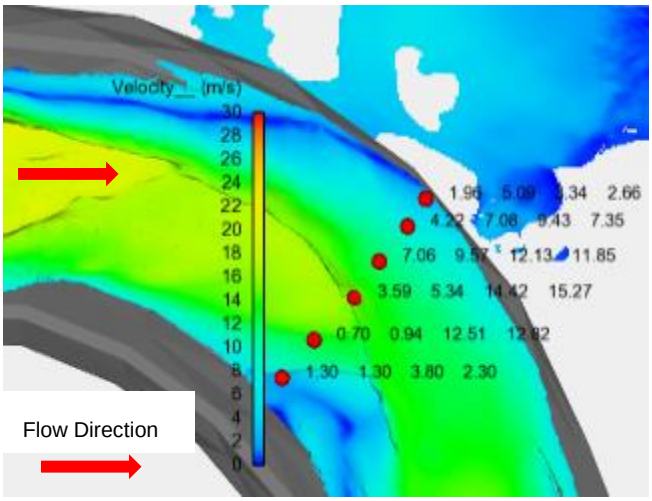

3 : 3D model result as per the design

- At bend high velocity and wavy flow.
- Overtopping due to superelevation.
- Depth of flow and velocity across the cross section varies significantly.

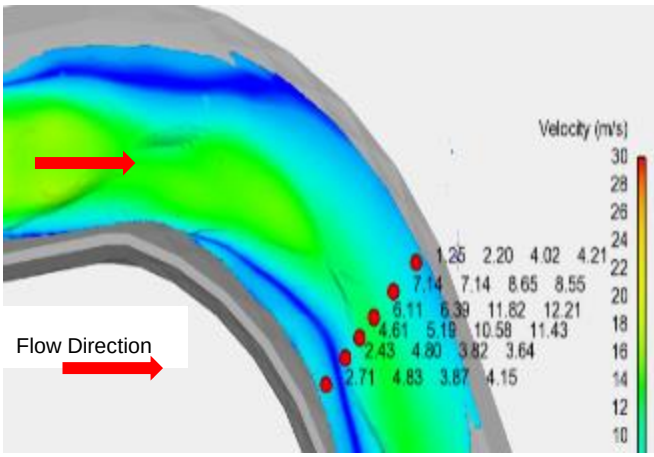

4 : 3D model result as per the design

- At bend lower velocity and has less turbulence or uneven distribution of flow in across the channel.
- No significant variation in depth across the spillway section.
- Depth of flow and velocity across the cross section did not vary significantly.

Figure 5- 17 Flow at Bend

5.7.10 At Downstream Channel

The Downstream Channel capacity was designed with ¼ PMF which is 850 m^3/s. The channel section is trapezoidal with bed width 45 m and side slopes on 1 Vertical to 1 Horizontal. The design report stated that overtopping is allowable since it will create minor lose and will require minor maintenance. However, after the bend there was no overtopping. The overtopping was occurred along the bend due to superelevation. Due to overtopping, flood entered into Main Canal which caused significant damage in Main Canal for 17 km and affected the irrigated fields. Such damage cannot be considered as a minor damage because, the damage was not only in the Downstream Spillway Channel, but it was along the Main Canal and the irrigation field.

The analysis was carried out in both flows which is ½ PMF 1700 m^3/s and ¼ PMF 850 m^3/s. For the flow at Downstream Channel CH 0+ 165, the results are as follow. In 3D model since it was observed an overflow, comparison was made only for modified design. Hence, for full flow as per modified of 3D average 3.46 m and for reduced flow it was 2.28 m depth. For full flow, 3D maximum flow depth was 3.67 m for modified condition and for reduced flow it was 2.25 m depth. As per the design report, the velocity was 1.6 m/s however, as per modified for 3D average 9.43 m/s and for reduced flow it was 7.68 m/s. Table 5- 1 shows detail information.

Table 5- 1 3D Model results along Downstream Channel

Flow Discharge (m^3/s)	Average Depth (m)	Maximum Depth (m)	Designed Velocity (m/s)	Average Velocity (m/s)	Maximum Velocity (m/s)
½PMF 1700 m^3/s	3..46	3.67	1.6	9.43	10.23
¼ PMF 850 m^3/s	2.28	2.25		7.68	8.43

To be conservative, the downstream boundary condition of the river at the outlet was set as an outlet flow condition. Hence, the analysis was done under no blocking head at the outlet.

The 3D numerical model clearly showed that across the cross section of the channel, the velocity of the flow which has a potential to scour the channel. Therefore, modification in the channel section is required since the current section is not sufficient to accommodate the flood.

As it was mentioned earlier, the bed width of the channel is 45 m with 1:1 trapezoidal section. Therefore, the proposed section by the researcher is, to increase the bed width from 45 m to 300 m with the same side slope for the last 100 m of the channel. For this proposal it was checked by 1D model since there is no complex flow condition at the outlet. For full flow, the depth of flow at the outlet will be 1.63 m with the velocity 3.16 m/s and for reduced flow, the flow depth will be 1.08 m with the velocity of 2.37 m/s. In addition, it is required to increase the roughness of the channel by placing boulders that can properly operate with both flow conditions. Thus, this proposed section will safely operate for both flow conditions. Figure 5- 18 to Figure 5- 20 show detail information of the results.

Downstream Channel at 0+165

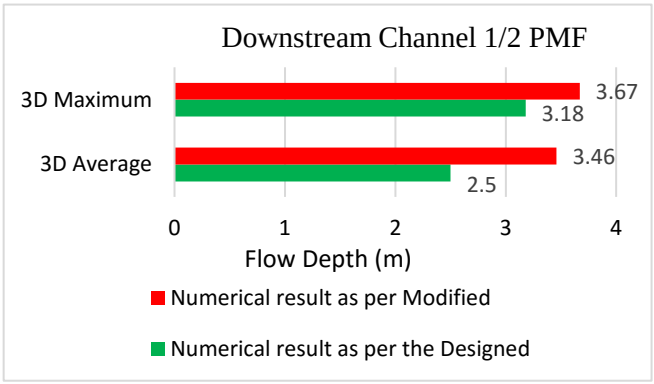

1: Depth comparison for ½ PMF

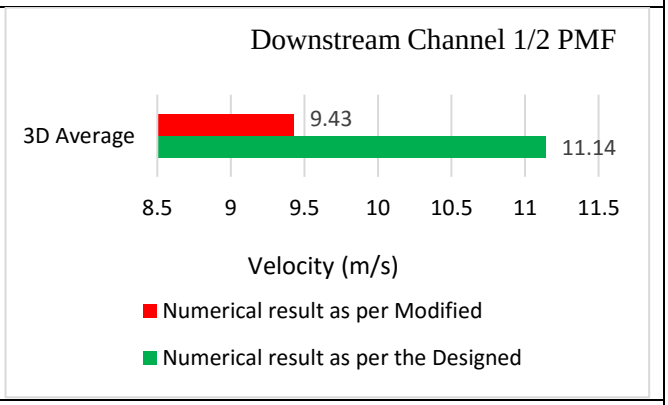

2: Velocity comparison ½ PMF

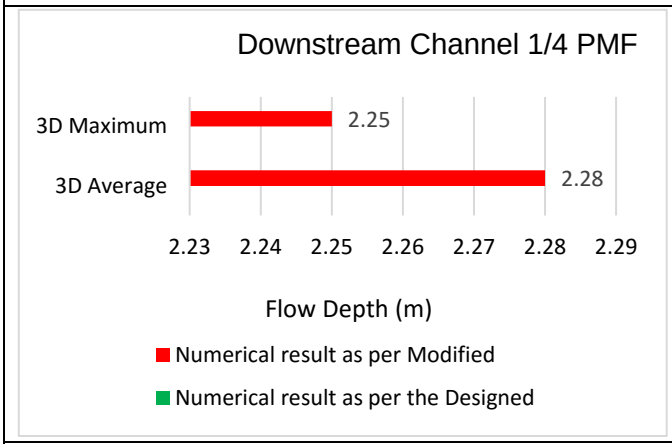

3: Depth comparison 1/4 PMF

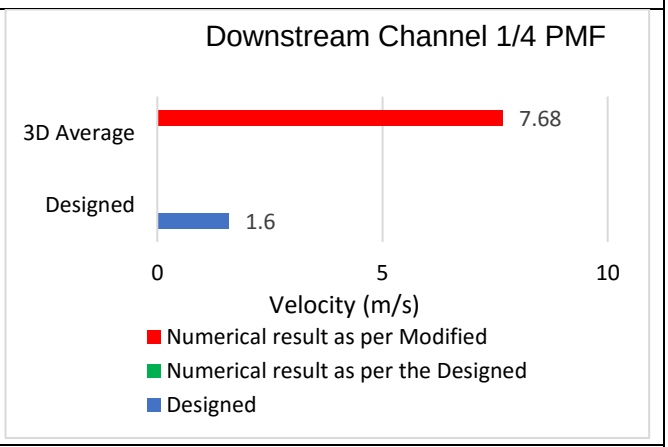

4: Velocity comparison 1/4 PMF

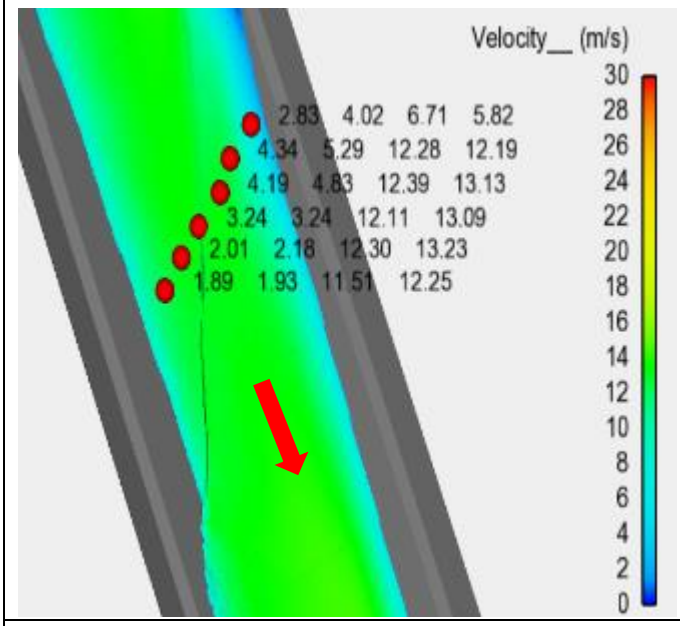

5: 3D model result with Full Flow as per design

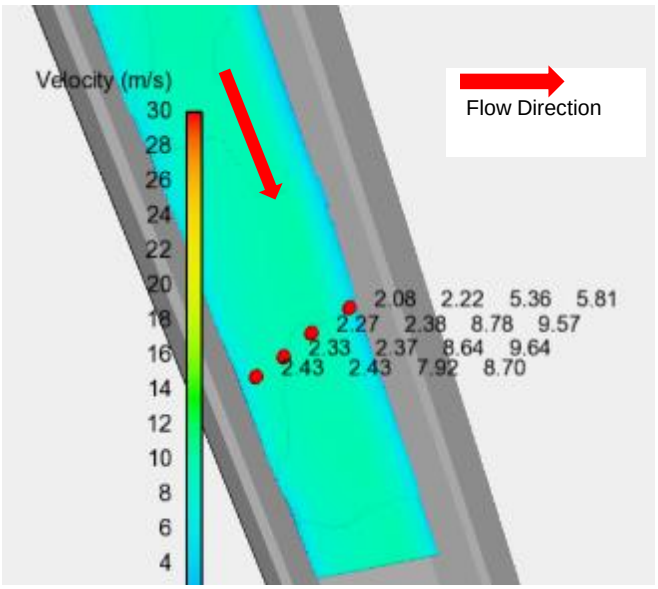

6: 3D model result with ¼ PMF as per modified

Downstream Channel at 0+165	
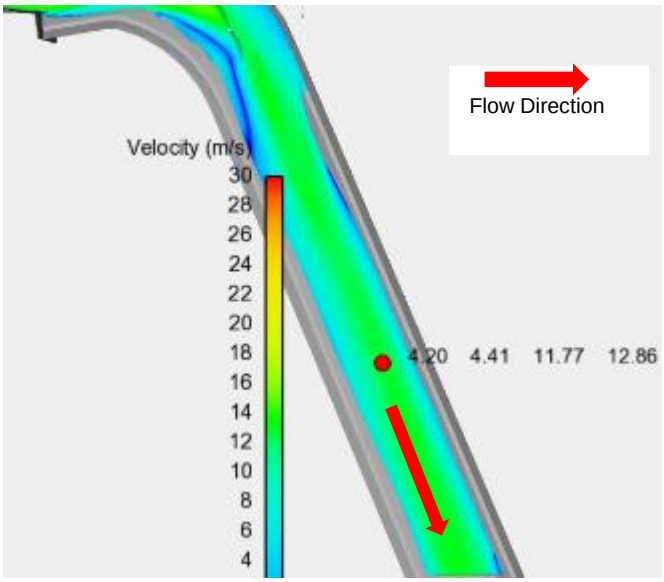	- The Downstream Channel capacity was designed with ¼ PMF which is 850 m^3/s. - No overtopping - In both flow conditions there was high velocity
7: 3D model result for Hydraulic data	

Figure 5- 18 Downstream Channel

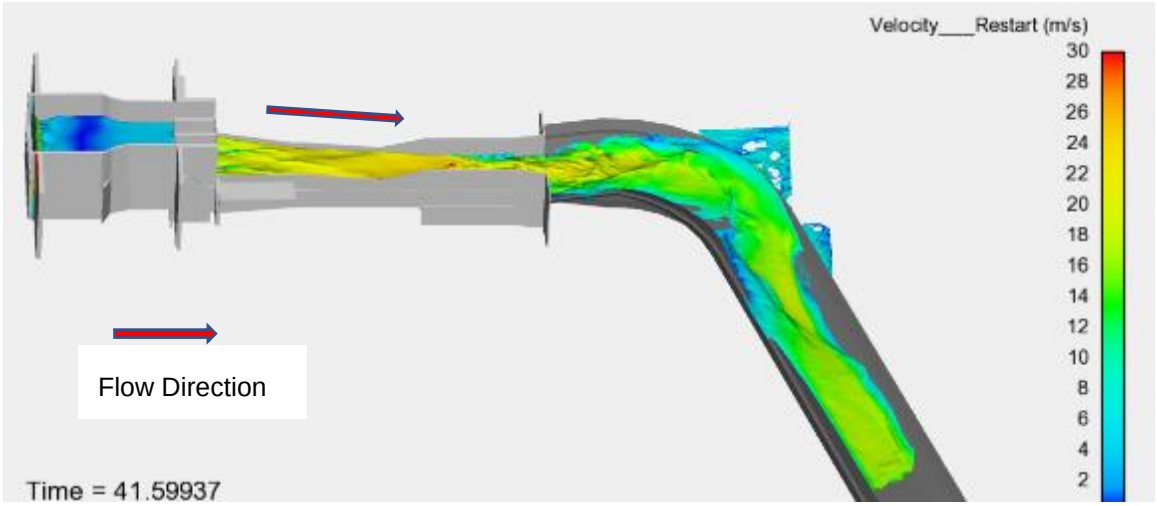

Figure 5- 19 3D model result as per the design in reference to flow velocity

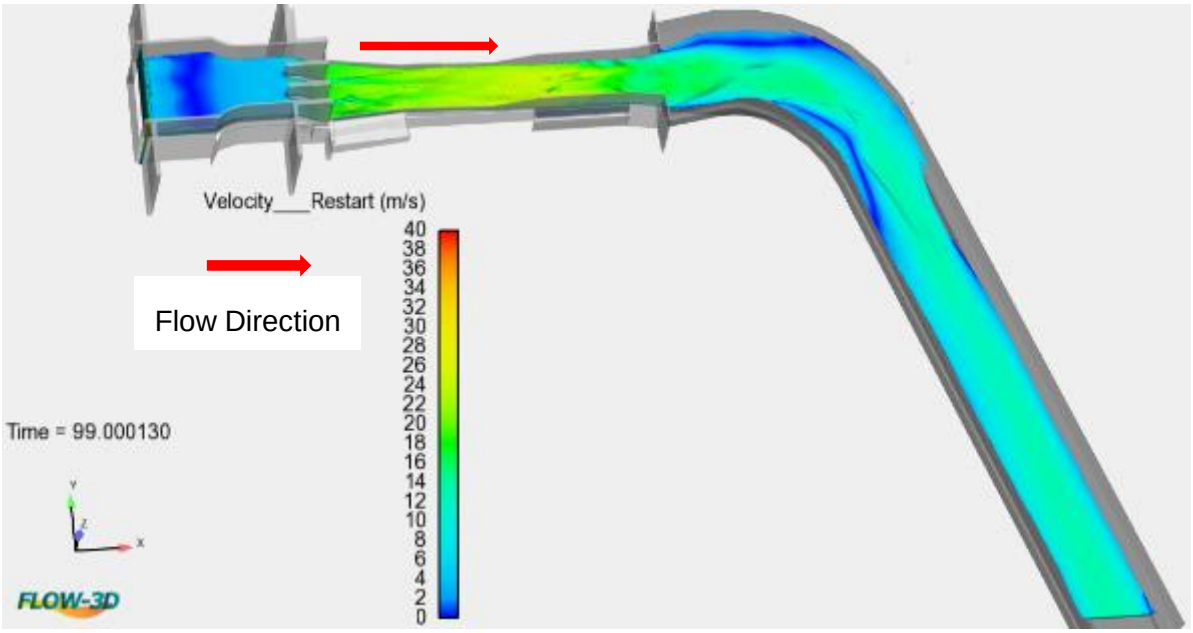

Figure 5- 20 3D model result as per the proposed adjustment in reference to flow velocity

5.7.11 Performance Indicators

The statistical parameters for the spillway upstream of stilling basin has been assessed as per the 3D model and design results. Since from the stilling basin downstream, the section has complex hydraulic section, it is not included in the statistical comparison. Accordingly, the spillway performance indicators for 3D model result with design result for depth of flow R^2 = 0.886, NSCE = 0.857 and Rbais = -7.324%. For design result of velocity of flow R^2 = 0.956, NSCE = 0.82 and Rbais = -13.748%. For further information refer Table 5- 2,Table 5- 3 and Annex C.

Table 5- 2 Summary result of depth of flow form 3D model and design output

Measurement Location	3D from Research (m)	Flow from Design (m)	Percentage difference (%)
At Approach channel	11.43	12.4	-7.82
At the Crest of Spillway	5.37	8.4	-56.42
At the Spillway Toe	3.88	2.34	39.69
End of Convergence	3	2.91	3
Along the Chute Channel	2.83	2.91	-2.83
Upstream of Stilling Basin	2.72	2.58	5.15
Sum	29.23	31.54	-7.9
Average	4.872	5.257	-7.9
	R^2 =	0.886	
	NSCE =	0.857	
	Rbias =	-7.324	

Table 5- 3 Summary result of velocity of flow form 3D model and design output

Measurement Location	Velocity of flow from 3D model (m/s)	Velocity of flow from Design (m)	Percentage difference (%)
At Approach channel	3.52	3.5	0.57
At the Crest of Spillway	8.4	6.86	18.33
At the Spillway Toe	13.31	19.4	-45.76
End of Convergence	18.25	21.25	-16.44
Along the Chute Channel	19.31	21.25	-10.05
Upstream of Stilling Basin	20.15	23.9	-18.61
Sum	82.94	96.16	-15.94
Average	13.823	16.027	-15.94
	R^2 =	0.956	
	NSCE =	0.820	
	Rbias =	-13.748%	

5.8 DISCUSSIONS

A complex hydraulic structure such as a spillway of dam design must be verified by 3D hydrodynamic numerical model rather than finalizing its design with only 1D model. The study undertaken at the University of Queensland shows the numerical limitations of 1D hydraulic models [67]. Typical limitations of 1D Hydraulic Models has been practically seen in Ethiopia Tendaho Dam Spillway where, the design was finalized with only 1D model and was not verified with a physical model or 3D numerical model. As a result, significant losses occurred during its operation. Therefore, verification of the original design for Tendaho Dam Spillway was done using FLOW 3D hydrodynamic numerical model. According to the original design, the spillway sections including the approach channel, ogee crest and chute channel are safe for the spillway operation. However, stilling basin, downstream channel, along bend and after bend, the spillway is not safe while in operation. Therefore, modification of the spillway section at the stilling basin was undertaken and after modification the design was verified using FLOW-3D hydrodynamic model and the result showed that the spillway is safe for operation.

Dam overtopping is checked for full PMF if for some reason, one of the control gates is faulty. The 3D model result for depth of flow from the design was lower than the design flow depth over the crest even though the spillway will operate only by two bays. This shows that the dam is safe from overtopping during malfunction of one gate.

The designed and constructed stilling basin cannot dissipate the energy of the flow which was also seen in numerical model. Accordingly, modification was done at stilling basin by lowering the bed level to a depth of 15 m. According to the original design section, after dissipation in stilling basin, the depth of water was raised up to 19.85 m as per 3D model. The downstream flow depth was 3 m. Therefore, more than 15 m depth of water needs to be dissipated before it joins the downstream channel. Accordingly, the stilling basin was lowered by 15 m in order to reduce the hydraulic head in the stilling basin. After reducing the stilling basin level using the AUTO CAD 3D mode, the section was prepared and exported to the FLOW-3D model. The selected level with section was analysed by the 3D model and the results showed that after modification, the velocity was considerably reduced from 19 m/s to 6 m/s. Furthermore, the energy dissipated before modification was decreased from 23 m to 20 m. On the other hand, the energy dissipated after modification decreased from 23 m to 13 m. This shows that modification will dissipate the energy significantly.

Without modification, after the stilling basin which is at the beginning of downstream channel, the flow had wavy and high fluctuating in depth with a velocity of 20 m/s. Such a result was also seen during the problem and became the cause of destruction along the bed and sides of the channel where the concrete blocks and structures were taken away by the flood. On the other hand, after modification, the numerical model showed that, the variation in depth was significantly decreased, and the velocity was reduced from 19 m/s to 6 m/s.

During the flooding time, there was an overtopping channel at the bend and this condition could not be identified during design. On the other hand, the FLOW-3D numerical model showed that what happened in the time of flood where there was an

overtopping due to superelevation. Meanwhile, no overtopping was seen after modification of the stilling basin. This is one of the advantages to using a 3D hydrodynamic model in order to identify whether a section is safe for its operation or not. Whenever, it is not safe, another hydraulic section should be proposed by the designer and verified by the 3D hydrodynamic model.

The 3D model has the ability to show the turbulence condition [68] in the model and gives the outputs in both average depth, maximum depth, etc. at different points across and along the channel.

5.9 RECOMMENDATIONS AND CONCLUSION

Tendaho Dam Spillway was constructed over 10 years ago. However, the design safety for its operation has not been confirmed either with a physical model or 3D numerical model. In these durations, one flood season has occurred, and it caused significant loss. On the other hand, after damages, maintenance on the spillway has been undertaken based on the original design. Therefore, the following recommendations are put forward to minimize further loss:

- The stilling basin must be modified by at least lowering the floor level by 15 m otherwise the spillway is not safe. As per the design, the flow will not dissipate its energy and will have high velocity that can create erosion at the downstream channel. In addition, due to superelevation at the bend, the water will overtop the channel and enter into the Main Canal and will create a significant loss.
- From the stilling basin up to the bend, the channel bed and side slopes need to be constructed with concrete blocks that can resist a high velocity and increase the roughness of the channel.

- Due to significant superelevation, the water overtopped the channel. This result can only be identified by a 3D numerical model since flow at such curve has a three-dimensional feature. Therefore, a 3D numerical model must be used to check if there is superelevation so as to control water overtopping the channel.
- The Downstream Channel has high velocity which can scour the channel. Therefore, especial provision has to be provided to reduce the flow velocity or provide structures that will resist velocity up to 10 m/s.
- In order to safely join the flow from the spillway downstream channel into the river, the last portion of the channel needs to be wide enough to increase the cross-sectional area and reduce the flow energy. Thus, the channel bed width requires to be widened from 45 m to 300 m and maintaining the same side slope and gradient since the widening has no limitation in the topography.
- It is a significant technological development to use a 3D hydrodynamic numerical model for the design of complex hydraulic structures. Flow condition at the curve or complex section cannot be seen by a 1D numerical model. Therefore, any complex hydraulic structure design such as spillway of the dam must be verified with a 3D hydrodynamic model.
- A 3D hydrodynamic modelling must be used because it helps the designers to improve the hydraulic performance of existing or new hydraulic structures.

Due to the development of science and technology, the emergency of the 3D numerical model is one of the base lines for the design of the complex hydraulic structures that can operate safely. Modelling flow in a complex geometry using the state- of- art of 3D numerical model will not only help to enhance and recognize the complex hydrodynamic flow conditions but it also helps to ensure uniform velocity

distribution, depth variation, energy dissipation, etc. This will enable the engineers to provide the required sections with greater accuracy, appropriate energy dissipation methods and safe hydraulic structure. Therefore, for a complex flow structure the design or verification must be done with at least with 3D numerical model.

CHAPTER SIX

6 APPLICATION OF FLOW-3D ON RIBB DAM SPILLWAY ETHIOPIA

6.1 INTRODUCTION

Dams and spillways are hydraulic structures built across a stream to facilitate the storage of water. The storage of water can then be utilized for different means, such as for power generation, water supply, stabilization of the water flow, irrigation, flood control and navigation to name a few. A dam is defined as a large structure built across a valley to store water in the upstream reservoir [38], [7], [69], . In general, the upstream water level should not overtop the dam at any possible flow conditions, as dam overtopping may indeed lead to dam erosion and destruction of the dam and associated structures. To ensure this, spillways are built. For conventional designs a spillway is designed to "spill" excess water under controlled and safe conditions. If the spillway discharge capacity is insufficient the upstream water level will rise and risks the dam structure. Downstream of the spillway the kinetic energy of the flow needs to be dealt with to prevent erosion in the downstream channel and transport the water back to the original riverbed [39], [37].

Ribb Dam has been proposed in the premises of embankment dam with an impervious clay core material and this type of dam needs sufficient capacity of spillway for the safety of the dam. The safety of the dam cannot be secured only with provision of sufficient discharging capacity of the spillway; the hydraulic design of spillway must

also adequate to convey and dissipate the energy associated with water from pond level of the reservoir to the discharging natural stream.

The side channel spillway has certain advantages which makes it adaptable to topography where the overflow is most economically returned to the original streamed by deep, narrow channel or by open channel flow through tunnel, [70], [69]. In view of the complex nature of flow, hydraulic model studies are normally required to ensure adequate and economical details for the final design [51], [71]. The flow in a side channel spillway is an example of a spatially varied non-uniform flow that is best solved by the application of the momentum principle. Side channels should not submerge the reservoir outflow due to complex interactions between the overflow and the downstream channel [7], [72], [61]

The Ribb dam spillway is a U-shaped side channel spillway which is designed to accommodate the inflow half PMF flood within the storage space above the full retention level of the reservoir and prevents the dam to be overtopped in the event of occurrence of PMF flood. As per the design the actual length of the crest is 153 m however, for design it has been taken 107 m for half PMF and 123 m for full PMF for considering the complexity of flow at U-shaped. Accordingly, for uncontrolled spillway with a crest length of 107.0 m and the routed maximum outflow discharge for half PMF is 1060 m^3/s and for PMF outflow discharge is 2,378 m^3/s. These correspond to design head over the crest 3 m for half PMF and 5 m for full PMF respectively [73].

3D hydrodynamic numerical modelling of the spillway was carried out for Ribb Dam Spillway, Ethiopia, which is constructed with a routed half PMF (Probable Maximum Flood) design flow rate of 1,060 m^3/s. The routed hydrograph is characterized by the

attenuation of flood peak of the inflow hydrograph. The design results were compared with FLOW-3D model results [36]. As per the result, the design head for both half PMF and full PMF is over estimated. In addition, the spillway length is also uneconomical. The stilling basin wall requires modification since the provided wall height is not sufficient. The other sections of the spillway dimensions agree with the 3D model result.

Using 3D hydrodynamic model, Ribb Spillway hydraulic performance was assessed and it is found that the side channel spillway length is excessively enough which lead designing uneconomical hydraulic structure. The unconventional type of stilling basin requires also modification to avoid overtopping. For such complex flow condition, it is recommended that before construction the design has to be verified with at least 3D hydrodynamic numerical model.

6.2 BACKGROUND

Ribb Dam is located in the Ribb River, on the eastern side of Lake Tana Basin, in the South Gondar Zone of Amhara National Regional State in Ethiopia. The dam axis is located in between the geographic grid ref. UTM E 392174.64, N1330225.76 and E 390813.45, N 1330018.02, at an altitude of 1880 m to 1970 m. The height of the dam is 71 m and the construction has been completed in 2018 [73].

The proposed dam project will supply water for 20,000 ha of Irrigation land, thereby generating a demand for agricultural support services, and will enable farmers to fully benefit from more reliable access to sources of water [73].

The spillway has designed discharge of 1,060 m^3/s with 3 m head over the crest for half PMF. The spillway was also confirmed not to be overtopped for full PMF which is 2,340 m^3/s with 5 m head over the crest. In order to shorten the length of the side channel, it is designed a spillway from both sides of the side channel and at its end forming U-shaped side channel. Figure 6- 1 the Plan and Section of the Spillway. As per the design report, the effective length of the spillway is 123 m and due to reduction in discharge coefficient in case of full PMF a length of 107 m was considered. The designed spillway has a subcritical in the trough and it will not be submerged. However, such flow condition is three dimensional and the estimated length of the spillway crest was not verified with either physical scale model or 3D hydrodynamic model [73].

Flow in the side channel trough is spatially varied, and the side channel trough bed width at the exit to the trough is kept equal to the crest length of the control section, which is 20.0 meter with 1/1100 slope of side channel trough. The side channel section was designed for half PMF discharge and was checked for PMF discharge not to cause overtopping the dam. Accordingly, the elevation of side channel bottom is fixed based on PMF [73].

Control section is where the section has minimum energy and the flow is changed from sub critical in the side channel trough to supercritical in the conveyance chute called chute channel. The design of the rectangular control section has critical flow condition and girder length of the bridge is 20.0 m with sufficient clearance between bridge deck bottom and water level top in the control section [73], [74].

Flow released through the control structure is conveyed to the stilling basin through a rectangular cross section chute excavated along ground surface. The chute has combined slope of 0.045 and 0.33 a milder slope at the upper reach and steeper slope at the lower reach respectively. Width of the chute at the starting point of channel chute is 20.0 m, equal to the length of the control structure, which diverges to 47.0-meter chute width up to stilling basin entry. The channel section is designed for half PMF discharge [73].

The energy associated with the flow is dissipated by formation of hydraulic jump in the stilling basin. The required size of stilling basin has been assessed for half PMF flows. As per the design the velocity and the depth of flow at the end of inclined chute are 29.03 m/s and 0.78 m respectively. The Froude number of flows entering the basin equals to 10.5. For Froude number higher than 4.5 and velocity greater than 18.0 m/s type II stilling basin is appropriate. For flow velocities greater than 15 m/s provision of basin blocks is not important, therefore the installation of accessory devices is limited to chute blocks and end sill to stabilize the effect of the jump. Hence to control the jump two sharp-crested weirs are designed in the stilling basin. The width of the stilling basin is fixed to be the same as the chute section width, which is 47.0 m.

The flow in exit channel, in excess of design discharge, may scour the channel bed/side slopes or may over flank the channel banks. According to the design, there is no risk to human life and the risk may only be limited to some minimal loss of property. Hence, the section of exit channel is proposed to be designed to cater to the half of the rated flow over spillway, i.e., 740.0 m^3/s [73].

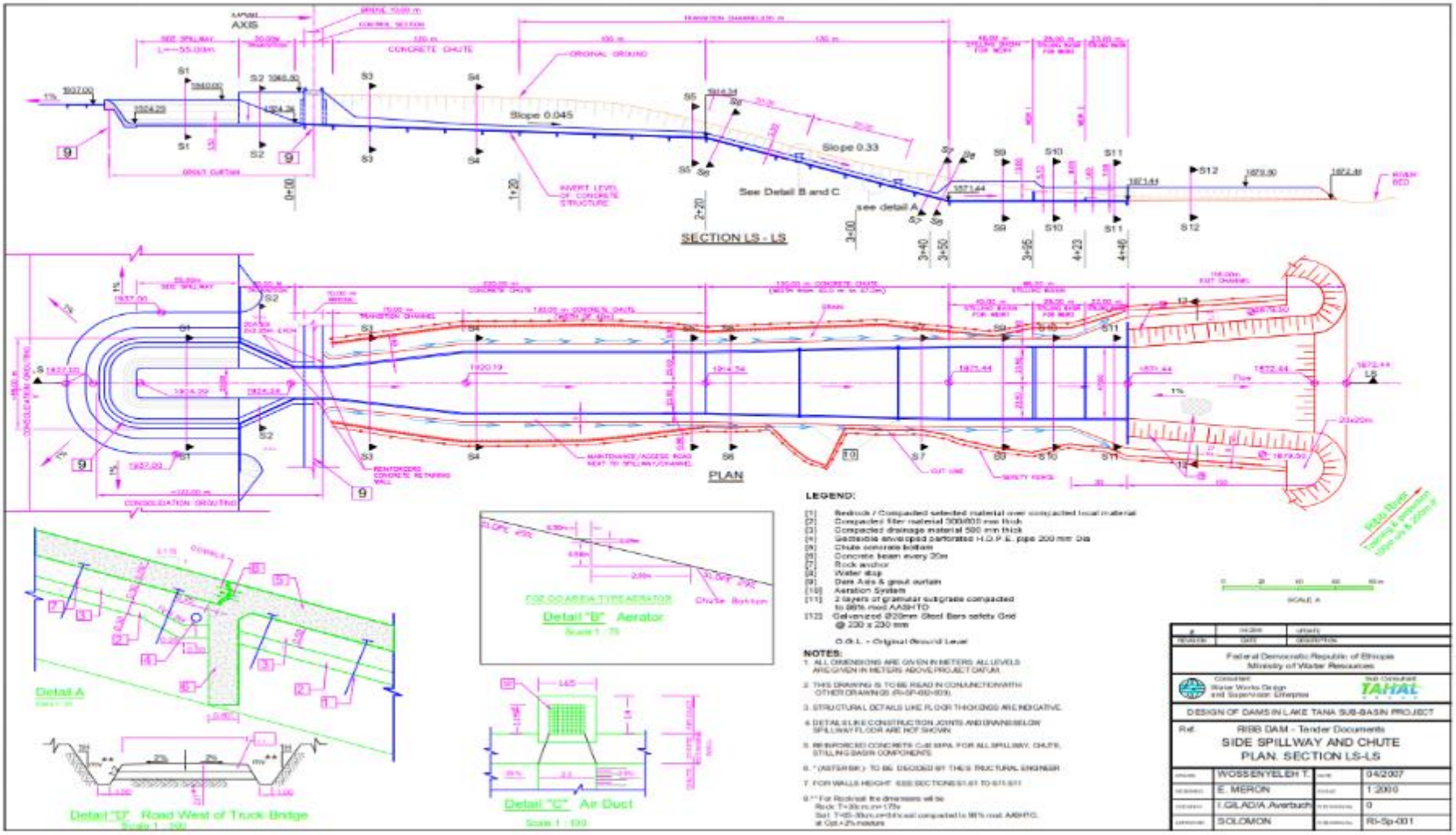

Figure 6- 1 Plan and Section of the Spillway as per the Design [73]

6.3 STATEMENT OF THE PROBLEM

The U-shaped side channel spillway have a curvature at the commencing point of the side channel trough and this maximizes the use of side channel trough length for spilling. The hydraulic design was done based on 1D model. However, this 1D model cannot show the performance of the hydraulic structure that accommodates flow from all directions. In addition, the side channel is a structure where the subcritical flow condition will be changed to critical and these flow exhibits 3-dimenssional in nature. Even if there is hydraulic complexity in the side channel trough, the U-shaped side channel spillway is selected from the topographic perspective of the area but the design has not been verified with either physical model or 3D hydrodynamic model.

The stilling basin has two weir structures for dissipating the energy. Since as per the design it requires stilling basin type II, the provided weir type of dissipation is not conventional type of energy dissipation. In addition, the proposed type of dissipation with weir has not been verified with the physical model or 3D hydrodynamic model.

6.4 OBJECTIVE OF THE STUDY

The objective of the study is to check the design of Ribb Dam side channel spillway using FLOW-3D numerical model. The study is mainly focused on the stilling basin with two weir type of energy dissipaters and their capability to dissipate excess energy and ensure

safe operation of the structure at a range of operating conditions. In addition, verification of the hydraulic performance of the hydraulic structures over the entire length of the spillway has been done. The control section (side channel ogee spillway), mild slope chute channel and steep slope chute channel are also included in the study. Meanwhile, proposing possible improvements for modification of the section will be done if required.

6.5 METHODS

6.5.1 Boundary and Initial Conditions

FLOW-3D hydrodynamic model has been used for verification and modification of the Ribb dam side channel spillway design. Since the flow domain is defined as a hexagonal in the Cartesian coordinates, there are different boundaries on each mesh block. The boundaries on the mesh and their coordinate directions were set as follows.

For optimal simulation, the spillway was modelled in three mesh blocks. The boundary condition for flow data in Block 1, the upstream boundary condition (X_{min}) was defined as volume flow rate 1,060 m^3/s at the inlet of the spillway, the downstream boundary condition (X_{max}) was defined as symmetry. The bottom boundary (Z_{min}) was defined as the Wall (no-slip condition) and the top boundary (Z_{max}) was set as Specified Pressure (with Fluid Fraction = 0). In Block 3 at the outlet, Y_{min} was given as an outflow. All the other blocks between Block 1 and 3 were either Symmetry or Wall condition. Symmetry means a zero-gradient condition which is continuative at the boundary. Wall means no-

slip condition at the boundary as well as a zero-velocity condition normal to the boundary [22]. Figure 6- 2 shows the boundary conditions. The initial conditions that represent on the upstream sides of the spillways at the same level as the specified fluid heights were proposed fluid elevation. The free surface water elevation option was given as an initial condition at the Block 1. The Z_{max}-coordinate of the free surface was fixed for the estimated initial condition.

6.5.2 Numerical Simulations Options

In most cases, the default selections were used; however, in case of momentum advection algorithm, the default momentum advection algorithm is a first-order upwind differencing method. In this numerical simulation second order momentum advection was given since there is a bend or U-shaped side channel. Starting from smaller time steps that is from 0.5 seconds upto 70 seconds, were given to get the final numerical simulation result. Implicit pressure solver was used.

6.5.3 Discretization Approach

FLOW-3D uses the finite volume method to solve the Navier-Stokes system of equations in three dimensions to simulate the flow of fluid. In this numerical model three numerical hexagonal meshes blocks were built to properly capture the geometry of the structure and correctly simulate the water flow from the reservoir to the outlet. Various computational trials are conducted with different grid cells size in x, y and z directions and

it was observed that the cells at the ogee, the weirs in stilling basin were not resolved well when the grid size was given above 0.5 m. Hence, 0.5 m width was given for all hexagonal grid widths. Figure 6- 3 shows the plan of the spillway and mesh blocks prepared for the model.

6.5.4 Model Geometry

The numerical analysis was carried out based on the original design and modified section of the side channel spillway. In addition, the designed data obtained from the report was also compared with the numerical results of design and modified numerical results. The total length of the spillway model is 630 m.

Another geometry option, that remained constant for all spillway modeling completed as part of this study was the inclusion of surface roughness value applied on the surface of all spillway geometry. The roughness friction factor = 0.013 for a concrete lined channel is also included. The numerical model comprises the approach ogee side channel crest, trough, control section, chute channel and stilling basin [59]. Figure 6- 4 shows the computational domain.

The runs were developed in a personal computer with a Pentium 4 Ghz processor and 16 GB of RAM; the evolution in time was used as a relaxation to the final steady state. Simulation time was given as 70 second and accordingly 3 days were taken to finalize simulation. The required output memory size was 84 GB carried out with eight multi processes parallel.

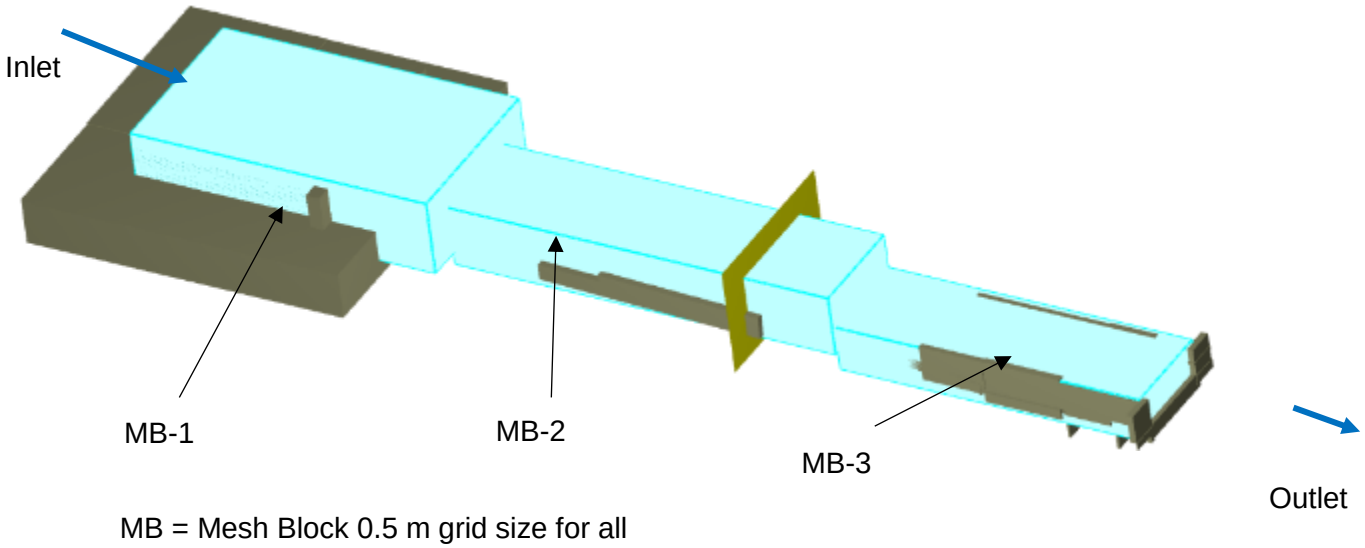

Figure 6- 2 Different mesh blocks for the spillway model 0.5 m grid length for all grid

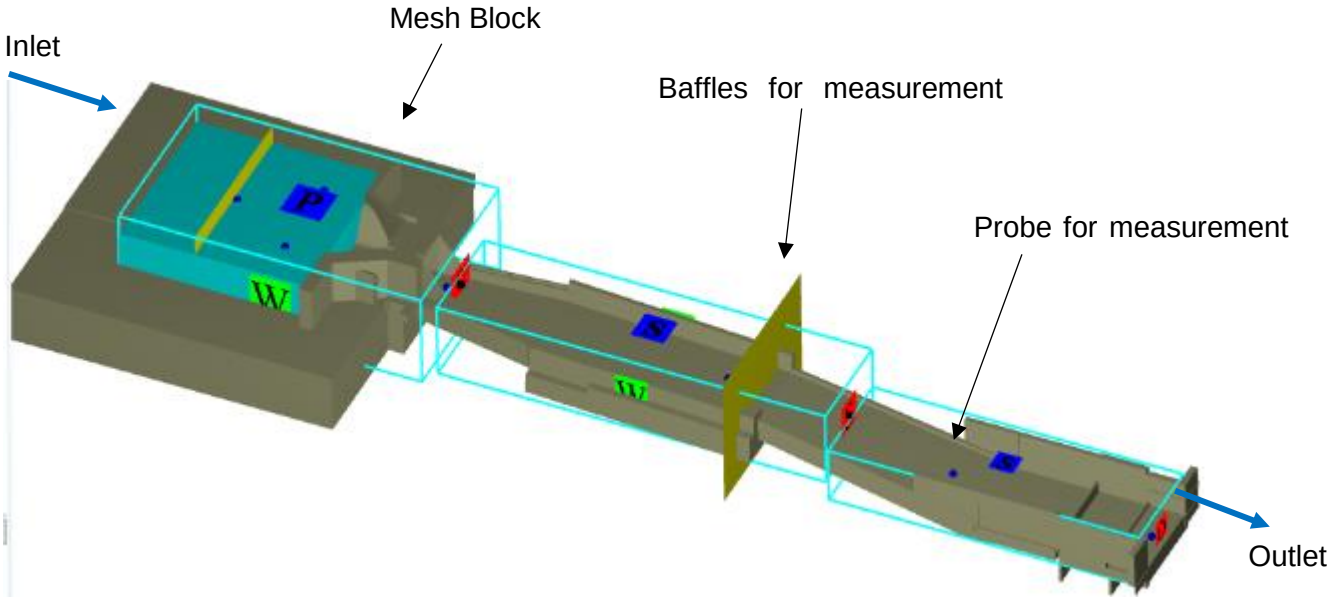

Figure 6- 3 Boundary conditions and location of hydraulic measuring devices

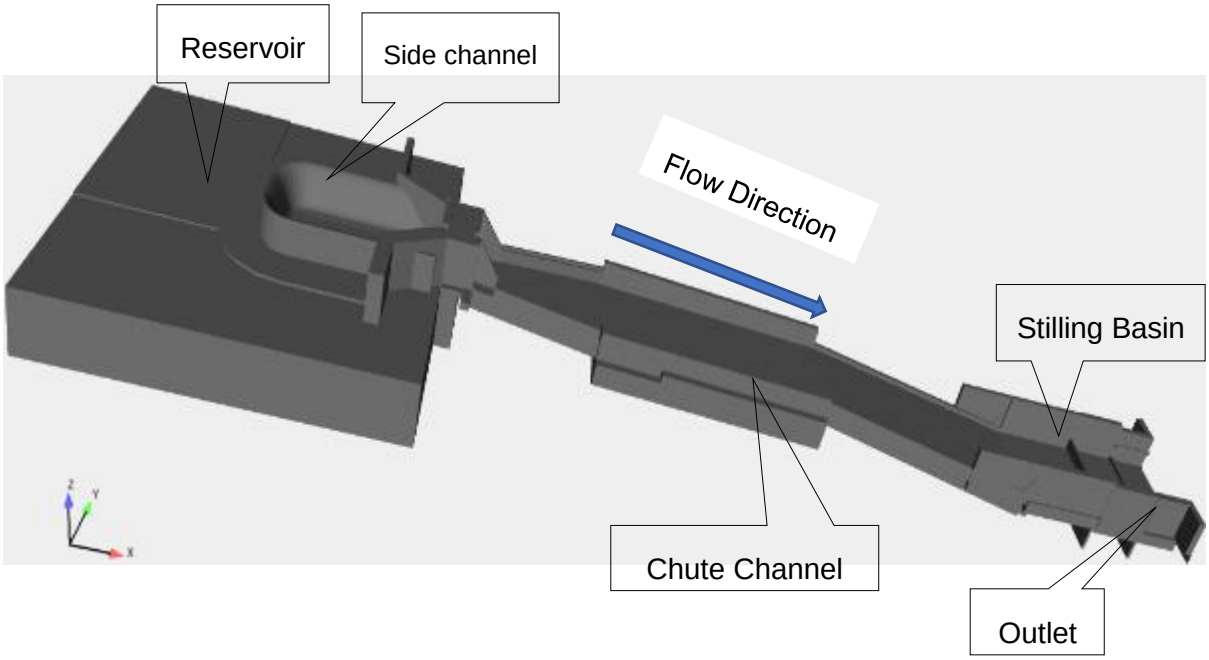

Figure 6- 4 Computational domain of the Spillway

6.6 RESULTS

6.6.1 Flow over the Spillway Crest

The routed half PMF flow which is 1,060 m^3/s was considered for design and checked for full PMF which is 2,340 m^3/s. As per the design, flow depth for half PMF is 3 m and for full PMF 5 m. Since water flows over the two side channels and the front section, data was taken in 3D model at three points and the average result was taken. As per the design the actual length of the crest is 153 m however, for design it has been taken 107 m for half PMF and 123 m for full PMF for considering the complexity of flow at U-shaped.

Therefore, as per the 3D model 1.3 m depth of flow for half PMF and 2.5 m for full PMF were the results. The design result is more than 50 % from the model result. Due to such large difference, the researcher modified the side channel spillway length reducing by 50 m and run the simulation for reduced length. Accordingly, the 3D model result depth of flow over the crest for full PMF was 3.0 m. It is required to note that 3 m flow depth is designed for half PMF in the design report. Therefore, the flow depth over the crest will not reach 5 m even with full PMF and reduced section. This indicates that, the designed length is excessively large which shows uneconomical design. According to the results, no overtopping and the wing walls are sufficient for all cases including PMF flow. Figure 6- 5 and Figure 6- 6 show for the half PMF and full PMF as per the design section. Figure 6- 7 shows the reduced section with full PMF. Since there was high fluctuation for the first 20 seconds, average depth was taken after 20 seconds.

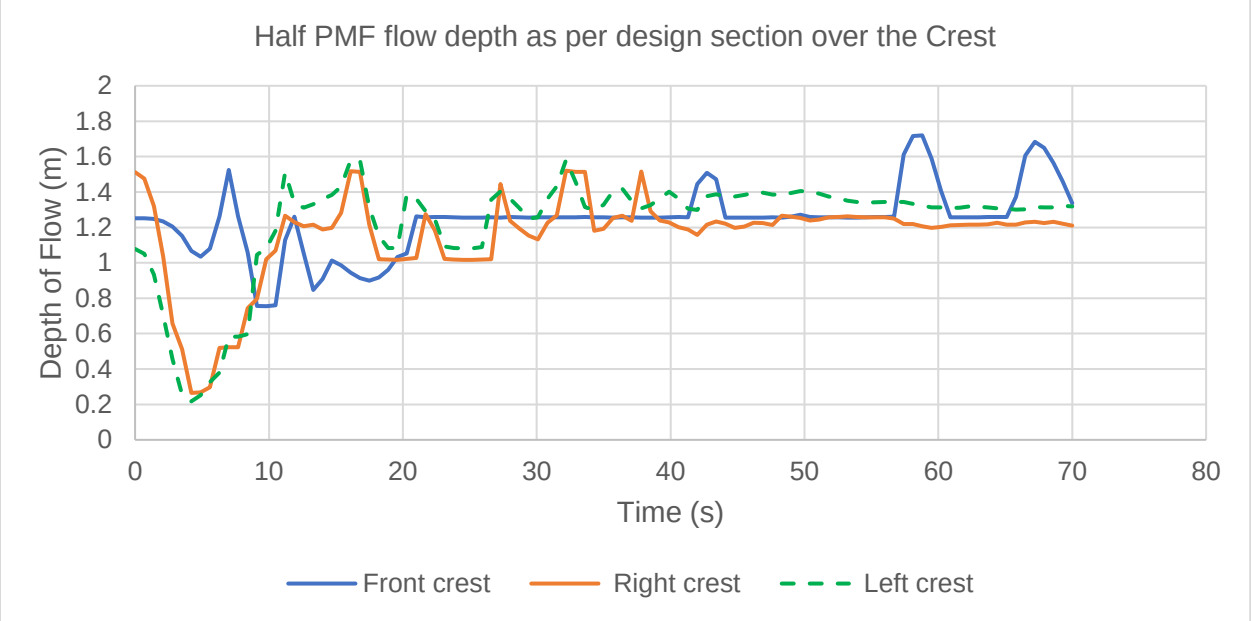

Figure 6- 5 Half PMF flow depth as per design section over the Crest

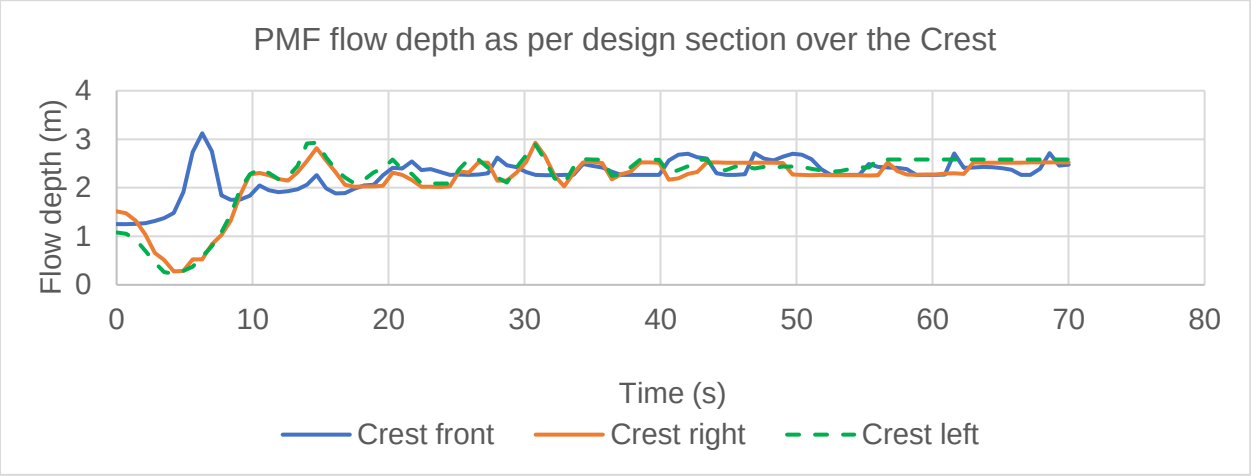

Figure 6- 6 PMF flow depth as per design section over the Crest

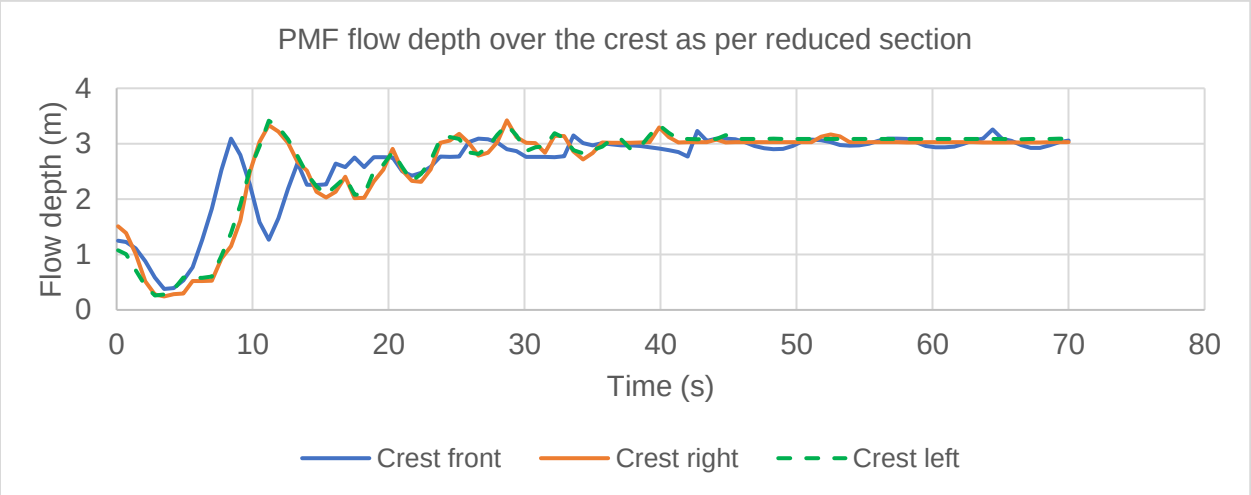

Figure 6- 7 PMF flow depth over the crest as per reduced section

6.6.2 Side Channel Trough

As per the design report the flow in the side channel trough to be subcritical and not submerged flow. Accordingly, the 3D model result for both half PMF and full PMF was subcritical and not submerged flow for the design section. Meanwhile, the trough was also checked with the reduced section and the result showed that it was subcritical and not submerged flow. Figure 6- 8 shows the half PMF Froude number result showing less than one implies the flow is subcritical.

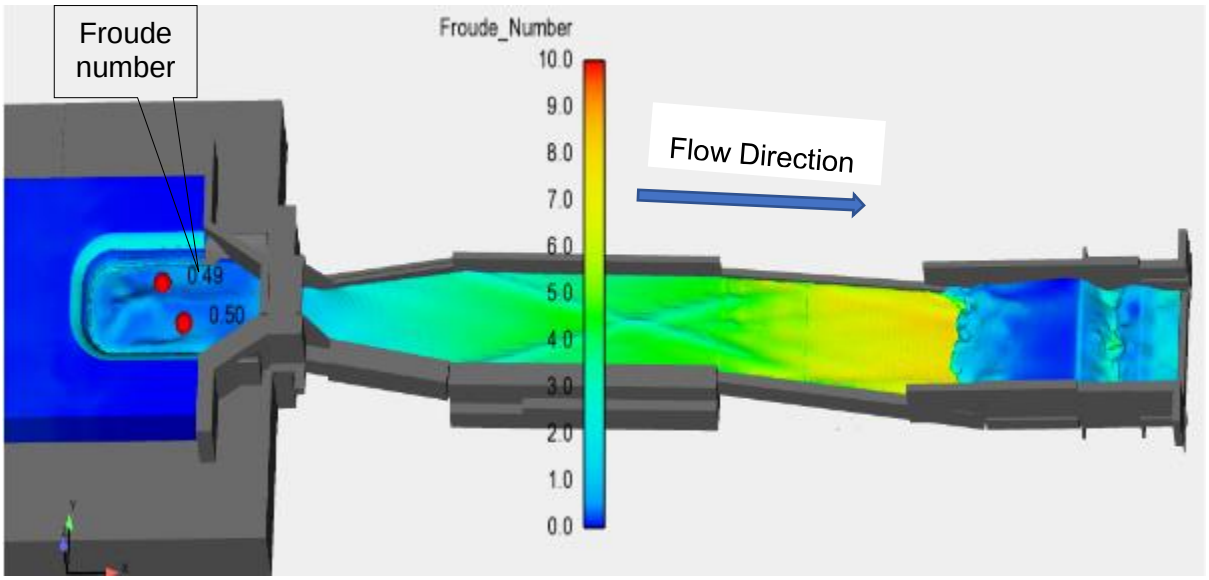

Figure 6- 8 3D model result showing Froude number

6.6.3 Control Section and Water Profile in Side Channel Trough

Control section is where the section has minimum energy and the flow is changed from sub critical in the side channel trough to supercritical in the conveyance chute channel. As per the 3D model in both flow conditions half PMF and full PMF, the control section is sufficient to pass the flow without overtopping.

There is sufficient clearance between bridge deck bottom and water level top in the control section. Therefore, the bridge will not be overtopped with either the design or the worst condition of the full PMF. Thus, the 3D model properly showed the flow condition which has 3-dimensional flow condition. Figure 6- 9 shows the full PMF flow depth for trough and control section.

Over the Crest 0+800

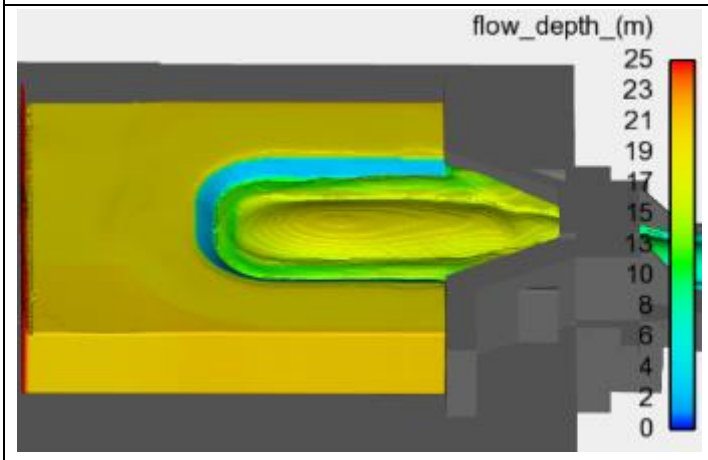

1 : 3D model result at with full PMF plan

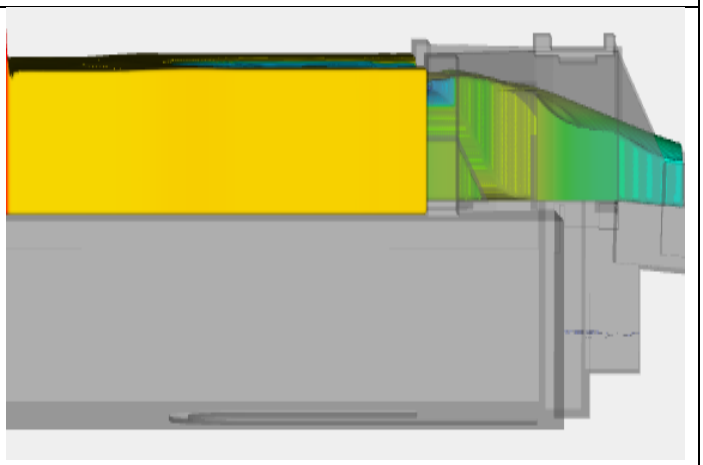

2 : 3D model result at with full PMF profile at the control

Figure 6- 9 3D model result for PMF flow as per the design section for control section

6.6.4 Along Chute Channel

As per the design, the chute channel starts from the outlet of the control section from ch 0+000 to 0+350 m until it joins the stilling basin. Refer Figure 6- 10 . Accordingly, Table 6- 1 shows the results as per the design and the 3D model. The first 20 m had difference

in depth of flow and the last part of the chute from ch 0+300 to 0+350 the difference was significant. The main reason for the last part was that the hydraulic jump was not considered in 1D model. As per the 3D model from ch 0+320 to 0+350 it was in hydraulic jump condition. This flow condition can be seen only with 3D model. The other section from ch 0+020 to 0+300 m the 3D model result agrees with the design result. The main reason for such good agreement was that the chute channel has no complex section. The 3D model result for depth of flow in the channel cross section at different location are shown in Figure 6- 11 . In addition, Figure 6- 12 shows the longitudinal profile with velocity contour.

The statistical parameters for the chute channel as per the 3D and design result was as flow. Chute channel performance indicators for 3D model result with Design result for depth of flow R^2 = 0.986, NSCE = 0.959 and Rbais = -0.123. For velocity R^2 = 0.993, NSCE = 0.992 and Rbais = -0.006. For further information refer Annex D.

Table 6- 1 Ribb chute channel performance indicators 3D with Design for Depth of flow (m)

Measurement Location	Depth of flow from 3D model (m)	Depth of flow from Design (m)	Percentage difference (%)
0	5.59	6.591	-15.19
20	3.52	4.997	-29.56
90	1.74	1.78	-2.25
220	1.48	1.59	-6.92
240	1.31	1.3	0.77
260	1.18	1.12	5.36
280	1.1	1.01	8.91
300	1.01	0.92	9.78
Sum	16.93	19.308	
Average	2.116	2.414	

R^2 =	0.977
NSCE =	0.900
Rbias =	-12.316

Table 6- 2 Ribb chute channel performance indicators 3D with Design for velocity (m/s)

Measurement Location	Velocity of flow from 3D model (m/s)	Velocity of flow from Design (m/s)	Percentage difference (%)
0	9.46	0.84	1026.19
20	12.05	10.61	13.57
90	15.51	14.88	4.23
220	18.47	16.71	10.53
240	20.03	19.96	0.35
260	21.18	22.49	-5.82
280	22.23	24.53	-9.38
300	23.61	26.16	-9.75
Sum	142.54	136.18	
Average	17.818	17.023	

R^2 =	0.960
NSCE =	0.808
Rbias =	4.670

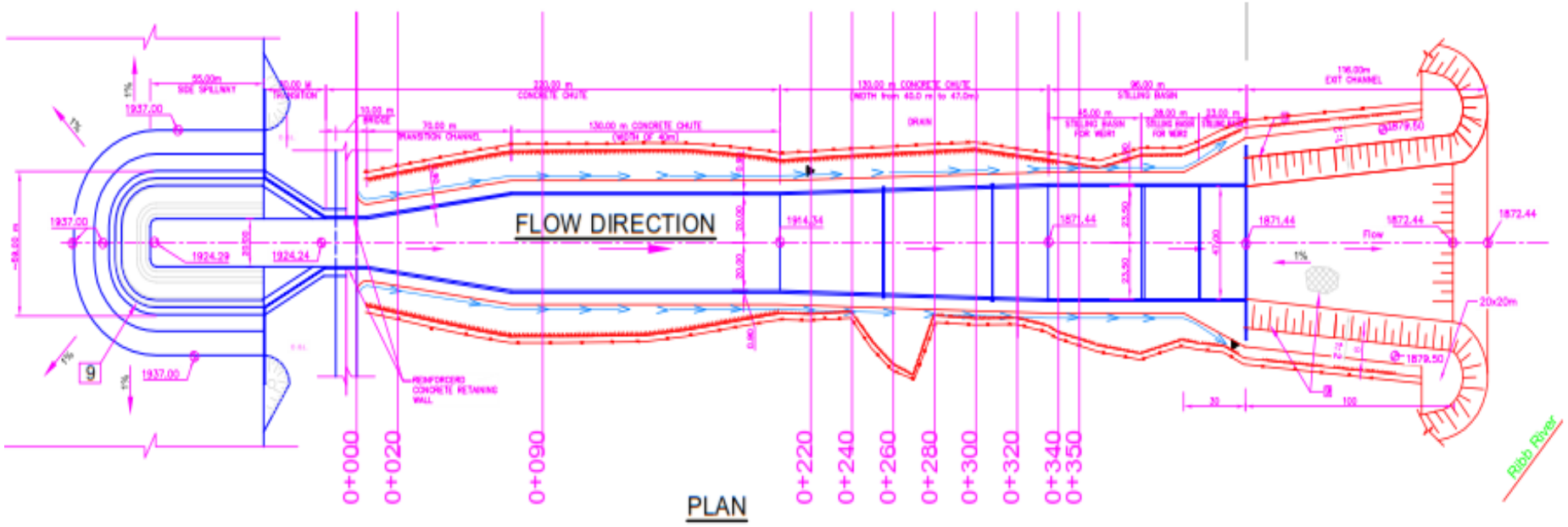

Figure 6- 10 Plan and Section of the Spillway showing chainage for chute channel [73]

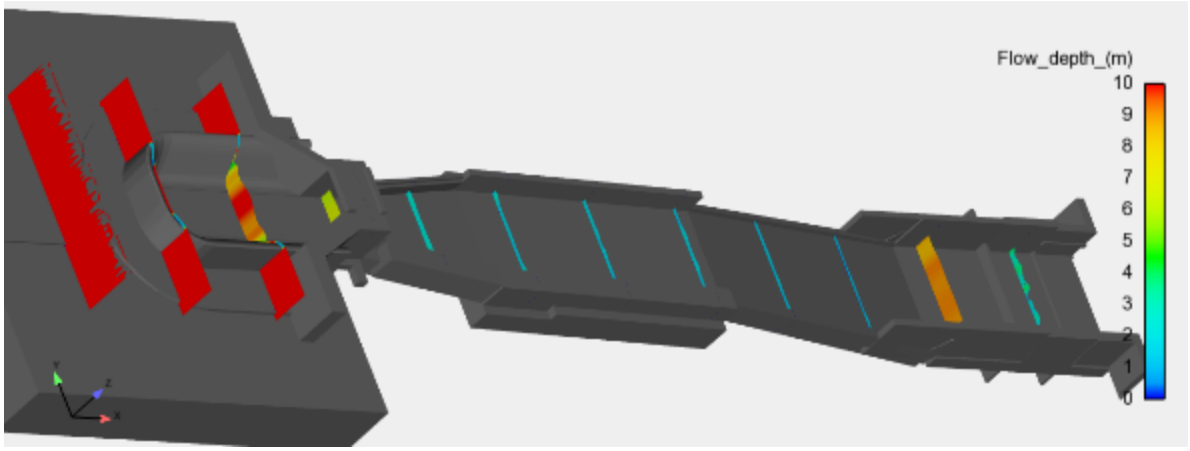

Figure 6- 11 Depth of flow across the spillway channel from inlet to outlet

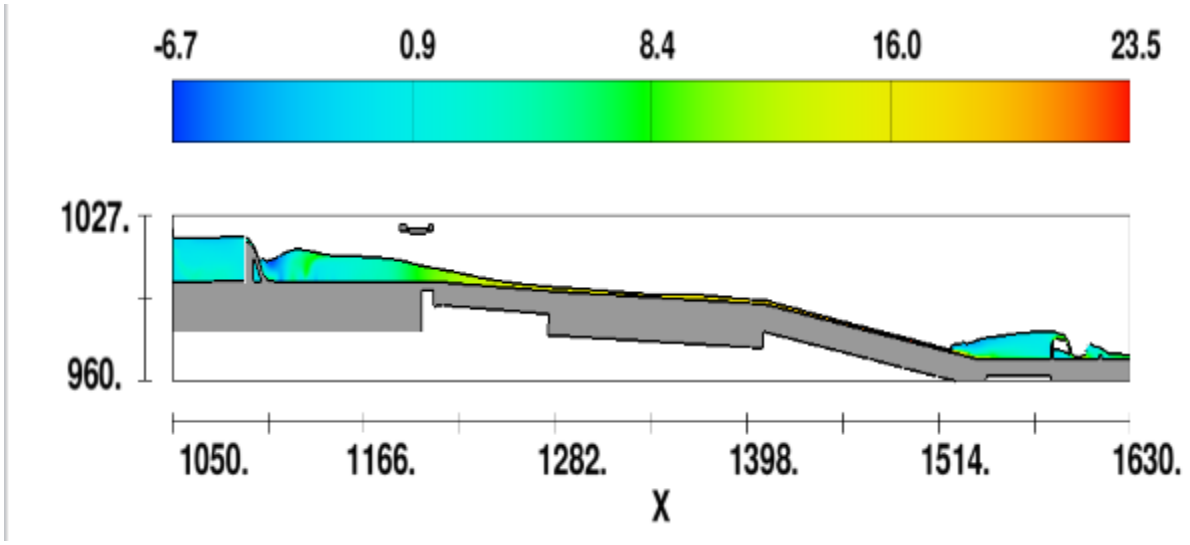

Figure 6- 12 Longitudinal profile with contours showing velocity

6.6.5 At Stilling Basin

As per the design the stilling basin has two sharp crested weirs for dissipation of the hydraulic energy. The first weir height is 5 m and the second is 3 m height. The depth of hydraulic jump as per the design is 7 m at the first weir and 5.66 m at second weir. According to 3D model the hydraulic jump created by the first weir was 18.63 m and by second weir was 9.25 m. According to the design, the wall height at stilling basin for weir-1 is 13 m which is not sufficient to protect overflow. Therefore, wall height needs to be raised for additional 7 m. After modification of the wall height by raising additional 7 m, the 3D model shows that the spillway is safe from overtopping. Meanwhile, wall height for weir-2 is sufficient and no need of modification. Figure 6- 13 and Figure 6- 14 show flow profile at stilling basin before modification and after modification. Figure 6- 15 shows detail information at weir 1 and weir 2.

As per the design report, for any problem for downstream channel it will be acceptable to be maintained. Hence, the 3D model result at the outlet showed that there was high velocity.

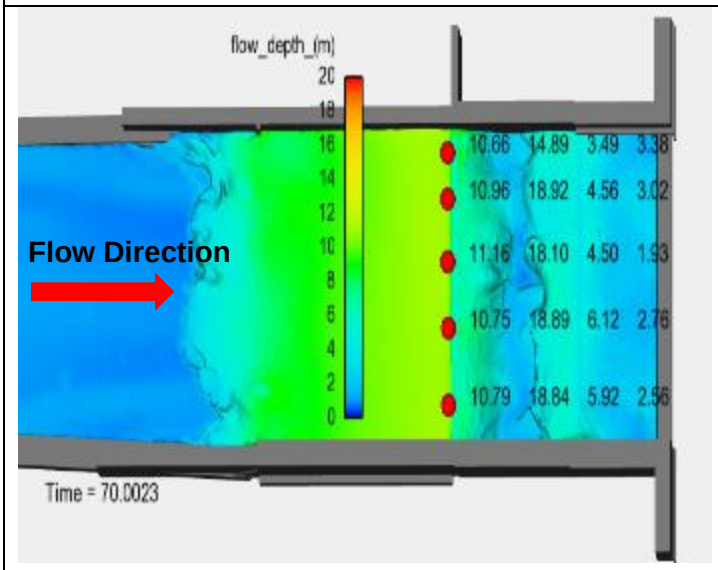

1 : 3D model result at Weir 1

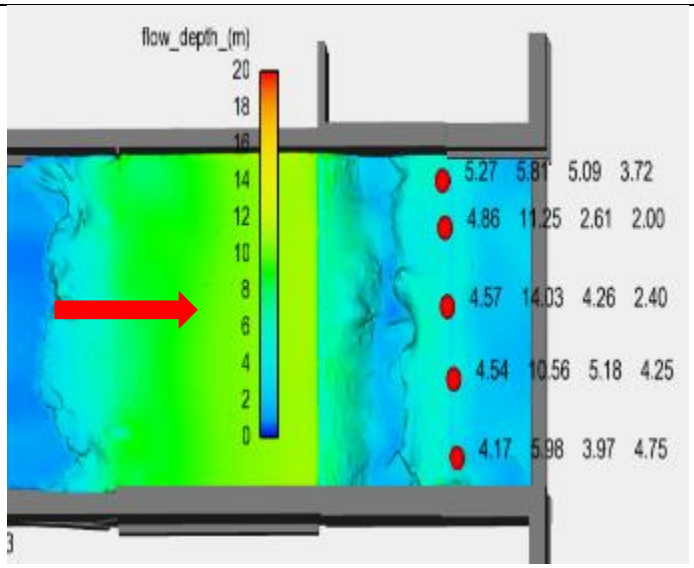

2 : 3D model result at Weir 2

Figure 6- 13 Flow Profile of 3D in stilling basin as per the proposed design modification

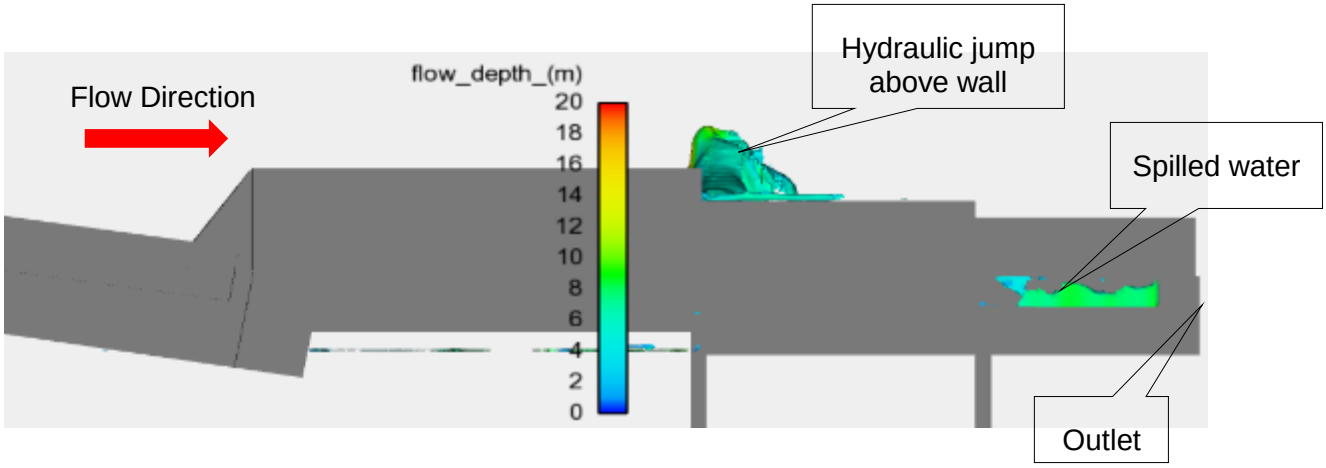

Figure 6- 14 Flow profile at Stilling Basin as per the design

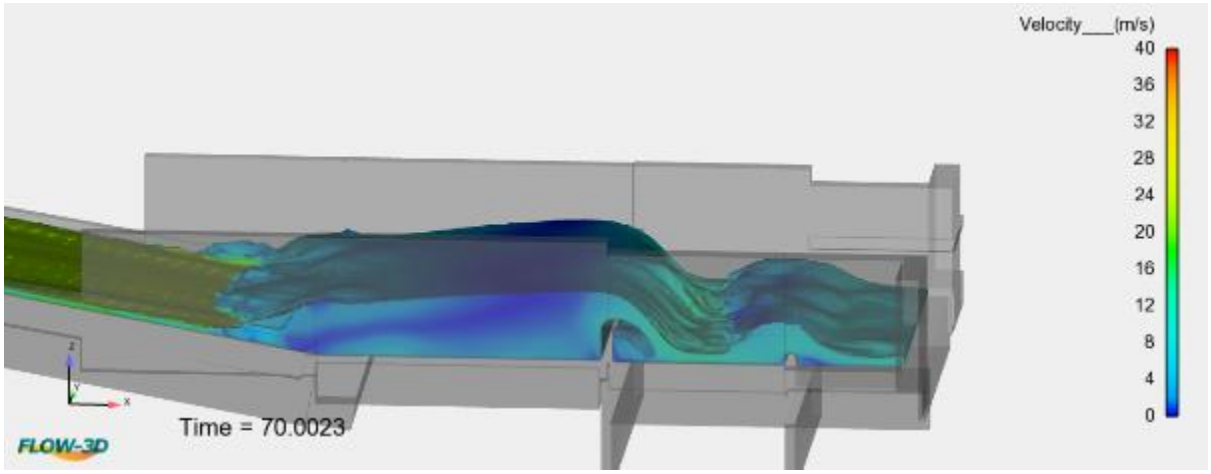

Figure 6- 15 Flow Profile of 3D in stilling basin as per the proposed design modification

6.7 DISCUSSIONS

The general objective of the study is to verify the hydraulic performance of the hydraulic structures over the entire range of possible operating conditions and suggest possible improvements of the original reference design. This has been done for Ribb side channel spillway.

Ribb side channel spillway is a U-shaped side channel spillway which is designed and constructed recently in Ethiopia. However, the design has not been verified with at least 3D hydrodynamic model before construction. The performance of the U-shaped side channel has been checked using FLOW-3D hydrodynamic numerical model and found that it is uneconomical design. During research, the design has been checked by reducing the spillway length by 50 m and it can operate for PMF flow with lower design head. Such result obtained using the state– of– art of 3D hydrodynamic model indicates that for any similar complex structure, it is advisable to check the design with either 3D model or physical model.

Ribb side channel spillway is constructed by excavating 15 m depth of rock and an estimated concrete quantity for a length of 50 m and rock excavation could have been saved up to 2M USD. This is also could play an important role in reducing construction time.

In addition, the unconventional stilling basin of the Ribb dam spillway has been also checked with 3D hydrodynamic model and found that the designed and constructed wall height will be overtopped. Hence, the wall height requires to be raised by 7 m, otherwise the spillway as well as the dam are not safe for operation.

Since, the chute channel has no complex section, there is good agreement between the 3D model result and design data. Therefore, FLOW-3D model can properly predict the flow condition and it has the ability to show the flow condition in a complex section in detail in three dimensions.

6.8 RECOMMENDATIONS AND CONCLUSION

The construction of Ribb Dam Spillway has been completed in 2018. However, the design safety for its operation has not been confirmed either with a physical model or 3D numerical model. Therefore, the following recommendations is that: -

- To avoid unnecessary extra cost expenditure and prolonged construction time, before construction of any complex hydraulic structure, the design should be verified with at least 3D hydrodynamic model.
- the stilling basin must be modified by increasing the wall height by 7 m otherwise the dam is not safe for the operation.
- A 3D hydrodynamic modelling must be used because it helps the designers to improve the hydraulic performance of existing or new hydraulic structures.

Due to the development of science and technology, the emergency of the 3D numerical model is one of the base lines for the design of the complex hydraulic structures that can operate safely. Modelling flow in a complex geometry using the state- of- art of 3D numerical model will not only help to enhance and recognize the complex hydrodynamic flow conditions but it also helps to ensure uniform velocity distribution, depth variation, energy dissipation, etc. This will enable the engineers to provide the required sections with greater accuracy, appropriate energy dissipation methods and safe hydraulic structure. Therefore, for a complex flow structure the design or verification must be done with at least 3D numerical model.

CHAPTER SEVEN

7 CONCLUSION AND RECOMMENDATIONS

7.1 CONCLUSION

The objective of this research is to design hydraulically safe structure for complex section using the state-of-art of 3D hydrodynamic modelling a case study of Tendaho Dam Spillway and Ribb Dam Spillway in Ethiopia. In order to enhance the design of such complex hydraulic structure, FLOW-3D hydrodynamic numerical model has been selected. Accordingly, performance assessment of the FLOW-3D was done based on the physical model result and designed data of Zarema May Day Dam Spillway. The verification work was focused on the flow depth and velocity distribution, water surface profile, bend super elevation, nappe uniformity and energy dissipation. FLOW-3D model has good agreement with the physical model especially along the approach channel, at the crest, after the guide wall, along the chute channel, before the bend, at the baffles and cascade drops.

Tendaho Dam Spillway was constructed over ten years ago. However, the design safety for its operation has not been confirmed either with physical model or 3D numerical model. In these durations, one flood season has occurred, and it caused significant loss. On the other hand, after damages, maintenance on the spillway has been done based on the original design. After assessing the performance of FLOW-3D, it was applied to identify the problem of Tendaho Dam Spillway problem. The numerical modelling shows that FLOW-3D predicted

the flow pattern agrees with the general flow conditions at the stilling basin and downstream of stilling basin and along bend where there was a serious problem. To overcome this problem, modification has been done and verified with FLOW-3D hydrodynamic modelling.

The design of Tendaho dam spillway is sized to pass the routed half Probable Maximum Flood (½ PMF) and dam overtopping is checked for full PMF. Furthermore, dam overtopping is checked for full PMF if for some reason, one of the control gates is faulty. The routed peak discharge for half PMF is 1,700 m^3/s with 8.4 m depth of water above the spillway crest and the routed discharge for full PMF is 2,194 m^3/s with 9.2 m depth of water above the spillway crest for 30.0 m crest length of spillway (3 bays of 10.5 m each). The routed discharge for full PMF is 2,194 m^3/s for the worst condition that is if one of the three control gates malfunctions, restricting the overflow length to 21.0 m only (2 bays of 10.5 m each) with 10.4 m depth of water above the spillway crest.

During research simulation has been done for two scenarios to check the performance of the spillway control section based on the design. The first simulation was for half PMF and the second simulation was for full PMF to check the safety of the dam from being overtopped if for some reason, one of the control gates is faulty. For the worst condition that is one of the three control gates malfunctions, restricting the overflow length to 21.0 m only. The depth of flow as per the design is 10.4 m without overtopping of the dam. The 3D model result for depth of flow over the crest was 7.75 m. The 3D model result for depth of flow from the design was lower than the design flow which shows that the dam is safe from overtopping.

The performance of the Ribb dam U-shaped side channel spillway has been checked using FLOW-3D hydrodynamic numerical model and found that it is safe for the operation, however

it is uneconomical design. During research, the design has been checked by reducing the spillway control crest length by 50 m. Accordingly, with the reduced section it can operate for PMF flow with lower head than design head. Such result obtained using the state – of – art of 3D hydrodynamic model indicates that for any similar complex structure, it is advisable to check the design with either 3D model or physical model.

In addition, the unconventional stilling basin of the Ribb dam spillway has been also checked with 3D hydrodynamic model and found that the designed and constructed wall height will be overtopped. Hence, the wall height requires to be raised by an additional 7 m, otherwise the spillway as well as the dam are not safe for operation.

For the area where there is no complex section, there is good agreement between FLOW-3D result and physical model as well as design results. For complex section, FLOW 3D can well predict the flow condition. Therefore, 3D hydrodynamic numerical model increases the level of confidence in designing hydraulic structures comprising critical issue for decision in dam design process. Cost savings in spillway through proper design is important to ensure the safety of the dam as well as guiding the engineers for design of complex hydraulic structures. The 3D hydrodynamic numerical model capability gives engineers the power to quickly and inexpensively explore different design options and often demonstrates how a water resource project can be constructed and or operated more efficiently.

Due to the development of science and technology, the emerging of the 3D numerical model is one of the base lines for the design of the complex hydraulic structures that can operate safely. Modelling flow in a complex geometry using the state- of- art of 3D numerical model will not only help to enhance and recognize the complex hydrodynamic flow conditions but it

also helps to have uniform velocity distribution, depth variation, energy dissipation, etc. This will enable the engineers to provide the required sections with greater accuracy, appropriate energy dissipation methods and safe hydraulic structure. Therefore, for a complex flow structure the design or verification must be done with 3D numerical model.

7.2 RECOMMENDATIONS

The verification of FLOW-3D results showed that, the numerical solution can well predict the flow depth and velocity along approach channel, over the crest, along chute channel, at bend and along the cascade drops for Zarema May Day Dam Spillway.

The overall recommendation forwarded by researcher is that, it is a significant technological development to use 3D hydrodynamic numerical model for design of complex hydraulic structures. Flow condition at the curve or complex section cannot be seen by 1D or 2D numerical model. Therefore, any complex hydraulic structure design such as spillway of the dam must be verified by 3D hydrodynamic numerical model. 3D hydrodynamic numerical modelling must be used for it helps the designers to improve the hydraulic performance of existing or new hydraulic structures.

The successful application of 3D hydrodynamic numerical model analysis in the design of complex hydraulic structures is a major step towards increasing the industry's confidence in the use of 3D hydrodynamic numerical model techniques to assist in all types of hydraulic design like dam design, hydropower design, irrigation design, water supply design or flood control design.

The followings are the main recommendations: -

- 3D hydrodynamic numerical modelling must be used for it helps the designers to improve the hydraulic performance of existing or new hydraulic structures.
- For open channel flow, depth and velocity are the main parameters to be checked in supercritical flow however, other hydraulic conditions are also useful for design.
- There should be a standard for the design methodology to be followed for verification of complex hydraulic structures before construction. The design verification must be done with at least 3D numerical model before construction.
- The Dynamic structural design of spillway should be done using the result of 3D model which can be obtained from Y and Z velocity components.

8 REFERENCE

[1] W. Wu, Computational River Dynamics, Mississippi,USA: National Centre for Computational Hydroscience and Engineering, 2007.

[2] M. D. M. a. E. Napoli, "3D Numerical Simulation of Curved Open Channel Flows," *Proceedings of the 2006 IASME/WSEAS Int. Conf. on Water Resources, Hydraulics & Hydrology, Chalkida, Greece,* pp. 86-91, May 11-13-2006.

[3] W. Syme, "Modelling of Bends and Hydraulic Structures," *The Institution of Engineers, Australia Conference on Hydraulics in Civil Engineering,* 30 November 2001.

[4] M. Zhenwei, Z. Zhiyan and Z. Tao, "Numerical Simulation of 3-D Flow Field of Spillway based on VOF Method," *International Conference on Modern Hydraulic Engineering ,* pp. 808 - 8012, 2012.

[5] E. Fadaei-Kermani and G. Barani, "Numerical simulation of flow over spillway based on the CFD method," *Scientia Iranica ,* pp. 91 - 97, 2014.

[6] J. Willy, T. Ewing, B. Wark and E. Lesleighter, "Complementary use of physical and numerical modelling techniques in spillway design refinement," in *COMMISSION INTERNATIONALE DES GRANDS BARRAGES* , Kyoto AUSTRALIA , Juin 2012.

[7] P. Novak, A. Moffat and C. Nalluri, Hydraulic Structures, New York: Taylor & Francis , 2007.

[8] U.S. Department of the Interior Bureau of Reclamation, "Appurtenant Structures for Dams (Spillways and Outlet Works) Design Standard," in *Reclamation Managing Water in the West (Design Standards No. 14)*, vol. 3, U.S. Department of the Interior Bureau of Reclamation, Bureau of Reclamation Technical Service Center , August 2014, pp. 3-1 to 3-147.

[9] D.K.H.Ho, B.W.Cooper and K. &. S. Donohoo, "Application of numerical modelling to spillways in Australia," *Dams and Reservoirs, Societies and Environment in the 21st Century Taylor and Francis Group,* p. 951 959, 2006.

[10] E. Teklemariam, B. W. Korbaylo, J. L. Groeneveld and D. M. Fuchs, "COMPUTATIONAL FLUID DYNAMICS: DIVERSE APPLICATIONS IN HYDROPOWER PROJECT's DESIGN AND ANALYSIS," *Water Mannagment in Chainging "Climate" ,* June 11-14, 2002.

[11] D.K.H.Ho and K. a. S. Donohoo, "Investigation of Spillway Behavior under Increased Maximum Flood by Computational Fluid Dynamics Technique," in *14th Australian Fluid Mechanics Conference*, Adelaide, Australia, 10-14 December 2001.

[12] H. David, B. Karen, D. Shane and C. Brian, "Numerical Analysis for Spillways," *43re ANCOLD Conference ,* 2003.

[13] R. R. O. M. R. T. C. Foias, Navier-Stokes Equation and Turbulence, Cambridge : Encyclopaedia of Mathematics and Its Applications Cambridge University, 2001.

[14] F. L. E. Y. R. S. Y. Cheng, "A comparison of large Eddy simulations with a standard k–ε Reynolds-averaged Navier–Stokes model for the prediction of a fully developed turbulent flow over a matrix of cubes," *Journal of Wind Engineering and Industrial Aerodynamics ,* pp. 1301-1328, 2003.

[15] A. H. G. I. a. J. M. Brethour, “On the Implementation of Two-equation Turbulence Models in FLOW-3D,” *Flow Science, Inc. ,* pp. 1-47, November 2009 .

[16] L. Davidson, Fluid mechanics, turbulent flow and turbulence modeling, Sweden: Chalmers University of Technology, November 23, 2015.

[17] C. 9. 1. 0. P. 3. C. R. P. V. U. OPTEK, Turbulence Handbook for Experimental, Skovlunde, Denmark : Dantec Dynamics A/S, September 2012.

[18] S. A. M. Al-Hashimi, H. M. Madhloom, R. M. Khalaf, T. N. Nahi and N. A. Al-Ansari, “Flow over Broad Crested Weirs: Comparison of 2D and 3D Models,” *Journal of Civil Engineering and Architecture ,* pp. 769 - 779, 2017.

[19] D. Valero, R. García-Bartual and J. Marco, “Optimization of Stilling Basin Chute Blocks Using a Calibrated Multiphase RANS Model,” in *5th International Junior Researcher and Engineer Workshop on Hydraulic Structures* , SPAIN, 28-30 August 2014 .

[20] SadeghDehdar-behbahani and A. Parsiae, “Numerical modeling of flow pattern in dam spillway’s guide wall. Case study: Balaroud dam, Iran,” *ELSEVIER Alexandria Engineering Journal,* vol. 55, no. 1, pp. 467- 473, March 2016.

[21] R. Gabl, J. Seibl and B. G. a. M. Aufleger, “3-D numerical approach to simulate the overtopping volume caused by an impulse wave comparable to avalanche impact in a reservoir,” *Natural Hazard and Earth Scienses,* pp. 2617 - 2630, December 2015.

[22] FLOW 3D , “Flow 3D User Manual,” 2014.

[23] F. A. Bombardelli, I. Meireles and J. Matos, “Laboratory measurements and multi-block numerical simulations of the mean flow and turbulence in the non-aerated skimming flow region of steep stepped spillways,” *Environ Fluid Mech Department of Civil and Environmental Engineering, University of California,* August 2010.

[24] I. S. A. Lu´cio, “Numerical modeling of skimming flow over stepped spillways: application on small embankment dams,” Lisboa, Portugal , December 2015.

[25] M. C. Johnson, M.ASCE and a. B. M. Savage, “Physical and Numerical Comparison of Flow over Ogee Spillway in the Presence of Tail water,” *Journal of Hydraulic Engineering,* pp. 1353 - 1357, December 2006.

[26] C. W. H. a. B. D. Nichols, “Volume of Fliud (VOF) Method for the Dynamics for Free Boundaries,” *Journal of Computational Physics,* 1979.

[27] D. VELIOGLU, N. D. TOKYAY and A. E. DINCER, “Numerical and Experimental Study on the Characteristics of Hydraulic Jumps on Rough Beds,” in *E-proceedings of the 36th IAHR World Congress*, The Hague, the Netherlands , 28 June – 3 July, 2015.

[28] C. Jose and e. al., “https://www.flow3d.com,” FLOW-3D, 2014. [Online]. Available: https://www.flow3d.com/wp-content/uploads/2014/08/A-Numerical-and-Experimental-Study-of-Hydraulic-Jump-Stilling-Basin.pdf. [Accessed 08 November 2018].

[29] S. Bruce M, J. Michael C and A. Members, “Flow over Ogee Spillway: Physical and Numerical Model Case Study,” *JOURNAL OF HYDRAULIC ENGINEERING /,* pp. 640 - 649, AUGUST 2001.

[30] N. S. a. A. R. Ravorji, “Experimental and numerical study of the effect of fow separation on dissipating energy in compond bucket,” *2nd International conference on civil engineering,* 2013.

[31] S. Z. Y. Yuehua WANG, Bin WANG, Hongqing ZHANG, Ziming WANG, “Three-dimensional Numerical Simulation on Stilling Basin of Sluice in Low Head,” *5th International Conference on Civil, Architectural and Hydraulic Engineering (ICCAHE),* pp. 503 - 509, 2016.

[32] H. D. Boyes, ,. K. Donohoo and S. Cooper, “Numerical analysis for spillway,” *ANCOLD conference. Hobart, Tasmania,* 2003.

[33] B. Savage and M. Johunson, “Flow over ogee spillway: Physical and numerical model case study,” *Journal of Hydraulic Engineering. 127: 640-649,* 2001.

[34] S.-r. Sabbagh-yazdi, F. Rostami, H. Rezaei-manizani and a. N. E. Mastorakis, “Comparison of the results of 2D and 3D numerical modeling of flow over the spillway chutes with vertical curvature,” *International journal of computer issue 4 volume 1,* 2007.

[35] I. S. A. L´ucio, “Numerical modeling of skimming flow over steeped spillways: application of small dams,” *Instituto Superior T''ecnico Lisboa,* 2015.

[36] S. Y. Kumcu, “Investigation of Flow Over Spillway Modeling and Comparison between Experimental Data and CFD Analysis,” *KSCE Journal of Civil Engineering ,* June 2016.

[37] USACE, Simulation of Tailrace hydrodynamics using Computational Fluid Dynamics models, IC Northwest National Laboratory , May 2001. .

[38] H. Chanson, The Hydraulics of Open Channel Flow: An Introduction Basic principle, sediment motion, hydraulic modelling, design of hydraulic structures, The University of Quenssland, Australia, 2004.

[39] A. Gunnarsson, “Physical Model Investigation on the Hvammur HEP Spillway,” *Faculty of Civil and Environmental Engineering University of Iceland 2012 Faculty of Civil and Environmental Engineering University of Iceland,* 2012.

[40] L.Toombes and H. Chanson, “Numerical Limitations of Hydraulic Models,” *34th IHAR World Congress - Balance and uncertainty,* 26 June - 1 July 2011.

[41] J. Groeneveld, C. Sweeney, C. Mannheim, C. Simonsen and K. Moen, “Comparison of Intake Pressures in Physical and Numerical Models of the Cabinet Gorge Dam Tunnel,” *Waterpower,* pp. 079 (1-15), 2007.

[42] HEC RAS, Reference Manual, “HEC RAS Hydraulic Reference Manual,” USACE Hydrologic Engineerig Center, Davis, 2016.

[43] G. Andri, Physical Model Investigation on the Hvammur HEP Spillway, Reykjavik: Faculty of Civil and Environmental Engineering University of Iceland, January 2012.

[44] W. Chen and J. Richard, The Civil Engineering Handbook 2nd Edition, CRC PRESS, 2003.

[45] Jeff Burnham, PE, LEEP AP, “Modeling Dams with Computational Fluid Dynamics: Past Success and New Directions”.

[46] C. W. H. A. B. D. NICHOLS, “Volume of Fluid (VOF) Method for the Dynamics of Free Boundaries,” *JOURNAL OF COMPUTATIONAL PHYSICS ,* pp. 39, 201-225 , 1981.

[47] Studio Galli Ingeneria and Sembenelli Consulting, “Zarema May Day Dam and Auppertenant Structures Detailed Design Spillway,” Federal Democratic Republic of Ethiopia Sugar Corporation, Addis Ababa, 2014.

[48] J. H. Ferzjger, Compuational Methods for Fluid Dyanamics, New York: Springer, 2002.

[49] D. N. Moriasi, J. G. Arnold, M. W. V. Liew, R. L. Bingner, R. D. Harmel and T. L. Veith, “Model Evaluation Guidelines for Systematic Quantification of Accuracy in Watershed Simulations,” *American Society of Agricultural and Biological Engineers ,* vol. 50(3), p. 885−900 , 2007.

[50] M. E. Coffey, S. R. Workman, J. L. Taraba and A. W. Fogle, “Statistical Procedures for Evaluating Daily and Monthly Hydrologic Model Predictions,” *Biosystems and Agricultural Engineering,* vol. 47(1), pp. 59-68, 2004.

[51] U. A. C. o. E. USACE, Hydraulics Design of Spillway Engineering Manual 1110-2-1603, 1992.

[52] E. A. W. a. M. R. Liaqat A. Khan, “A 3D CFD model analysis of the hydraulics of an outfall structure at a power plant,” *Journal of Hydroinformatics,* pp. 283-290, 2005.

[53] E. K. a. R. C. Michael Tran, “The United Nations World Water Development Report WATER AND JOBS Facts and Figures,” United Nations World Water Assessment Programme, Colombella, Perugia, Italy, 2016.

[54] Water_Resources_and_Irrigation_Development_in_Ethiopia, “Water_Resources_and_Irrigation_Development_in_Ethiopia,” 2016. [Online]. Available: https://www.researchgate.net/publication/42765483_Water_Resources_and_Irrigation_Development_in_Ethiopia. [Accessed 15 November 2018].

[55] I. S. IS 6934: 1998, “Hydraulic Design of High Ogee Overflow Spillways Recommendations,” Bureau of Indian Standard, New Delhi, December 1998.

[56] I. S. IS 4997- 1995, “Criteria for Design of Hydraulic Jump Type Stilling Basin with Horizontal and Sloping Apron,” Bureau of Indian Standard , New Delhi, 1995.

[57] USBR, Design of Small Dams, U.S. Bureau of Reclamation,, 1987.

[58] W. W. D. a. S. E. WWDSE/WAPCOS, “Tendaho Dam & Irrigation Project Main Report Final,” Water Works Design and Supervision Enterprise, Addis Ababa Ethiopia, 2005.

[59] W. W. D. a. S. E. WWDSE/ WAPCOS, “Design of Dam and Appurtenant Works Final Report,” Water Works Design and Supervision Enterprise, Addis Ababa Ethiopia, 2005.

[60] W. W. D. a. S. E. WWDSE/ WAPCOS, “Tendaho Dam & Irrigation Project Main Report Final,” Water Works Design and Supervision Enterprise, Addis Ababa Ethiopia, 2005.

[61] V. T. Chow, Open Channel Hydraulics, 1976.

[62] G. S. Ghahfarokhi and P. v. G. a. J.K.Vrijling, “Evaluation of superelevation in open channel bends with probabilistic analysis methods,” *World Environmental and Water Resources Congress ,* 2008.

[63] W. W. D. a. S. E. (. WWDSE), “Emergency Action Plan for Tendaho and Logia Dam,” WDSE, Addis Ababa, Ethioia, January 2017.

[64] W. W. D. a. S. E. WWDSE/WAPCOS, “Design of Dam and Appurtenant Works Final Report,” Water Works Design and Supervision Enterprise, Addis Ababa Ethiopia, 2005.

[65] T. S. Davidsen, Numerical studies of flowin curved channels, Department of Mathematics University of Bergen, November 2007.

[66] M. K. a. J. Z. G. Constantinescu, “Simulation of flow in an open channel bend of strong curvature using Detached Eddy Simulation,” *River Flow 2010 - Dittrich, Koll, Aberle & Geisenhainer (eds) Bundesanstalt für Wasserbau ISBN 978-3-939230-00-7,* 2010.

[67] H. Chanson and L.Toombes, “Numerical Limitations of Hydraulic Models,” *34th IHAR World Congress - Balance and uncertainty,,* 26 June - 1 July 2011.

[68] K. I. F. A. a. D. A. Benoumessad Kamel, “3D simulation of velocity profile of turbulent flow in open channel with complex geometry,” *ScienceDirect Eight International Conference on Material Sciences (CSM8-IMS5),* pp. 119-128, 2014.

[69] USBR , Design of Small Dams, U.S. Bureau of Recalamation, , 1987.

[70] N. L. A. L. W. H. H. F. a. R. M. B. J. Lucas, “Side-Channel Flow: Physical Model Studies,” *ASCE Journal of Hydraulic Engineering ,* May 2015 .

[71] D. K. a. V. C. P. Admane, “Physical model study of side channel spillway,” *International Journal of Civil Engineering and Technology (IJCIET),* Vols. vol. 9, no. 7, p. 774–782, July 2018.

[72] D. Vischer and W. Hager, Dam Hydraulics, Switzerland: JOHN WILEY & SONS, 1996.

[73] WWDSE, “Lake Tana sub-basin four dams project Ribb Dam Proect,” WWDSE, Addis Ababa Ethiopia, 2008.

[74] G. J. C.Y., “Critical Flow Section in a Collector Channel,” *Hydraulic Engineering, ,* Vols. 125, No. 4, April 1999.

[75] V. T. Chow, Open Channel Hydraulics, 1976.

[76] USACE, Hydraulic Design of Flood Control Channel Engineering Manual EM 1110-2-1601, U.S. Army of Corps of Engineers , 1994.

[77] R. Szymkiewicz, Numerical Modeling In Open Channel Hydraulics, Poland: Springer , 2010.

[78] M. H. Chaudhry, Open-Channel Flow, Columbia: Springer, 2008.

[79] A. O. Akan, Open Channel Hydraulics, Canada: Elsevier, 2006.

[80] P. S. Jayanti, “Computational Fluid Dynamics,” 16 July 2012. [Online]. Available: http://nptel.iitm.ac.in.

[81] J. E. Lombard, Introduction to Structured Grid Generation for Aeronautics, Swiss Institute of Technology Lausanne, September 27 2011.

[82] T. W. Strum, Open Channel Hydraulics, Singapore: McGraw-Hill Higher Education, 2001.

[83] C. Canale, Numerical methods for Engineers, The McGraw Hill Companies Fourth Edition , 2001.

[84] M. Szydłowski, “Implicit versus Explicit Finite Volume Schemes for Extreme, Free Surface Water Flow Modelling,” *Archives of Hydro-Engineering and Environmental Mechanics,* pp. Vol. 51, No3, 287-303 , 2004.

[85] R.L.Johnston, Numerical Methods A Software Approach, New York: John Wiley and Sons, 1982.

[86] Lars Davidson, An Introduction to Turbulence Models, G¨oteborg, Sweden: Department of Thermo and Fluid Dynamics CHALMERS, September 6, 2016.

[87] P. Majumdar, “Computational Fluid Dynamics Analysis of Turbulent Flow,” 5 July 2011. [Online]. Available: http://cdn.intechweb.org/pdfs/16392.

[88] L. A. P. C. O. J. A. D. I. R. R. Enciso, “Computational Fluid Dynamics Characterization of a Rotating Cylinder Electrochemical Reactor using an RANS-RNG Turbulence Model,” *International Journal of ELECTROCHEMICAL SCIENCE,* pp. 12181 - 12192, 2012.

[89] H. CHANSON, “Steeped Spillway Flows and Air Entrainment,” *Can. Jl of Civil Eng. Vol. 20, No. 3, June, pp 422-435 (ISSN 0315-1468) ,* 1993.

[90] CHANSON H. and etl., Hydraulics of Nape Flow Regime Above Steeped Chute and Spillways, Australian Civil Engineering Transanctions IEAust, Vol. CE36 No. 1, 1994.

[91] HEC RAS 2D User's Manual, “River Analysis System 2D Modeling User's Manual,” *USACE Hydrologic Engineerig Center,* 2016.

[92] F. A. B. ·. I. M. ·. J. Matos, “Laboratory measurements and multi-block numerical simulations of the mean flow and turbulence in the non-aerated skimming flow region of steep stepped spillways.,” 2010.

[93] H. CHANSON, “Hydraulics of Napw Flow Regime Above Steeped Chute and Spillways,” *Australian Civil Engineering Transaction, JEAust, Vol. CE36 No. 1,* 1994.

[94] C. H, Stepped Spillway Flows and Air Entrainment, 1993.

[95] A. Gunnarsson, Physical Mode Investigation on the Hvammur HEP Spillway, Faculty of Civil and Environmental Engineering University of Iceland, 1012.

[96] S.-y. F. R. H. R.-m. a. N. E. M. Saeed-reza, “Comparison of the results of 2D and 3D Numerical Modeling of Flow Over Spillway Chutes with Vertical Curvatures,” *International Journal of Computers,* pp. 296-302, 2007.

[97] I. S. IS 5186:1994, “Design of Chute and Side Channel Spillways,” Bureau of Indian Standard , New Delhi , 1994.

[98] R. H. French, Openchannel Hydraulics, Singapore: McGraw-Hill Book Company, 1987.

[99] D. G. K. a. J. H. Park, “Analysis of Flow Structure over Ogee-Spillway in Consideration of Scale and Roughness Effects by Using CFD Model,” *Water Engineering, KSCE Journal of Civil Engineering,* pp. 161-169, 2005.

[100] H.-J. L. a. S.-D. A. Sung-Duk Kim, “Improvement of hydraulic stability for spillway using CFD model,” *International Journal of the Physical Sciences Vol. 5(6),* pp. 774-780, June 2010.

[101] D. T. a. J. S. Date V, “Numerical Modeling of Flow over an Ogee Crested Spillway under Radial Gate: VOF and MMF Model,” *Journal of Applied Mechanical Engineering Volume 6 • Issue 5 • 1000287,* 2017.

[102] C. W. H. A. B. D. NICHOLS, “Volume of Fluid (VOF) Method for the Dynamics of Free Boundaries,” *Journal of Computational Physics,* pp. 39, 201-225, 1981.

[103] P. G. C. a. J. C. Doering, “Assesment of Spillway Modeling Using Computational Fluid Dynamics,” *Technical Note Canada,* p. 1482, 2008.

[104] G. S. S. K. &. S. A. Kutsi S. Erduran, “3D Numerical Modelling of Flow Around Skewed Bridge Crossing,” *Engineering Applications of Computational Fluid Mechanics,* pp. Vol. 6, No. 3, pp. 475–489, 2012.

[105] D. Getnet k, H. Dereje and S. Yima, “Performance Assessment of Numerical 3D Hydraulic Model Using Spillway Physical Model and Design Results,” 2018.

ANNEX A

ZAREMA MAY DAY DAM SPILLWAY

1. HYDRAULIC DESIGN

1.1 DISCHARGE CAPACITY OVER UN-CONTROLLED OGEE CRESTS

The following design report is taken from the design report and checked during the research time. For additional required output, the researcher added for computation of rating curve and computation at the bend.

The discharge capacity of the ogee crest may be estimated through the general weir equation:

$$Q = CL_eH_e^{1.5} \quad ----(1.1)$$

Where

Q is the discharge (m^3/s)

C is variable discharge coefficient

L_e is effective length of the crest (m)

H_e is actual head being considered including velocity head that is the total specific energy above the crest (m).

The discharge coefficient, C, is influenced by several factors, such as i) the depth of approach, ii) relation of the actual crest shape to the ideal nappe shape, iii) upstream face slope, iv) downstream apron interference, and v) downstream submergence. Plate A/ 1 , Plate A/ 2 and from Plate A/ 5 to Plate A/ 7 show for details and for contraction coefficients.

The effective length of the crest L_e can be expressed as:

$$L_e = L - 2\left(K_a + nK_p\right) ----(1.2)$$

Where

L is the net length = 30 - 1 = 29 m

n is the number of piers = 1

K_p is the pier contraction coefficient= 0.02

K_a the abutment contraction coefficient = 0.15

The pier nose is rounded to reduce the flow contraction. This configuration also allows the pier profile to extend downstream beyond the zone where negative pressures may occur to prevent aeration of the nappe, nappe separation and undulation, which may cause losing part of the under design beneficial effects. The overall pier length is around 26 m.

1.2 CREST SHAPE

The ogee crest is elliptical and conforms to the recommendations [51]. The crest shape approximates that of a fully ventilated nappe of water flowing on a sharp-crested weir.

The shape of the ogee crest approximates the lower nappe of a flow over a sharp-crested weir and can be divided into two quadrants with the apex on the crest axis (El. 946.4 m). The shape is proportionally based on the design head H_d = 4 m.

The equation for the upstream elliptical quadrant can be expressed as:

$$\frac{X^2}{A^2} + \frac{(B-Y)^2}{B^2} = 1 - - - - - (1.3)$$

Where

X is the horizontal coordinate positive downstream (m)

Y is the vertical coordinate positive downward (m)

A and B respectively the one-half horizontal and vertical axes of ellipse (m)

The semi-axes of the ellipse A and B has been computed through the following relations based on the Plate A/ 1 and valid for an approach condition $P/H_d = 0.5$, where P is the approach depth upstream from the ogee = 2 m (El. 446.4 – 944.4 m):

$$A = 0.244H_d = 0.974\,m$$

$$B = 0.143H_d = 0.571\,m$$

The equation of the downstream quadrant can be expresses as:

$$X^n = KH_d^{n-1}\,Y \quad ----(1.4)$$

Where

X is the horizontal coordinate positive downstream (m)

Y is the vertical coordinate positive downward (m)

n is variable, however usually set = 1.85

K is variable and dependent on the approach condition. According on Plate A/ 1, for P/H_d = 0.5, the parameter K = 2.047.

The surface of the nappe, which is also the crest shape, must meet tangentially the slopes of the ogee crest both upstream and downstream, to avoid discontinuity that may disrupt the flow boundary. The location of the tangent intersection has been computed geometrically:

tg u/s slope = vertical = A = 0.974 m

tg d/s slope = 2H: 1V = 2.361 m

1.3 SPILLWAY RATING CURVE

The spillway profile can be designed only for one head which is called design head. The lower nape profile is the result of the design head. Practically the head over the spillway operate either lower or higher than design head. For lower heads, the pressure on the crest will be above atmospheric but still less than hydrostatic. For higher heads, on the other hand, the pressure will be lower than atmospheric, and it may become so low that separation in flow will occur. Plate A/ 3 and Plate A/ 4 can be used to determine the coefficient of discharge for heads other than the design head. Thus, rating curve of the spillway was computed, and cross checked with the design.

The effect due to interference caused by the downstream apron, in terms of variation of (C_s/C), the ratio of modified coefficient to free discharge coefficient, with respect to apron effect, has been studied

in terms of variation of the parameter (h_d + d)/He as shown in Plate A/4. When this parameter exceeds about 1.7, the downstream floor has practically no effect on the discharge coefficient. The effect of submergence of crest by tail water on discharge coefficient is studied in terms of parameter (h_d/H_e), also called degree of submergence. The coefficient of discharge begins to be influenced by the submergence when the degree of submergence expressed as the depth of tail water above the crest/head on crest exceeds about significant.

Accordingly, the downstream submergence at Zarema Dam will not exceed 25% which shows that downstream submergence will not have an effect for the coefficient of discharge. On the other hand, the effect of apron is computed by comparing the design rating curve and checked during the research using the results are matching except at some higher discharges [69]. The differences are small, and it could be a difference in taking the data from the graph. On the other hand, the research result and the physical model result at the end have closer agreement than the design. The result of the physical model and design are obtained from the design report. Meanwhile, submerged flow after ogee is clearly seen in the FLOW-3D model.

The performance indicator of flow depth comparison between 3D model result and physical model result are as follow: R^2= 0.9998, NSCE = 0.833 and Rbias =-3.584%. The performance indicator of flow depth comparison between 3D model result and design results are as follow: R^2= 0.902, NSCE = 0.860 and Rbias = -0.804%.

Table A.1. 1 Rating curve computed

H_e/H_o	H_e	C/C_o	C_i	hd+d	(hd+d) /He	Cs/C	Cs	$CsHe^{3/2}$	He+P	va (approx.)	ha	s	Entrance loss, 0.1ha	Total approach losses	Gross head	Total discharge (Q= CsLHe3/2)	He	Total discharge (Q= $CsLHe^{3/2}$)
	ft			ft					ft	ft/s	ft			ft	ft	ft3/s	m	m3/s
0.14	1.82	0.835	3.21	8.32	4.57	1	3.21	7.9	8.32	0.95	0.014	0.00001	0.00	0.00	1.82	750.5	0.6	21.25
0.21	2.73	0.857	3.29	9.23	3.38	1	3.29	14.8	9.23	1.6	0.04	0.00003	0.00	0.01	2.74	1406	0.8	39.81
0.28	3.64	0.875	3.36	10.14	2.79	1	3.36	23.3	10.14	2.3	0.08	0.0001	0.01	0.02	3.66	2213.5	1.1	62.68
0.33	4.29	0.89	3.42	10.79	2.52	1	3.42	30.4	10.79	2.82	0.12	0.0001	0.01	0.03	4.32	2888	1.3	81.78
0.38	4.94	0.895	3.44	11.44	2.32	1	3.44	37.8	11.44	3.3	0.17	0.0001	0.02	0.03	4.97	3591	1.5	101.69
0.42	5.46	0.904	3.47	11.96	1.41	1	3.47	44.3	11.96	3.43	0.18	0.0001	0.02	0.04	5.50	4208.5	1.7	119.17
0.47	6.11	0.91	3.49	12.61	2.06	1	3.49	52.7	12.61	4.18	0.27	0.0001	0.03	0.05	6.16	5006.5	1.9	141.77
0.51	6.63	0.922	3.54	13.13	1.98	1	3.54	60.4	13.13	4.6	0.33	0.0002	0.03	0.06	6.69	5738	2	162.48
0.55	7.15	0.93	3.57	13.65	1.91	1	3.57	68.3	13.65	5	0.39	0.0002	0.04	0.07	7.22	6488.5	2.2	183.73
0.59	7.67	0.938	3.6	14.17	1.85	1	3.6	76.5	14.17	5.4	0.45	0.0002	0.05	0.08	7.75	7267.5	2.3	205.79
0.67	8.71	0.95	3.65	15.21	1.75	1	3.65	93.8	15.21	6.17	0.59	0.0002	0.06	0.10	8.81	8911	2.7	252.33
0.76	9.88	0.962	3.69	16.38	1.66	0.998	3.68	114.3	16.38	6.98	0.76	0.0003	0.08	0.12	10.00	10858.5	3	307.48
0.84	10.92	0.978	3.76	17.42	1.6	0.995	3.74	135	17.42	7.75	0.93	0.0003	0.09	0.15	11.07	12825	3.3	363.16
0.91	11.83	0.982	3.77	18.33	1.55	0.988	3.72	151.4	18.33	8.26	1.06	0.0003	0.11	0.16	11.99	14383	3.6	407.28
0.98	12.74	0.995	3.82	19.24	1.51	0.984	3.76	171	19.24	8.89	1.23	0.0004	0.12	0.19	12.93	16245	3.9	460.01
1.05	13.65	1	3.84	20.15	1.48	0.98	3.76	189.6	20.15	9.41	1.37	0.0004	0.14	0.20	13.85	18012	4.2	510.04
1.13	14.69	1.015	3.9	21.19	1.44	0.97	3.78	212.8	21.19	10.04	1.57	0.0004	0.16	0.23	14.92	20216	4.5	572.45
1.19	15.47	1.02	3.92	21.97	1.42	0.966	3.79	230.6	21.97	10.5	1.71	0.0004	0.17	0.24	15.71	21907	4.7	620.34
1.26	16.38	1.035	3.97	22.88	1.4	0.961	3.82	253.2	22.88	11.07	1.9	0.0004	0.19	0.27	16.65	24054	5	681.13
1.33	17.29	1.04	3.99	23.79	1.38	0.945	3.77	271	23.79	11.39	2.01	0.0004	0.20	0.28	17.57	25745	5.3	729.02

Table A.1.2 Comparison of Rating Curve over spillway crest

Elevation	Designed Flow	Flow from Research	Physical model result	
			Elevation	Flow
(m)	(m^3/s)	(m^3/s)	(m)	(m^3/s)
946.94	20	21.25	946.4	0
947.24	40	39.81	947.92	100
947.49	60	62.68	948.02	113.54
947.7	80	81.78	948.1	138.97
947.9	100	101.69	948.5	180.52
948.08	120	119.17	949.08	262.48
948.25	140	141.77	949.34	306.27
948.42	160	162.48	949.98	422.17
948.57	180	183.73	950.24	444.15
948.72	200	205.79	951.23	671.87
949.07	250	252.33	951.48	703.24
949.4	300	307.48	951.51	727.08
949.71	350	363.16		
950.01	400	407.28		
950.3	450	460.01		
950.58	500	510.04		
950.86	550	572.45		
951.13	600	620.34		
951.39	650	681.13		
951.65	700	729.02		

1.4 CREST PRESSURE

Thus, when He/Hd ≤ 1 the pressures on the crest are essentially atmospheric (+), as H_e/H_d > 1 the pressures drop below atmospheric (-). Such negative pressures produce a sort of suction effect on the lower nappe that increases the discharge coefficient C over that of a ventilated sharp-crested weir. Negative pressure may lead to cavitation damages and should be limited. Chow “Harmful cavitation may develop if the design head exceeded by at least 50%” [75].

Cavitation on the crest would be incipient at the average pressure of -7.6 m of water column. The ogee crest should be designed so that the maximum expected head will result in an average pressure no lower than -4.6 m. Plate A/ 8 shows the relationship between He and Hd defining the maximum limit of under design permitted in relation to the minimum acceptable water pressure. During the research pressure was checked. Since the head over the crest was not high, the design is adequate to avoid development of cavitation on the crest boundary for all range of operating conditions.

1.5 WATER SURFACE PROFILE

i) Water Surface Profile Along Approach Channel

The approach channel conveys the flow from the reservoir to the ogee crest and extends for approximately 55 m, with an average width of around 40 m.

As per the design the computation from the ogee crest to the reservoir was done by means of the following expression:

$$H = H_e + \Delta H_f + \Delta H_c \quad ----(1.5)$$

Where

H_e is total specific energy on the crest from eq. 1.3 (m)

ΔH_f is the friction head loss (m)

ΔH_c is the concentrated head loss (m)

H is the total head in the upstream reservoir

The friction head loss may be estimated through the Manning formula:

$$\Delta H_f = L\frac{n^2 v^2}{R^{4/3}} \quad \text{----------(1.6)}$$

Where

L is the length of the head channel = 55 m

V is the mean flow velocity in the channel (m/s)

R is the hydraulic radius (m),

n is the Manning friction factor, which has been assumed = 0.025 for a relatively straight and smooth channel excavated in rock.

The concentrated head loss may be expresses as:

$$\Delta H_c = K\frac{v^2}{2g} \quad ----------(1.7)$$

Where

V is the mean flow velocity in the channel (m/s)

K is a coefficient function of the geometry = 0.1 is usually adequate [69].

g is the gravitational acceleration (m/s^2)

The solution of eq. 1.5 is summarized in Table A.1.3.

Table A.1.3 Computation of the water depth for Approach channel

He =	4.99	m	From rating curve
v =	3.4	m/s	From rating curve
L =	55	m	
n =	0.025		
A = w*(Hd+P) =	240	m^2	
P = 2*(Hd+P)+w =	52	m	
R = (A/P)^(4/3)	7.68		
∆Hf =	0.05	m	
k =	0.1		
g =	9.81	m/s^2	
∆Hc =	0.06	m	
H = He + ∆Hf + ∆Hc =	5.1	m	

ii) Depth of water at control section

The flow depth is computed during rating curve computation. Hence, for detail information refer section 1.3.

iii) Water Surface Profile at the Toe of Ogee

The flow depth at the toe of the ogee crest has been computed with Bernoulli equation. Given the short length of the downstream crest profile, the friction losses have been disregarded:

$$H_e + P = y_0 + \frac{1}{2g}\frac{Q^2}{b^2 y_0^2} - - - - - - - - - - (1.8)$$

Where

H_e is the total specific energy over the ogee crest (m)

P is the approach depth (m)

Q is the discharge (m^3/s)

y_o is the flow depth at the toe of the ogee crest (m)

b is the channel width (m)

g is gravitational acceleration (m/s^2)

iv) Water Surface Profile along the Spill Channel or Chute

The flow depth at specific cross-sections along the spillway channel has been computed according to the standard step method, which is applicable also to non-prismatic channel:

$$S_0 \Delta x + y_1 + \frac{1}{2g}\frac{Q^2}{b_1^2 y_1^2} = y_2 + \frac{1}{2g}\frac{Q^2}{b_2^2 y_2^2} + h_f - - - - - (1.9)$$

Where

S_0 is the channel slope = 0.005 m/m

Δx is the length between two cross-sections (m)

y is the flow depth (m)

b is the channel width (m)

h_f is friction loss, which may be estimated as:

$$h_f = S_f \Delta x = \frac{1}{2}(S_1 + S_2)\Delta x \quad -----(1.10)$$

Where

S_f the friction slope is taken as the average of the slopes at the two cross-sections.

The computation is carried on by steps and iteratively from station index 1 to station index 2, where the hydraulic characteristics are estimated. When the Manning formula is used, the friction slope S_f is expressed as:

$$S_f = \frac{n^2 v^2}{R^{4/3}} \quad -----(1.11)$$

Where

S_f is friction slope

V is flow velocity (m/s),

R is hydraulic radius (m),

n is the Manning friction factor = 0.013 for a concrete lined channel.

v) Water Surface Profile Along Channel Transition

The flow depth was computed with similar procedure in Equation 1.9. However, due to convergence, the channel transition has been designed to minimize formation of shock waves and flow disturbance. The design best practice recommends, for straight-lined walls, a minimum convergence factor of angular variation of flow boundaries not exceeding that produced by the Equation 1.9. According to equation (1.12) it is possible for flare angle up to

27 degree. However, as per the design it is less than 5 degrees hence there will not be cross wave, wave runup and uneven distribution of flow in across the channel.

$$\tan \propto = \frac{1}{3F} - - - - - - - - (1.12)$$

Where $F = \frac{v}{\sqrt{gd}}$

$\propto$ = Angular variation of sidewall with respect to the channel centre line

v = velocity at the start of transition (m/s)

g = Gravitational acceleration (m/s^2)

d = Flow depth at the start of transition (m)

Table A. 1.4 shows the result from the design report at different sections of the spillway. For verification, the maximum flow was taken. In a similar way Table A. 1.5 shows the result of the physical model result at different section of the chute channel.

Table A.1.4 Depth at different cross-sections as per the design

Discharge (Q)	ogee crest toe	crest pier end	contraction entrance	contraction end	channel end
m^3/s	m	m	m	m	m
650	2.35	2.35	2.25	3.35	3.06
700	2.5	2.5	2.39	3.6	3.25

The maximum water depth of physical model result measured in the spillway channel along the sidewalls, immediately upstream from the deflecting walls, scaled to prototype is summarized in the following Table A.1.5.

Table A.1.5 Maximum Water Depth in the spillway channel as per Physical model

TR	Qp	hw right	hw left
years	m^3/s	m	M
PMF	709	6.18	6.24

vi) Water Surface Profile along Channel Bend

Difficulty in the design arises because of the complexity of the flow around a curved path, that is not readily subject to any analytical solutions. Hence it was not possible to predict the depth of flow at the bend. To reduce the superelevation guide walls are proposed. With the standard step method, it was not mentioned in the design report for the depth of the flow along the bend. However, during research, the required superelevation was checked with the USACE [76].

For supercritical flow EM 110-2-1601 provides the superelevation of water surface as flows traverse around a curve:

$$\Delta h = CW\frac{V^2}{gr}$$

Table A.1.6 Superelevation as per the USACE

Where			Remark
W = Channel width at elevation of centre line water surface (m)			
V = Average velocity (m/s)			
g = Acceleration to gravity (m/s^2)			
r = Centre line radius of curvature			
C =	1	For rectangular Channel	
∆h = Superelevation (m)			
W	14.56	m	From design
V	5	m	From design
g	9.81	m/s^2	
C	1		
r	8	m	From design
Fr	6		Supercritical
∆h =	4.64	m	
Normal depth of flow			
Q =	680	m/s^3	From design
For one Chamber = 680/3	227	m/s^3	
A = Area = Q/V =	45.4	m^2	
Depth of flow = A/W =	3.12	m	
Total wall height required including Superelevation =	7.76	m	
Recommended height =	8	m	

PERFORMANCE STATISTICS

$$R^2 = \left[\frac{\sum_{i=1}^{n}(\mathrm{SIM}_i - \overline{\mathrm{SIM}})\,(\mathrm{OBS}_i - \overline{OBS})}{\sqrt{\sum_{i=1}^{n}(\mathrm{SIM}_i - \overline{\mathrm{SIM}})^2}\sqrt{\sum_{i=1}^{n}(\mathrm{OBS}_i - \overline{\mathrm{OBS}})^2}}\right]^2, \quad \mathrm{NSE} = 1 - \left[\frac{\sum_{i=1}^{n}(\mathrm{SIM}_i - \mathrm{OBS}_i)^2}{\sum_{i=1}^{n}(\mathrm{OBS}_i - \overline{\mathrm{OBS}})^2}\right]$$

$$\mathrm{Rbias} = \frac{\sum_{i=1}^{n}(\mathrm{SIM}_i - \mathrm{OBS}_i)}{\sum_{i=1}^{n}\mathrm{OBS}_i} * 100$$

For detail information refer section 4.5.3.1.

Zarema May Day Dam performance indicators over the crest Physical and 3D Model

Elevation (m)	Flow from 3D model (m^3/s)	Flow from Physical model (m^3/s)	SIM-Av_SIM		OBS-AVOBS	(OBS-AV_OBS)^2	(SIM-Av_SIM)(OBS-AV_OBS)		
1	2	3	4	5	6	7	8	9	10
				(4)^2		(7)^2	(4)*(6)	(2)-(3)	(9)^2
946.94	21.25	0	248.238	61622.11	280.714	78800.35	69683.88	21.25	451.563
947.9	101.69	100	167.798	28156.17	180.714	32657.55	30323.45	1.69	2.856
948.08	119.17	138.97	150.318	22595.5	141.744	20091.36	21306.68	-19.8	392.04
948.57	183.73	180.52	85.758	7354.435	100.194	10038.84	8592.437	3.21	10.304
949.07	252.33	262.48	17.158	294.397	18.234	332.479	312.859	-10.15	103.023
949.4	307.48	306.27	37.992	1443.392	25.556	653.109	970.924	1.21	1.464
950.01	407.28	422.17	137.792	18986.64	141.456	20009.8	19491.51	-14.89	221.712
950.3	460.01	444.15	190.522	36298.63	163.436	26711.33	31138.15	15.86	251.54
950.86	572.45	671.87	302.962	91785.97	391.156	153003	118505.4	-99.42	9884.336
Sum	2425.39	2526.43	1338.538	268537.2	1443.204	342297.8	300325.3	-101.04	11318.84
Average	269.488	280.714	148.726	29837.47	160.356	38033.09	33369.48	-11.227	1257.649
			SQRT =	518.2058		585.0622			

R^2 =	0.981
NSCE =	0.967
Rbias =	-4.00%

Note: - OBS= Observed, SIM = Simulated, AV_ Average

Zarema May Day Dam performance indicators 3D with Physical Model for flow depth

Measurement Location	Depth of flow from 3D model (m)	Depth of flow from Physical Model (m)	SIM-Av_SIM		OBS-AV_OBS	(OBS-AV_OBS)^2	(SIM-Av_SIM)(OBS-AV_OBS)			Percentage difference (%)
1	2	3	4	5	6	7	8	9	10	11
				(4)^2		(7)^2	(4)*(6)	(2)-(3)	(9)^2	
At the Crest of Spillway	4.460	4.880	1.100	1.210	0.887	0.786	0.975	-0.420	0.176	-8.610
Before Bend	6.160	6.240	0.600	0.360	0.473	0.224	0.284	-0.080	0.006	-1.300
At Bend	6.060	6.180	0.500	0.250	0.413	0.171	0.207	-0.120	0.014	-1.940
Sum	16.680	17.300	2.200	1.820	1.773	1.181	1.466	-0.620	0.197	
Average	5.560	5.767	0.733	0.607	0.591	0.394	0.489	-0.207	0.066	
			SQRT =	1.349		1.087				

R^2 =	0.9998
NSCE =	0.833
Rbias =	-3.584%

Zarema May Day Dam performance indicators 3D with Design or 1D model for flow depth

Measurement Location	Depth of flow from 3D model (m)	Depth of flow from Design or 1D model (m)	SIM-Av_SIM		OBS-AV_OBS	(OBS-AVOBS)^2	(SIM-Av_SIM)(OBS-AV_OBS)			Percentage difference (%)
1	2	3	4	5	6	7	8	9	10	11
				(4)^2		(7)^2	(4)*(6)	(2)-(3)	(9)^2	
At Approach channel	5.94	5.4	1.006	1.012	0.426	0.181	0.429	0.54	0.292	10
At the Crest of Spillway	4.46	4.99	0.474	0.225	0.016	0	0.008	-0.53	0.281	-10.62
At the Spillway Toe	2.83	2.5	2.104	4.427	2.474	6.121	5.205	0.33	0.109	13.2
At the End of Divide Wall	2.76	2.5	2.174	4.726	2.474	6.121	5.378	0.26	0.068	10.4
Before Convergence	6.12	5.87	1.186	1.407	0.896	0.803	1.063	0.25	0.063	4.26
End of Convergence	5.37	4.5	0.436	0.19	0.474	0.225	0.207	0.87	0.757	19.33
Along the Chute Channel	3.32	3.25	1.614	2.605	1.724	2.972	2.783	0.07	0.005	2.15
At Bend	6.06	7.76	1.126	1.268	2.786	7.762	3.137	-1.7	2.89	-21.91
Along Cascade	7.55	8	2.616	6.843	3.026	9.157	7.916	-0.45	0.203	-5.63
Sum	44.41	44.77	12.736	22.703	14.296	33.342	26.126	-0.36	4.668	
Average	4.934	4.974	1.415	2.523	1.588	3.705	2.903	-0.04	0.519	
		SQRT =		4.765		5.774				

R^2 =	0.902
NSCE =	0.860
Rbias =	-0.804%

Zarema May Day Dam performance indicators 3D with Design for Velocity

Measurement Location	Velocity of flow from 3D model (m/s)	Velocity of flow from Design or 1D model (m/s)	SIM-Av_SIM		OBS-AV_OBS	(OBS-AVOBS)^2	(SIM-Av_SIM)(OBS-AV_OBS)			Percentage difference (%)
1	2	3	4	5	6	7	8	9	10	11
				(4)^2		(7)^2	(4)*(6)	(2)-(3)	(9)^2	
At Approach channel	3.81	3.4	2.21	4.884	2.377	5.65	5.253	0.41	0.168	10.76
At the Crest of Spillway	5.35	4.1	0.67	0.449	1.677	2.812	1.124	1.25	1.563	23.36
Before Convergence	5.44	3.95	0.58	0.336	1.827	3.338	1.06	1.49	2.22	27.39
End of Convergence	5.28	6.57	0.74	0.548	0.793	0.629	0.587	-1.29	1.664	-24.43
Along the Chute Channel	7.85	6.67	1.83	3.349	0.893	0.797	1.634	1.18	1.392	15.03
Before Bend	6.88	6.1	0.86	0.74	0.323	0.104	0.278	0.78	0.608	11.34
At Bend	7.53	9.65	1.51	2.28	3.873	15	5.848	-2.12	4.494	-28.15
Sum	42.14	40.44	8.4	12.586	11.763	28.33	15.784	1.7	12.109	
Average	6.02	5.777	1.2	1.798	1.68	4.047	2.255	0.243	1.73	
		SQRT =		3.548		5.323				

R^2 =	0.698
NSCE =	0.573
Rbias =	4.204%

The design drawings for the dam is shown in Annex B.

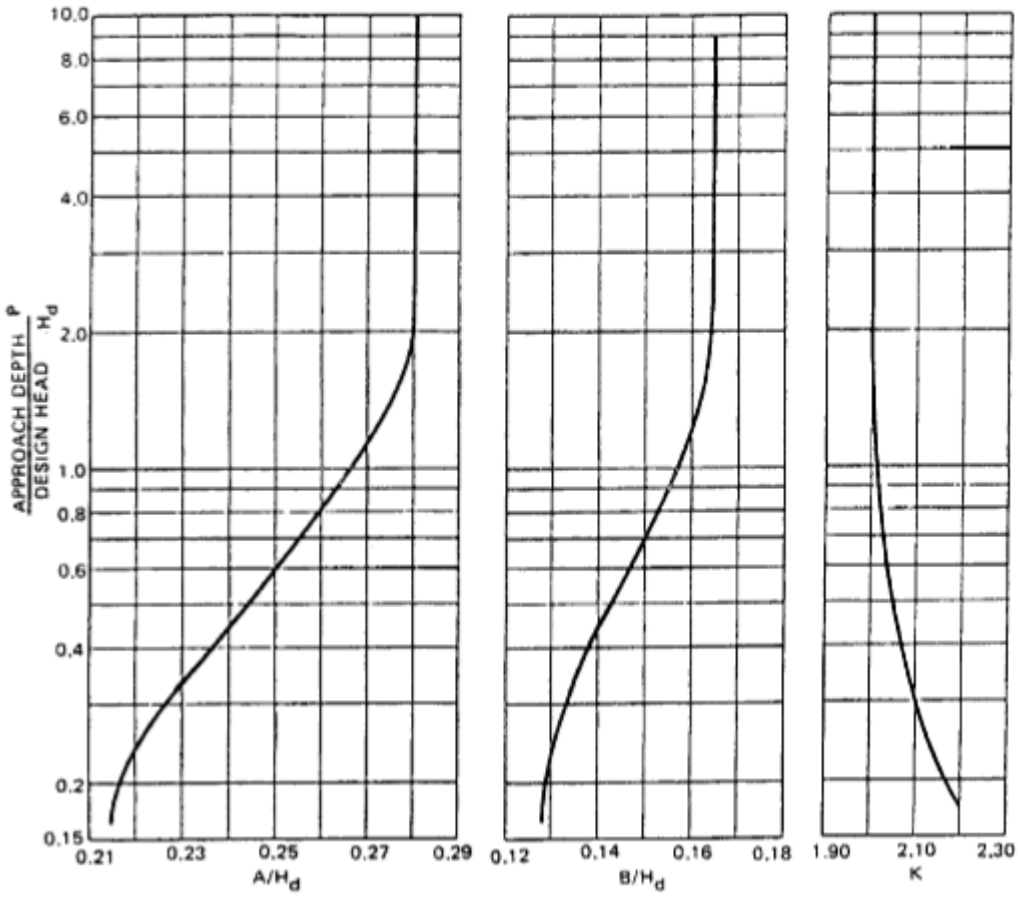

-

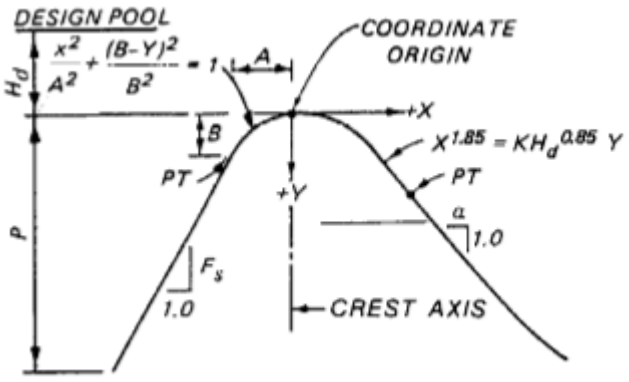

Plate A/ 1 Shape of the ogee crest, extracted from the USACE

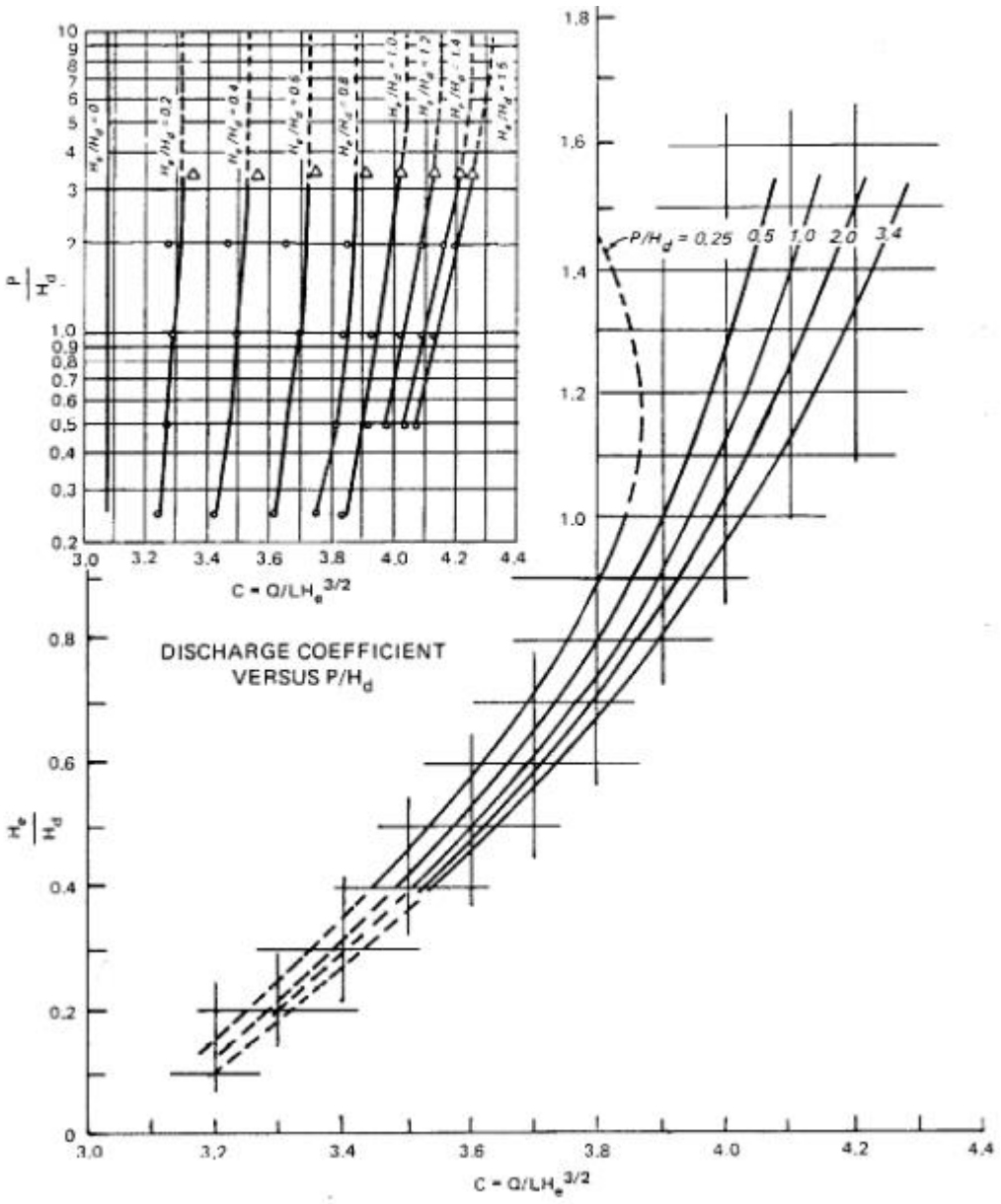

Plate A/ 2 Discharge coefficient for upstream ogee crest slope >1H:1V, extracted from the USACE

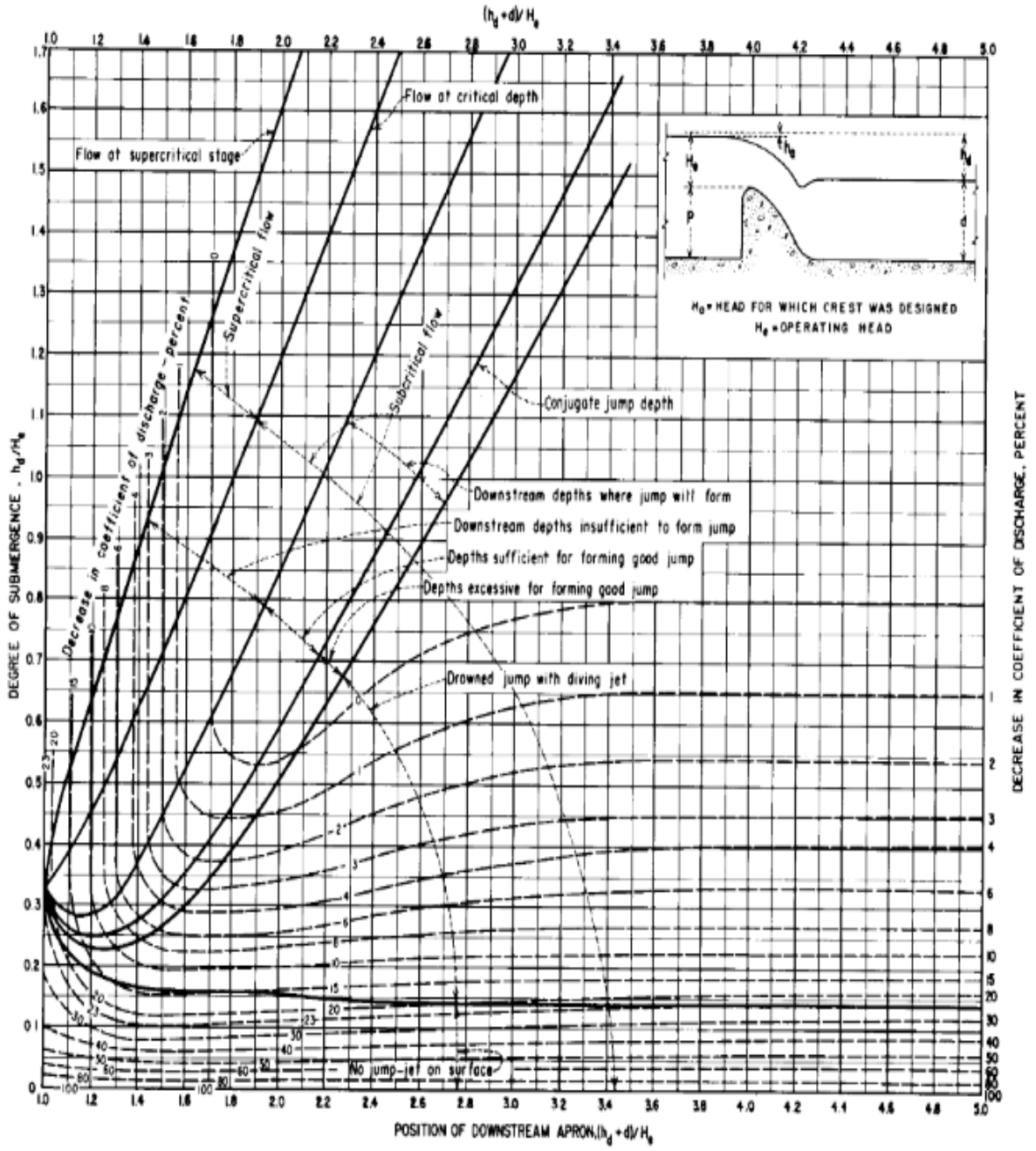

Plate A/ 3 Effects of the tailwater and downstream apron on the discharge coefficient, extracted from USBR

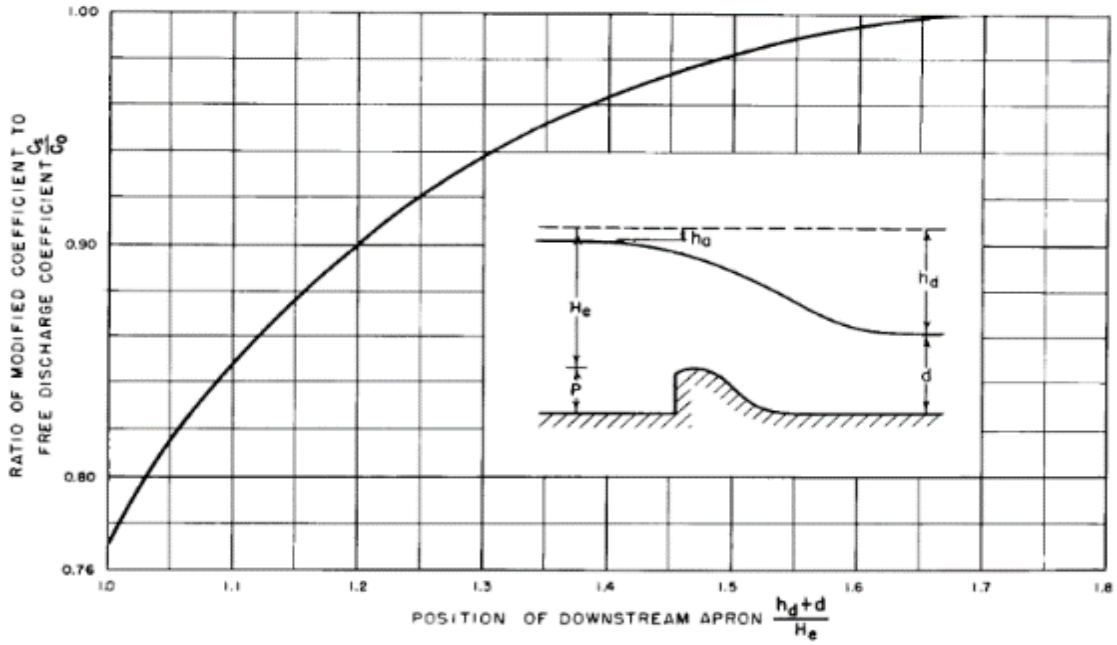

Plate A/ 4 Effect of the back-pressure on the discharge coefficient, extracted from USBR

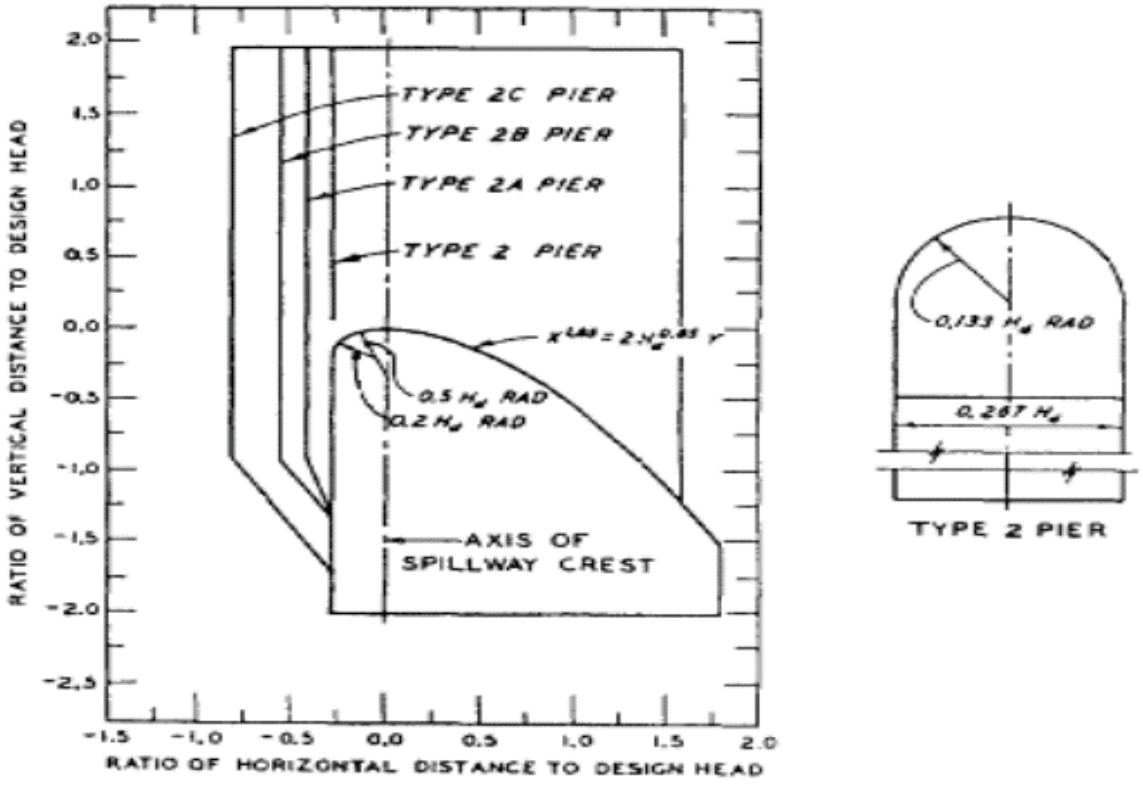

Plate A/ 5 High Gated Overflow Crests, extracted from USACE

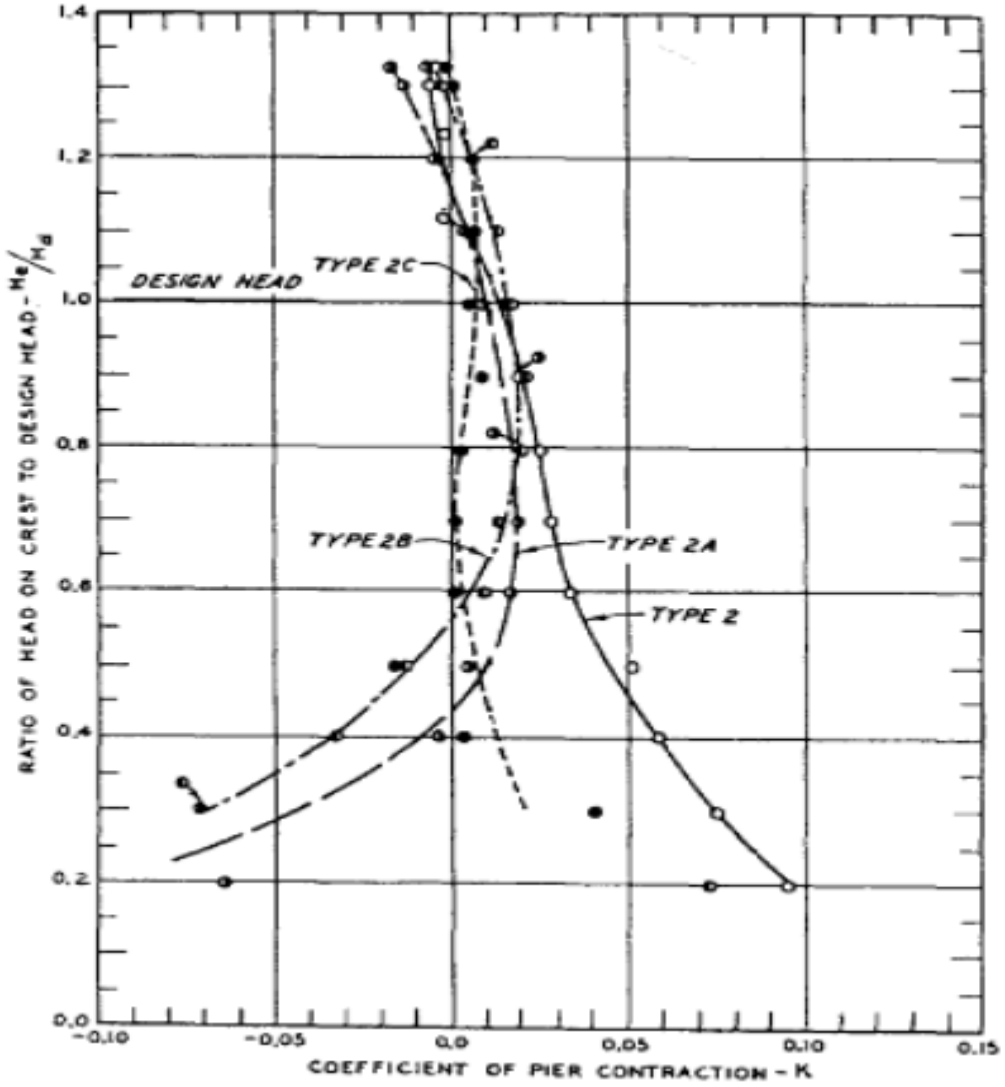

Plate A/ 6 Pier contraction coefficient, extracted from USACE

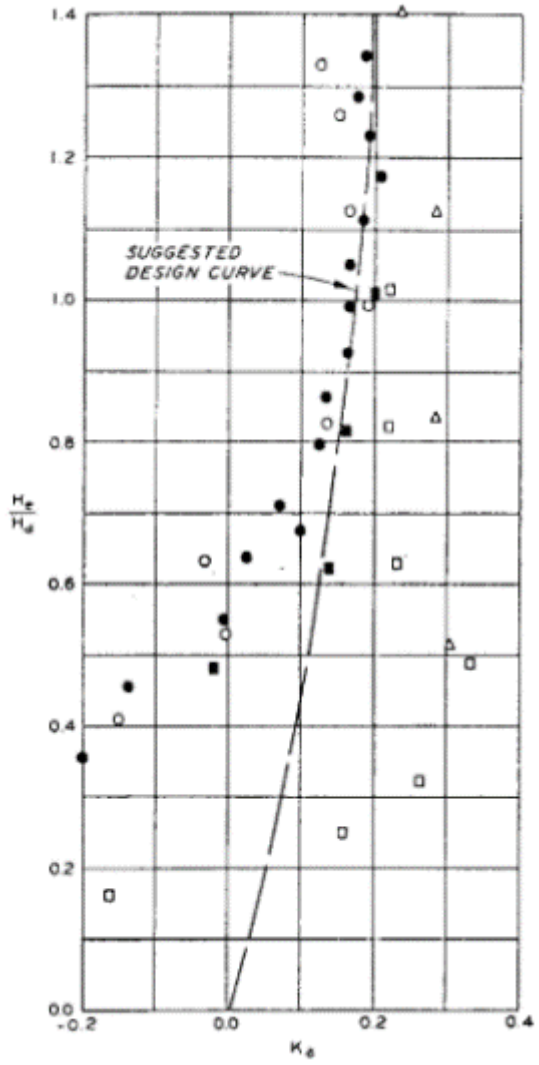

BASIC EQUATION

$$Q = C\left[L' - 2\left(NK_p + K_\Delta\right)H_e\right]H_e^{3/2}$$

WHERE:
- Q = DISCHARGE, CFS
- C = DISCHARGE COEFFICIENT
- L' = NET LENGTH OF CREST, FT
- N = NUMBER OF PIERS
- K_p = PIER CONTRACTION COEFFICIENT
- K_Δ = ABUTMENT CONTRACTION COEFFICIENT
- H_e = ENERGY HEAD ON CREST, FT

LEGEND

SYMBOL	PROJECT	R	W/L	W/H
□	DORENA	2	5.60	10.7
■	DORENA	4	5.60	10.7
○	RED ROCK*	7.8	3.42	16.5
●	CARLYLE*	9	8.44	75.5
△	WALTER F. GEORGE*	4	5.44	55.3

*GATED SPILLWAY WITH PIERS

NOTE: R = RADIUS OF ABUTMENT, FT
W = WIDTH OF APPROACH REPRODUCED IN MODEL, FT
L = GROSS WIDTH OF SPILLWAY, FT
H = DEPTH OF APPROACH IN MODEL, FT
H_d = DESIGN HEAD ON CREST, FT

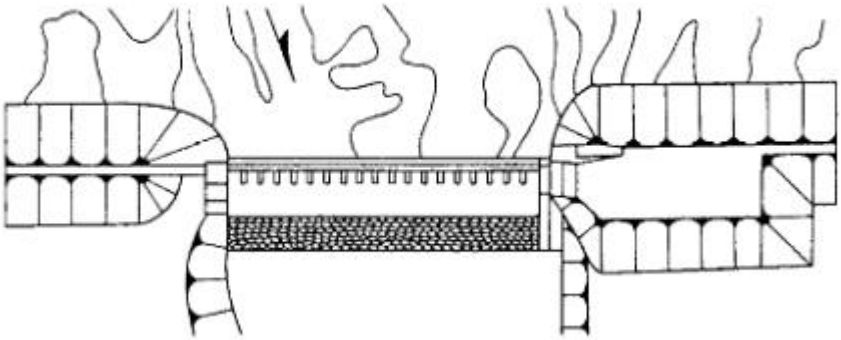

Plate A/ 7 Abutment contraction coefficient, extracted from USACE

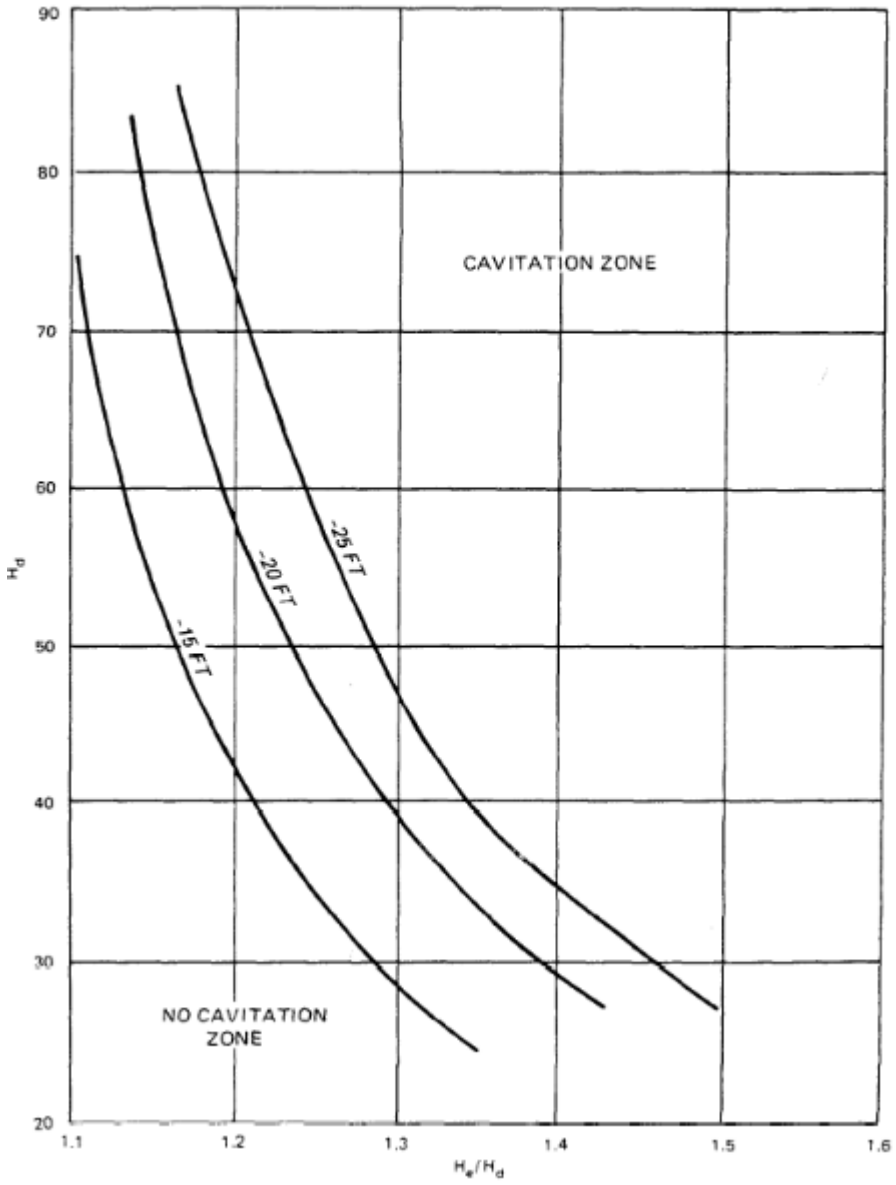

Plate A/ 8 Cavitation safety curve for flow over an ogee crest, extracted from USACE

ANNEX B

DETAILS OF DRAWINGS

CHANNEL (S1-S2') - PROFILE

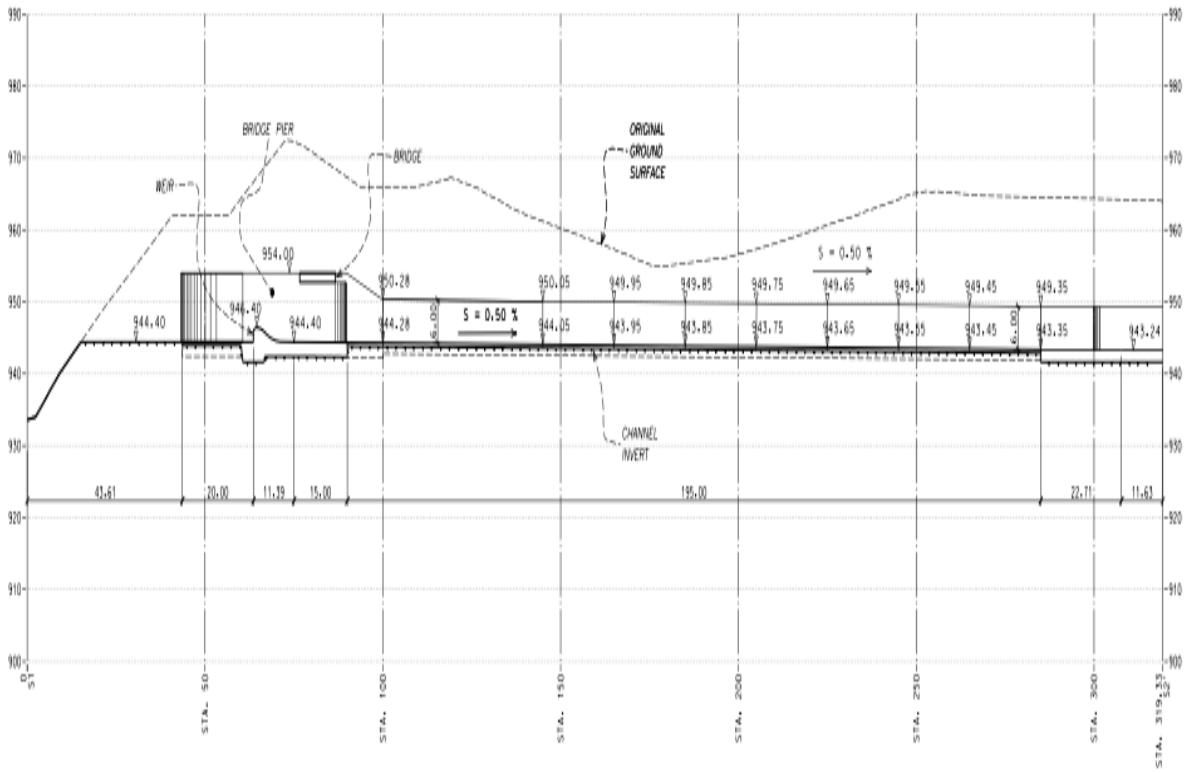

CHANNEL (S1-S2') - TYPICAL CROSS SECTION

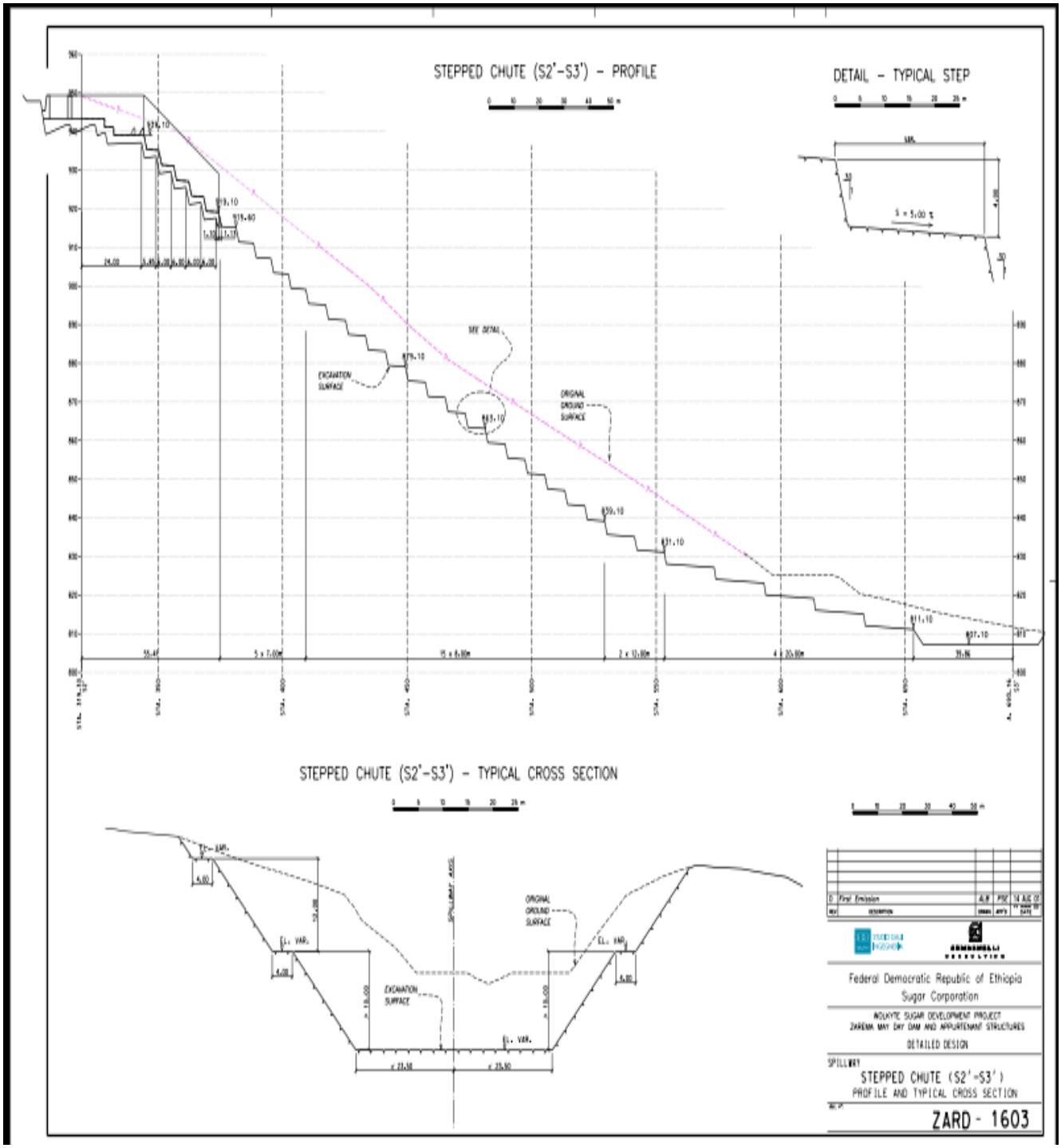
STEPPED CHUTE (S2'-S3') - PROFILE
DETAIL - TYPICAL STEP
EXCAVATION SURFACE
ORIGINAL GROUND SURFACE
STEPPED CHUTE (S2'-S3') - TYPICAL CROSS SECTION
Federal Democratic Republic of Ethiopia
Sugar Corporation
WOLKYTE SUGAR DEVELOPMENT PROJECT
ZAREMA MAY DAY DAM AND APPURTENANT STRUCTURES
DETAILED DESIGN
SPILLWAY
STEPPED CHUTE (S2'-S3')
PROFILE AND TYPICAL CROSS SECTION
ZARD - 1603

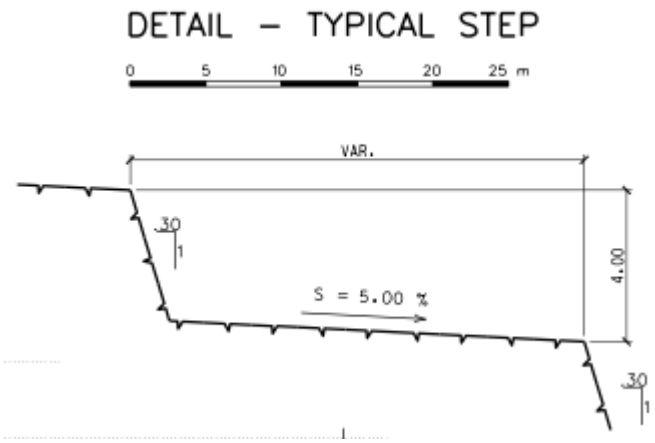
DETAIL – TYPICAL STEP
0 5 10 15 20 25 m
VAR.
3
0
1
S = 5.00 %
4.00
3
0
1

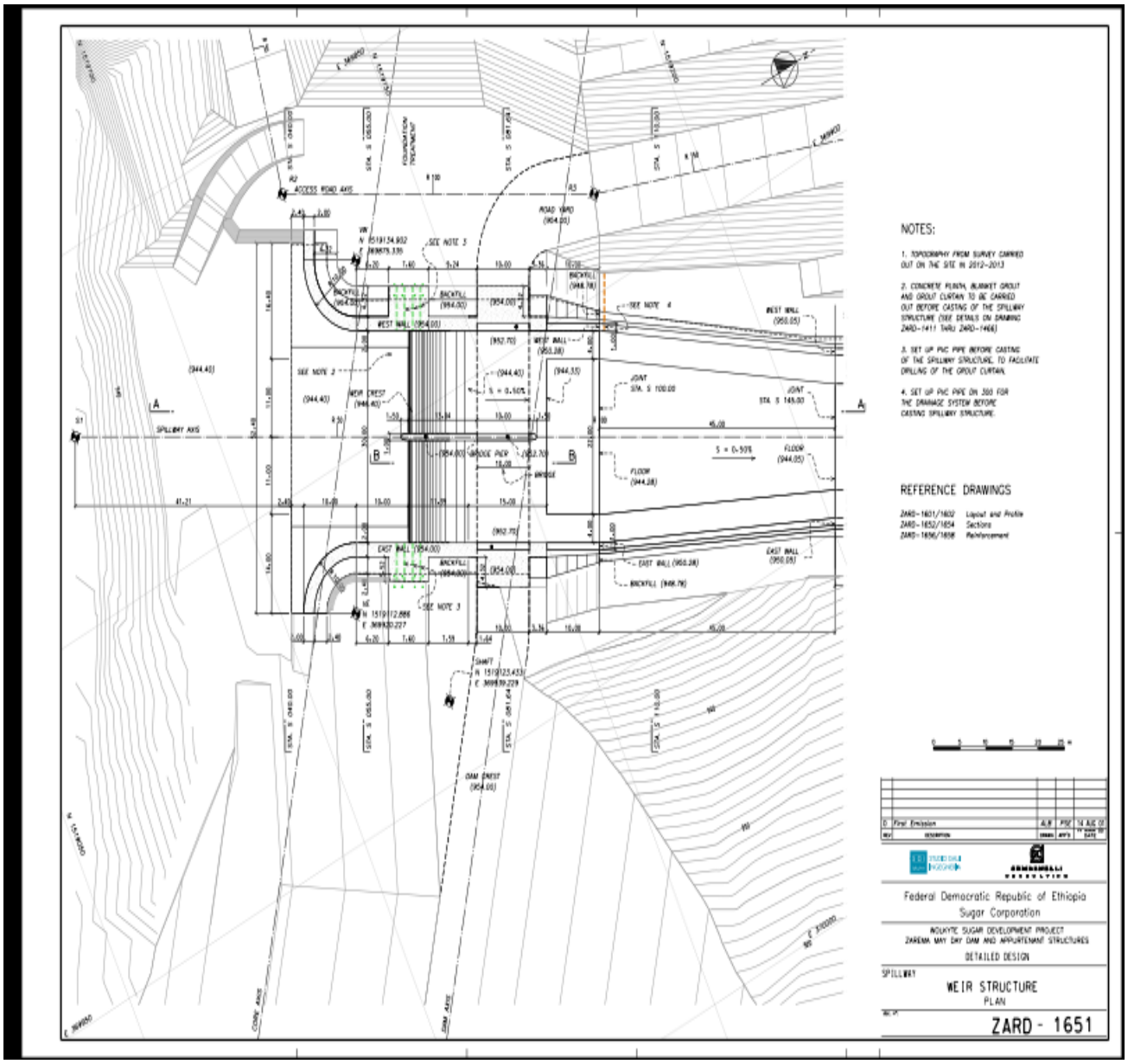
NOTES:
REFERENCE DRAWINGS
Federal Democratic Republic of Ethiopia
Sugar Corporation
WEIR STRUCTURE
PLAN
ZARD - 1651

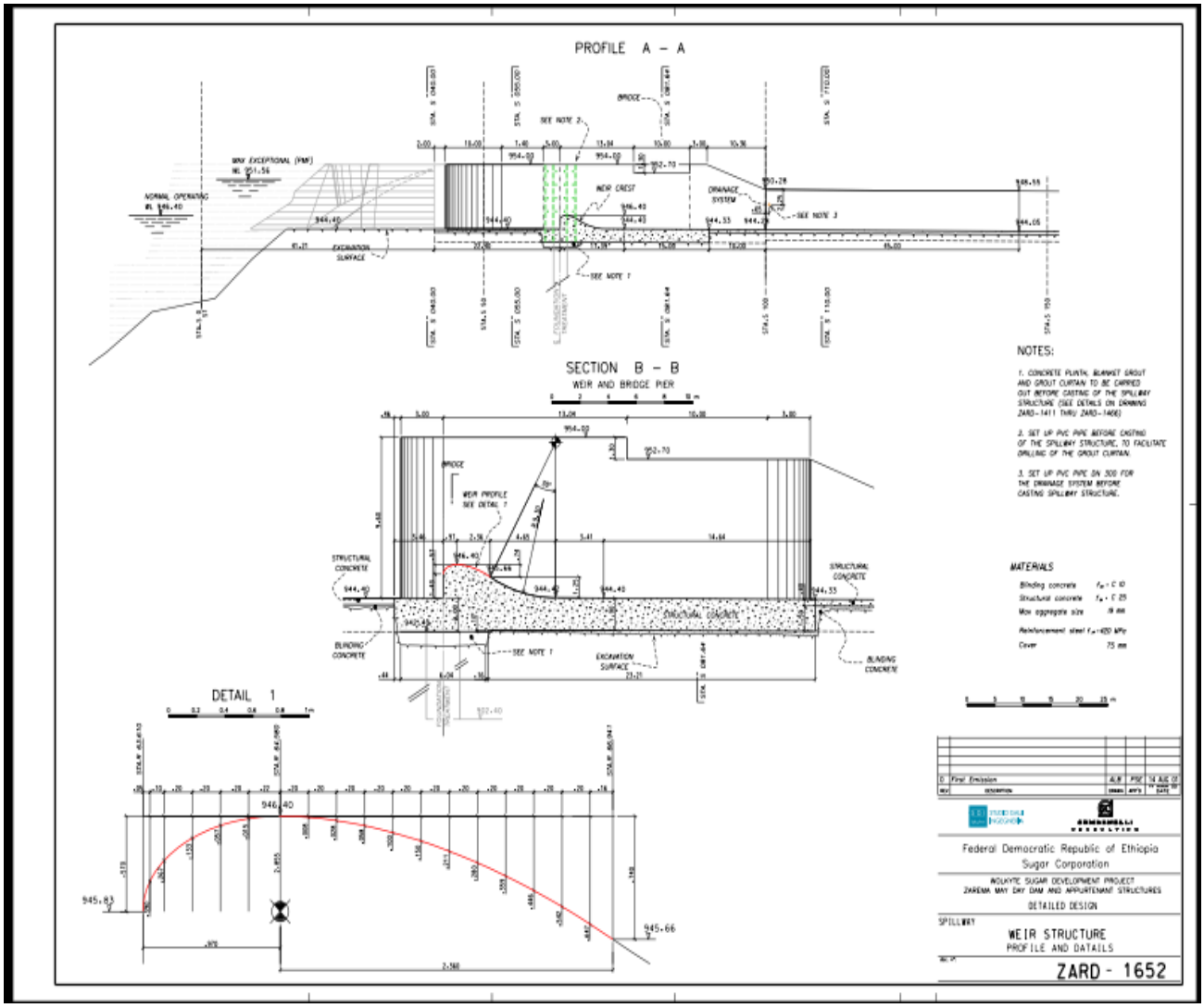
PROFILE A – A
SECTION B – B
WEIR AND BRIDGE PIER
DETAIL 1
NOTES:
MATERIALS
Federal Democratic Republic of Ethiopia
Sugar Corporation
WOLKYTE SUGAR DEVELOPMENT PROJECT
ZAREMA MAY DRY DAM AND APPURTENANT STRUCTURES
DETAILED DESIGN
SPILLWAY
WEIR STRUCTURE
PROFILE AND DATAILS
ZARD - 1652

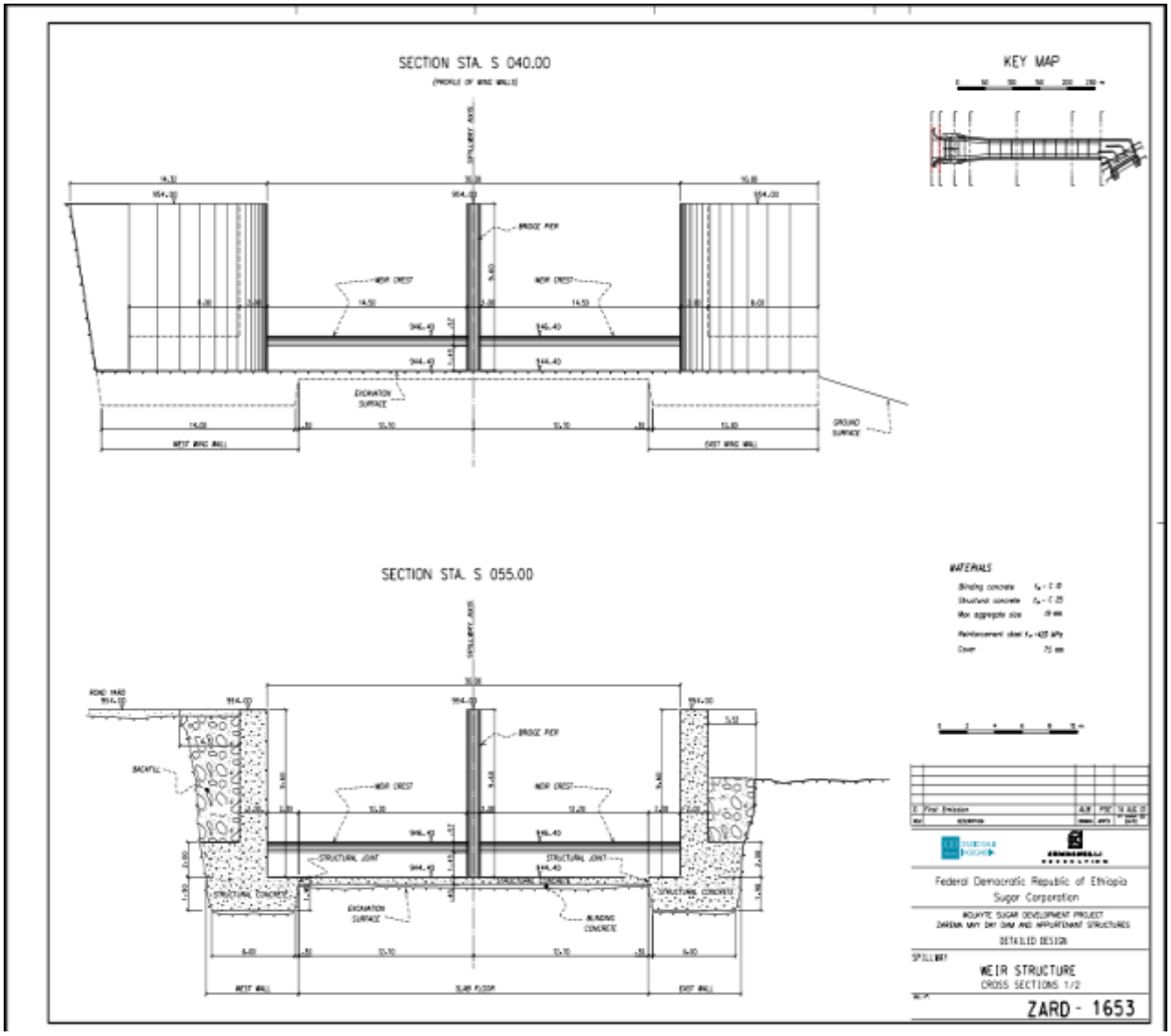
SECTION STA. S 040.00
KEY MAP
SECTION STA. S 055.00
MATERIALS
Federal Democratic Republic of Ethiopia
Sugar Corporation
DETAILED DESIGN
WEIR STRUCTURE
CROSS SECTIONS 1/2
ZARD - 1653

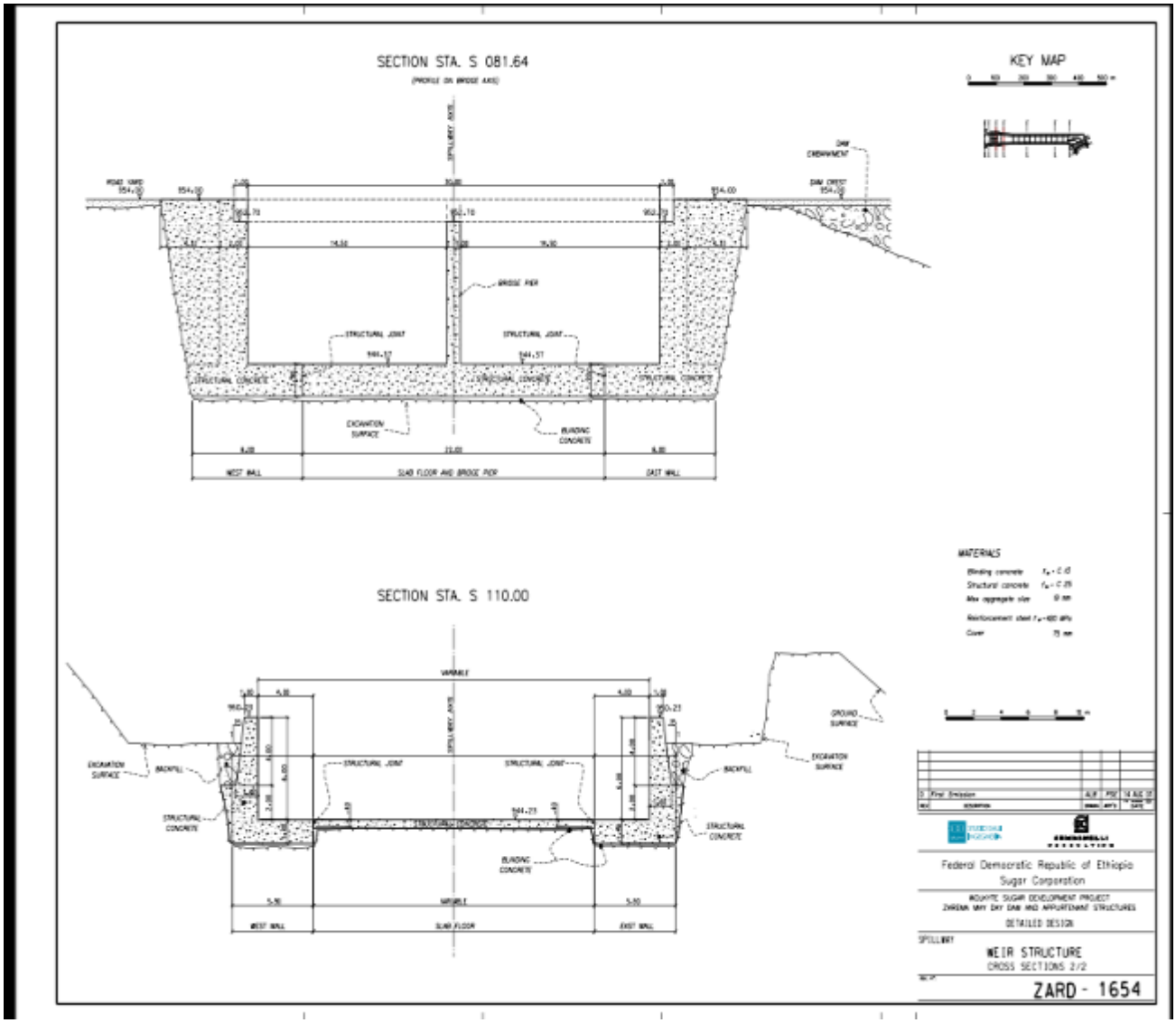
SECTION STA. S 081.64
KEY MAP
SECTION STA. S 110.00
MATERIALS
Federal Democratic Republic of Ethiopia
Sugar Corporation
DETAILED DESIGN
WEIR STRUCTURE
CROSS SECTIONS 2/2
ZARD - 1654

ANNEX C

TENDAHO DAM SPILLWAY

PROFILE OF OGEE WEIR

The maximum head over the spillway crest in passing the design discharge can be estimated by the relation:

$$Q = \frac{2}{3} * \sqrt{2g} * C * L * H^{3/2}$$

Where L is the effective length of the control structure,

Expression $\frac{2}{3} * \sqrt{2g} * C$ denoted by Cd is the discharge co-efficient.

Considering H equal to 8.4 m and Cd equal to 2.15 as first approximation, effective length of the control structure:

L = L'- 2H (N.kp + ka)

=31.5 - 2 x 8.4 (2 x .01 + 0.1)

=29.5 m

Hence, 1700 = 2.15 x 29.5x $H_e^{3/2}$

or H_e = 9.0 m

Velocity of approach, Va = 1700/(37.5 x 13.0)

=3.5 m/s

$H_a = Va^2 /2g$ = 0.62m

Maximum head of overflow, H = H_e – H_a = 8.38 m, which is close to the assumed value of 8.4 m.

Selecting the design head equal to 82% of this anticipated maximum head,

H_d = 0.8 x 8.38 = 6.87 m

Let us select H_d as 6.9 m

Coefficient of Discharge

$$C_d = \frac{2}{3} * \sqrt{2g} * C$$

C is read from IS 6934 and depends on ratio P / H_d

Where P is the height of the spillway crest measured from the bed of approach channel.

Thus, P = El 400 – El 396

= 4.0 m

P / H_d= 4.0 / 6.9 = 0.58

For P/H_d = 0.58, c = 0.722

$$C_d = \frac{2}{3} * \sqrt{2g} * 0.722 = 2.13$$

Which is close to the assumed value of 2.15.

Hence, for selected scheme, H_d = 6.9 and Cd = 2.15

Shape of the Ogee Profile

The profile of ogee weir consists of two quadrants, the upstream quadrant and the downstream quadrant.

The upstream quadrant of the crest shall conform to the ellipse:

X12 / A12 + Y12 / B12 = 1

The magnitudes of A1 and B1 are determined with reference to parameter P/H_d from the graph given in Fig 2 in IS : 6934.

For P/H_d = 0.58, A1/H_d = 0.248 and B1/H_d = 0.145

So A1 = 0.248 x 6.9 = 1.71

B1 = 0.145 x 6.9 = 1.00

Hence, profile of upstream quadrant is given by the equation:

X12 / 1.712 + Y12 / 12 = 1

Or $0.34 * X_1^2 + Y_1^2 = 1$

The upstream face will meet the bed of approach channel in a slope of 1:1. The coordinates of tangent point are given by x = - 1.48, y = 0.50. Downstream profile:

As per IS: 6934, the downstream profile of the crest may conform to the equation:

$$X_2^{1.85} = K_2 * H_d * Y_2$$

For P/H_d = 0.58, K2 = 2.04

Hence equation of downstream profile:

$$X_2^{1.85} = 2.04 * H_d * Y_2$$

Or $X_2^{1.85} = 9.56 * Y_2$

Considering the topography and the geology of the spillway area, the upstream end of inclined chute, which is also the downstream toe of the control structure, is set at El 387.5m. The downstream profile of the weir meets the floor of the inclined chute in a curve of 20 m radius. The coordinates of the point D denoting the start of circular curve are given by, X = 8.34, Y = 5.47. The total length of the control structure is 26.6 m.

Inclined chute

Flow released through the control structure is conveyed to the stilling basin through an inclined chute excavated along ground surface. A rectangular section of inclined chute has been selected for chute spillway. The inclination of chute is 1 in 9. Width of the chute at the point of its joining with the control structure is 37.5 m, equal to the length of the control structure which comprises 3 bays of 10.5 m each and two intermediate piers of 3.0 m thickness.

The design discharge of spillway being only 1700 m^3/s, the consideration of discharge intensity permits to adopt a width lesser than 37.5 m. Keeping this in view, it is proposed to reduce the width of the inclined chute, downstream of control structure, to 27.5 m. The Indian standard, IS: 5186 specifies that the channel section downstream of control structure may be converged on economic considerations, with due care to ensure that the side wall convergence in discharge channel is made gradual to avoid 'waves ride ups' on the walls and uneven distribution of flow across that channel. For this purpose, the code specifies that the side transition for convergence should be provided at an angle given by the equation:

$$\tan\alpha = \frac{1}{3F}$$

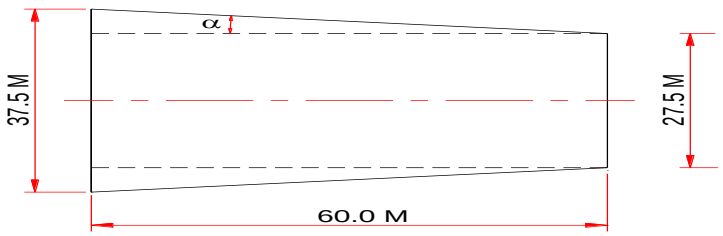

Where α = angle of convergence, and

F = Froud number given by $\frac{V}{\sqrt{gd}}$

Where,

V = average of the velocities at the beginning and end of convergence:

g = acceleration due to gravity; and

d = average of the depths of flow at the beginning and end of transition

The channel of inclined chute is proposed to be converged from 37.5 m width to 27.5 m in a length of 60 m.

Check for Convergence Length

Calculation of velocity and flow depth at the start of chute:

Let v be the velocity and d the flow depth at the toe of Ogee weir.

Neglecting head loss in flow over weir,

$400 + 9.0 = 387.5 + v^2/2g + d$

or $v^2/2g + 1700/(37.5xv) = 21.5$

Solving v = 19.4 m/s, d = 2.34 m

Calculation of velocity and flow depth at 60 m distance

Let v be the velocity and d the flow depth at this section.

Head loss in 60 m length can be calculated by Manning formula-

$h_f = v^2 n^2 L / R^{4/3}$

Considering n equal to 0.016, head loss in 60 m length of the chute works out to 2.28 m.

Applying Bernoulli's theorem, the velocity and depth at this section work out to 21.25 m/s and 2.91 m respectively.

Average velocity = (19.4 + 21.25)/2 = 20.325 m/s

Average depth = (2.34 + 2.91)/2 = 2.625 m

$F = v/\sqrt{gd}$

= 4.0

$\tan \alpha = 5.0/L = 1/3F$

$S_o L = 5 \times 3 \times F = 60$ m.

Hence, the considered convergence length of 60 m is in order.

Height of Chute Walls

IS: 5186 specifies that the freeboard provided for discharge channel where flow is supercritical should not be less than the one given by the following formula:

Freeboard = $0.61 + 0.0378\ v\ d^{1/3}$

For maximum values of v and d, the required freeboard works out to1.75 m.

The height of walls in the chute part has been kept as 4.7 m.

Stilling basin

The flow from the inclined chute enters the stilling basin in supercritical state. The energy associated with the flow is dissipated by formation of hydraulic jump in the stilling basin. The jump form and the flow features in the stilling basin are related to the Froud number parameter of the flow entering the stilling basin.

The velocity and the depth of flow at the end of inclined chute work out to 23.9 m/s and 2.58 m respectively. The Froud number of flows entering the basin equals to 4.75. For Froud number higher than 4.5, IS: 4997 recommends adopting Basin type II, which is similar to type III basin recommended by USBR for such cases. A true hydraulic jump forms in this type of basin. The installation of accessory devices such as chute blocks, basin blocks and end sill produce a stabilizing effect on the jump, which permits shortening the basin length and guard against sweep-out caused by inadequate tail water depth. The Codes further recommend that the basin blocks should not be provided when flow velocities at the location of basin bocks exceeds 15 m/s. Accordingly, the stilling basin of Tendaho spillway is provided with only chute blocks at the start of the basin and a dentated sill at the end of the basin.

Water depths at the beginning and the end of the hydraulic jump are related by the formula:
D2 / D1 = 0.5 ((1 + 8 F12)1/2 -1)

For the present case of F1 = 4.75 and D1 = 2.58 m, D2 works out to 16.1 m Required length of the basin is a function of F1 and D2. From IS: 4997, Lb / D2, for F1 equal to 4.75, reads out to 2.8. Thus, the minimum length of the basin as per IS: 4997 is 45.1 m. But, as per recommendations of USBR, the length of the jump for F1 = 4.75 is 3.8 times the D2, that works out to 61.2 m. A length of 60.0 m has been adopted for stilling basin of Tendaho spillway.

As per recommendations made by USBR Design of Small Dams, floor of the basin is required to be located at a distance HT below FRL where HT has certain relationship to discharge intensity and D2. Guided by this consideration, the floor of the stilling basin is set at El 372.0.

IS: 5186 recommends to provide a freeboard equal to 0.1 (v1 + D2) for flow in the stilling basin, that works out to 4.0 m. Accordingly, the height of wall in stilling basin is kept as 20.0 m. The scheme of spillway is shown in below.

Downstream discharge channel

The flow over the spillway, after dissipation of energy in stilling basin, will be conveyed to the river by an Outlet Channel (being referred here as downstream Discharge Channel). Unlike the spillway structure which is designed for an inflow flood equal to half of PMF due to higher risks involved if the structure fails to function properly under design flood condition, no such high risks are involved with performance of Discharge Channel. The flow in Discharge channel, in excess of design discharge, may scour the channel bed/side slopes or may over flank the channel banks. In any such case, there is no risk to human life and the risk may only be limited to some minimal loss of property. Hence, the section of Discharge Channel is proposed to be designed to cater to the half of the rated flow over spillway i: e 850 m^3/s.

The proposed section channel bed will have a down slope of l in 8000, the bed levels at upstream and downstream ends being 372.0 and 371.93 m respectively. The bed slope has

been so selected that the flow velocities are limited to 1.6 m/s for design discharge of 850 m^3/s. Accordingly, a channel of cross-sectional area equal to 532.5 m^2 has been provided. Sufficiently hard ground strata are expected at grade of the channel bed. Further, since the channel will only infrequently be called upon to cater to the design discharge, no lining is proposed to be provided in the Discharge Channel, except for first 110 m length immediately downstream of stilling basin. The channel, in this part, is provided with 2.0 m thick dumped rock riprap and concrete cladding on side slopes. The thickness of concrete cladding in first 25 m shall be 1000 mm while a 600 mm thick cladding is provided in remaining length. In case of occurrence of some damages to the channel section following heavy flood, the same can be made good by necessary repairs.

PERFORMANCE STATISTICS

Tendaho spillway performance indicators 3D with Design for Depth of flow (m)

Measurement Location	3D from Research (m)	Flow from Design (m)	SIM-Av_SIM		OBS-AV_OBS	(OBS-AVOBS)^2	(SIM-Av_SIM)(OBS-AV_OBS)			Percentage difference (%)
1	2	3	4	5	6	7	8	9	10	11
				(4)^2		(7)^2	(4)*(6)	(2)-(3)	(9)^2	
At Approach channel	11.43	12.4	6.558	43.007	7.143	51.022	46.844	-0.97	0.941	-7.82
At the Crest of Spillway	5.37	8.4	0.498	0.248	3.143	9.878	1.565	-3.03	9.181	-56.42
At the Spillway Toe	3.88	2.34	0.992	0.984	2.917	8.509	2.894	1.54	2.372	39.69
End of Convergence	3	2.91	1.872	3.504	2.347	5.508	4.394	0.09	0.008	3
Along the Chute Channel	2.83	2.91	2.042	4.17	2.347	5.508	4.793	-0.08	0.006	-2.83
Upstream of Stilling Basin	2.72	2.58	2.152	4.631	2.677	7.166	5.761	0.14	0.02	5.15
Sum	29.23	31.54	14.114	56.544	20.574	87.591	66.251	-2.31	12.528	-7.9
Average	4.872	5.257	2.352	9.424	3.429	14.599	11.042	-0.385	2.088	-7.9
		SQRT =		7.52		9.359				

R^2 =	0.886
NSCE =	0.857
Rbias =	-7.324

ANNEX D

Ribb Calculation of the Chute Stilling Basin and Sharp-crested Weirs

CALCULATION OF THE CHUTE

Paremeter	Formula	Symbol	Unit	Result										
points			unit	0	1	2	3	4	5	6	7	8	9	10
chainage			m	0	20	90	220	240	260	280	300	320	340	350
discharge		Q	m^3/s	1060										
dist.between sections		dl	m	0	20	70	130	20	20	20	20	20	20	10
dist.between datum and elevation	$z_2=z_1-(s-sfav)*dl$	z	m	0	-0.86	-3.20	-5.95	-11.75	-17.05	-21.79	-25.95	-29.54	-32.56	-33.86
channel slope		s		0.045	0.045	0.045	0.045	0.330	0.330	0.330	0.330	0.330	0.330	0.330
depth		y	m	6.591	4.997	1.78	1.59	1.30	1.12	1.01	0.92	0.86	0.81	0.78
width		b	m	20	20	40	40	41.0	42.0	43.0	44.0	45.0	46.0	47.0
Manning coefficient		n		0.013	0.013	0.013	0.013	0.013	0.013	0.013	0.013	0.013	0.013	0.013
Hydraulic radius	R=(y*b)/(b+2*y)	R		3.97	3.33	1.64	1.47	1.22	1.07	0.96	0.88	0.83	0.78	0.75
friction slope	$sf=(n^2*V^2)/(R^{4/3})$	sf			0.004	0.019	0.028	0.052	0.079	0.107	0.136	0.165	0.193	0.208
average slope between two successive steps	$sfav=(sf_1+sf_2)/2$	sfav			0.002	0.012	0.024	0.040	0.065	0.093	0.122	0.151	0.179	0.200
channel slope-sf	s-sfav	s-sfav			0.043	0.033	0.021	0.290	0.265	0.237	0.208	0.179	0.151	0.130
area	A=b*y	A	m2	131.8	99.9	71.2	63.4	53.1	47.1	43.2	40.5	38.6	37.1	36.5
mean velocity	V=Q/A	V	m/sec	8.04	10.61	14.88	16.71	19.96	22.49	24.53	26.16	27.49	28.59	29.03
Froude number	$Fr=V/(g*y)^{0.5}$	Fr		1.0	1.51	3.56	4.24	5.60	6.78	7.81	8.70	9.48	10.17	10.51
Total Energy	z+y+V2/2g+hf	E+hf	m	9.9	9.9	9.9	9.9	9.9	9.9	9.9	9.8	9.8	9.9	9.9
local losses	$hl=0.45*(V_1-V_2)^2/(2*g)$	hl	m											
Freeboard for side wall	$\Delta y=2.0+0.025*V*y^{1/3}$ (lb)	Δy	m	1.17	1.28	1.28	1.33	1.42	1.48	1.52	1.55	1.58	1.60	1.60
Wall height	$y+\Delta y$		m	7.76	6.28	3.06	2.92	2.71	2.60	2.53	2.48	2.44	2.40	2.38

STILLING BASIN

Paremeter	Formula	Symbol	Unit	Result
depth above the jamp		d_1	m	0.78
Froude number		Fr		10.5
depth below the jamp	$d_2=d_1*0.5*[(1+8*Fr_1^2)^{0.5}-1]$	d_2	m	11.17
Lengh of jamp	$L=4.3*d_2$	L	m	48.03
Freeboard for side wall	0.1(V1+d2)	Δy	m	4.02

SHARP-CRESTED WEIR

Weir 1

Paremeter	Formula	Symbol	Unit	Result
discharge		Q	m	1,060
width		w	m	47.00
depth below the jamp		d_2	m	11.17
height	h=d2-H	h	m	5.71
H	$H=(Q/(bm*(2g)^{0.5})^{0.667}$	H	m	5.46
velocity	V=Q/(B+d2)	V2	m/sec	2.02
Total Energy in 2	$E2=0.95*(h+H+V2^2/2*9.81)$	E2	m	10.81
Total Energy in *	$E^*=d^*1+V^{*2}/2*g$	E*	m	10.81
approaching depth	d1	d*1	m	1.69
velocity	V*=Q/B*d*1	V*1	m/sec	13.38
Froude number	$Fr=V^*/(g*d^*1)^{0.5}$	Fr*		3.29
approaching depth	$d_2=d_1*0.5*[(1+8*Fr_1^2)^{0.5}-1]$	d*2	m	7.04
Lengh of jamp	$L=4*d_2$	L*	m	28.18
Freeboard for side wall	0.1(V*1+d*2)	Δy	m	2.04

Weir 2

Paremeter	Formula	Symbol	Unit	Result
depth below the jamp		d_2	m	7.04
height	h=d2-H	h	m	1.58
H	$H=(Q/(bm*(2g)^{0.5})^{0.667}$	H	m	5.46
velocity	V=Q/(B+d2)	V2	m/sec	3.20
E2	$E2=0.95*(h+H+V2^2/2*9.81)$	E2	m	7.19
E*	$E^*=d^*1+V^{*2}/2*g$	E*	m	7.19
approaching depth	d1	d*1	m	2.30
velocity	V*=Q/B*d*1	V*	m/sec	9.79
Froude number	$Fr=V^*/(g*d^*1)^{0.5}$	Fr*		2.06
approaching depth	$d_2=d_1*0.5*[(1+8*Fr_1^2)^{0.5}-1]$	d*2	m	5.66
Lengh of jamp	$L=4*d_2$	L*	m	22.63
Freeboard for side wall	0.1(V*1+d*2)	Δy	m	1.54

Ribb chute channel performance indicators 3D with Design for Depth of flow (m)

Measurement Location	Depth of flow from 3D model (m)	Depth of flow from Design (m)	SIM-Av_SIM		OBS-AV_OBS	(OBS-AV_OBS)^2	(SIM-Av_SIM)(OBS-AV_OBS)			Percentage difference (%)
1	2	3	4	5	6	7	8	9	10	11
				(4)^2		(7)^2	(4)*(6)	(2)-(3)	(9)^2	
0	5.59	6.591	3.474	12.069	4.177	17.447	14.511	-1.001	1.002	-15.19
20	3.52	4.997	1.404	1.971	2.583	6.672	3.627	-1.477	2.182	-29.56
90	1.74	1.78	0.376	0.141	0.634	0.402	0.238	-0.04	0.002	-2.25
220	1.48	1.59	0.636	0.404	0.824	0.679	0.524	-0.11	0.012	-6.92
240	1.31	1.3	0.806	0.65	1.114	1.241	0.898	0.01	0	0.77
260	1.18	1.12	0.936	0.876	1.294	1.674	1.211	0.06	0.004	5.36
280	1.1	1.01	1.016	1.032	1.404	1.971	1.426	0.09	0.008	8.91
300	1.01	0.92	1.106	1.223	1.494	2.232	1.652	0.09	0.008	9.78
Sum	16.93	19.308	9.754	18.366	13.524	32.318	24.087	-2.378	3.218	
Av	2.116	2.414	1.219	2.296	1.691	4.04	3.011	-0.297	0.402	
			SQRT =	4.286		5.685				

R^2 =	0.977
NSCE =	0.900
Rbias =	-12.32%

Ribb chute channel performance indicators 3D with Design for velocity (m/s)

Measurement Location	Velocity of flow from 3D model (m/s)	Velocity of flow from Design (m/s)	SIM-Av_SIM		OBS-AV_OBS	(OBS-AV_OBS)^2	(SIM-Av_SIM)(OBS-AV_OBS)			Percentage difference (%)
1	2	3	4	5	6	7	8	9	10	11
				(4)^2		(7)^2	(4)*(6)	(2)-(3)	(9)^2	
0	9.46	0.84	8.358	69.856	16.183	261.889	135.258	8.62	74.304	1026.19
20	12.05	10.61	5.768	33.27	6.413	41.127	36.99	1.44	2.074	13.57
90	15.51	14.88	2.308	5.327	2.143	4.592	4.946	0.63	0.397	4.23
220	18.47	16.71	0.652	0.425	0.313	0.098	0.204	1.76	3.098	10.53
240	20.03	19.96	2.212	4.893	2.937	8.626	6.497	0.07	0.005	0.35
260	21.18	22.49	3.362	11.303	5.467	29.888	18.38	-1.31	1.716	-5.82
280	22.23	24.53	4.412	19.466	7.507	56.355	33.121	-2.3	5.29	-9.38
300	23.61	26.16	5.792	33.547	9.137	83.485	52.922	-2.55	6.503	-9.75
Sum	142.54	136.18	32.864	178.087	50.1	486.06	288.318	6.36	93.387	
Average	17.818	17.023	4.108	22.261	6.263	60.758	36.04	0.795	11.673	
			SQRT =	13.345		22.047				

R^2 =	0.960
NSCE =	0.808
Rbias =	4.67%

ANNEX E

1. THEORETICAL BACKGROUND FOR NUMERICAL MODELLING

1.1 FLUID PROPERTIES

The term “hydraulics” is related to the application of the Fluid Mechanics principles to water engineering structures, civil and environmental engineering facilities, especially hydraulic structures (e.g. canal, river, dam, reservoir and water treatment plant).

The main parameters of a hydraulic study are the geometry of the channel (e.g. width, slope and roughness), the properties of the flowing fluid (e.g. density and viscosity) and the flow parameters (e.g. velocity and flow depth).

Viscosity and Other Properties

The quantities such as pressure, temperature, and density are primary thermodynamic variables which characterize specific fluid- mechanical behaviour. The most important of these is viscosity, which relates the local stresses in moving fluid to the strain rate of the fluid element.

Viscosity: - The resistance to the movement of one layer of fluid over an adjoining one is referred to as the viscosity of fluid. Newton’s law of viscosity postulates that, for the straight parallel motion of a given fluid, the tangential stress between two adjacent layers is proportional to the velocity gradient in a direction perpendicular to the layers:

$$\tau = \mu \frac{dV}{dy} \quad -------- (2.1)$$

Where τ is the shear stress between adjacent fluid, μ is the dynamic viscosity of the fluid, V is the velocity and y is the direction perpendicular to the fluid motion. Fluid that obey Newton’s law of viscosity are called Newtonian fluids. The common fluids such as air, water and light petroleum oils, are Newtonian fluids [38]. The ratio of viscous and inertial forces is defined as the Reynolds number.

Reynolds Number: - $R_e = \frac{\rho VL}{\mu} = \frac{VL}{\nu} \quad ---------(2.2)$

Where V and L are characteristic velocity and length scales of the flow. The second form of Re illustrates that the ratio of μ to ρ has its own name, the kinematic viscosity:

$\nu = \text{kinematic viscosity}$

$\nu = \frac{\mu}{\rho}$

1.2 THE FUNDAMENTAL EQUATIONS

The law of conservation of mass states that the mass within a closed system remains constant with time [48]:

$$\frac{dm}{dt} = 0 \quad -------(2.3)$$

On the other hand, momentum can be changed by the action of forces and its conservation equation in Newton's second low of motion [48]:

$$\sum F = \frac{d}{dt}(mv) \quad ------(2.4)$$

Where $\sum F$ refers to the resultant of all external forces acting on the system including body forces such as gravity, v stands for the velocity, m for mass and t for time. This application is called motion equation.

The above equations must be applied to a control volume. A control volume is a specific region of space selected for analysis. It refers to a region in space where fluid enters and leaves. The boundary of a control volume is its control surface. The concept of control volume used in conjunction with the differential form of the continuity, momentum and energy equations, is an open system [38]. In this research three-dimensional modelling is seen in more detail than one- and two-dimensional modelling.

1.3 ONE DIMENSIONAL MODELLING OF OPEN-CHANNEL FLOWS

The general equations for unsteady nonuniform open-channel flows are the Saint-Venant equations or the dynamic wave equations [77], [78], [79]. The derivation of the Saint-Venant equations is based on the shallow-water approximation where the vertical pressure distribution is hydrostatic and the vertical acceleration is small. It is also assumed that the channel bottom slope is

$$\frac{\partial A}{\partial t} + \frac{\partial Q}{\partial x} - q_1 = 0 \quad ---------(2.5\ )$$

and the momentum equation which describes the force balance of the control volume has the form

$$\frac{\partial Q}{\partial t} + \frac{\partial}{\partial x}(QV) = gA(S_0 - S_f) \quad -------(2.6)$$

Where A is the cross-sectional area of the flow which depends of the geometry of the channel cross section and the flow depth, V is the average velocity perpendicular to the cross section, and Q = AV is the flow rate. q1 in the continuity equations is the lateral inflow rate per unit channel length. In the momentum equations, $S_o = -\partial z/\partial x$ is the water surface slope and z is the surface elevation. Sf is the friction slope which is a function of flow and stage. The friction slope is determined by the resistance equation, such as Manning and Chezy equations. In derivation, it is assumed the momentum associated with the lateral inflow can be neglected.

1.4 TWO- DIMENSIONAL MODELLING OF OPEN-CHANNEL FLOWS

Two-dimensional modelling [78] of open-channel flows usually uses the depth-averaged shallow water equations (SWEs) where the vertical acceleration of the fluid is ignored. The governing equations for the one-dimensional modelling in the previous section can be viewed as a special case of SWEs where one spatial derivative vanishes. Both 1D and 2D modelling equations belong to the broad category of hyperbolic partial differential equations which has a natural connection with conservation laws. It is noted that there are also two-dimensional

models with one dimension being the vertical and the other one being along the river. This modelling methodology is applicable when the variation across the river is small and the emphasis is to model the vertical motion and transport.

Two-dimensional shallow- water equations can be written in normal conservation law form as

$$\frac{\partial h}{\partial t}+\frac{\partial(uh)}{\partial x}+\frac{\partial(vh)}{\partial y}=0 \quad ---------(2.7)$$

$$\frac{\partial uh}{\partial t}+\frac{\partial(u^2h+\frac{1}{2}gh^2)}{\partial x}+\frac{\partial(uvh)}{\partial y}=ghS_{ox}-ghS_{fx}+\frac{\tau_{wx}}{\rho}+hfu \quad ---------(2.8)$$

$$\frac{\partial(vh)}{\partial t}+\frac{\partial(uvh)}{\partial x}+\frac{\partial(v^2h+\frac{1}{2}gh^2)}{\partial y}=ghS_{oy}-ghS_{fy}+\frac{\tau_{wx}}{\rho}+hfu \quad -----(2.9)$$

Where h is the water depth, u and v are the depth-average velocities in x and y directions respectively, g is the gravity constant, ρ is the water density, τ_{wx} and τ_{wy} are surface wind shear stresses, f is the Coriolis parameter, and ν the Kinematic eddy viscosity. S_{0x} and S_{0y} are the bed slopes in the x and y direction; S_{fx} and S_{fy} are the friction slopes in the x and y directions, respectively, which can be estimated using Manning's formula

$$S_{fx}=n^2u\sqrt{u^2+v^2} \quad ----------(2.10)$$

$$S_{fy}=n^2v\sqrt{u^2+v^2} \quad ----------(2.11)$$

Where n is Manning's roughness coefficient.

1.5 THREE-DIMENSIONAL MODELLING OF OPEN-CHANNEL FLOWS

1.5.1 Navier-Stokes equations

The conservation equations of mass, momentum and energy for incompressible flows will be described generally in this part. First, a derivation to the equations in the most general form is shown. The mathematical equations that exemplify the physical principles could be extracted

by applying the suitable fundamental physical principle into an appropriate model of flow. The fluid flow has been modelled with infinitesimal control volume fixed in space and the fluid moving through it. As a result, the equations are proposed in a differential conservation form.

Conservation laws can be derived by considering a given quantity of matter or control mass (CM) and its extensive properties, such as mass, momentum and energy [77]. This approach is used to study the dynamics of solid bodies, where the CM (sometimes called the system) is easily identified. In fluid flows, however, it is difficult to follow a parcel of matter. It is more convenient to deal with the flow within a certain spatial region called a control volume (CV), rather than in a parcel of matter which quickly passes through the region of interest. This method of analysis is called the control volume approach [48].

The main fluid properties are noted as u, v, w, ρ, p, and t, for the velocity vector, scalar velocities in the x-, y-, and z direction, density, pressure, and viscous stresses, respectively [80].

Conservation of Mass

Conservation of mass on the fluid in a control volume (CV)

Rate of accumulation of mass in the CV = Rate of inflow mass – Rate of out flow mass

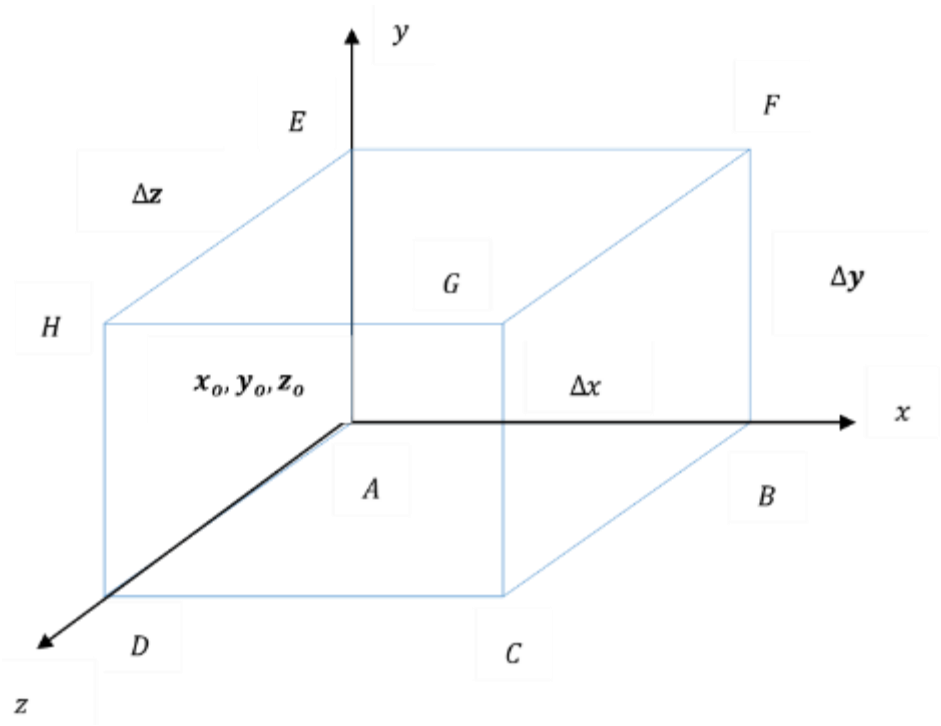

Mass in the CV = ρ(Voume) = $\rho\Delta x\Delta y\Delta z$

Mass flow rate through any face $= \rho$ (Velocity)(area normal to U) = ρUA =

$$\frac{\partial}{\partial t}(\rho\Delta x\Delta y\Delta z) = inflow\ rate\ through\ sides\ ADHE, ABCD\ \&\ ABFE - out\ flow\ rate\ through\ face\ BCGF, EFGH\ \&\ DCGH$$

$$\frac{\partial}{\partial t}(\rho\Delta x\Delta y\Delta z) = \rho u\Delta y\Delta z\ at\ x_0 + \rho v\Delta x\Delta z\ at\ y_0 + \rho w\Delta x\Delta y\ at\ z_0 - \rho u\Delta y\Delta z\ at\ x_0 + x_{\Delta x} - \rho v\Delta x\Delta z\ at\ y_0 + y_{\Delta y} - \rho w\Delta x\Delta y\ at\ z_0 + z_{\Delta z}$$

Divide by $\Delta x\Delta y\Delta z$ and take limit as lim as $\Delta x\rightarrow 0$, $\Delta y\rightarrow 0$ and $\Delta z\rightarrow 0$

$$\frac{\partial\rho}{\partial t} = \frac{\rho u\ at\ x_0 - \rho u\ at\ x_0+\Delta x}{\Delta x} + \frac{\rho v\ at\ y_0 - \rho v\ at\ y_0+\Delta y}{\Delta y} + \frac{\rho w\ at\ z_0 - \rho w\ \ at\ z_0+\Delta z}{\Delta z}$$

$$\lim_{\Delta x \to 0} = \frac{(\rho u)\ at\ x_0 - (\rho u)\ at\ x_0 + \Delta x}{\Delta x}$$

$$= \frac{-\partial(\rho u)}{\partial x}\ at\ x_0$$

$$\frac{\partial \rho}{\partial t} = -\frac{\partial(\rho u)}{\partial x}\ at\ x_0 - \frac{\partial(\rho v)}{\partial y}\ at\ y_0 - \frac{\partial(\rho w)}{\partial z}\ at\ z_0$$

$$\frac{\partial \rho}{\partial t} + \frac{\partial(\rho u)}{\partial x} + \frac{\partial(\rho v)}{\partial y} + \frac{\partial(\rho w)}{\partial z} = 0$$

For incompressible

$$\frac{\partial(u)}{\partial x} + \frac{\partial(v)}{\partial y} + \frac{\partial(w)}{\partial z} = 0 \quad \text{or} \quad \nabla \vec{V} = 0 \qquad \text{(continuity Equation)}$$

Momentum Conservation

Rate of accumulation of momentum in the CV = Rate of inflow momentum – Rate of out flow momentum + net external forces within CV.

Rate of accumulation in x direction = rate of inflow of x momentum – rate of out flow of x momentum + ∑F acting in x direction

X -momentum = mass * velocity

$= \rho \Delta x \Delta y \Delta z\ V_x$

$= (\rho \Delta x \Delta y \Delta z)\ U$

$$\frac{\partial}{\partial t}(u \rho \Delta x \Delta y \Delta z)$$

$$= inflow\ rate\ of\ x\ momentum\ through\ side$$

$$- outflow\ rate\ of\ x\ momentum\ through\ side + \sum F_x$$

$$\frac{\partial}{\partial t}(u\rho\Delta x\Delta y\Delta z)$$

$$= (\rho u\Delta y\Delta zu)\ at\ x_0 + (\rho v\Delta x\Delta zu)\ at\ y_0 + (\rho w\Delta x\Delta yu)\ at\ z_0 - (\rho u\Delta y\Delta zu) at\ x_{0+\Delta x}$$

$$- (\rho v\Delta x\Delta zu) at\ y_{0+\Delta y} - (\rho w\Delta x\Delta yu) at\ z_{0+\Delta z} + \sum F_{net\ x}$$

$$\frac{\partial(\rho u)}{\partial t} = \lim_{\Delta x\to 0} \frac{(\rho u^2)\ at\ x_0 - (\rho u^2)\ at\ x_0+\Delta x}{\Delta x} + \lim_{\Delta y\to 0} \frac{(\rho vu)\ at\ y_0 - (\rho vu)\ at\ y_0+\Delta y}{\Delta y} +$$

$$\lim_{\Delta z\to 0} \frac{(\rho wu)\ at\ x_0 - (\rho wu)\ at\ z_0+\Delta z}{\Delta z}$$

$$\frac{\partial(\rho u)}{\partial t} + \frac{\partial(\rho u^2)}{\partial x} + \frac{\partial(\rho vu)}{\partial y} + \frac{\partial(\rho wu)}{\partial z} = \sum \frac{F_{net\ x}}{\Delta x\Delta y\Delta z}$$

$\sum \boldsymbol{F_{net}}$

- Gravitational Force (external spread all over the volume)
- Pressure Force (external exerts on the surface)
- Viscosity (internal)

External fore $= F_{body} + \sigma * A$

Pressure Force (exerts on the surface) = Normal compressive stress

$F_{body} = F_{gravity} = m\vec{g} = \rho\Delta x\Delta y\Delta z.\vec{g}$

$$\lim_{\substack{\Delta x\to 0\\ \Delta y\to 0\\ \Delta z\to 0}} \frac{F_{body}}{\Delta x\Delta y\Delta z} = \rho\vec{g} = \rho g_x$$

$\bar{\bar{\sigma}} \cong \sigma_{ij} \implies$ Stress acting on the ith plain in the ^{jth} direction

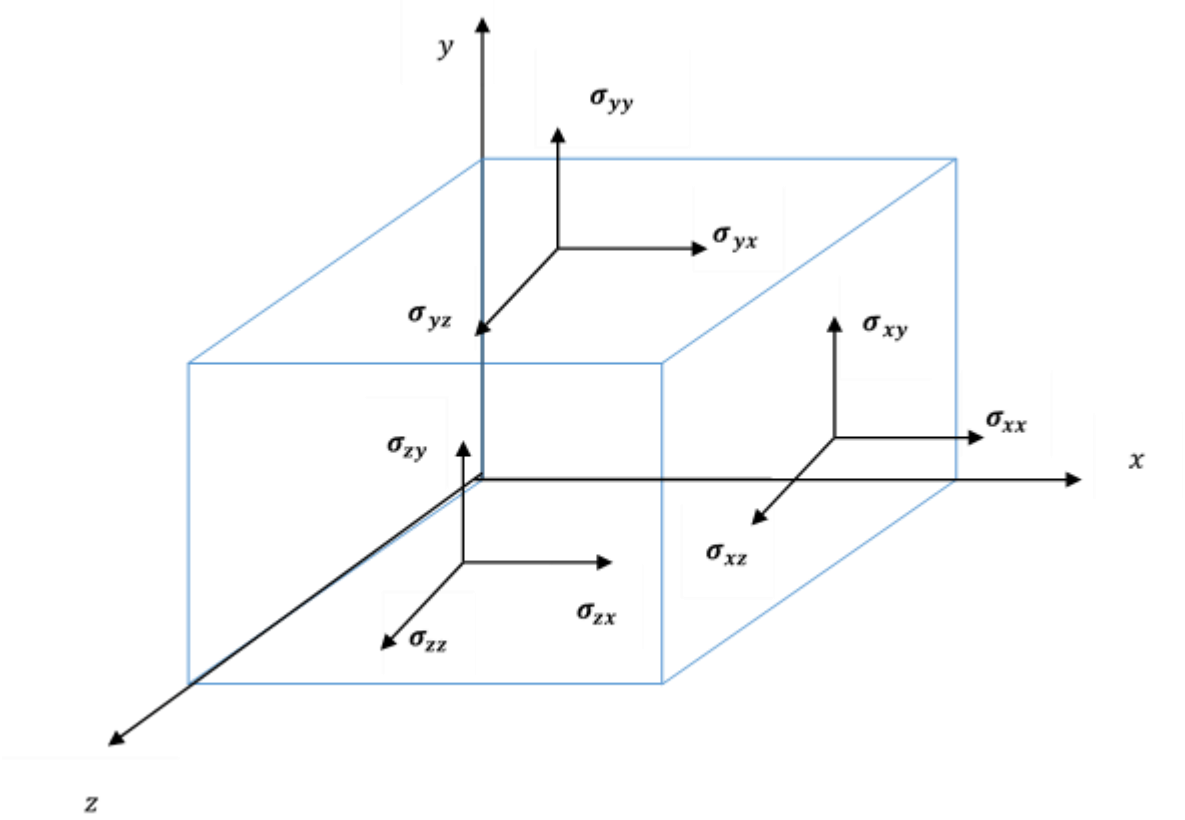

X direction only the x-direction stress.

$$\sum \frac{F_{external\,x}}{\Delta x\Delta y\Delta z} = \frac{\rho g_x\,\Delta x\Delta y\Delta z}{\Delta x\Delta y\Delta z} + \frac{\sigma_{xx}\,\Delta y\Delta z\ at\ x_0 + \Delta x - \sigma_{xx}\,\Delta y\Delta z\ at\ x_0}{\Delta x\Delta y\Delta z} +$$

$$\frac{\sigma_{yx}\,\Delta x\Delta z\ at\ y_0 + \Delta y - \sigma_{yx}\,\Delta x\Delta z\ at\ y_0}{\Delta x\Delta y\Delta z} + \frac{\sigma_{zx}\,\Delta x\Delta y\ at\ z_0 + \Delta z - \sigma_{zx}\,\Delta x\Delta y\ at\ z_0}{\Delta x\Delta y\Delta z}$$

$$\lim_{\substack{\Delta x\to 0\\ \Delta y\to 0\\ \Delta z\to 0}} \sum \frac{F_{external\,x}}{\Delta x\Delta y\Delta z}$$

$$\sum \frac{F_{external\,x}}{\Delta x\Delta y\Delta z} = \rho g_x + \frac{\partial(\sigma_{xx})}{\partial x} + \frac{\partial(\sigma_{yx})}{\partial y} + \frac{\partial(\sigma_{zx})}{\partial z}$$

$$\frac{\partial(\rho u)}{\partial t} + \frac{\partial(\rho u^2)}{\partial x} + \frac{\partial(\rho vu)}{\partial y} + \frac{\partial(\rho wu)}{\partial z} = \frac{\partial(\sigma_{xx})}{\partial x} + \frac{\partial(\sigma_{yx})}{\partial y} + \frac{\partial(\sigma_{zx})}{\partial z} + \rho g_x \quad --- \quad \text{(x- momentum)}$$

$$\frac{\partial(\rho v)}{\partial t}+\frac{\partial(\rho uv)}{\partial x}+\frac{\partial(\rho v^2)}{\partial y}+\frac{\partial(\rho wv)}{\partial z}=\frac{\partial(\sigma_{xy})}{\partial x}+\frac{\partial(\sigma_{yy})}{\partial y}+\frac{\partial(\sigma_{zy})}{\partial z}+\rho g_y \quad --- \text{ (y- momentum)}$$

$$\frac{\partial(\rho w)}{\partial t}+\frac{\partial(\rho uw)}{\partial x}+\frac{\partial(\rho vw)}{\partial y}+\frac{\partial(\rho w^2)}{\partial z}=\frac{\partial(\sigma_{xw})}{\partial x}+\frac{\partial(\sigma_{yw})}{\partial y}+\frac{\partial(\sigma_{ww})}{\partial z}+\rho g_w \quad --- \text{ (z- momentum)}$$

There are 12 variables but only 4 equations. One continuity equation and three momentum equations.

The variables are as follows.

$u, v, w, \sigma_{xx}, \sigma_{yx}, \sigma_{zx}, \sigma_{xy}, \sigma_{yy}, \sigma_{zy}, \sigma_{xw}, \sigma_{yw}\ and\ \sigma_{ww}$

Internal forces

There is a change in shape due to variation in viscosity.

Three components which changes in shape [80].

1) Rotation strain rate
2) Shear strain rate
3) Extension strain rate

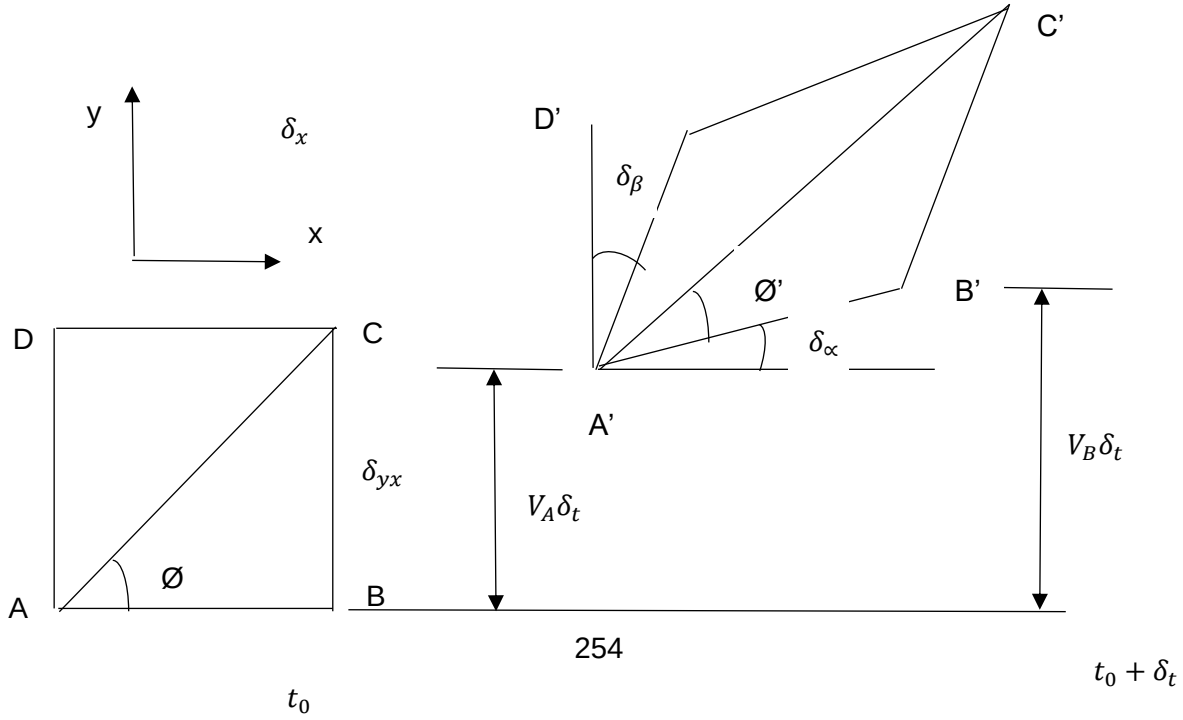

- Measure angle in counter clock wise

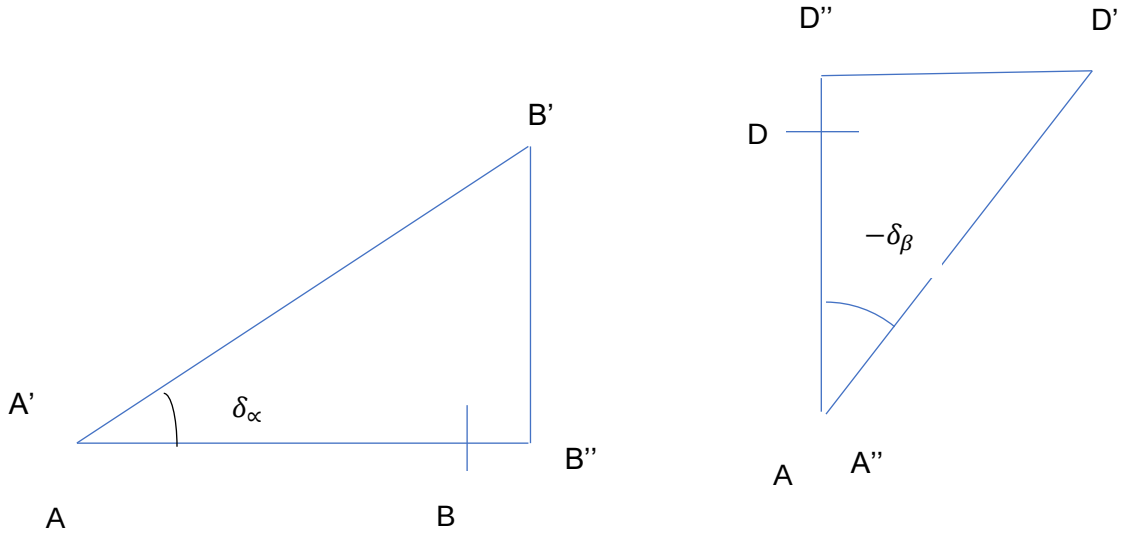

1) Rotational Strain

$$\text{Rotational Strain} = \text{Ø'} - \text{Ø} = \frac{1}{2}(\delta_\alpha + \delta_\beta)$$

$$\delta_\alpha = \frac{B'B''}{AB''}$$

$$\delta_\alpha = \frac{(V_B - V_A)\delta_t}{AB + BB"}$$

$$\delta_\alpha = \frac{(V_B - V_A)\delta_t}{AB + (u_B - u_A)\delta_t}$$

$$\frac{\left(\frac{\partial v}{\partial x}\right)\delta_x\delta_t}{\delta_x + \left(\frac{\partial u}{\partial x}\right)\delta_x\delta_t} = \delta_x \quad neglecting\ small\ terms$$

$$\frac{\left(\frac{\partial v}{\partial x}\right)\delta_x\delta_t}{\delta_x} = \delta_x$$

$$\delta_x = \frac{\partial v}{\partial x}\delta_t$$

$$\delta_\beta = \frac{D'D''}{AD + DD"}$$

$$\delta_\beta = \frac{(u_B - u_A)\delta_t}{\delta_y + (v_D - v_A)\delta_t}$$

$$= \frac{\left(\frac{\partial u}{\partial y}\right)\delta_y \delta_t}{\delta_y + \left(\frac{\partial v}{\partial y}\right)\delta_y \delta_t} \quad neglecting\ small\ terms$$

$$= \frac{\left(\frac{\partial u}{\partial y}\right)\delta_y \delta_t}{\delta_y}$$

$$\delta_\beta = \frac{\partial u}{\partial y}\delta_t$$

$$\therefore Rotational\ Strain = Ø' - Ø = \frac{1}{2}(\delta_\alpha + \delta_\beta)$$

$$= \frac{1}{2}(\frac{\partial v}{\partial x} - \frac{\partial u}{\partial y})\delta_t$$

$$The\ rate\ of\ rotational\ strain = \frac{1}{\delta_t}(Ø' - Ø) = \frac{1}{2}(\frac{\partial v}{\partial x} - \frac{\partial u}{\partial y})$$

2) Shear Strain

Shear Strain = $\frac{1}{2}(\delta_\alpha - \delta_\beta) = \frac{1}{2}(\frac{\partial v}{\partial x} + \frac{\partial u}{\partial y})\delta_t$

Rate of Shear Strain = $\frac{1}{2}(\frac{\partial v}{\partial x} + \frac{\partial u}{\partial y})$

3) Extension strain rate

Extension strain (x-distance) = $\frac{B'B'' - AB}{AB}$

Extension strain (x-distance) = $\frac{AB + (u_B - u_A)\delta_t - AB}{AB}$

$$= \frac{\left(\frac{\partial u}{\partial x}\right)\delta_x\delta_t}{\delta_x} = \frac{\partial u}{\partial x}\delta_t$$

Rate of Extension strain (y-direction) = $\frac{\partial u}{\partial y}$

Therefore, all strain rates are expressed in velocity gradient.

The various combination of velocity gradient describes the rate of strain that the fluid particle is suffering as it going to the flow. This shows that stress strain rate can be expressed in linear rate of relation [80].

$\tau_{ij} \propto \epsilon_{kl}$

$\epsilon_{kl} = \epsilon_{kl} = \frac{\partial u_k}{\partial x_l}$

$$\epsilon = \begin{vmatrix} \frac{\partial \mathrm{u}}{\partial \mathrm{x}} & \frac{\partial \mathrm{u}}{\partial \mathrm{y}} & \frac{\partial \mathrm{u}}{\partial \mathrm{z}} \\ \frac{\partial \mathrm{v}}{\partial \mathrm{x}} & \frac{\partial \mathrm{v}}{\partial \mathrm{y}} & \frac{\partial \mathrm{v}}{\partial \mathrm{z}} \\ \frac{\partial \mathrm{w}}{\partial \mathrm{x}} & \frac{\partial \mathrm{w}}{\partial \mathrm{y}} & \frac{\partial \mathrm{w}}{\partial \mathrm{z}} \end{vmatrix}$$

Stress component is proportional to velocity component.

$$\tau_{\mathrm{yx}} = \mu\frac{\partial \mathrm{u}}{\partial \mathrm{y}}$$

As a sample

$$\tau_{\mathrm{xx}} = \mathrm{a}_1\frac{\partial \mathrm{u}}{\partial \mathrm{x}} + \mathrm{a}_2\frac{\partial \mathrm{u}}{\partial \mathrm{y}} + \mathrm{a}_3\frac{\partial \mathrm{u}}{\partial \mathrm{z}} + \mathrm{a}_4\frac{\partial \mathrm{v}}{\partial \mathrm{x}} + \mathrm{a}_5\frac{\partial \mathrm{v}}{\partial \mathrm{y}} + \mathrm{a}_6\frac{\partial \mathrm{v}}{\partial \mathrm{z}} + \mathrm{a}_7\frac{\partial \mathrm{w}}{\partial \mathrm{x}} + \mathrm{a}_8\frac{\partial \mathrm{w}}{\partial \mathrm{y}} + \mathrm{a}_9\frac{\partial \mathrm{w}}{\partial \mathrm{z}}$$

$$\tau_{\mathrm{xy}} = \mathrm{b}_1\frac{\partial \mathrm{u}}{\partial \mathrm{x}} + \mathrm{b}_2\frac{\partial \mathrm{u}}{\partial \mathrm{y}} + \mathrm{b}_3\frac{\partial \mathrm{u}}{\partial \mathrm{z}} + \mathrm{b}_4\frac{\partial \mathrm{v}}{\partial \mathrm{x}} + \mathrm{b}_5\frac{\partial \mathrm{v}}{\partial \mathrm{y}} + \mathrm{b}_6\frac{\partial \mathrm{v}}{\partial \mathrm{z}} + \mathrm{b}_7\frac{\partial \mathrm{w}}{\partial \mathrm{x}} + \mathrm{b}_8\frac{\partial \mathrm{w}}{\partial \mathrm{y}} + \mathrm{b}_9\frac{\partial \mathrm{w}}{\partial \mathrm{z}}$$

Similarly $\tau_{xz,}\tau_{yx,}\tau_{yy,}\tau_{yz,}\tau_{wx,}\tau_{wy,}\tau_{ww}$

Hence there are 81 constants.

$\tau_{ij} = \epsilon_{kl} \Rightarrow \tau_{ij} = A_{ij}\epsilon_{kl}$

A_{ij} are 81 constants

81 constants are the properties of the fluid which is difficult to get and not necessary. The following assumptions are used.

1) Using symmetry, the equations will be reduced from 9 to 6 which accordingly the number of constants will reduce accordingly to 6 X 6 = 36 constants.

$\tau_{xy} = \tau_{yx}$

2) When there is no hydrostatic motion or relative motion, then there is no viscus stress

$\bar{\bar{\sigma}} = -P\bar{\bar{\sigma}} + \bar{\bar{\tau}}$

$\bar{\bar{\tau}}\ is\ viscus\ tenssor = 0, P = presure$

3) Under pure rotation $\tau = 0$

$\epsilon_{kl} = \frac{\partial u_k}{\partial x_l} = \frac{1}{2}\left(\frac{\partial u_k}{\partial x_l} - \frac{\partial u_l}{\partial x_k}\right) + \frac{1}{2}\left(\frac{\partial u_k}{\partial x_l} + \frac{\partial u_l}{\partial x_k}\right)$

Under pure rotation $\tau = 0 = \frac{\partial u_k}{\partial x_l} - \frac{\partial u_l}{\partial x_k}$

$\Rightarrow \epsilon_{kl} = \frac{1}{2}\left(\frac{\partial u_k}{\partial x_l} + \frac{\partial u_l}{\partial x_k}\right)$

4) Linear relation between $\tau_{ij} = \epsilon$ any length can be converted to principal stress

$\tau_{\bar{x}\bar{x}}, \tau_{\bar{y}\bar{y}}, \tau_{\bar{z}\bar{z}} \neq 0$

$\tau_{\bar{x}\bar{y}} = \tau_{\bar{y}\bar{z}} = \tau_{\bar{x}\bar{z}} = 0$

$\tau_{ij} \Rightarrow \tau_{\bar{x}\bar{y}}$

$\tau_{ij}\ has\ 6\ components\ and\ \tau_{\bar{x}\bar{y}}\ three\ components$

$\tau_{11} = a_1\epsilon_{11} + a_2\epsilon_{22} + a_3\epsilon_{33}$

$\tau_{22} = b_1\epsilon_{11} + b_2\epsilon_{22} + b_3\epsilon_{33}$

$\tau_{33} = c_1\epsilon_{11} + c_2\epsilon_{22} + c_3\epsilon_{33}$

5) The fluid is isotropic. (Fluid which gives same stress strain relation in all directions.

Using isotropy substitute $\tau_{11}\ to\ \tau_{33}$ that is 11 will be changed into 33 and 33 to 11

$\tau_{11} = c_1\epsilon_{33} + c_2\epsilon_{22} + c_3\epsilon_{11}\ therfore\ c_1 = a_3,\ c_2 = a_2,\ c_3 = a_1$

substitute $\tau_{22}\ to\ \tau_{33}$

$\tau_{33} = b_1\epsilon_{33} + b_2\epsilon_{33} + b_3\epsilon_{22}\ therfore\ b_1 = c_1,\ b_2 = c_3,\quad b_3 = c_2$

substitute $\tau_{11}\ to\ \tau_{22}$

$\tau_{11} = a_1\epsilon_{22} + a_2\epsilon_{11} + a_3\epsilon_{33}\ therfore\ a_1 = b_2,\ a_2 = b_1,\ a_3 = b_3$

$\therefore\ c_1 = a_3 = b_3 = c_2 = a_2 = b_1 = \lambda_1$

$c_3 = a_1 = b_2 = c_3 = \lambda_2$

From above the nine independent constants becomes two independent constants. Hence it can be expressed as follows.

$\tau_{11} = \lambda_1\epsilon_{11} + \lambda_2(\epsilon_{11} + \epsilon_{22} + \epsilon_{33})$

$\tau_{22} = \lambda_1\epsilon_{22} + \lambda_2(\epsilon_{11} + \epsilon_{22} + \epsilon_{33})$

$\tau_{33} = \lambda_1\epsilon_{33} + \lambda_2(\epsilon_{11} + \epsilon_{22} + \epsilon_{33})$

The above three equations obey the condition of isotropy and invariant to coordinate transformations as well as symmetry [80].

$\tau_{ij} = \mu\left(\frac{\partial u}{\partial x_i} + \frac{\partial u}{\partial x_i}\right) + \lambda\left(\frac{\partial u_k}{\partial x_k}\right)\delta_{ij}$

$\tau_{xx} = \mu\left(\frac{\partial u}{\partial x} + \frac{\partial u}{\partial x}\right) + \lambda\left(\frac{\partial u}{\partial x} + \frac{\partial v}{\partial y} + \frac{\partial w}{\partial z}\right)$

$$\tau_{yx} = \mu\left(\frac{\partial v}{\partial x} + \frac{\partial u}{\partial x}\right) + \lambda\left(\frac{\partial u}{\partial x} + \frac{\partial v}{\partial y} + \frac{\partial w}{\partial z}\right)\delta_{yx}$$

Since $x \neq y = 0$

$$\tau_{yx} = \mu\left(\frac{\partial v}{\partial x} + \frac{\partial u}{\partial x}\right)$$

x-momentum balance

$$\frac{\partial(\rho u)}{\partial t} + \frac{\partial(\rho u^2)}{\partial x} + \frac{\partial(\rho v u)}{\partial y} + \frac{\partial(\rho w u)}{\partial z} = \frac{\partial(\sigma_{xx})}{\partial x} + \frac{\partial(\sigma_{yx})}{\partial y} + \frac{\partial(\sigma_{zx})}{\partial z} + \rho g_x \; - - -$$ (x-momentum)

$$\sigma_{ij} = -P\sigma_{ij} + \tau_{ij}$$

$$\tau_{ij} = \mu\left(\frac{\partial u_i}{\partial x_j} + \frac{\partial u_j}{\partial x_i}\right) + \lambda\left(\frac{\partial u_k}{\partial x_k}\right)\delta_{ij}$$

x-momentum balance

μ = dynamic viscosity

λ = second coefficient of viscosity

$$\delta_{ij} = 1, if\ i = j\ else\ 0\ if\ i \neq j$$

x-momentum

$$\frac{\partial(\rho u)}{\partial t} + \frac{\partial(\rho u^2)}{\partial x} + \frac{\partial(\rho v u)}{\partial y} + \frac{\partial(\rho w u)}{\partial z}$$

$$= \rho g_x - \frac{\partial p}{\partial x} + \frac{\partial}{\partial x}\left[2\mu\frac{\partial u}{\partial x} + \lambda\left(\frac{\partial u}{\partial x} + \frac{\partial v}{\partial y} + \frac{\partial w}{\partial z}\right)\right] + \frac{\partial}{\partial y}\left[\mu\left(\frac{\partial u}{\partial y} + \frac{\partial v}{\partial x}\right)\right]$$

$$+ \frac{\partial}{\partial z}\left[\mu\left(\frac{\partial w}{\partial x} + \frac{\partial u}{\partial z}\right)\right]$$

y-momentum

$$\frac{\partial(\rho v)}{\partial t}+\frac{\partial(\rho uv)}{\partial x}+\frac{\partial(v^2)}{\partial y}+\frac{\partial(\rho vw)}{\partial z}$$
$$=\rho g_y+\frac{\partial}{\partial x}\left[\mu\left(\frac{\partial u}{\partial y}+\frac{\partial v}{\partial x}\right)\right]-\frac{\partial p}{\partial y}+\frac{\partial}{\partial y}\left[2\mu\frac{\partial v}{\partial y}+\lambda\left(\frac{\partial u}{\partial x}+\frac{\partial v}{\partial y}+\frac{\partial w}{\partial z}\right)\right]$$
$$+\frac{\partial}{\partial z}\left[\mu\left(\frac{\partial w}{\partial y}+\frac{\partial v}{\partial z}\right)\right]$$

z-momentum

$$\frac{\partial(\rho w)}{\partial t}+\frac{\partial(\rho uw)}{\partial x}+\frac{\partial(vw)}{\partial y}+\frac{\partial(\rho w^2)}{\partial z}$$
$$=\rho g_z+\frac{\partial}{\partial x}\left[\mu\left(\frac{\partial u}{\partial z}+\frac{\partial w}{\partial x}\right)\right]+\frac{\partial}{\partial z}\left[\mu\left(\frac{\partial w}{\partial y}+\frac{\partial v}{\partial z}\right)\right]-\frac{\partial p}{\partial z}$$
$$+\frac{\partial}{\partial z}\left[2\mu\frac{\partial w}{\partial z}+\lambda\left(\frac{\partial u}{\partial x}+\frac{\partial v}{\partial y}+\frac{\partial w}{\partial z}\right)\right]$$

Total variables are 4 and total equations are 4.

Variables = u, v, w, p

Properties ρ, μ and λ

Four equations and four variables. These equations are called Navior-Stocks Equation.

The above equations are basically developed based on the following conditions.

1) An isotropic fluid
2) Linear relation between viscous stress and deformation rate

Such types of fluids are called Newtonian fluid.

For incompressible flow, density is constant. Hence the Navior-Stocks Equation is reduced as follows.

Continuity equation:

$$\frac{\partial u}{\partial x} + \frac{\partial v}{\partial y} + \frac{\partial w}{\partial z} = 0 \qquad ---(2-13)$$

X-momentum

$$\frac{\partial(u)}{\partial t} + \frac{\partial(u^2)}{\partial x} + \frac{\partial(vu)}{\partial y} + \frac{\partial(wu)}{\partial z} = g_x - \frac{1}{\rho}\frac{\partial p}{\partial x} + \nu\left(\frac{\partial^2 u}{\partial x^2} + \frac{\partial^2 u}{\partial y^2} + \frac{\partial^2 u}{\partial z^2}\right) ---(2-14\text{A})$$

Y-momentum

$$\frac{\partial(v)}{\partial t} + \frac{\partial(vu)}{\partial x} + \frac{\partial(v^2)}{\partial y} + \frac{\partial(wv)}{\partial z} = g_x - \frac{1}{\rho}\frac{\partial p}{\partial y} + \nu\left(\frac{\partial^2 v}{\partial x^2} + \frac{\partial^2 v}{\partial y^2} + \frac{\partial^2 v}{\partial z^2}\right) ---(2-14\text{B})$$

Z-momentum

$$\frac{\partial(w)}{\partial t} + \frac{\partial(wu)}{\partial x} + \frac{\partial(wv)}{\partial y} + \frac{\partial(w^2)}{\partial z} = g_x - \frac{1}{\rho}\frac{\partial p}{\partial z} + \nu\left(\frac{\partial^2 w}{\partial x^2} + \frac{\partial^2 w}{\partial y^2} + \frac{\partial^2 w}{\partial z^2}\right) ---(2-14\text{C})$$

1.5.2 Discretization Approach

After selecting the mathematical model, one has to choose a suitable discretization method, i:e a method of approximating the differential equations by a system of algebraic equations for the variables at some set of discrete locations in space and time. There are many approaches, but the most important of which are: finite difference, finite volume and finite element methods. Other methods, like spectral schemes, boundary element methods, and cellular automata are used in CFD but their use is limited to special classes of problems [48]. Finite difference and finite volume are explained in this study.

Solving the Navir-Stokes equations numerically relies on their spatial discretization (and temporal for non-stationary cases). The volume around the geometry is divided into smaller sub-volumes on each of which the discretized governing equations are computed. Discretization is achieved by one of the three methods that are finite element (partial differential equations are approximated by ordinary differential equations and then integrated with Runge-Kutta or Euler methods), finite differences (derivatives are approximated by difference quotients) and finite volume (based on integral form of conservation laws over small control volumes) [81].

To perform numerical modelling for open-channel flows as well as in other areas of fluid mechanics, the basic process includes pre-processing, computation, and post-processing. At the pre-processing stage, the majority of the work is to prepare the data in the format required by the specific numerical code. In the case of three-dimensional modelling, the pre-processing stage can be a major portion of the whole process. One of the difficulties during this stage is to generate a reasonable mesh that represents the domain of interest and has a good quality. Most of the commercial codes have their own pre-processing and mesh generation tools. One general suggestion is to make a mesh with good quality and at affordable resolution.

1.5.3 Finite Difference Method

Analytical solutions of partial differential equations involve closed form expressions which give the variation of the dependent variables continuously throughout the domain. In contrast, numerical solutions can give answers at only discrete points in the domain, called grid points. So this is what discretization means. All methods in CFD utilize some form of discretization.

The starting point is the conservation equation in differential form. The solution domain is covered by a grid. At each grid point, the differential equation is approximated by replacing

the partial derivatives by approximations in terms of the nodal values of the functions. The result is one algebraic equation per grid node, in which the variable value at that and a certain number of neighbour nodes appear as unknowns.

Taylor series expansion or polynomial fitting is used to obtain approximations to the first and second derivatives of the variables with respect to the coordinates. When necessary, these methods are also used to obtain variable values at locations other than grid nodes (interpolation).

On structured grids, the FD method is very simple and effective. It is especially easy to obtain higher- order schemes on regular grids. The disadvantage of FD methods is that the conservation is not enforced unless special care is taken. Also, the restriction to simple geometries is a significant disadvantage in complex flows. The following shows sample of 2D grid.

The terms that were deleted from the right-hand sides are called the truncation errors; they measure the accuracy of the approximation and determine the rate at which the error decreases as the spacing between points is reduced [82]. In particular, the first truncated term is usually the principal source of error.

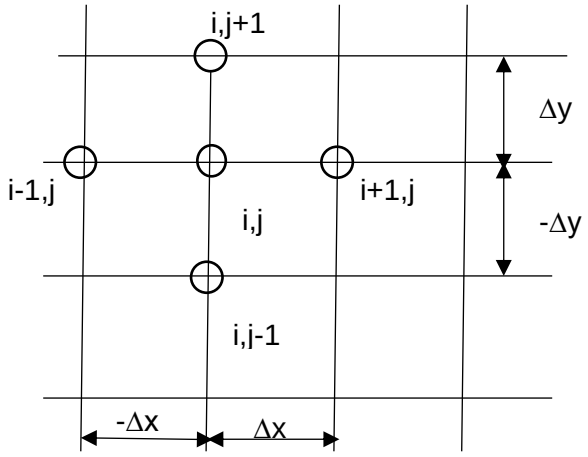

Figure shows 2D Sample grid

From Tailor Series Expansion [83]

Forward Difference Scheme

$$u_{i+1,j} = u_{i,j} + \Delta x\left(\frac{\partial u}{\partial x}\right)_{i,j} + \frac{\Delta x^2}{2!}\left(\frac{\partial^2 u}{\partial x^2}\right)_{i,j} + \frac{\Delta x^3}{3!}\left(\frac{\partial^3 u}{\partial x^3}\right)_{i,j} + \frac{\Delta x^4}{4!}\left(\frac{\partial^4 u}{\partial x^4}\right)_{i,j} \ldots + \frac{\Delta x^n}{n!}\left(\frac{\partial^n u}{\partial x^n}\right)_{i,j} - - - - -$$

$$- (2-15)$$

$$u_{i+1,j} - u_{i,j} = \Delta x\left[\left(\frac{\partial u}{\partial x}\right)_{i,j} + \frac{\Delta x}{2!}\left(\frac{\partial^2 u}{\partial x^2}\right)_{i,j} + \frac{\Delta x^2}{3!}\left(\frac{\partial^3 u}{\partial x^3}\right)_{i,j} + \frac{\Delta x^3}{4!}\left(\frac{\partial^4 u}{\partial x^4}\right)_{i,j} \ldots + \frac{\Delta x^{n-1}}{n!}\left(\frac{\partial^n u}{\partial x^n}\right)_{i,j}\right]$$

$$\frac{u_{i+1,j} - u_{i,j}}{\Delta x} = \left(\frac{\partial u}{\partial x}\right)_{i,j} + \frac{\Delta x}{2!}\left(\frac{\partial^2 u}{\partial x^2}\right)_{i,j} + \frac{\Delta x^2}{3!}\left(\frac{\partial^3 u}{\partial x^3}\right)_{i,j} + \frac{\Delta x^3}{4!}\left(\frac{\partial^4 u}{\partial x^4}\right)_{i,j} \ldots + \frac{\Delta x^{n-1}}{n!}\left(\frac{\partial^n u}{\partial x^n}\right)_{i,j}$$

$$\left(\frac{\partial u}{\partial x}\right)_{i,j} = \frac{u_{i+1,j} - u_{i,j}}{\Delta x} - \underbrace{\left[\frac{\Delta x}{2!}\left(\frac{\partial^2 u}{\partial x^2}\right)_{i,j} + \frac{\Delta x^2}{3!}\left(\frac{\partial^3 u}{\partial x^3}\right)_{i,j} + \frac{\Delta x^3}{4!}\left(\frac{\partial^4 u}{\partial x^4}\right)_{i,j} \ldots + \frac{\Delta x^{n-1}}{n!}\left(\frac{\partial^n u}{\partial x^n}\right)_{i,j}\right]}$$

Truncation Error

$$\boxed{\left(\frac{\partial u}{\partial x}\right)_{i,j} = \frac{u_{i+1,j} - u_{i,j}}{\Delta x} + O(\Delta x)} \quad - - - - \text{ Forward Difference (FD)}$$

Similarly, FD with respect to y

$$\boxed{\left(\frac{\partial v}{\partial y}\right)_{i,j} = \frac{v_{i,j+1}-v_{i,j}}{\Delta y} + O(\Delta y)} \quad --- \quad \text{Forward Difference (FD)}$$

Backward Difference Scheme

$$u_{i-1,j} = u_{i,j} - \Delta x\left(\frac{\partial u}{\partial x}\right)_{i,j} + \frac{\Delta x^2}{2!}\left(\frac{\partial^2 u}{\partial x^2}\right)_{i,j} - \frac{\Delta x^3}{3!}\left(\frac{\partial^3 u}{\partial x^3}\right)_{i,j} + \frac{\Delta x^4}{4!}\left(\frac{\partial^4 u}{\partial x^4}\right)_{i,j} \ldots + \frac{\Delta x^n}{n!}\left(\frac{\partial^n u}{\partial x^n}\right)_{i,j} \quad ---$$

$---------$ (2-16)

$$u_{i-1,j} - u_{i,j} = -\Delta x\left[\left(\frac{\partial u}{\partial x}\right)_{i,j} - \frac{\Delta x}{2!}\left(\frac{\partial^2 u}{\partial x^2}\right)_{i,j} + \frac{\Delta x^2}{3!}\left(\frac{\partial^3 u}{\partial x^3}\right)_{i,j} - \frac{\Delta x^3}{4!}\left(\frac{\partial^4 u}{\partial x^4}\right)_{i,j} \ldots + \frac{\Delta x^{n-1}}{n!}\left(\frac{\partial^n u}{\partial x^n}\right)_{i,j}\right]$$

$$\frac{u_{i,j} - u_{i-1,j}}{\Delta x} = \left(\frac{\partial u}{\partial x}\right)_{i,j} - \frac{\Delta x}{2!}\left(\frac{\partial^2 u}{\partial x^2}\right)_{i,j} + \frac{\Delta x^2}{3!}\left(\frac{\partial^3 u}{\partial x^3}\right)_{i,j} - \frac{\Delta x^3}{4!}\left(\frac{\partial^4 u}{\partial x^4}\right)_{i,j} \ldots + \frac{\Delta x^{n-1}}{n!}\left(\frac{\partial^n u}{\partial x^n}\right)_{i,j}$$

$$\boxed{\left(\frac{\partial u}{\partial x}\right)_{i,j} = \frac{u_{i,j}-u_{i-1,j}}{\Delta x} + O(\Delta x)} \quad --- \quad \text{Backward Difference}$$

Note that $O(\Delta x)$ $is\ first\ order\ of\ accuracy$

Similarly, FD with respect to y

$$\boxed{\left(\frac{\partial v}{\partial y}\right)_{i,j} = \frac{v_{i,j}-v_{i,j-1}}{\Delta y} + O(\Delta y)} \quad --- \quad \text{Backward Difference (BD)}$$

To get first order derivative for central difference Eq (2-15) – Eq (2-16):

$$u_{i+1,j} - u_{i-1,j} = 2\Delta x\left(\frac{\partial u}{\partial x}\right)_{i,j} + 2\frac{\Delta x^3}{3!}\left(\frac{\partial^3 u}{\partial x^3}\right)_{i,j} + 2\frac{\Delta x^5}{5!}\left(\frac{\partial^5 u}{\partial x^5}\right)_{i,j} + \cdots$$

$$u_{i+1,j} - u_{i-1,j} = 2\Delta x\left[\left(\frac{\partial u}{\partial x}\right)_{i,j} + 2\frac{\Delta x^2}{3!}\left(\frac{\partial^3 u}{\partial x^3}\right)_{i,j} + 2\frac{\Delta x^4}{5!}\left(\frac{\partial^5 u}{\partial x^5}\right)_{i,j} + \cdots\right]$$

$$\boxed{\left(\frac{\partial u}{\partial x}\right)_{i,j} = \frac{u_{i+1,j}-u_{i-1,j}}{2\Delta x} + O(\Delta x)^2} \quad --- \quad \text{Central Difference}$$

Note that $O(\Delta x)^2$ $is\ second\ order\ of\ accuracy$

Similarly, FD with respect to y

$$\boxed{\left(\frac{\partial u}{\partial y}\right)_{i,j} = \frac{u_{i,j+1}-u_{i,j-1}}{2\Delta y} + O(\Delta y)^2} \quad ---$$ Central Difference

To get second order derivative for central difference Eq(2-15) + Eq (2-16) :

$$u_{i+1,j} + u_{i-1,j} = 2u_{i,j} + 2\frac{\Delta x^2}{2!}\left(\frac{\partial^2 u}{\partial x^2}\right)_{i,j} + 2\frac{\Delta x^4}{4!}\left(\frac{\partial^4 u}{\partial x^4}\right)_{i,j} \ldots + \frac{\Delta x^n}{n!}\left(\frac{\partial^n u}{\partial x^n}\right)_{i,j}$$

$$\frac{u_{i+1,j} + u_{i-1,j} - 2u_{i,j}}{\Delta x^2} = \left(\frac{\partial^2 u}{\partial x^2}\right)_{i,j} + \frac{\Delta x^2}{2!}\left(\frac{\partial^4 u}{\partial x^4}\right)_{i,j} \ldots + \frac{\Delta x^n}{n!}\left(\frac{\partial^n u}{\partial x^n}\right)_{i,j}$$

$$\boxed{\left(\frac{\partial^2 u}{\partial x^2}\right)_{i,j} = \frac{u_{i+1,j}+u_{i-1,j}-2u_{i,j}}{\Delta x^2} + O(\Delta x)^2} \quad --$$ Central Difference for Second Order PDE

1.5.4 Finite Volume Method

Converting the conservation equation by differential form into algebraic equation is FDM and converting the integral form equations into algebraic equation is FVM. The FV methods uses the integral form of the conservation equations as its starting point. The solution domain is subdivided into a finite number of continuous Control Volumes (CVs), and the conservation equations are applied to each CV. At the centroid of each CV lies a computational node at which the variable values are to be calculated. Interpolation is used to express variable values at the CV surface in terms of the nodal (CV- centre) values. Surface and volume integrals are approximated using suitable quadrature formulae. As a result, one obtains an algebraic equation for each CV, in which a number of neighbour nodal values appear [48].

The FV method can accommodate any type of grid, so it is suitable for complex geometries. The grid defines only the control volume boundaries and need not be related to a coordinate system. The method is conservative by construction, so long as surface integrals (which

represent convective and diffusive fluxes) are the same for the CV's sharing the boundary [48].

The FV approach is perhaps the simplest to understand and to program. All terms that need be approximated have physical meaning which is why it is popular with engineers [48].

The disadvantage of FV methods compared to FD schemes is that methods of order higher than second are more difficult to develop in 3D. This is due to the fact that the FV approach requires three levels of approximation: interpolation, differentiation, and integration [48], [84].

The solution domain is subdivided into a finite number of small control volumes (CVs) by a grid which, in contrast to the finite difference (FD) method, defines the control volume boundaries, not the computational nodes [48].

Finite Volume schemes can be applied to irregular flow domains and at the same time they are as easy to implement as finite difference schemes. The main advantages of this scheme are its simplicity and of implementation. It can also handle sharp gradients in the water surface profile if they are present. A finite volume scheme which is an explicit scheme and is second order accurate in space and time, is presented below. It is a two-step predictor-corrector scheme. The finite volume grid need not be orthogonal as in the case of a finite difference grid [48].

The volume in integrals of predicted variables (Ø) are calculated on small volume cells with volume V by calculating the quantities entering and leaving the cell.

$$\boxed{\frac{\partial}{\partial t}(V\emptyset) = \sum_{i=1}^{N} f_i} \quad ------ \quad ---(2-17)$$

Where fi the flux of Ø through edge i. The finite volume can also be derived by discretizing the flux form of the advection equation. Constant density flow is divergence free($\nabla . u = 0$) and so two forms of the linear advection equation are equivalent

$$\frac{\partial \emptyset}{\partial t} + u.\nabla\emptyset = 0 \; ------advective\; form$$

$$\frac{\partial \emptyset}{\partial t} + \nabla.(\mathrm{u}\emptyset) = 0 \; ------flux\; form$$

The flux or conservative form can be discretised using Gauss's divergence theorem

$$\nabla.\mathrm{u}\emptyset = \frac{1}{V}\int_v \nabla.u\emptyset dv = \frac{1}{V}\int_s \emptyset u.ds = \frac{1}{V}\sum_i f_i \; ------(2-18)$$

Where volume V has surface S, ds is the outward pointing normal to surface S and $f_i = \emptyset u.ds$ is the flux over edge i.

In typical Figure shown below the 2D Cartesian control volumes are shown together with the notation that can be used. The CV surface consists of four (in 2D) or six (in 3D) plane faces, denoted by lower-case letters corresponding to their direction (e, w, n, s, t, and b) with respect to the central node (P). The 2D case can be regarded as a special case of the 3D one in which the dependent variables are independent of z.

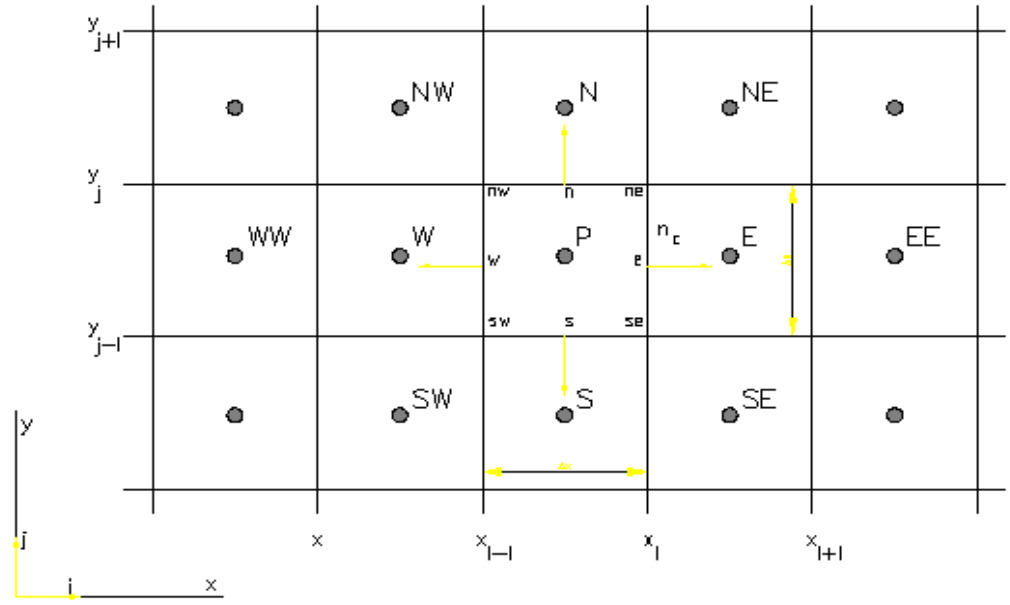

Figure A Typical CV and Notation used for a Cartesian 2D Grid

1.6 NUMERICAL SOLUTION SCHEMES

1.6.1 Implicit vs. Explicit Numerical Methods

Numerical solution schemes are often referred to as being explicit or implicit. Explicit finite difference methods advance the solution to the end of the time step at a single grid node, using an explicit function of the dependent variables already determined for several grid nodes at the beginning of the time step. Implicit methods, on the other hand, approximate the derivatives using values of dependent variables both at the beginning of the time step, where they are known, and at the end of the time step for more than one grid node, where the dependent variables are unknown. In the latter case, a system of simultaneous equations must be solved to advance the solution by onetime step.

By definition, in an explicit approach each different equation contains only one unknown and therefore can be solved explicitly for this unknown in a straightforward manner. When we chose to represent $\frac{\partial u}{\partial x}$ with a forward difference and $\frac{\partial^2 u}{\partial x^2}$ with a central second difference, leading to the particular form of the difference equation given by Eq (2-19) below:

$$\frac{T_i^{k+1} - T_i^k}{\Delta t} = \frac{\alpha\left(T_{i+1}^k - 2T_i^k + T_{i-1}^k\right)}{(\Delta x)^2} \qquad -------(2-19)$$

With some rearrangement, this equation can be written as in straightforward manner.

$$T_i^{k+1} = T_i^k + \alpha\frac{\Delta t}{(\Delta x)^2}\left(T_{i+1}^k - 2T_i^k + T_{i-1}^k\right) ------(2-20)$$

By definition, an implicit approach is one where the unknowns must be obtained by means of a simultaneous solution of the difference equations applied at all the grid points arrayed at a given time level. Because of this need to solve large systems of simultaneous algebraic equations, implicit methods are usually involved with the manipulations of large matrices.

1.6.2 Properties of Numerical Solution Methods

Accuracy

Numerical solutions of fluid flow and heat transfer problems are only approximate solutions.

In addition to the errors that might be introduced in the course of the development of the solution algorithm [83], [85], in programming or setting up the boundary conditions, numerical solutions always include three kinds of systematic errors:

- Modelling errors, which are defined as the difference between the actual flow and the exact solution of the mathematical model;
- Discretization errors define as the difference between the exact solution of the conservation equations and the exact solution of the algebraic system of equations obtained by discretizing these equations, and
- Iteration errors, defined as the difference between the iterative and exact solutions of the algebraic equations systems.

Consistency

The discretization should become exact as the grid spacing tends to zero. The difference between the discretized equation and the exact one is called the truncation error. It is usually estimated by replacing all the nodal values in the discrete approximation by a Taylor series expansion about a single point. As a result, one recovers the original differential equation plus a remainder, which represents the truncation error. For a method to be consistent, the truncation error must become zero when the mesh spacing $\Delta t \rightarrow 0$ and/ or $\Delta xi \rightarrow 0$. Truncation error is usually proportional to a power of the grid spacing Δxi and/ or the time step Δt. If the most important term is proportional to $(\Delta x)k$ or $(\Delta t)k$ we call the method an n^{th}-order approximation; $n>0$ is required for consistency. Ideally, all terms should be discretized with approximations of the same order of accuracy; however, some terms (e,g convective terms in high Reynolds number flows or diffusive terms in low Reynolds number flows) may be

dominate in a particular flow and it may be reasonable to treat them with more accuracy than the others.

Some discretization methods lead to truncation errors which are functions of the ratio of Δxi to Δt or vice versa. In such a case the consistency requirement is only conditionally fulfilled: Δxi and Δt must be reduced in a way that allows the appropriate ratio to go to zero.

Even if the approximations are consistent, it does not necessarily mean that the solution of the discretized equation system will become the exact solution of the differential equation in the limit of small step size. For this to happen, the solution method has to be stable; this is defined below.

Stability

A numerical solution method is said to be stable if it does not magnify the errors that appear in the course of numerical solution process. For temporal problems, stability guarantees that the method produces a bounded solution whenever the solution of the exact equation is bounded. For iterative methods, a stable method is one that does not diverge. Stability can be difficult to investigate, especially when boundary conditions and non- linarites are present. For this reason, it is common to investigate the stability of a method for linear problems with constant coefficients without boundary conditions. Experience shows that the results obtained in this way can often be applied to more complex problems but there are notable exceptions.

When solving complicated, non- linear and coupled equations with complicated boundary conditions, there are few stability results so we may have to rely on experience and intuition. Many solution schemes require that the time step be smaller than a certain limit or that under-relaxation be used. A larger time step will lead to numerical instabilities and nonphysical results. Hence, smaller time steep has to be taken.

Convergence

A numerical method is said to be convergent if the solution of the discretized equations tends to the exact solution of the differential equation as the grid spacing tends to zero. For linear initial value problems that satisfies the consistency condition, stability is the necessary and sufficient condition for convergence.

For non- linear problems which are strongly influenced by boundary conditions, the stability and convergence of a method are difficult to demonstrate. Therefore, convergence is usually checked using numerical experiments, i.e. repeating the calculation on a series of successively refined grids. If the method is stable and if all approximations used in the discretization process are consistent, we usually find that the solution does converge to a grid-independent solution. For sufficiently small grid sizes, the rate of convergence is governed by the order of principal truncation error component. This allows us to estimate the error in the solution.

FLOW-3D uses the self-corrective procedure as well as an automatic setting of the convergence criteria that adjusts to whatever is happening during the course of a solution. Generalized Minimum Residual (GMRES) method is strongly preferred due to its rapid convergence and parallel efficiency.

1.7 TURBULENCE MODELLING

1.7.1 General

Turbulent flow in which the fluid undergoes irregular fluctuations, or mixing, in contrast to laminar flow, in which the fluid moves in smooth paths or layers. In turbulent flow the speed of the fluid at a point is continuously undergoing changes in both magnitude and direction [13], [14]. In a laminar flow, transport of momentum mostly occurs through viscosity (diffusion),

while in a turbulent flow, transport can occur through the random motion embodied by the fluctuating terms.

The origin of turbulence rests in small perturbations imposed on the flow; for instance, by wall roughness, by small variations in fluid density, by mechanical vibrations, etc. At low Re numbers such disturbances are damped out by the fluid viscosity and the flow remains laminar, but at high Re (when convective momentum transport dominates over viscous forces) they can grow and propagate, giving rise to the chaotic phenomena perceived as turbulence.

Turbulence or turbulent flow is a flow regime in fluid dynamics characterized by chaotic changes in pressure and flow velocity in contrast to a laminar flow regime, which occurs when a fluid flows in parallel layers, with no disruption between those layers.

There is no definition on turbulent flow, but it has several characteristic features such as:

- Fluctuating is very rapid
- Well contained fluctuations this mans the fluctuation do needs care. Chaotic behaviour of the flow properties. By Chaotic means immediately tells it is unpredictable. But the overall flow is well contained.
- Turbulent flows are never steady, never 1D or 2D flow property. It is always 3D
- It is highly diffusive eddies are present Extra diffusivity is a strong function such as Reynold number or friction factor. Reynolds numbers are very high. For example, the transition to turbulent flow in pipes occurs that ReD ≃ 2300, and in boundary layers at Rex ≃ 500 000.

1.7.2 Statistical Averaging of the Differential Equations of Fluid Mechanics

The differential equations of mass, momentum and energy balance express fundamental physical laws and therefore hold for turbulent flow just as they do for laminar flow. If all the

perturbations acting on the flow can be also mathematically modelled, then these equations could be solved for the flow properties (velocity, pressure, etc.) of interest. However, this is generally too difficult problem. An easier task is to solve "time-averaged" versions of these equations in which some of the fluctuation contributions are averaged out. As we shall see the solution to such equations provides less detailed, but still very useful, information [80]. Figure below shows detail information shows sample of Reynold Time Average is the most widely equation used for turbulent flow. In turbulent flow, we usually divide the velocities in one time-averaged part $\bar{v}_(i)$, which is independent of time (when the mean flow is steady), and one fluctuating part $v^{\prime}$ so that $v_(i) = \bar{v}_(i) + v^{\prime}$.

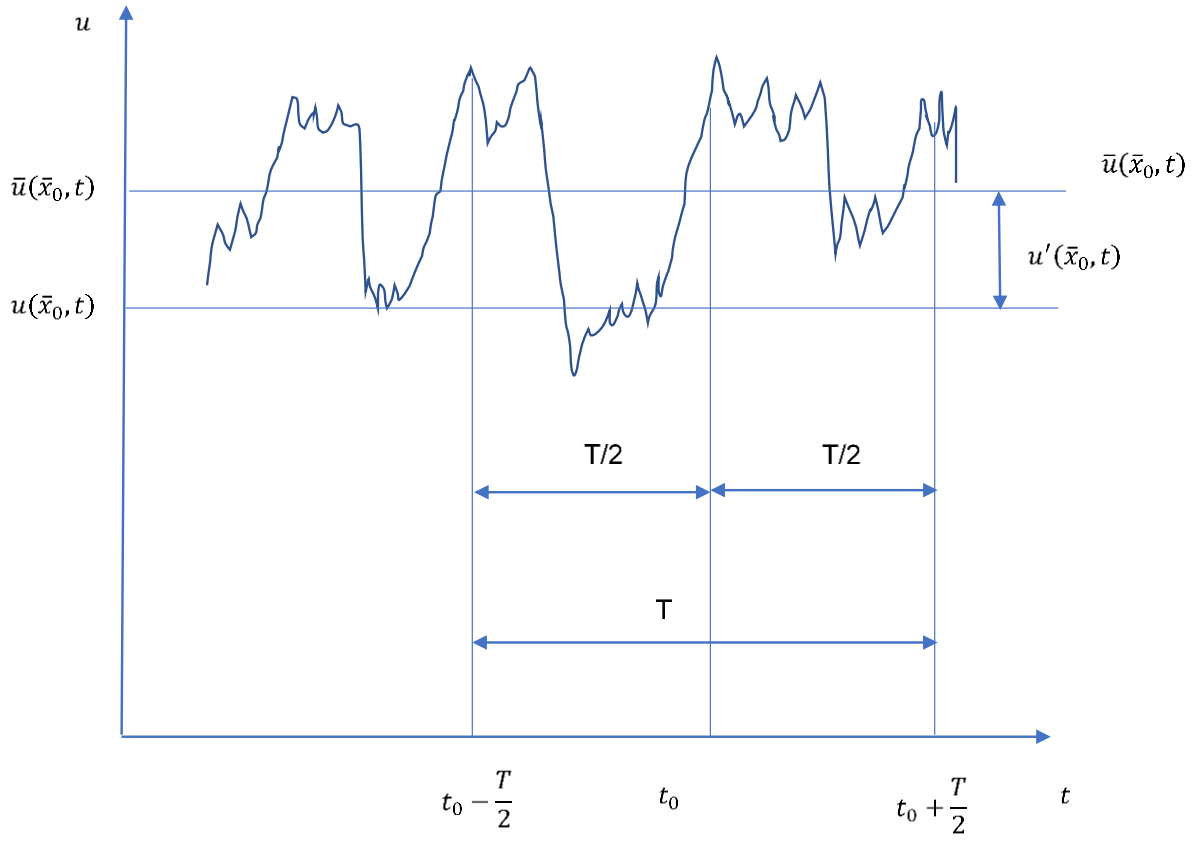

Figure Graphical depiction of components of Reynolds decomposition

T is the average time period. It is sufficiently large enough to smoothen out the turbulence fluctuations and not so large not suppress inheritance time dependent of the system itself [80].

u^- is, the time average velocity.

$$\bar{u}(\bar{x}_0,t) = \frac{1}{T}\int_{t_0-\frac{T}{2}}^{t_0+\frac{T}{2}} u dt \quad -----(2-21)$$

$$\bar{u}(\bar{x}_0,t) = \bar{u}(\bar{x}_0,t) + u'(\bar{x}_0,t)$$

$u^{\wedge\prime}$ is fluctuation component. It is ± in graphical depiction of components of Reynolds number.

Figure Graphical depiction of components of Reynolds decomposition

.

$u = \bar{u} + u^{\wedge\prime}$

$v = \bar{v} + v^{\wedge\prime}$

$w = \bar{w} + w^{\wedge\prime}$

$p = \bar{p} + p'$

$$\frac{\partial \bar{u}_k}{\partial x_k} = 0$$

$$\frac{\partial \bar{u}_i}{\partial t} + \frac{\partial(\bar{u}_i\,\bar{u}_j)}{\partial x_j} = -\frac{1}{\rho}\frac{\partial \bar{p}}{\partial x_i} + \nu\nabla^2\bar{u}_i - \frac{\partial(\overline{u'_\iota\, u'_\jmath})}{\partial x_j}$$

It is useful to begin by recalling the nature of velocity profiles of turbulent flow in duct. This is depicted in Figure below shows typical velocity distributions in turbulent flow near wall.

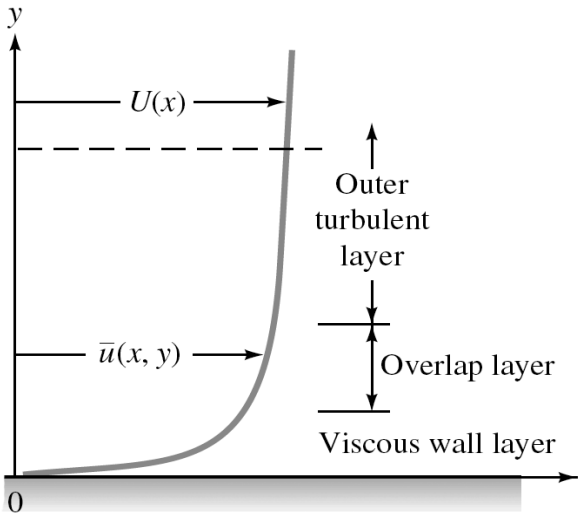

Figure Typical velocity distributions in turbulent flow near wall

1.7.3 Turbulence Models in FLOW-3D

In FLOW-3D, there are six turbulence models available:

1. the Prandtl mixing length model

2. the one-equation

3. the two- equation $k-\varepsilon$

4. the two- equation $k-\omega$ models

5. RNG

6. Large eddy simulation, LES, model

FLOW-3D formulation differs slightly from other formulations in that it includes the influence of the fractional areas/volumes of the FAVOR method and have generalized the turbulence production (or decay) associated with buoyancy forces. The latter generalization, for example, includes buoyancy effects associated with non-inertial accelerations.

i) The Prandtl mixing length model

Eddies in turbulent flow around similar to the manner in which molecules move about in a gas. By drawing an analogy to viscosity expressions for gases from kinetic theory, it is suggested that:

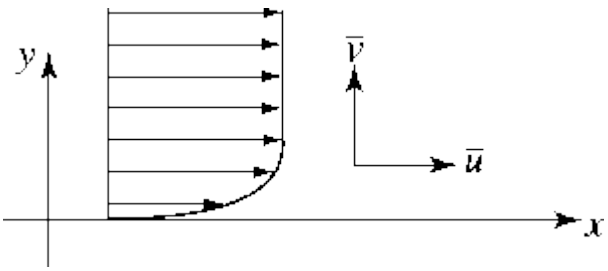

Figure Two-dimensional boundary flow

For 2D channel flows, there is only one significant tangential stress component, namely, $\tau = (u^{\prime} v^{\prime})^{-}$ and velocity gradient $\partial u/\partial y$. Prandtl postulated that the velocity scale v_t of the fluctuation motion is equal to the velocity gradient times a length scale L_m which is called the mixing length, namely,

$$V_t = \left|\frac{\partial \bar{u}}{\partial \bar{y}}\right|$$

The eddy viscosity is given by

$$\mu_t = \rho L_m^2 \left|\frac{\partial \bar{u}}{\partial y}\right| \quad ----------(2-22)$$

where the mixing length L_m is prescribed algebraically, and according to the eddy viscosity model equation gives

$$\tau = \mu_t \frac{\partial \bar{u}}{\partial y} \quad ----------(2-23)$$

From equations (2-22) and (2-23) we obtain

$$\tau = \rho L_m^2 \left|\frac{\partial \bar{u}}{\partial y}\right| \frac{\partial \bar{u}}{\partial y} \quad ----------(2-24)$$

ii) One Equation Models

In one equation models a transport equation is often solved for the turbulent kinetic energy. The unknown turbulent length scale must be given, and often an algebraic expression is used. This length scale is, for example, taken as proportional to the thickness of the boundary layer, the width of a jet or a wake [86].

A one-equation model can be used to model the SubGrid Scale (SGS) turbulent kinetic energy. The equation can be written on the same form as the RANS k-equation [86], i.e.

$$\frac{\partial k_{sgs}}{\partial t} + \frac{\partial}{\partial x_j}\left(\bar{v}_j k_{sgs}\right) = \frac{\partial}{\partial x_j}\left[\left(v + v_{sgs}\right)\frac{\partial k_{sgs}}{\partial x_j}\right] + P_{ksgs} - \in \quad -------(2-25)$$

$$v_{sgs} = c_k \Delta k_{sgs}^{\frac{1}{2}}, \quad P_{ksgs} = 2v_{sgs}\bar{s}_{ij}\bar{s}_{ij}, \quad \in = C_\epsilon \frac{k_{sgs}^{\frac{3}{2}}}{\Delta}$$

Note that the production term, P_ksgs, is equivalent to the SGS dissipation in the equation for the resolved turbulent kinetic energy.

Where,

c_k = where the Kolmogorov constant CK= ≃ 1.5. This is a very important law (Kolmogorov spectrum law or the - 5/3 law) which states that, if the flow is fully turbulent (high Reynolds number), the energy spectra should exhibit a -5/3 decay in the inertial region

k_sgs = The SGE kinetic energy (m^2/s^2) = $k_{sgs} = \frac{3}{2} C_k \left(\frac{\Delta \in}{\pi}\right)^{2/3}$

SGS Sub-Grid Scale

Δ Difference

∈ = dissipation (m^2/s^3)

v = viscosity

s_ij Symmetric tensor called strain-rate tensor

iii) The two- equation $k-\in$

Standard k– ∈ (SK∈) model [86]

- The most widely-used engineering turbulence model for industrial applications
- Robust and reasonably accurate
- Contains sub models for compressibility, buoyancy, combustion, etc.

Limitations

- The ∈ equation contains a term which cannot be calculated at the wall. Therefore, wall functions must be used.

- Generally, performs poorly for flows with strong separation, large stream line
- curvature, and large pressure gradient.
- In the $k-\in$ model the modelled transport equations for k and $\in$ are solved. The turbulent length scale is obtained from

$$l = \frac{k^{3/2}}{\in} \quad ----------(2-26)$$

The turbulent viscosity is computed from:

$$v_t = c_u k^{1/2} l = c_u \frac{k^2}{\in} \quad ----------(2-27)$$

$$\frac{\partial k}{\partial t} + \bar{v}_j \frac{\partial k}{\partial x_j} = v_t \left(\frac{\partial \bar{v}_i}{\partial x_j} + \frac{\partial \bar{v}_j}{\partial x_j}\right)\frac{\partial \bar{v}_i}{\partial x_j} + g_i \beta \frac{v_t}{\sigma_\theta}\frac{\partial \bar{\theta}}{\partial x_i} - \in + \frac{\partial}{\partial x_j}\left[\left(\nu + \frac{v_t}{\sigma_k}\right)\frac{\partial k}{\partial x_j}\right] ---(2-28)$$

In the same way, the modelled $\in$ equation is obtained from Eq. (D)

$$\frac{\partial \in}{\partial t} + \overline{\upsilon}_j \frac{\partial \in}{\partial x_j} = \frac{\in}{k} c_{(\in 1)} v_t \left(\frac{\partial \overline{\upsilon}_i}{\partial x_j} + \frac{\partial \overline{\upsilon}_j}{\partial x_j}\right)\frac{\partial \overline{\upsilon}_i}{\partial x_j} + c_{\in 1} g_i \frac{\in}{k}\frac{v_t}{\sigma_\theta}\frac{\partial \overline{\theta}}{\partial x_i} - c_{\in 2}\frac{\in^2}{k} + \frac{\partial}{\partial x_j}\left[\left(\nu + \frac{v_t}{\sigma_\in}\right)\frac{\partial \in}{\partial x_j}\right] ---(2-29)$$

The turbulent viscosity is computed as

$$v_t = c_\mu \frac{k^2}{\in} --------(2-30)$$

The standard values for the coefficients read

$$c\_\mu, c\_(\in 1), c\_(\in 2), \sigma\_k, \sigma\_ \in) = 0.09, 1.44, 1.92, 1, 1.3) ----(2-31)$$

iv) The two- equation $k-\omega$

In this model [86], the standard k equation is solved, but as length determining equation ω is used. This quantity is often called specific dissipation from its detention $\omega \propto \in / k$. The modelled k and ω equation read

$$\left(\rho\bar{U}_j k\right)_{,j} = \left[\left(\mu + \frac{\mu_t}{\sigma_k^{\omega}}\right)k_{,j}\right]_{,j} + P_k - \beta^*\omega k \quad ----------(2-32)$$

$$\left(\rho\bar{U}_j \omega\right)_{,j} = \left[\left(\mu + \frac{\mu_t}{\sigma_{\omega}}\right)\omega_{,j}\right]_{,j} + \frac{\omega}{\kappa(c_{\omega 1}P_k - c_{\omega 2}\rho\omega)} -------(2-33)$$

$\mu_t = \rho\frac{k}{\omega},\ \epsilon = \beta^*\omega k$

The constants are determined as $\beta^* = 0.09, c_{\omega 1} = \frac{5}{9},\ c_{\omega 2} = \frac{3}{40}$, $\sigma_k^{\omega} = 2\ and\ \sigma_{\omega} = 2$

When wall functions are used k and ω are prescribed as

$$k_{wall} = (\beta^*)^{-\frac{1}{2}}u_*^2, \qquad \omega_{wall} = (\beta^*)^{-\frac{1}{2}}\frac{u_*}{ky} \quad -----(2-34)$$

In regions of low turbulence when both k and ϵ go to zero, large numerical problems for the $k-\omega$ model appear in the ϵ equation includes as k becoms zero. The destruction term in the ϵ equation includes $\frac{\epsilon^2}{k}$, and this causes problems as $k \to 0$ even ϵ also goes to zero; they must both go to zero at a correct rate to avoid problems, and this is often not the case. On the contrary, no such problems appear in the ω equation. If $k \to 0$ in the ω turbulent diffusion term simply goes to zero. Note that the production term in the ω equation does not include k since

$$\frac{\omega}{k}c_{\omega 1}P_k = \frac{\omega}{k}c_{\omega 1}\mu_t\left(\frac{\partial\bar{U}_i}{\partial x_j} + \frac{\partial\bar{U}_j}{\partial x_i}\right)\frac{\partial\bar{U}_i}{\partial x_j} = c_{\omega 1}\beta^*\left(\frac{\partial\bar{U}_i}{\partial x_j} + \frac{\partial\bar{U}_j}{\partial x_i}\right)\frac{\partial\bar{U}_i}{\partial x_j} \quad ------(2-35)$$

The $k-\omega$ model was used to predict transitional, recirculating flow.

v) Renormalization Group, RNG model

The RNG k - ϵ model was derived using a rigorous statistical technique (called renormalization group theory) [87] and [88]. It is similar in form to the standard k - ϵ model, but includes the following refinements:

- The RNG model has an additional term in its ∈ equation that significantly improves the accuracy for rapidly strained flows.
- The effect of swirl on turbulence is included in the RNG model, enhancing accuracy for swirling flows.
- The RNG theory provides an analytical formula for turbulent Prandtl numbers, while the standard k - ∈ model uses user specified, constant values.
- While the standard k - ∈ model is a high-Reynolds-number model, the RNG theory provides an analytically-derived differential formula for effective viscosity that accounts for low-Reynolds-number effects. Effective use of this feature does, however, depend on an appropriate treatment of the near-wall region.

These features make the RNG k - ∈ model more accurate and reliable for a wider class of flows than the standard k - ∈ model [87].

The RNG k - ∈ model has similar form to the standard k - ∈ model:

$$\frac{\partial}{\partial t}(\rho k) + \frac{\partial}{\partial x_i}(\rho k u_i) = \frac{\partial}{\partial x_j}\left(\alpha_k \mu_{eff} \frac{\partial k}{\partial x_j}\right) + G_k + G_b - \rho \in -Y_M + S_k \quad (2-36)$$

and

$$\frac{\partial}{\partial t}(\rho \in) + \frac{\partial}{\partial x_i}(\rho \in u_i) = \frac{\partial}{\partial x_j}\left(\alpha_\in \mu_{eff} \frac{\partial \in}{\partial x_j}\right) + C_{1\in}\frac{\in}{k}(G_k + C_{3\in}G_b) - C_{2\in}\rho\frac{\in^2}{k} - R_\in + S_\in \quad (2-37)$$

In these equations, G_k represents the generation of turbulence kinetic energy due to the mean velocity gradients, represent the contribution of fluctuating dilatation in compressible turbulence to the overall dissipation rate. Since the scope is for incompressible, it will be neglected. The quantities α_k and $\alpha_\in$ are the inverse effective Prandtl numbers for k and ∈, respectively. S_k and $S_\in$ are user-defined source terms.

vi) Large Eddy Simulation, LES, model

The LES equations read

$$\frac{\partial \bar{v}_i}{\partial t} + \frac{\partial \bar{v}_i \bar{v}_j}{\partial x_j} = -\frac{1}{\rho}\frac{\partial \bar{p}}{\partial x_i} + \nu \frac{\partial^2 \bar{v}_i}{\partial x_i \partial x_j} - \frac{\partial \tau_{ij}}{\partial x_j}$$

$$= -\frac{1}{\rho}\frac{\partial \bar{p}}{\partial x_i} + \frac{\partial}{\partial x_j}\left(\left(\nu + \nu_{sgs}\right)\frac{\partial \bar{v}_i}{\partial x_j}\right) \quad ----------(2-38)$$

Note that the time dependence term (the first term on the left side of the first line) has been retained, because the large, time dependent turbulent (i.e. the resolved) fluctuations are part of $\bar{v}_i$ and $\bar{p}$ and are not modelled with the turbulence model. The last term on the first line includes the Reynolds stresses of the small eddies, which are called SGS (Sub-Grid Stresses). This term must also be modelled, and at the second line it has been modelled with an SGS turbulent viscosity, ν_{sgs}. The difference of ν_{sgs} compared to ν_t is that it includes only the effect of the small eddies [87] and [86].

2. THEORETICAL BASIS AND SOLUTIONS FOR STEADY FLOW ANALYSIS IN HEC RAS

2.1 Equation for basic profile calculation

Water surface profiles computed from one cross section to the next by solving the Energy Equation with an iterative procedure called Standard step Method.

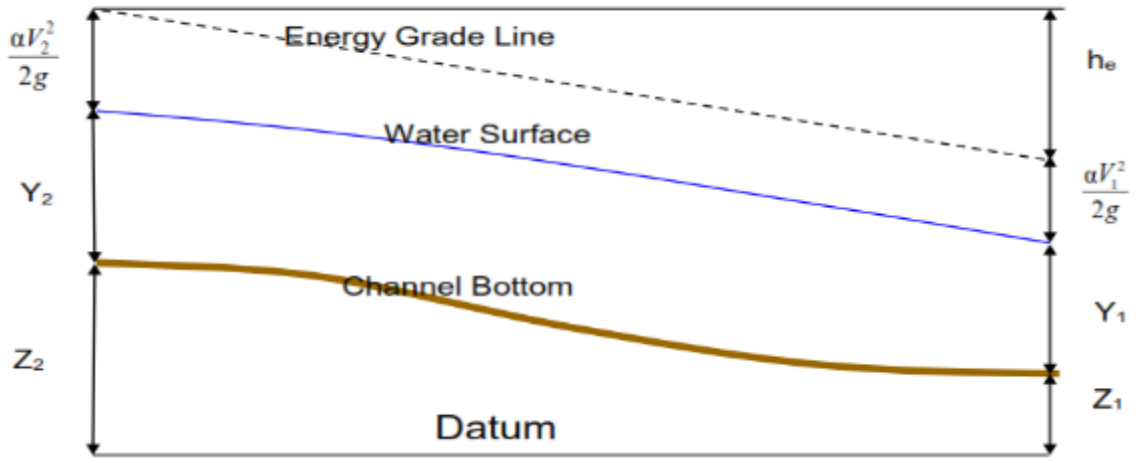

Figure Terms in the Energy equation

$$Z_2 + Y_2 + \frac{\alpha_2 v_2^2}{2g} = Z_1 + Y_1 + \frac{\alpha_1 v_1^2}{2g} + h_c \quad (3-1)$$

Where Z_1, Z_2 elevations of the main channel inverts, Y_1, Y_2: Depth of water at a cross section; v_1, v_2 Average velocity total (discharge/flow area), α_1, α_2: Velocity weighing coefficient alpha, g: Gravitational force and h_c is the energy head loss.

Energy head loss between cross sections: - Friction, Contraction and Expansion loss

Energy head loss (hc): $h_c = L\overline{S}_f + C\left|\frac{\alpha_2 v_2^2}{2g} - \frac{\alpha_1 v_1^2}{2g}\right| \quad (3-2)$

Where L is discharge weighted reach length; $\overline{S}_f$ Representative friction slope between sections; C: Contraction or Expansion loss coefficient

Discharge weighted reach length (L)

$$L = \frac{L_{lob}\overline{Q}_{lob} + L_{ch}\overline{Q}_{ch} + L_{rob}\overline{Q}_{rob}}{\overline{Q}_{lob} + \overline{Q}_{ch} + \overline{Q}_{rob}} \quad (3-3)$$

Where L_{lob}, L_{ch}, L_{rob} :XS reach length for flow in the Left, main channel and Right overbank $\overline{Q}_{lob}; \overline{Q}_{ch}; \overline{Q}_{rob}$: Average of the flow between section for the lob (leftover bank), ch (centre channel) & rob (right overbank) [42].

Applications of the Momentum Equation

The energy equation is only applicable to gradually varied flow situations. Whenever the WS passes through critical depth, the energy equation is not applicable. Transition from subcritical to supercritical or supercritical to subcritical is a rapidly varying flow instances that flow in transition categorized as rapidly varying situation. If significant changes in channel slope, structures, bridge constrictions, drop and weirs, and stream junctions. During these instances obtaining an answer may be achieved using Empirical equations for drop & weirs or applying momentum equation. Within HEC RAS, the momentum equation can be applied for specific problems: Occurrence of a hydraulic jump; Low flow hydraulics at bridges; and stream junctions [42].

The momentum equation from Newton's second law of motion:

$\sum F_x = ma \; ----3-4$

Applying Newton's second law of motion to a body of water enclosed by two XSs 1 and 2

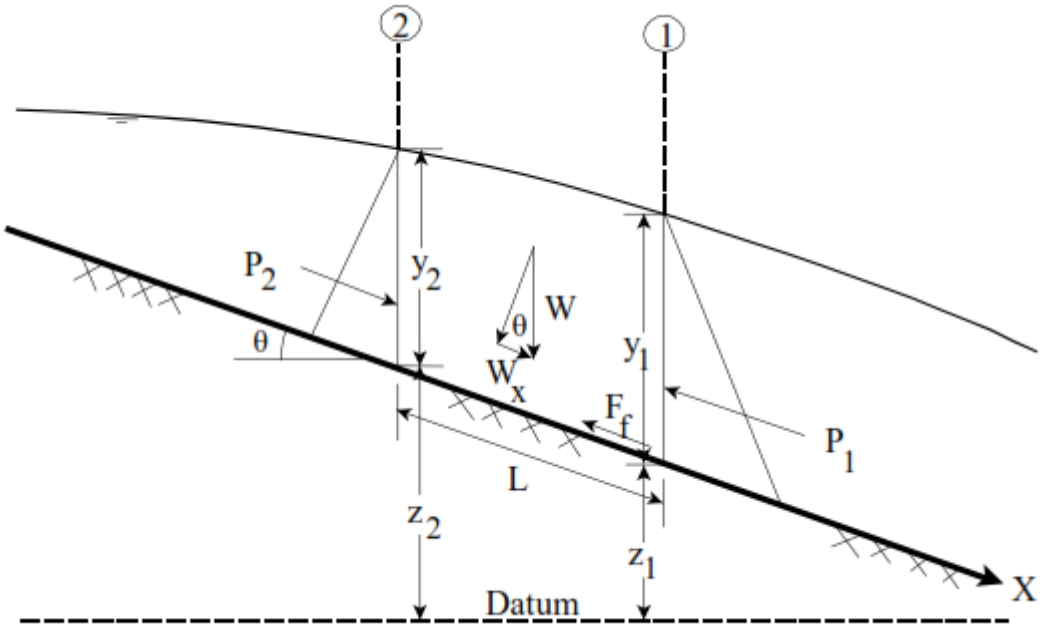

Figure: Application of momentum principle on a longitudinal profile of a channel

The change in momentum over a unit time can be written;

$$P_2 - P_1 + W_x - F_f = Q\rho\Delta V_x \quad ----------(3-5)$$

Where P is hydrostatic pressure force at location 1 & 2, W_x Force due to the weight of the water in the X direction, F_f Force due to the external friction losses from 2 and 1, ΔV_x Change on velocity from 2 to 1 in the x direction, Q = discharge, and ρ is density of water [42].

Hydrostatic Pressure Force:

The force in the X direction due to hydrostatic pressure is:

$$P = \gamma A\overline{Y}Cos\,\theta \quad ---------- \quad (3-6)$$

The assumption of a hydrostatic pressure distribution is only valid for slopes less then 1:10. The cos θ for a slope of 1:10 (approximately 6 degrees) is equals to 0.995. Because the slope of ordinary channels is far less than 1:10, the cosθ correction for depth can be set to 1.0 (chow, 1959). Therefore, the equations for hydrostatic pressure force at sections 1 and 2 are as follows [42]:

$$P_1 = \gamma A_1\overline{Y_1} \quad ---------- \quad (3-7)$$

$$P_2 = \gamma A_2\overline{Y_2} \quad ---------- \quad (3-8)$$

Where γ is unit weight of water; A_i area of the cross section at location 1 and 2; $\overline{Y_i}$ depth measured at the WS to the centroid of the cross-sectional area at point1 and 2

Gravity component of Weight of water force:

Weight of water = (unit weight of water) X (Volume of water)

$$W = \gamma\left[\frac{A_1+A_2}{2}\right]L \quad ---------- \quad (3-9)$$

$$W_x = WSin\theta \quad ---------- \quad (3-10)$$

$$Sin\theta = \frac{Z_2 - Z_1}{L} = S_0 \quad ---------- \quad (3-11)$$

$$W_x = \gamma \left[\frac{A_1 + A_2}{2}\right] L S_0 \quad ---------- \quad (3-12)$$

Where L distance between section 1 and 2 along the x axis; S_0slope of the channel based on mean elevations; Z_i mean bed elevation at location 1 and 2 [42].

Force of external Friction:

$$F_f = \tau L \overline{P} \quad ---------- \quad (3-13)$$

Where τ is Shear stress; $\overline{P}$ average wetted perimeter between section 1 and 2

$$\tau = \gamma \overline{S}_f * \overline{R} \quad ---------- \quad (3-14)$$

Where $\overline{R}$ is average hydraulic radius (R=A/P); $\overline{S}_f$ slope of the energy grade line (friction slope)

$$F_f = \gamma \frac{\overline{A}}{P} \overline{S}_f \, L \, \overline{P} \quad ---------- \quad (3-15)$$

$$F_f = \gamma \left[\frac{A_1 + A_2}{2}\right] \overline{S}_f \, L \quad ---------- \quad (3-16)$$

As Mass X acceleration:

$$\mathrm{ma} = \mathrm{Q}\rho\Delta\mathrm{V_x} \quad ---------- \quad (3-17)$$

But $\rho = \frac{\gamma}{g}$ and $\Delta V_x = [\beta_1 V_1 - \beta_2 V_2]$ $---------- \quad (3-18)$

$$ma = \frac{Q\gamma}{g}[\beta_1 V_1 - \beta_2 V_2] \quad ---------- \quad (3-19)$$

Where β is momentum coefficient that account for a varying velocity distance in irregular channels [42].

Collecting individual Forces acting on CV and substituting into equation 18 and assuming Q can vary from 2 to 1

$$\gamma A_2 \overline{Y}_2 - \gamma A_1 \overline{Y}_1 + \gamma \left\{\frac{A_1 + A_2}{2}\right\} L S_0 - \gamma \left[\frac{A_1 + A_2}{2}\right] L \overline{S}_f = \frac{Q_1 \gamma}{g} \beta_1 V_1 - \frac{Q_2 \gamma}{g} \beta_2 V_2 \quad ----(3-20)$$

$$\frac{Q_2\beta_2V_2}{g} + A_2\overline{Y}_2 + \left\{\frac{A_1+A_2}{2}\right\}LS_0 - \left[\frac{A_1+A_2}{2}\right]L\overline{S}_f = \frac{Q_1\beta_1V_1}{g} + A_1\overline{Y}_1 \quad (3-21)$$

$$\frac{Q_2^2\beta_2}{gA_2} + A_2\overline{Y}_2 + \left\{\frac{A_1+A_2}{2}\right\}LS_0 - \left[\frac{A_1+A_2}{2}\right]L\overline{S}_f = \frac{Q_1^2\beta_1}{gA_1} + A_1\overline{Y}_1 \quad (3-22)$$

All applications of the momentum equation within HEC RAS are derived from equation 3-22 [42].